

4-14-2015 12:00 AM

Methods and Systems for Fault Diagnosis in Nuclear Power Plants

Jianping Ma, *The University of Western Ontario*

Supervisor: Jin Jiang, *The University of Western Ontario*

A thesis submitted in partial fulfillment of the requirements for the Doctor of Philosophy degree
in Electrical and Computer Engineering

© Jianping Ma 2015

Follow this and additional works at: <https://ir.lib.uwo.ca/etd>



Part of the [Signal Processing Commons](#)

Recommended Citation

Ma, Jianping, "Methods and Systems for Fault Diagnosis in Nuclear Power Plants" (2015). *Electronic Thesis and Dissertation Repository*. 2737.

<https://ir.lib.uwo.ca/etd/2737>

This Dissertation/Thesis is brought to you for free and open access by Scholarship@Western. It has been accepted for inclusion in Electronic Thesis and Dissertation Repository by an authorized administrator of Scholarship@Western. For more information, please contact wlsadmin@uwo.ca.

METHODS AND SYSTEMS FOR FAULT DIAGNOSIS IN NUCLEAR POWER
PLANTS

(Thesis format: Monograph)

by

Jianping Ma

Graduate Program in Engineering Science
Department of Electrical and Computer Engineering

A thesis submitted in partial fulfillment
of the requirements for the degree of
Doctor of Philosophy

The School of Graduate and Postdoctoral Studies
The University of Western Ontario
London, Ontario, Canada

© Jianping Ma, 2015

Abstract

This research mainly deals with fault diagnosis in nuclear power plants (NPP), based on a framework that integrates contributions from fault scope identification, optimal sensor placement, sensor validation, equipment condition monitoring, and diagnostic reasoning based on pattern analysis. The research has a particular focus on applications where data collected from the existing SCADA (supervisory, control, and data acquisition) system is not sufficient for the fault diagnosis system. Specifically, the following methods and systems are developed.

A sensor placement model is developed to guide optimal placement of sensors in NPPs. The model includes 1) a method to extract a quantitative fault-sensor incidence matrix for a system; 2) a fault diagnosability criterion based on the degree of singularities of the incidence matrix; and 3) procedures to place additional sensors to meet the diagnosability criterion. Usefulness of the proposed method is demonstrated on a nuclear power plant process control test facility (NPCTF). Experimental results show that three pairs of undiagnosable faults can be effectively distinguished with three additional sensors selected by the proposed model.

A wireless sensor network (WSN) is designed and a prototype is implemented on the NPCTF. WSN is an effective tool to collect data for fault diagnosis, especially for systems where additional measurements are needed. The WSN has distributed data processing and information fusion for fault diagnosis. Experimental results on the NPCTF show that the WSN system can be used to diagnose all six fault scenarios considered for the system.

A fault diagnosis method based on semi-supervised pattern classification is developed which requires significantly fewer training data than is typically required in existing fault diagnosis models. It is a promising tool for applications in NPPs, where it is usually difficult to obtain training data under fault conditions for a conventional fault diagnosis model. The proposed method has successfully diagnosed nine types of faults physically simulated on the NPCTF.

For equipment condition monitoring, a modified S-transform (MST) algorithm is developed by using shaping functions, particularly sigmoid functions, to modify the window width of the existing standard S-transform. The MST can achieve superior time-frequency resolution

for applications that involves non-stationary multi-modal signals, where classical methods may fail. Effectiveness of the proposed algorithm is demonstrated using a vibration test system as well as applications to detect a collapsed pipe support in the NPCTF. The experimental results show that by observing changes in time-frequency characteristics of vibration signals, one can effectively detect faults occurred in components of an industrial system.

To ensure that a fault diagnosis system does not suffer from erroneous data, a fault detection and isolation (FDI) method based on kernel principal component analysis (KPCA) is extended for sensor validations, where sensor faults are detected and isolated from the reconstruction errors of a KPCA model. The method is validated using measurement data from a physical NPP.

The NPCTF is designed and constructed in this research for experimental validations of fault diagnosis methods and systems. Faults can be physically simulated on the NPCTF. In addition, the NPCTF is designed to support systems based on different instrumentation and control technologies such as WSN and distributed control systems. The NPCTF has been successfully utilized to validate the algorithms and WSN system developed in this research.

In a real world application, it is seldom the case that one single fault diagnostic scheme can meet all the requirements of a fault diagnostic system in a nuclear power. In fact, the values and performance of the diagnosis system can potentially be enhanced if some of the methods developed in this thesis can be integrated into a suite of diagnostic tools. In such an integrated system, WSN nodes can be used to collect additional data deemed necessary by sensor placement models. These data can be integrated with those from existing SCADA systems for more comprehensive fault diagnosis. An online performance monitoring system monitors the conditions of the equipment and provides key information for the tasks of condition-based maintenance. When a fault is detected, the measured data are subsequently acquired and analyzed by pattern classification models to identify the nature of the fault. By analyzing the symptoms of the fault, root causes of the fault can eventually be identified.

Keywords

Fault diagnosis, optimal sensor placement, semi-supervised classification, S-transform, kernel principal component analysis, nuclear power plant, wireless sensor network

Acknowledgements

I am grateful to my supervisor Dr. Jin Jiang for the opportunity to work on this exciting research. It would have been impossible without his guidance, inspiration, and patience.

Thanks to the members of the CIES research group for the help that came in many ways. Dr. Ataul Bari and Mr. Drew Rankin played instrumental roles in the design and commissioning of the NPCTF. The wireless system is also mainly configured by Dr. Bari. Dr. Ervin Sejdić has shared a lot of his experiences with time-frequency analysis. The management skills of Dr. Xinhong Huang have made the research a much smoother process. Drew Rankin has always been ready to lend a hand over the years -- both technical and nontechnical. Mr. Quan Wang made valuable contributions to the electronics work involved in the research. Dr. Sungwhan Cho and Dr. Ataul Bari provided constructive review of this manuscript. The friendship of many more members of the research group will be cherished for the rest of my life.

The research has benefited from the generousities of many outside the research group. The vibration data acquisition system is set up by Mr. Dave Lunn. Dr. H. M. Hashemian provided the IAEA benchmark data for validation of the sensor FDI algorithm. I have also learned from many people in the Canadian nuclear industries.

This research is financially supported by the Natural Sciences and Engineering Research Council of Canada (NSERC) and the University Network of Excellence in Nuclear Engineering (UNENE).

Finally, I would like to express my heartfelt gratitude to my wife Fang Li, my daughters Carolyn and Alice, and my family in China, for their everlasting love, understanding, encouragement, and support. They always fill my heart with happiness and hope under all circumstances.

Table of Contents

ABSTRACT.....	ii
KEYWORDS.....	iv
ACKNOWLEDGEMENTS.....	v
TABLE OF CONTENTS.....	vi
LIST OF TABLES.....	ii
LIST OF FIGURES	xiii
LIST OF APPENDICES.....	xvii
LIST OF SYMBOLS	xviii
NOMENCLATURE	xxv
1 INTRODUCTION	1
1.1 BACKGROUND	1
1.2 A FRAMEWORK FOR FAULT DIAGNOSIS IN NPPs	4
1.2 OBJECTIVES.....	8
1.3 INVESTIGATED METHODS AND SYSTEMS.....	9
1.4 SCOPE OF THE THESIS.....	10
1.5 CONTRIBUTIONS.....	10
1.6 ORGANIZATION	11
2 LITERATURE SURVEY	12
2.1 FAULT DIAGNOSIS METHODS.....	12

2.1.1	<i>Data-Driven Methods</i>	16
2.1.2	<i>Signal-Based Methods</i>	19
2.1.3	<i>Pattern Recognition Methods</i>	23
2.1.4	<i>Data Fusion Methods</i>	26
2.1.5	<i>Model-Based Methods</i>	28
2.2	SENSOR PLACEMENT METHODS	29
2.3	INSTRUMENTATION SYSTEMS	32
2.4	APPLICATIONS OF FDD IN NPP	34
2.5	SUMMARY	43
3	SENSOR PLACEMENT FOR FAULT DIAGNOSIS	45
3.1	PROBLEM STATEMENT	46
3.2	SYSTEM MODELING	49
3.3	FAULT DIAGNOSABILITY CRITERION.....	60
3.4	SENSOR PLACEMENT FOR DIAGNOSABILITY	62
3.5	EXPERIMENTAL VALIDATIONS	63
3.6	CONCLUSION	76
4	WIRELESS SENSOR NETWORKS FOR FAULT DIAGNOSIS	77
4.1	WIRELESS SENSOR NETWORK DESIGN	78
4.2	DIAGNOSTIC MODELS USED IN A PROTOTYPE WSN	80
4.3	PROTOTYPE IMPLEMENTATIONS	83

4.4	EXPERIMENTAL RESULTS	84
4.5	CONCLUSION	88
5	SEMI-SUPERVISED CLASSIFICATION FOR FAULT DIAGNOSIS	90
5.1	FAULT DIAGNOSIS AS A SEMI-SUPERVISED CLASSIFICATION PROBLEM.....	91
5.2	SEMI-SUPERVISED CLASSIFICATION ALGORITHMS FOR FAULT DIAGNOSIS.....	96
5.3	EXPERIMENTAL VALIDATIONS	100
5.3.1	<i>Case study using CANDU NPP simulator.....</i>	<i>101</i>
5.3.2	<i>Case study using NPCTF.....</i>	<i>104</i>
5.4	CONCLUSION	114
6	EQUIPMENT CONDITION MONITORING USING MODIFIED S-TRANSFORM.....	115
6.1	S-TRANSFORM FOR TIME-FREQUENCY ANALYSIS.....	116
6.2	MODIFIED S-TRANSFORM.....	120
6.3	EXPERIMENTAL VALIDATIONS	125
6.4	CONCLUSION	142
7	SENSOR VALIDATIONS USING KPCA	143
7.1	SENSOR FAULTS ON DIAGNOSIS PERFORMANCE.....	143
7.2	SENSOR FAULT DETECTION AND ISOLATION USING KPCA	147
7.2.1	<i>KPCA for sensor FDI.....</i>	<i>147</i>
7.2.2	<i>Numerical validations.....</i>	<i>154</i>
7.3	CONCLUSION	159

8	SUMMARY, CONCLUSION, AND FUTURE WORK.....	160
8.1	SUMMARY	160
8.2	CONCLUSION	161
8.3	FUTURE WORK.....	164
	BIBLIOGRAPHY	165
	APPENDICES	198
	APPENDIX A: NPP PROCESS CONTROL TEST FACILITY	198
	APPENDIX B: FMEA OF SELECTED NPCTF LOOPS.....	203
	CURRICULUM VITAE.....	204

List of Tables

Table 2-1: Summary of fault detection and diagnosis methods.....	14
Table 2-2: Fault diagnosis applications of data fusion methods.....	27
Table 2-3: Applications of fault diagnosis methods in NPPs	35
Table 3-1: Illustration of a S matrix.....	51
Table 3-2: Illustration of a C matrix	51
Table 3-3: Illustration of a y matrix	51
Table 3-4: Complete S matrix for a system with subsystems	53
Table 3-5: Complete S matrix for a system with subsystems	54
Table 3-6: B matrix for the example process	65
Table 3-7: C matrix for the example process.....	65
Table 3-8: Summary of NPCTF subsystems	67
Table 3-9: Fault effect matrix for water cooling subsystem.....	68
Table 3-10: System model results for NPCTF subsystems	69
Table 3-11: State propagation matrices for NPCTF subsystems	70
Table 3-12: Total fault-effect matrix of the NPCTF.....	71
Table 3-13: Incidence matrix for process control sensors of the NPCTF.....	71
Table 3-14: Fault diagnosability matrix of the NPCTF with process control sensors.....	72
Table 3-15: Fault diagnosability matrix of NPCTF with three additional sensors	73
Table 3-16: Summary of NPCTF experiments	73

Table 4-1: Faults and sensors used for prototype WSN system	80
Table 4-2: <i>A priori</i> distributions for local diagnosis models	82
Table 4-3: NPCTF settings for normal steady state operation.....	84
Table 4-4: Fault hypotheses for WSN test.....	84
Table 5-1: Validation data sets using CANDU NPP simulator	102
Table 5-2: NPCTF faults considered for SSC-based fault diagnosis model.....	105
Table 5-3: NPCTF settings for normal steady state operation.....	106
Table 5-4: Statistics of normal NPCTF operation data.....	106
Table 5-5: NPCTF fault detection thresholds	107
Table 5-6: Labeled data generation for NPCTF fault diagnosis	108
Table 5-7: Labeled data for SSC model.....	108
Table 6-1: Frequency domain window widths of two MST for example frequencies	120
Table 6-2: Frequency domain window width of MST-3 for example frequencies.....	122
Table 6-3: Summary of experimental case studies using vibration test system	126
Table 6-4: Frequency localization index for the data shown in Figure 6-6	129
Table 6-5: Frequency domain window widths for three MST-3 parameter settings	130
Table 6-6: Frequency localization index for the data shown in Figure 6-7	130
Table 6-7: Frequency localization index for vibration signals with different SNRs	136
Table 6-8: Summary of pipe vibration tests.....	138
Table 6-9: Time and frequency localization index for pipe vibration Test-I.....	139

Table 7-1: Summary of case studies with sensor faults	144
Table 7-2: NPP sensors used for KPCA validations.....	154
Table 7-3: NPP data set for KPCA validation	155
Table A-1: Control loops of the considered NPCTF system	200
Table A-2: FMEA of selected NPCTF loops.....	203

List of Figures

Figure 1-1: A framework for fault diagnosis in NPPs	4
Figure 2-1: Classification of fault detection and diagnosis methods	13
Figure 2-2: Typical usages of different categories of FDD methods.....	15
Figure 3-1: Illustration of a system.....	50
Figure 3-2: System model of a complex system.....	52
Figure 3-3: An example process to illustrate system modeling.....	64
Figure 3-4: Diagram of selected NPCTF loops	67
Figure 3-5: Model structure of NPCTF processes	68
Figure 3-6: Illustration of NPCTF experimental data.....	74
Figure 3-7: Further illustration of NPCTF experimental data	74
Figure 3-8: Illustration NPCTF experimental data with additional sensors	75
Figure 4-1: Architecture of prototype WSN for NPCTF fault diagnosis.....	79
Figure 4-2: Illustration of CV-1 fault experiment, (a), (c) and (e) sensor readings, and (b), (d) and (f), fault hypotheses probabilities computed by local diagnosis nodes in Cluster-1, 2 and 3, respectively.	85
Figure 4-3: Illustration of final diagnosis results by the central station for test with CV-1 fault.	87
Figure 4-4: System status diagnosis under normal condition and faults FV-2, FV-1, CV-12, CV-34 and heater, (a) measurement signals, (b) fault class level as classified by the central station.....	87

Figure 5-1: Supervised classification based on (a) 1-nearest neighbor; (b) semi-supervised classification	95
Figure 5-2: An example data graph	97
Figure 5-3: Proposed fault diagnosis scheme based on SSC	99
Figure 5-4: Illustration of CANDU NPP classification results.....	102
Figure 5-5: Computed class labels for the CANDU NPP data sets with: (a) normal operation $H0$; (b) BLCV fault $H1$; (c) SBV fault $H2$; and (d) MSSV fault $H3$	103
Figure 5-6: Diagram of selected NPCTF loops	104
Figure 5-7: Estimated class labels of NPCTF test data	110
Figure 5-8: Diagnosis results of test data with loss of coolant inventory faults	111
Figure 5-9: Illustration of the classification results of NPCTF test data	112
Figure 5-10: Further illustration of the classification results of NPCTF test data.....	113
Figure 6-1: Frequency domain window width of two MST algorithms	119
Figure 6-2: Effect of parameter b for $MST-3(a, b)$	122
Figure 6-3: Setup of vibration test system	125
Figure 6-4: Results of case study I as TFDs produced by (a) ST; (b) $MST-3(0.4, 2.2)$; (c) $MST-2(0.9083)$; and (d) $MST-1(1.8345)$	127
Figure 6-5: Threshold of the results in Figure 6-4 at 0.5	127
Figure 6-6: Results of case study II as TFDs produced by (a) ST; (b) $MST-4(462)$; (c) $MST-2(0.8963)$; and (d) $MST-1(2.0)$	129
Figure 6-7: Results of case study III as TFDs produced by (a) $MST-3(0.9315, 0.5)$; (b) $MST-3(1.4462, 0.5)$; (d) $MST-3(0.4, 2.2)$; and (d) standard ST	130

Figure 6-8: Results of case study IV as TFDs produced by (a) ST; (b) MST-3 (0.42, 3.0); (c) MST-2 (0.9157); (d) MST-1 (1.7472); (e) MST-2 (0.995); and (f) MST-1 (1.03)	132
Figure 6-9: TFDs produced by short-time Fourier transform for the signal in Fig. 8 using (a) narrow time domain window and (b) wide time domain window	133
Figure 6-10: TFDs of sweep signals produced by (a) ST for sweep signal one; (b) ST for sweep signal two; (c) MST-3(0.4, 2.2) for sweep signal one; (d) MST-3(0.4, 2.2) for sweep signal two; (e) MST-4(462) for sweep signal one; and (f) MST-4(462) for sweep signal two	134
Figure 6-11: Comparison of TFDs with different SNRs for (a) ST without noise; (b) sigmoid MST (0.4, 2.2) without noise; (c) ST with 6 dB SNR; (d) sigmoid MST (0.4, 2.2) with 6 dB SNR; (e) ST with 0 dB SNR; and (f) sigmoid MST (0.4, 2.2) with 0 dB SNR.....	135
Figure 6-12: Illustration of the pipe vibration monitoring system.....	137
Figure 6-13: Picture of the pipe vibration monitoring system.....	137
Figure 6-14: Results of pipe vibration Test-I as TFDs produced by (a) ST and (b) MST-3(0.3, 2.0). The TFDs are threshold at 0.368 and shown in (c) for ST and (d) for MST-3(0.3, 2.0)	139
Figure 6-15: Results of pipe vibration Test-II as TFDs produced by (a) ST and (b) MST-3(0.3, 2.0). The TFDs are threshold at 0.368 and shown in (c) for ST and (d) for MST-3(0.3, 2.0)	140
Figure 6-16: Results of pipe vibration test -III and test-IV as TFDs produced by (a) ST for test-III; (b) MST-3(0.3, 2.0) for test-III; (c) ST for test-IV; and (d) MST-3(0.3, 2.0) for test-IV	141
Figure 7-1: Classification results of NPCTF test data with positive bias in T2	144
Figure 7-2: Classification results of NPCTF test data with negative bias in T2.....	145
Figure 7-3: Classification results of NPCTF test data with positive bias in P1.....	146

Figure 7-4: Classification results of NPCTF test data with negative bias in P1	147
Figure 7-5: Illustration of advantages of nonlinear PCA.....	149
Figure 7-6: Results of fault detection in NPP data using KPCA	155
Figure 7-7: Average reconstruction errors (absolute value) of KPCA for NPP data.....	156
Figure 7-8: Average reconstruction errors (percentage) of KPCA for NPP data	157
Figure 7-9: Fault indices for selected sensors of NPP data	158
Figure A-1: Front view of the NPCTF.....	198
Figure A-2: Diagram of selected NPCTF loops	199
Figure A-3: Pictures of selected components of the NPCTF I&C system	202

List of Appendices

APPENDIX A: NPP PROCESS CONTROL TEST FACILITY 198

APPENDIX B: FMEA OF SELECTED NPCTF LOOPS 203

List of Symbols

Chapter 3:

$A_{i,j}$: The effects of system states changes in subsystem i on the states in subsystem j

B : A fault effect matrix that models sensitivities of system states to faults

B_k : The fault effect matrix for the k -th subsystem

C : A sensor sensitivity matrix that models sensitivities of sensors to system states

C_a : Augmented C matrix

C_k : The sensor sensitivity matrix for the k -th subsystem

f : A set of faults in a system

$f(i)$: The i -th number of faults in a system

f_k : The faults in the k -th subsystem

F : A fault matrix

Γ : The total fault effect matrix

$H(y, f)$: A system model that obtains sensitivities between sensors y and faults f

η : A threshold of fault diagnosability

$\Lambda(a, b)$: A measure of differences between a and b

I_i : An identity matrix of the size i

λ_i : The i -th biggest singular value of matrix

nf : Total number of faults in a system

n_y : Total number of sensors in a system

nf_k : The number of faults for the k -th subsystem

ns_k : The number of system states for the k -th subsystem

ny_k : The number of sensors for the k -th subsystem

R : A fault diagnosability matrix

Φ : The total state propagation matrix

Φ_b : The backward state propagation matrix

Φ_f : The forward state propagation matrix

$s(i)$: The i -th state of a system

s_k : The system states for the k -th subsystem

S : A matrix comprising sensitivities of system states to faults

S_k^l : A matrix comprising sensitivities of system states of subsystem k to faults originated in the subsystem l

$\Xi_i(y, f(i))$: Sensitivities of sensors y to the fault $f(i)$

$\Xi(y, f)$: Sensitivities of sensors y to the faults f

Ξ_i : The i -th column of Ξ

y : A set of sensors in a system

y_k : The sensors in the k -th subsystem

$y(i)$: The i -th number of sensor in a system

\bar{y} : A set of additional sensors

\tilde{y} : A subset of y

Chapter 4:

$N(a,b)$: A distribution function with the parameters a and b

$R(a,b)$: A distribution function with the parameters a and b

$p(x|y=i)$: A *prior* distribution of x for the class $y=i$

$p(y=i)$: Distribution of the class label $y=i$

$p(y=i|x)$: Probability of the i class for the inputs x

x : A set of process measurements

y : Fault class labels

Chapter 5:

α : A constant

D : A degree matrix

D_{ii} : The i -th element of the matrix D

D^l : A set of training data

F : A classification matrix

F^* : The convergent value of the classification matrix F

$g_i(y=i|x)$: A classification function for the class i given the inputs x

H_i : Fault hypothesis number i

L : A Lagrangian for a graph

nl : The number of training samples

nu : The number of unlabeled data samples

$p(x | y = i)$: A *prior* distribution of x for the class $y=i$

$p(x | y = i, \theta)$: A *prior* distribution $p(x | y = i)$ with the parameters θ

$p(y = i)$: Distribution of the class $y=i$

σ : A constant

u : An eigenvector

w_{ij} : A weight assigned to two input points x_i and x_j

x_t : A set of process measurements at time t

x_i'' : A set of new measurements at time i

X : A matrix with both labeled and unlabeled inputs

X^l : Inputs for the set of training data

X'' : Inputs for the set of unlabeled data

y : Fault class labels

Y : A matrix comprising class labels for the data matrix with both labeled and unlabeled inputs

Y^l : Class labels for the set of training data

Chapter 6:

$erf(x)$: The Gauss error function

f : Frequency

f_0 : The analysis frequency for a Gaussian shaping function

\hat{f} : The width of a modified window function

f_m : The maximum analysis frequency

$S(f, \beta)$: A sigmoid function for the frequency f and the parameters β

$ST(t, f)$: The S-transform of a signal at time t for the frequency f

σ : The width of a window function

$w(t)$: A window function at time t

$W(\alpha, f)$: The Fourier transform of a window function evaluated at the frequency f

$\hat{W}(\alpha, f)$: A modified window function in frequency domain

$\tilde{W}(\alpha, f)$: A shaping function for the window function in frequency domain

$x(t)$: A signal at time t

$x_i(t)$: The i -th component of a signal $x(t)$

$X(\alpha)$: The Fourier transform of a signal $x(t)$

Chapter 7:

α : A vector of the coefficients α_i

α_i : Coefficients

c_α : Standard normal deviation corresponding to the upper $(1 - \alpha)$ percentile

C : The covariance matrix of the training data matrix

\bar{C} : The covariance matrix of the training data matrix in the feature space

e : The estimations errors of the measurement data x

h_0 : A parameter defined on θ

η_i : The ratio between and SPE_i and SPE

$k(a,b)$: A kernel function defined on inputs a and b

K : A kernel matrix

λ : Eigenvalues of the covariance matrix

λ_i : The i -th largest eigenvalue

m : The number of training data samples

μ : The average reconstruction error for a set of measurement data

n : The number of variables

p : Eigenvectors of the covariance matrix

p_i : The eigenvector for the i -th largest eigenvalue λ_i

P_i : A projection operator

$\Phi(x)$: The vector of training data in the feature space

$\Phi(x_i) \bullet \Phi(x_j)$: Inner product between $\Phi(x_i)$ and $\Phi(x_j)$

SPE : Squared prediction errors

SPE_i : The squared prediction errors with the i -th sensor reconstructed

θ : A parameter defined on the non-principal eigenvalues

w_i : Projection of the i -th principal component in the feature space

x : A vector of measurement data

\hat{x} : The estimations of the vector x

X : Training data matrix

z : Estimated value of a input vector

\bar{z} : Convergent value of z

Nomenclature

1-NN: 1-nearest neighbor

AAKR: Auto-associative kernel regression

ADC: Analog-to-digital converter

ANN: Artificial neural network

ARMA: Autoregressive moving average

BLCV: Boiler level control valve

BNN: Back-propagation neural networks

BSPM: Backward state propagation matrix

CANDU: Canada Deuterium Uranium

CSTR: Continuous stirred tank reactor

CUSUM: Cumulative sum

DAQ: Data acquisition

DBN: Deep belief network

DG: Directed graph

D-S: Dempster-Shafer

EKF: Extended Kalman filter

EWMA: Exponentially weighted moving average

FCM: Fuzzy c-means

FDA: Fisher discriminant analysis

FDD: Fault detection and diagnosis

FDI: Fault detection and isolation

FFT: Fast Fourier transform

FMEA: Failure mode and effect analysis

FOM: Figure of merit

FPSS: Full power steady state

FSPM: Forward state propagation matrix

HHT: Hilbert-Huang transform

HMM: Hidden Markov model

HX: Heat exchanger

I&C: Instrumentation and control

ICA: Independent component analysis

K-NN: K-nearest neighbor

KPCA: Kernel principal component analysis

LDA: Linear discriminant analysis

LOCC: Loss of cooling capacity

LOCI: Loss of coolant inventory

LPMS: Loose part monitoring systems

MCSA: Motor current signature analysis

MD: Mahalanobis distance

MLE: Maximum likelihood estimation

MSET: Multivariate state estimation technique

MSSV: Main steam safety valve

MST: Modified S-transforms

NPCTF: Nuclear power plant process control test facility

NPP: Nuclear power plant

OPG: Ontario Power Generation

PCA: Principal component analysis

PHTS: Primary heat transport system

PLS: Partial least squares

PSD: Power spectral density

RCS: Reactor coolant system

ROH: Reactor outlet header

SBV: Steam bleed valve

SCADA: Supervisory control and data acquisition

SDG: Signed digraph

SFSM: Sub fault-sensitivity matrix

SG: Steam generator

SOM: Self-organizing maps

SPE: Squared prediction error

SPND: Self-powered neutron detector

SPRT: Sequential probability ratio test

SSC: Semi-supervised classification

ST: S-transform

STFT: Short-time Fourier transform

SVD: Singular value decomposition

SVM: Support vector machine

SVI: Sensor validity index

TFA: Time frequency analysis

TFD: Time-frequency distribution

TFR: Time-frequency representation

TSPM: Total state propagation matrix

TSVM: Transductive support vector machine

WSN: Wireless sensor networks

WVD: Wigner-Ville distribution

WT: Wavelet transform

Chapter 1

1 Introduction

1.1 Background

Various faults, such as stuck valves, process fouling, broken pipes, sensor drift, and damaged motor bearings, can occur in the instruments, equipment, processes, and structures of an industrial system (Kesavan & Lee, 1997; Kidam, Hurme, & Hassim, 2010; Ma & Jiang, 2011). Faults can have a significant impact on system safety and performance for a nuclear power plant (NPP). For example, drift in steam generator (SG) feedwater flow sensors can result in reactor power output reduction by as much as 3% (Chan & Ahluwalia, 1992). A stuck open relief valve created a loss of coolant scenario in the Three Mile Island accident, which was a major reason for the disastrous outcome (Rogovin & Frampton, 1980; Broughton, Kuan, Petti, & Tolman, 1989).

A fault can be defined as “an unpermitted deviation of at least one characteristic property (feature) of the system from the acceptable, usual, standard condition”, and a failure can be defined as “a permanent interruption of a system’s ability to perform a required function under specified operating conditions” (Isermann & Balle, 1997; Isermann, 2006). For simplicity, the term fault is used to refer to both faults and failures herein. Fault detection and diagnosis (FDD) is the process to detect, isolate, and identify faults (Isermann & Balle, 1997). Fault diagnosis includes fault isolation and identification. This research mainly deals with diagnosis of process faults, such as stuck valve, broken pipe, and malfunctioning actuators in NPPs (Venkatasubramanian, Rengaswamy, Yin, & Kavuri, 2003).

A great variety of FDD methods have been developed for applications in industries such as power generation, petrochemical processes, manufacturing, and aviation. The FDD methods have been reviewed in a number of books and papers (Gertler, 1998; Chiang, Russell, & Braatz, 2000; Korbicz, Koscielny, Kowalczyk, & Cholewa, 2004; Isermann, 2006; Palade & Bocaniala 2006; Tavner, Ran, Penman, & Sedding, 2008; Ding, 2012;

Aldrich & Auret, 2013; Ding, 2014; Gertler, 1988; Frank, 1990; Wise & Gallagher, 1996; Dasarathy, 2003; Venkatasubramanian, Rengaswamy, & Kavuri, 2003; Venkatasubramanian, Rengaswamy, & Kavuri, 2003; Isermann, 2005; Widodo & Yang, 2007; Du, Chi, & Wu, 2008; Ma & Jiang, 2011; Qin, 2012; Zaytoon & Lafortune, 2013; Yan, Gao, & Chen, 2014; Wang & Man, 2014; Onchis, Yan, & Rajmic 2014). The FDD methods can be broadly classified to 1) signal-based methods, 2) data-driven methods, 3) model-based methods, 4) pattern recognition methods, and 5) data fusion methods. Signal-based methods, such as spectral analysis, have been widely used for equipment condition monitoring using vibrations, acoustic emissions, etc. Data-driven methods are popular choices for fault detection and isolation (FDI) in sensors. Model-based methods have interesting properties for fault diagnosis in dynamic systems. Pattern recognition methods such as the support vector machine (SVM) algorithm provide the intelligence to recognize different fault scenarios as a way to identify faults, which are becoming increasingly prominent for fault diagnosis. Data fusion methods combine information from multiple sources to arrive at refined diagnostic conclusions.

Besides the FDD methods, it is very important to optimally select a set of sensors so that faults considered in a fault diagnosis system can be uniquely identified using data collected from the sensors. For this purpose, a handful of sensor placement models are developed, in which a directed graph (DG) is mostly used to model a system. The sensors are selected by optimizing a figure of merit (FOM) defined based on the cause-effect relationships between faults and sensors (Bhushan & Rengaswamy, 2002).

In addition, digital instrumentation and control (I&C) technologies enable more cost-effective data acquisition and management, which have created opportunities for fault diagnosis. For example, digital sensors can be programmed to perform self-diagnostics (Kolen, 1994; Clarke, 2000; Powner & Yalcinkaya, 1995; Tombs, 2002; Ichtertz, 2007). Industrial wireless sensor networks (WSN) are easier to set up, more flexible to relocate, and less expensive to deploy, as compared to a conventional wired system; thus, WSN provides an effective way to collect data for fault diagnosis (Callaway, 2003; Hashemian et al., 2011; Jiang, *et al.*, 2014; Oppermann, Boano, & Römer, 2014).

Despite the tremendous progress of FDD technologies in the past few decades, to implement an effective fault diagnosis system in a NPP can still face several unique problems.

- In existing FDD methods, it has often been assumed that information required for fault diagnosis is available from the SCADA (supervisory, control, and data acquisition) system. However, the average age of the NPPs worldwide is close to 30 years. To implement fault diagnosis in a system designed decades ago, a problem can arise that data from the existing SCADA system are not sufficient for a diagnosis model to identify the exact fault.
- To solve the previous problem, additional measurements need to be set up so that undiagnosable faults can be identified with the additional dimensions of information. However, to the best knowledge of the author, a method to guide optimal placement of additional measurements in an existing system is not available. This issue has not been studied in the related literatures.
- Installation of new measurements in the harsh environment (e.g. radioactive) of a NPP is much more difficult than in an ordinary industrial system.
- Even though all the measurements required are available, a fault diagnosis system can still face the problem that reliable training data obtained under actual fault conditions are scarce for a NPP because one cannot simply create real faults in a NPP, and computer simulations will inevitably suffer from modeling errors. However, most available fault diagnosis models often require a large amount of such training data to work.
- Identification of a fault occurring in a process often involves local diagnosis of the conditions of the equipment (e.g., pumps and motors) in the process. Processing of multi-modal signals is common in equipment condition monitoring. However, classical signal processing algorithms may have difficulties in characterizing such signals satisfactorily.

The effectiveness of a fault diagnosis system for NPPs can be affected all of the above mentioned problems. The fault diagnosis system should be based on an integral framework where the following issues are addressed: 1) determination of the scope of

faults to be diagnosed; 2) determination of the optimal set of sensors to use in the system; 3) effective data acquisition (DAQ) systems to collect data from the sensors; 4) proper tools to analyze data collected from the SCADA system and additional new sensors to make reliable diagnostic decisions; and 5) effective signal processing methods to extract useful features for diagnostic analysis based on multi-modal signals. Two more factors should be considered. They are: 6) methods to validate the conditions of the sensors, and 7) dependable platforms to validate performance of the above mentioned methods and systems.

1.2 A Framework for Fault Diagnosis in NPPs

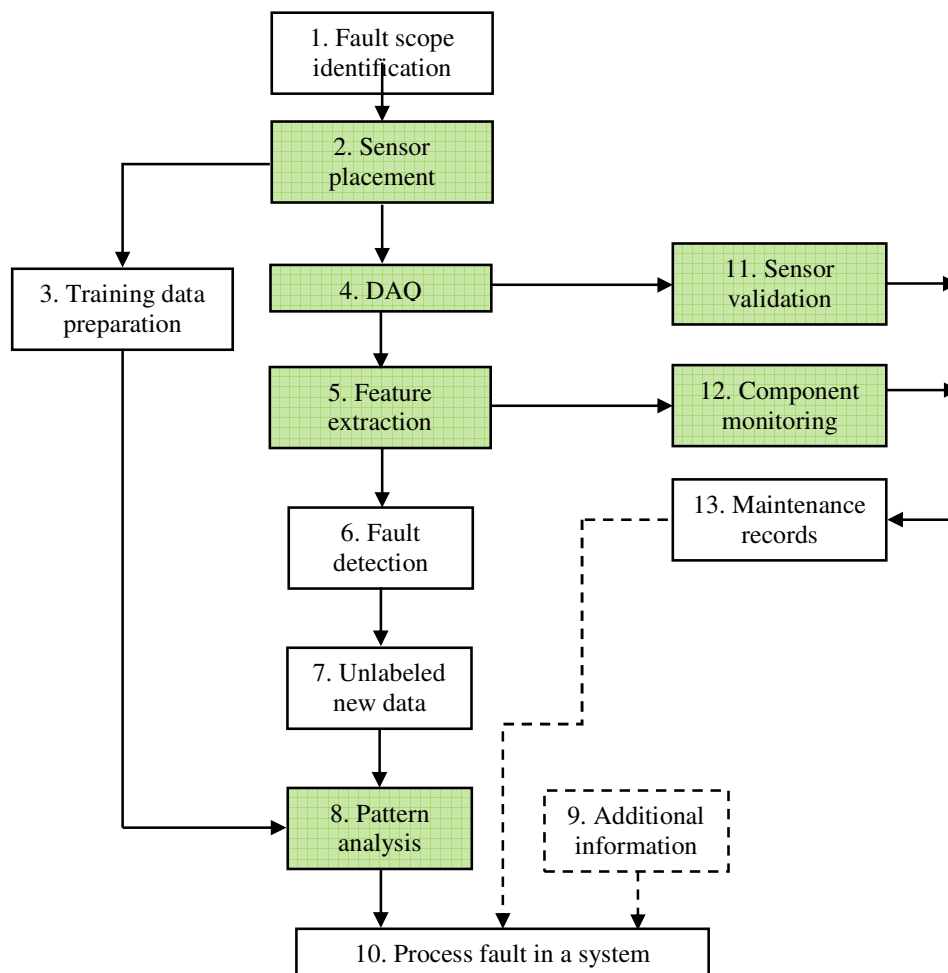


Figure 1-1: A framework for fault diagnosis in NPPs

A possible framework for fault diagnosis in NPPs is illustrated in Figure 1-1. It can be seen in Figure 1-1 that the framework has covered the previously discussed issues.

In the first step, faults that are to be considered in a FDD system are identified in advance. This step determines the scope of the diagnosis system. Since it is not realistic for a diagnosis system to inclusively cover all faults that can possibly happen in a complex system, this step ensures that faults critical to system performance and safety are handled with high priorities. Besides domain specific engineering judgement, the method of failure mode and effect analysis (FMEA) is particularly suitable for this purpose, the standard procedures of which have been well documented (Stamatis, 2003; Press, 2003). For a FDD system based on Figure 1-1, failure modes with high risk priority numbers are considered. Therefore, the FDD system will significantly reduce risks associated with the considered faults, and faults left outside the FDD system will have relatively low risks even if they remain undiagnosed.

Once the scope of faults is identified, a suite of sensors needs to be selected so that all faults identified in step one can be uniquely distinguished using data collected from the sensors. This is the purpose of step two in Figure 1-1. It is essentially a sensor placement problem, which is solved to search a minimum set of sensors so that fault diagnosability is ensured. If the existing SCADA system is not sufficient, the sensor placement step should also identify a set of additional sensors to achieve diagnosability of all faults.

Fault diagnosis is often based on pattern classification performed on data collected from the sensors identified in step two. Availability of training data is indispensable for such a pattern classification model. The training data characterize unique features of different fault conditions. The purpose of step three in Figure 1-1 is to prepare the necessary training data for a fault diagnosis model.

Step four deals with the data management infrastructure to support the necessary data acquisition, communication, and processing tasks. Sensors identified in step two must be installed in cost-effective ways, because excessive cost and complexity of the data management system will diminish the economical and technical viabilities of a fault diagnosis system. It is a particularly important issue for NPPs, because instrumentation

wiring in harsh environment of a NPP could cost as much as two thousand dollars per foot (Shankar, 2004; Kadri, Rao, & Jiang, 2009).

A fault diagnosis model often relies on features extracted from the measurement data collected from step four. If selected properly, a feature is able to characterize a faulty system better than the raw sensor outputs. Therefore, the quality of diagnosis can be improved for equipment condition monitoring (e.g., based on vibration monitoring) as well as process fault diagnosis (e.g., based on pattern classification). Step five in Figure 1-1 represents the feature extraction processes that can be considered for fault diagnosis.

Step six is the process to detect the presence of process faults. Limit checking of the measurement data at step four can be used for this purpose. A fault is considered if any measurements move outside the ranges regarded as normal. The fault detection step serves as a trigger of subsequent steps to diagnose what type of fault has happened.

If a fault is detected in step six, a pattern classification process will be activated to determine which type of fault has happened. Step seven and step eight are designed to fulfill this purpose. In step seven, a series of measurement data are collected following fault detection which are treated as new unlabeled data to be tested by a pattern classifier. The pattern classification process is represented by step eight, where fault classes that the new measurement data belong to are determined by a pattern classification model. In essence, a pattern classification model compares the unlabeled new data to the training data prepared in step three. Class label of the training data with the best match to the unlabeled data is assigned to the new data; thus, the fault hypothesis is determined. The quality of the pattern classification model has a direct impact on the performance of the fault diagnosis system.

At the end of step eight, the diagnosis system has detected that a fault has happened in the system and the most likely fault condition has been identified. However, if additional sources of relevant information are available, the diagnosis results may be enhanced by aggregating the additional information. Maintenance related information represented by step thirteen can be used for this purpose. Other sources of information such as operator inputs are collectively represented as step nine. The information provided by step eight,

step nine, and step thirteen can be combined by an information fusion model to arrive at a decision that is refined from that of step eight. Step ten is used to represent the information fusion process. Data fusion methods (to be surveyed in Chapter 2) can be considered for application here. If no diagnostic information is provided by step nine and step thirteen, the fusion steps can be disregarded. For this reason, dashed lines are used for the concerned connections.

The diagnosis system is only credible when data collected from the system are reliable. Sensor validation ensures that troublesome sensors can be detected promptly for repair or replacement so that the diagnosis system will not suffer from erroneous data. Step eleven in Figure 1-1 is designed for this purpose. Data-driven methods (to be reviewed in Chapter 2) can be used to detect and isolate sensor problems. Self-diagnostics in smart sensors can be another approach.

Step twelve in Figure 1-1 represents condition monitoring of other system components such as pumps, motors, pipes and valves. If abnormal process operation is caused by faulty equipment, the equipment condition monitoring system is able to provide timely indication of the fault location and characteristics. Trending of the equipment condition monitoring results can also be used to guide optimal maintenance practice. The maintenances not only can reduce the probabilities of fault occurrence, they can also provide evidences of fault precursors which can be considered in the decision making models in step ten. Equipment condition monitoring often relies on features extracted from monitoring signals such as vibration, acoustic emissions, and motor current. Therefore, it needs the feature extraction process of step five in Figure 1-1.

The research has a particular focus on the six steps highlighted in Figure 1-1, i.e. step two, four, five, eight, eleven, and twelve. One reason is that the performance of a fault diagnosis system may suffer more severely if those steps are not handled properly. Another reason is that these steps face problems unique to a NPP as previously discussed.

1.2 Objectives

Through a literature review as summarized later in Chapter 2, several gaps between existing FDD technologies and the framework (Figure 1-1) are identified. More specifically, some limitations can be summarized as follows.

- 1) Existing sensor placement models are difficult to use to investigate the effects of additional sensors on fault diagnosis. In addition, they lack quantifications of the fault-sensor relationships. A fault diagnosability criterion based on a conventional binary incidence matrix can create challenges for a practical fault diagnosis model.
- 2) It can be very expensive to install new measurements in a NPP using conventional wired I&C systems. In addition, data acquisition and processing are usually implemented in a centralized fashion which can create diagnosis latency and excessive demand on communication bandwidth.
- 3) Fault diagnosis models often require the availability of sufficient and reliable training data. The applicability of this important tool is challenged for applications in NPPs because training data can be difficult to acquire.
- 4) Vibration signals are important for equipment condition monitoring in NPPs. However, current signal processing methods have problems to extract the time-frequency characteristics of a time-varying, multi-modal vibration signal.
- 5) Nonlinear data-driven models, particularly kernel principal component analysis (KPCA), are suitable for detection and isolation of faults in sensors; however, the existing fault isolation index can be unreliable.

The objectives of this research are to develop methods and systems to relax those limitations. Specifically, the objectives include

- 1) Develop a model that can guide the optimal placement of additional sensors to enhance performance of a fault diagnosis system. The model is able to quantify the cause-effect relationships between faults and sensors of a complex system, and the model allows flexible model reconfigurations. It is for step two of the framework in Figure 1-1.

- 2) Develop a prototype WSN with distributed in-network diagnosis capabilities that supports effective implementation of a process fault diagnosis system. It is for step four of the framework in Figure 1-1.
- 3) Develop a pattern classification method for process fault diagnosis where labeled training data is scarce but unlabelled measurement data is easily accessible. It is for step eight of the framework in Figure 1-1.
- 4) Develop a time-frequency analysis (TFA) algorithm with improved time-frequency localization performance for equipment condition monitoring, where non-stationary multi-component signals are involved. It is for step five and twelve of the framework in Figure 1-1.
- 5) Improve the performance of data-driven sensor FDI methods especially for multi-fault scenarios. It is for step eleven of the framework in Figure 1-1.
- 6) It is desirable to validate the methods by physical systems where realistic faults can be created, so that feasibilities of the methods for real world applications can be tested. Therefore, another objective of the research is to develop a physical NPP simulator where realistic fault scenarios can be created to validate fault diagnosis methods.

By integrating the developed methods into a suite of diagnostic tools, the values and performance of diagnosis systems can potentially be enhanced. For this reason, another objective of this research is to demonstrate the advantages of implementing a fault diagnosis system that integrates the developed methods and systems.

1.3 Investigated Methods and Systems

The following methods and systems are studied in this research to achieve the objectives:

- 1) A sensor placement model is developed. It models a system in three layers 1) faults, 2) system states, and 3) sensors to obtain a quantitative incidence matrix. A complex system is decoupled to multiple less complicated problems and a mechanism is provided to model the couplings. A fault diagnosability criterion is proposed by measuring the degrees of singularities of the incidence matrix. A

sensor selection procedure is provided, so that faults considered in a diagnosis system are diagnosable, and the number of additional sensors is kept minimal.

- 2) A WSN with two levels of information aggregation is designed and implemented on a NPP process control test facility (NPCTF) for fault diagnosis, using commercial off-the-shelf products from the MEMSIC, Inc.
- 3) A fault diagnosis scheme based on semi-supervised classification (SSC) is developed as a solution to challenges of limited training data under fault conditions.
- 4) The standard S-transform (ST) is modified for TFA of non-stationary multi-modal signals. The solution is to modify the frequency domain window width using sigmoid functions and other appropriate shaping functions.
- 5) The KPCA-based sensor FDI methods are extended by utilizing the average reconstruction errors of a KPCA model to identify sensor faults.
- 6) A simplified physical NPP simulator (the NPCTF) is designed and built. A variety of faults can be physically simulated on the NPCTF. The studied fault diagnosis methods and systems are validated on the NPCTF.

1.4 Scope of the Thesis

Investigations of the FDD methods and systems are limited within the following scopes:

- 1) This research only deals with faults identified by a FMEA of a concerned system. The scope is further limited to scenarios where there can be, at most, one fault at a time.
- 2) Validation of the modified S-transform (MST) algorithm is limited to vibration signals.
- 3) For WSNs, classical algorithms such as Naive Bayes classifiers are preferred for implementations on the prototype.

1.5 Contributions

Contributions of this research can be summarized as follows:

- 1) Development of a sensor placement model to determine optimal placement of additional sensors to enhance fault diagnosability of a complex system.
- 2) Development of a WSN design and prototype with distributed in-network data processing for fault diagnosis.
- 3) Development of a process fault diagnosis method based on SSC, which can be applied to systems where reliable training data is difficult to obtain.
- 4) Development of an improved TFA algorithm, which achieves superior time-frequency resolution for equipment condition monitoring that involves non-stationary multi-component signals, where classical methods can fail.
- 5) Proposed an improvement to KPCA-based FDI techniques for sensor faults.
- 6) Design and commissioning of a physical NPP simulator for experimental validations of fault diagnosis methods and systems.

1.6 Organization

The rest of this thesis is organized as follows:

- A literature survey on FDD methods, sensor placement models, and industrial I&C technologies is provided in Chapter 2.
- The proposed model for optimal sensor placement is explained in Chapter 3.
- A prototype WSN to implement a fault diagnosis system is presented in Chapter 4.
- The fault diagnosis scheme based on SSC is discussed in Chapter 5.
- The principle and experimental validations of the proposed MST algorithm for vibration monitoring is presented in Chapter 6.
- Sensor FDI using KPCA is investigated in Chapter 7.
- Conclusions are drawn in Chapter 8, along with some future work directions suggested.
- Details about the NPCTF system design are summarized as Appendix A.

Chapter 2

2 Literature Survey

A survey of FDD methods is presented in this chapter. Since a great variety of FDD methods have been studied for a wide range of applications, it becomes non-realistic to include an all-encompassing survey; therefore, only some well-known methods related to this research are considered. In addition, only methods that rely on quantitative analysis of process measurement data are considered. Following the review of FDD methods, a brief survey of optimal sensor placement methods for fault diagnosis applications is presented. Furthermore, a brief review of popular I&C technologies is also included in this chapter because, as the tool to acquire, communicate, process, and manage the data used in a fault diagnosis system, the I&C systems have increasingly become integral parts for fault diagnosis. Finally, applications of FDD methods to NPPs are reviewed.

2.1 Fault Diagnosis Methods

As presented in Figure 2-1, the surveyed FDD methods are roughly classified into the following five categories: data-driven methods, signal-based methods, pattern recognition methods, data fusion methods, and model-based methods. Also listed in Figure 2-1, are some well-known algorithms of each class of methods. Some properties of the five categories of FDD methods are summarized in Table 2-1. Acronyms of the algorithms are used in Figure 2-1 for the interest of space. The full names are given in the nomenclature. Note that overlaps may exist between different categories of methods.

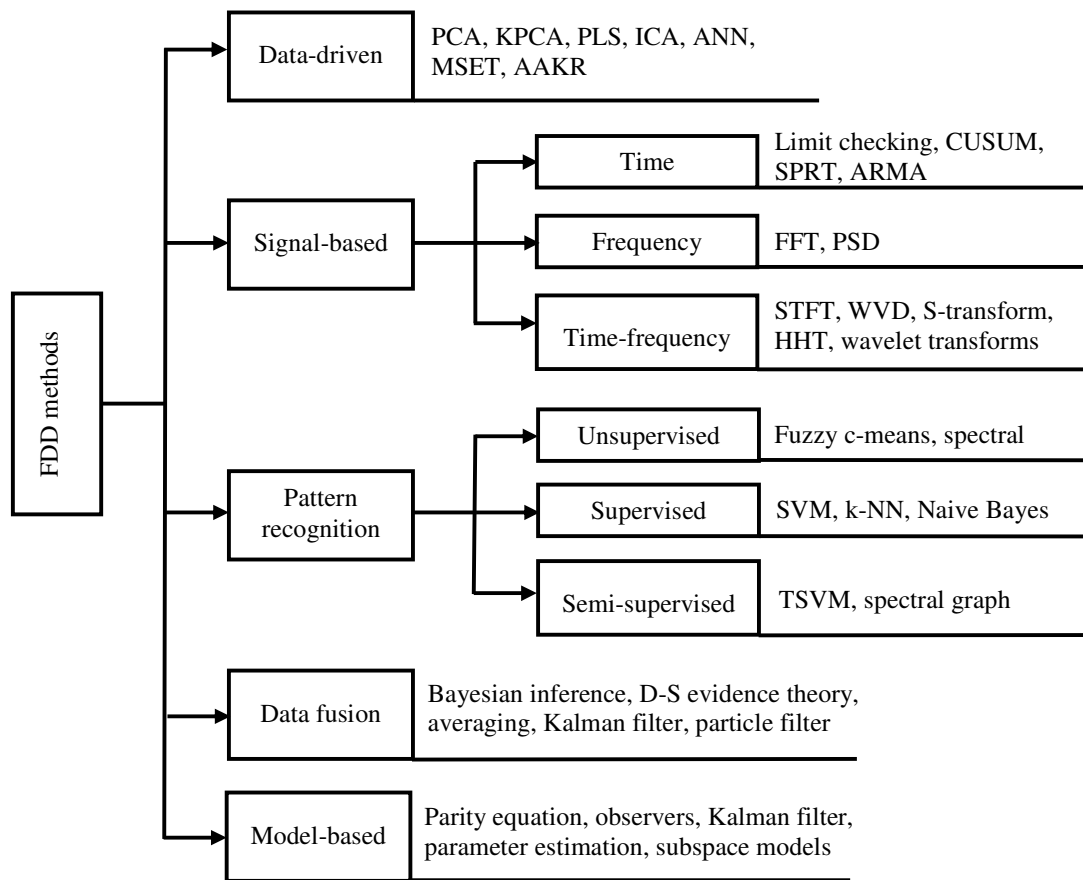


Figure 2-1: Classification of fault detection and diagnosis methods

Table 2-1: Summary of fault detection and diagnosis methods

Category of methods	General principle	Example algorithms	Typical applications
Data-driven methods	Test correlations in new data against historical data using multivariate statistics	PCA, KPCA, PLS, ICA, FDA, ANN, MSET, AAKR	FDI in sensors and processes for steady state systems
Signal-based methods	Compare features extracted from a signal to normal baseline values	PSD, STFT, WVD, wavelet transforms, ST, SPRT, ARMA, CUSUM, limit checking	Monitoring of machines and process parameters
Pattern recognition methods	Match features extracted from process measurements to ones with known faults	SVM, k-NN, Naive Bayes, ANN, fuzzy c-means, semi-supervised classifications	Fault diagnosis in sensors, machines and processes
Data fusion methods	Combine data from multiple sources to improve quality of diagnosis	Bayesian inference, Kalman filter, D-S evidence theory, ANN, fuzzy logic	FDD in machines and processes
Model-based methods	Compare actual system response to predictions based on system models	Parity equation, observers, parameter identification, Kalman filter, subspace models	FDI in dynamic systems

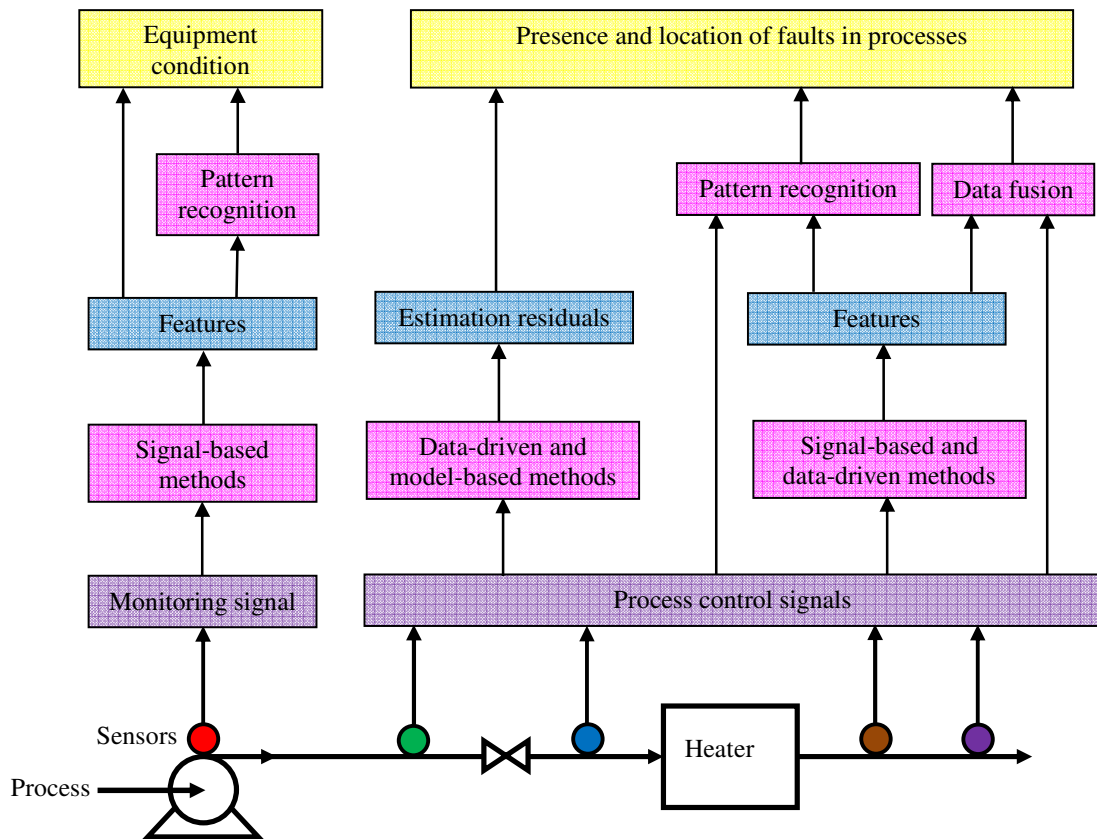


Figure 2-2: Typical usages of different categories of FDD methods

Typical usages of different categories of FDD methods are illustrated in Figure 2-2. At the bottom of Figure 2-2 is an example process that is instrumented with sensors to measure process control variables such as pressure, temperature, flow, and level, as well as monitoring sensors such as vibration sensors for motors and pipes.

Signal-based methods are often used to process monitoring signals to extract features that can characterise component conditions. Based on the features, health of the equipment can be assessed using engineering judgement. Pattern recognitions methods are also used to automate the assessment process.

Multivariate analysis is another way to detect and diagnose faults in a process. Data-driven methods and model-based methods are used for diagnostic analysis based on

analytical redundancy. Using those methods, the value of a process variable is estimated from other correlated measurements using a model, and the estimation is compared to the actual sensor measurement. An abnormal increase in the estimation residuals indicates that normal correlations captured in the models are violated due to faults. Testing the estimation residuals of data-driven methods and model-based methods enables detection and diagnosis of faults.

Pattern recognition methods and data fusion methods diagnose problems in a system based on analysis of features extracted from various process measurements. Pattern recognition methods match unique patterns in the features to specific fault conditions. Data fusion methods use various tools to combine the features to produce a conclusion e.g., the location and root cause of a fault. Signal-based methods and data-driven models are often used for pre-processing to extract the features used by pattern recognition and data fusion analyses. However, depending on the problem at hand, pattern recognition and data fusion methods may work directly on raw measurement data without the need of feature extraction.

2.1.1 Data-Driven Methods

Data-driven methods mainly use multivariate statistical analysis for FDD. They rely on relationships between multiple measurements of a system, but use them implicitly through analysis of historical data. For this reason, such methods are also referred to as process history-based methods (Venkatasubramanian, Rengaswamy, Kavuri, & Yin, 2003). Since the challenging task of explicit system modeling is not required, data-driven methods are attractive for practical FDD applications. They are particularly suitable for FDI in steady state systems. In fact, data-driven methods have been successfully used for FDI in sensors, machines, and processes of various industrial systems. However, a key limitation of data-driven methods is that a data-driven model only works well within the operational range represented by the training data.

Model-based methods can be used for fault diagnosis in two different approaches. The first approach is based on transformations of a set of measurements using model-based algorithms. Some popular algorithms using this approach include Principal component

analysis (PCA) (Dunia & Qin, 1998; Jolliffe, 2002; Wise & Gallagher, 1996), partial least squares (PLS) (Geladi & Kowalski, 1986; Wise & Gallagher, 1996; Kourti & MacGregor, 1996; Qin & McAvoy, 1992; Wold, 1994; Qin, 1998; Rosipal & Kramer, 2006), independent component analysis (ICA) (Hyvärinen & Oja, 2000; Ding, Gribok, Hines, & Rasmussen, 2004), Fisher linear discriminant analysis (FDA or LDA) (Chiang et al., 2000; Chiang et al., 2000; Chiang, Russell, & Braatz, 2000; Chiang, Kotanchek, & Kordon, 2004; He, Qin, & Wang, 2005), and nonlinear extensions to those algorithms (Mika, Ratsch, Weston, Scholkopf, & Muller, 1999; Baudat & Anouar, 2000; Bach & Jordan, 2003; Lee, Qin, & Lee, 2007; Zhang & Qin, 2007). In the second approach, fault is detected and isolated by comparing a set of measurement data with analytical estimations generated by a data-driven model. Popular algorithms in this approach include PCA, ANN (Mehrotra, Mohan, & Ranka, 1997; Venkatasubramanian, Rengaswamy, Kavuri, et al., 2003), MSET (Herzog, Wegerich, & Gross, 1998; Hines & Usynin, 2005), AAKR (Garvey & Hines, 2006), and cross calibration (Hashemian, 2006). ANN and MSET have been used for a large variety of FDD applications (Watanabe, Matsura, Abe, Kubota, & Himmelblau, 1989; Venkatasubramanian, Vaidyanathan, & Yamamoto, 1990; Kramer, 1992; Nieman & Singer, 2002; Hines & Davis, 2005; White, Gross, Kubic, & Wigeland, 1994; Gross, Wegerich, Singer, & Mott, 1996; Hines & Davis, 2005; GE, 2014).

It is interesting to note that PCA is one of the best known algorithms in both approaches. PCA is basically a linear projection of a set of data into a lower dimensional principal component subspace, where the maximum variances are captured. The principal components reveal how the variables are correlated to each. Projections to the non-principal subspace are considered residuals (Dunia & Qin, 1998; Jolliffe, 2002). Standard PCA can be conveniently trained by applying singular value decomposition (SVD) to the covariance matrix of some historical data (Wise & Gallagher, 1996). Faults in the measurement data will break down the normal correlations and increase the residuals. Fault detection can be achieved by comparing the squared prediction error (SPE) with a threshold. The faulty sensor can be isolated using techniques such as contribution plot and sensor reconstruction (Wise & Gallagher, 1996; Dunia, Qin, Edgar, & McAvoy, 1996; Qin, 2003; Qin, 2012). PCA has simple structure, is easy to train, and is a powerful

tool that captures the maximum variances in correlated data. It is a very popular choice for FDI in real systems (Kaistha & Upadhyaya, 2001; Upadhyaya, Zhao, & Lu, 2003; Ma & Jiang, 2009). Standard PCA has been extended to obtain variant algorithms such as recursive PCA (Li, Yue, Valle-Cervantes, & Qin, 2000), dynamic PCA (Ku, Storer, & Georgakis, 1995; Russell, Chiang, & Braatz, 2000; Chen & Liu, 2002; Lee, Choi, & Lee, 2004), multi-way PCA (Wise & Gallagher, 1996; Nomikos & MacGregor, 1994), and multi-scale PCA (Bakshi, 1999; Yoon & MacGregor, 2004). PCA has also been used in hybrids with model-based FDD methods to improve the performance (Gertler, Li, Huang, & McAvoy, 1999; Qin & Li, 1999; Li & Qin, 2001).

Standard PCA is a linear method. Large errors can be induced when PCA is applied to data containing nonlinearities. A few nonlinear PCA methods (Kramer, 1991; Webb, 1996; Dong & McAvoy, 1996) have been developed. However, complicated nonlinear optimization is often required, which has the risk of local optima. In addition, the model structures usually need to be specified *a priori*. What's more, existing fault isolation techniques for PCA, notably contribution plot (Kramer, 1991) and sensor validity index (SVI) based on sensor reconstruction (Dunia et al., 1996), may not give reliable isolation results if more than one sensor fault exists at the same time. A more recent development to PCA is the combination of kernel-based nonlinear learning methods to PCA to obtain nonlinear PCA (Schölkopf, Smola, & Müller, 1998; Mika, Schölkopf, et al., 1999). This technique has been adopted in some FDD studies (Lee, Yoo, Choi, Vanrolleghem, & Lee, 2004; Choi, Lee, Lee, Park, & Lee, 2005; Ma & Jiang, 2012). KPCA first maps measurements from the input space onto a feature space via nonlinear mapping functions. Procedures used in linear PCA can then be directly applied in the feature space. Through the use of kernel functions, dot products in the feature space can be computed implicitly (Aizerman, Braverman, & Rozonoer, 1964). Nonlinear optimizations and *a priori* model structure specifications as required in other nonlinear PCA techniques are not involved in KPCA. KPCA has been studied for fault detection applications (Lee et al., 2004; Choi et al., 2005) in analogy to PCA. For fault detection, a SPE in the feature space can be calculated and compared with a predetermined threshold (Lee et al., 2004; Choi et al., 2005). Fault isolation and identification is more difficult for KPCA (Schölkopf & Smola, 2002). One possible approach is to reconstruct new measurements from the training data.

After replacing the output of a sensor with the reconstructed value, a SVI, called fault index in (Choi et al., 2005), can be defined for this sensor as the ratio between the SPEs after and before the reconstruction. A sensor with considerably reduced fault index is considered faulty. However, the fault index may not provide reliable results if more than one fault exists at the same time. In addition, the direction and magnitude of a detected fault cannot be identified.

Overall, data-driven methods do not need an explicit model of a system. Therefore, they are flexible for applications in practical systems. In fact, they have been favorable choices for FDD in various industries. The major limitation is that the models only work well in the range of the training data. PCA is probably the most widely used algorithm in practical FDD systems. PCA has been extended for nonlinear applications using kernel functions; however, the techniques used to isolate faulty sensors can be unreliable.

2.1.2 Signal-Based Methods

Signal-based methods do not rely on analytical relationships between different variables. They make decisions by comparing features extracted from a signal to normal baseline values. Features in time domain, frequency domain, and joint time-frequency domain have been used.

Time domain features are usually related to statistical parameters extracted from a signal, such as the mean, cumulative sum (Montgomery, 2005), and exponentially weighted moving average (EWMA) (Hunt, 1986). Another group of signal-based methods rely on parameters of a signal model or predictions generated by a signal model. A group of time series analysis models are popular choices as the signal model, such as autoregressive moving average model (Box & Jenkins, 1970; Hamilton, 1994) and autoregressive (AR) model (Kitamura, 1989; Ueda, Tomobe, Setoguchi, & Endou, 2002). The models can detect faults causing deviations of the model parameters from the normal values.

The spectral information extracted from a signal is usually used as frequency domain features. The spectrum of a signal can be obtained using algorithms based on the fast Fourier transform (FFT). Spectral analysis is a useful tool to diagnose machine faults

using signals such as vibration, motor current (Benbouzid, 2000; Tavner et al., 2008), and acoustic emissions (Li & Li, 1995; Kunze, 1999; Lee, Lee, Kim, Luk, & Jung, 2006). In addition, spectral analysis of process noise is shown to be a useful tool to detect dynamic performance degradation of sensors (Hashemian, Thie, Upadhyaya, & Holbert, 1988; Demazière & Glöckler, 2004; Hashemian, 2006; Hashemian & Jiang, 2010) and to monitor nuclear reactor internal structures (Robinson, Hardy, Shamblin, & Wolff, 1977; Glöckler, 2003; Park et al., 2003). Higher order spectral analyses have also been utilized in FDD applications (Liang, Iwnicki, & Zhao, 2013; Saidia, Fnaiech, Henao, Capolino, & Cirrincione, 2013).

In the joint time-frequency domain, a time-frequency representation (TFR) maps a one-dimensional time series signal to a two-dimensional distribution function in both time and frequency, which shows the spectral variations over time. The joint time-frequency distribution (TFD) is an important tool for analysis of non-stationary signals that can be found in various fault detection and diagnosis applications in practice (Peng & Chu, 2004; Sejdić, Djurović, & Jiang, 2009; Feng, Liang, & Chu, 2013; Yan et al., 2014; Huang et al., 1998; Huang, Shen, & Long, 1999; Peng, Tse, & Chu, 2005; Yu, Yang, & Cheng, 2007; Antonino-Daviu, Riera-Guasp, Pineda-Sanchez, & Perez, 2009).

Time-frequency analysis methods have been widely investigated in the literature (Cohen, 1989; Hlawatsch & Boudreaux-Bartels, 1992; Cohen, 1995; Gröchenig, 2001). The short-time Fourier transform is often considered a standard TFA algorithm. STFT is the Fourier transform of a signal enveloped by a window function moving in time (Hlawatsch & Boudreaux-Bartels, 1992). Since the window function suppresses signals away from the analysis time, the STFT produces local spectral distributions running in time. Since the window function is fixed in STFT, the TFD has uniform time-frequency resolution across the frequency range.

Quadratic TFA methods compute the TFD of a signal's energy. A well-known quadratic TFA algorithm is the Wigner-Ville distribution; however, WVD contains interference cross terms due to the quadratic nature. The Cohen class TFA methods are developed to smooth the interference terms using kernel functions (Cohen & Posch, 1985; Cohen,

1989; Choi & Williams, 1989; Hlawatsch & Boudreaux-Bartels, 1992; Cohen, 1966). Quadratic TFRs can produce outstanding frequency resolutions; however, they may face challenges for transient signals with fast time-varying characteristics.

Wavelet transforms (WT) produce a time-scale representation of a signal by scaling and translation of a mother wavelet (Hlawatsch & Boudreaux-Bartels, 1992; Qian, 2002). The resolution of WT is frequency-dependent, i.e., finer frequency resolution for lower analysis frequencies and better time resolution for higher analysis frequencies. WT are effective tools for analysis of signals with discontinuities and spikes. They have been applied extensively for condition monitoring and fault diagnosis (Peng & Chu, 2004; Kunpeng, San, & Soon, 2009). WT have also been used for signal pre-processing to improve performance of other diagnosis models (Paya, Esat, & Badi, 1997; Aminian & Aminian, 2000; Aminian & Aminian, 2001; Wu & Liu, 2009).

A relatively recent TFA method is the S-transform (Stockwell, Mansinha, & Lowe, 1996) that combines features of the STFT and wavelet transforms. ST provides frequency-dependent resolution like WT while maintaining a direct relationship with the linear Fourier spectrum like STFT. The formulation of ST is based on the Fourier transform and uses a time-running window function, which is similar to the STFT (Stockwell et al., 1996); however, the width of the window function in time domain is set to be inversely proportional to the analysis frequency. Therefore, the window is wider at lower frequency regions and narrower at higher frequency regions. As a result, ST has finer frequency localization for lower frequency components and sharp time resolution for high frequency components, which is similar to wavelet transforms. ST is useful for analyzing transient signals of a short duration. Applications of ST can be found in several engineering and biomedical fields (McFadden, Cook, & Forster, 1999; Dash, Panigrahi, & Panda, 2003; Rehorn, Sejdic, & Jiang, 2006; Li et al., 2011).

ST and WT have similar features in that they both can produce sharp time resolutions for signals in high frequency regions. A major difference between WT and ST is that WT is based on dilation and translation of a mother wavelet, but ST retains a direct relation to Fourier transform (Qian, 2002). The WT have been extensively studied in the past few

decades with many variant algorithms developed for both continuous and discrete signals. In comparison, the ST is less visible in the literature on time-frequency analysis and time-scale analysis, but the relative simplicity of ST makes it an attractive alternative to WT for analysis of signals with transients and discontinuities.

Despite its important features, ST has limitations. First, because the window function is narrower in the time domain for higher analysis frequencies, inevitably the frequency localization becomes poorer. Such deteriorated frequency localization may lead to compromised performance, or even erroneous results in practical applications. Second, the amplitude of the noise could be magnified at high frequency regions (Pinnegar & Mansinha, 2003), which can lead to false conclusions when dealing with analysis of noise-corrupted signals.

To improve the performance of ST, different window functions have been investigated to develop modified S-transforms (MST). The use of asymmetrical and non-Gaussian windows for signal decomposition is proposed in (McFadden et al., 1999). In (Pinnegar & Mansinha, 2003b; Pinnegar & Mansinha, 2003a), asymmetrical windows are developed to achieve higher time-resolution in the forward direction to detect the onset of a sudden event, such as an earthquake. To achieve improved energy concentration, a general approach is to modify the width of a standard window by increasing the time domain window width at higher frequencies. In the work of (Djurovic, Sejdic, & Jiang, 2008), a new parameter p is introduced as a power of the analysis frequency. Optimization procedures can be used to obtain the optimal value of p for energy concentration (Sejdic, Djurovic, & Jiang, 2008). In another approach, the width of the standard window is scaled by a constant (Mansinha, Stockwell, Lowe, Eramian, & Schincariol, 1997) or a linear function of frequency (Assous & Boashash, 2012). It has been demonstrated that improved energy concentration can be achieved by these MST algorithms. However, they may not provide the most desirable tradeoff in time-frequency resolutions for multi-modal signals covering different frequency regions. The reason is that widths of the modified window functions still change nearly linearly with respect to the analysis frequency. For signal components in different frequency regions, a width desirable for one component can be problematic for another one; therefore, MST with more flexibility to tune the

window width profile will be a valuable improvement. In addition, it is known that the window function of ST is essentially a band-pass filter of frequency-shifted inputs in the frequency domain. To design an effective MST for specific frequency localization, it would be more straightforward to modify the window directly in the frequency domain.

In a summary, a large variety of signal-based methods have been used to detect undesirable performance changes in industrial systems. Condition monitoring of machines often involves analysis of time-varying signals, where TFA methods are effective tools. The S-transform possesses desirable properties of the classical STFT and wavelet transforms. Further modifications to the S-transform may enhance the performance when dealing with time-varying signals with multiple components.

2.1.3 Pattern Recognition Methods

Pattern recognition has become increasingly important for FDD application (Gottlieb, Arzhanov, Gudowski, & Garis, 2006; Zio & Gola, 2006; Moshkbar-Bakhshayesh & Ghofrani, 2013; Chiang et al., 2004; Widodo & Yang, 2007; Zhu & Song, 2011). Pattern recognition mainly deals with categorization (classification or clustering) of objects into particular groups based on features extracted from related measurement data, so that objects in the same group are similar to one another from certain perspectives (Duda, Hart, & Stork, 2000; Jain, Duin, & Mao, 2000; Murty & Devi, 2011; Webb & Copsey, 2011). In fault diagnosis applications, measurements from a system are analyzed by pattern classification models to test hypotheses for different fault classes. Pattern recognition is very closely related to the fields of artificial intelligence and machine learning (Bishop, 2006; Alpaydin, 2010). In fact, most methods used for FDD applications have been studied in all three fields. Many data-driven methods, such as PCA and KDA, can be used for pattern recognition as well.

If class labels of the groups are unknown, pattern recognition is a clustering problem where the objects are partitioned into clusters or groups whose labels are just the cluster identities. Pattern recognition is more often a pattern classification problem with class labels of the groups as known. Pattern classification methods used for fault diagnosis applications are mostly supervised models where the classifier is trained using labeled

training data and new unlabeled data is then tested on the classifier. However, for cases where labeled training data is scarce, but unlabeled data are abundant, semi-supervised pattern classification can be considered where both labeled data and unlabeled data are integrated to train the classifier.

Clustering divides a set of objects into clusters, so that objects in the same cluster are more similar to each other than to those in another cluster (Jain & Dubes, 1988; Jain, Murty, & Flynn, 1999; Gan, Ma, & Wu, 2007; Webb & Copsey, 2011). Fuzzy c-means (FCM) clustering is one of the most visual algorithms for FDD applications (House, Lee, & Shin, 1999; Teppola, Mujunen, & Minkkinen, 1999; Zio & Baraldi, 2005a; Zio & Baraldi, 2005b; Aydin, Karakose, & Akin, 2008; Liu, Ma, & Mathew, 2009; Pan, Chen, & Li, 2010; Sun, Xue, Du, & Sun, 2010; Baraldi, Razavi-Fara, & Zio, 2011). Spectral clustering is a relatively new algorithm (Shi & Malik, 2000; Ng, Jordan, & Weiss, 2001; Von Luxburg, 2007). Though spectral clustering has not been applied for FDD, it is the basis of a semi-supervised classification model used in this research.

In a supervised pattern classification model, a classifier is first trained using data whose class labels are known. The classifier is then applied to new measurement data to estimate the class labels. Pre-processing is often applied to the raw input data to extract a vector of features. The classifier is actually trained and tested using the features so that unique characteristics of different classes can be better revealed. A great variety of pattern classification methods have been developed such as k-nearest neighbor (k-NN), neural networks, Naive Bayes classifier, hidden Markov model (HMM), SVM, logistic regression, fuzzy logic, decision trees and rules, random forests, and the hybrid and ensemble of different models. Details regarding those models and the training processes can be found in the rich literature on pattern recognition and machine learning (Jain et al., 2000; Bishop, 2006; Murty & Devi, 2011; Webb & Copsey, 2011; Dougherty, 2013; Hsu & Lin, 2002). For a FDD application, the class labels are related to specific fault hypotheses. The classifier is trained offline using training data with known fault classes. When new measurement data become available, their class labels are estimated by the classifier; thus, the current condition of the system is determined from the class label assignment. Applications of pattern classification models to process fault diagnosis have

been extensive and are still growing fast. The growing research interests on this topic are reflected from one review of FDD application of the SVM algorithm alone (Widodo & Yang, 2007).

A supervised pattern classifier only produces credible results for scenarios covered by the training data. In some applications, reliable training data are very scarce due to excessive expenses to label the data or technical difficulties to acquire the data in the first place. However, unlabeled measurement data are easily available. Semi-supervised classification (SSC) models have been developed for such situations. In a SSC model, both labeled data and unlabeled data are utilized for model training. Additional information provided by the unlabeled data (e.g., data distribution and manifold structure) can help to achieve enhanced performance than using the labeled data alone. SSC is generally based on the *clustering assumption* which states that nearby data points likely belong to the same class, as well as the *manifold assumption*, which says that data points on the same manifold structure are likely to be in the same class (Chapelle, Weston, & Schölkopf, 2002; Belkin, Niyogi, & Sindhwani, 2006; Niyogi, 2013). A SSC model can achieve superior performance because the classifier can be designed to avoid cutting through high density regions or manifolds with the availability of unlabeled data. A number of SSC methods have been developed with different ways to realize the assumptions such as transductive SVM, co-training, and various graph-based methods using manifold regulations, graph minicut, harmonic functions, local and global consistency, and spectral graph transducer. More information about the methods can be found in the following research papers and surveys (Blum & Mitchell, 1998; Vapnik, 1998; Joachims, 1999; Blum & Chawla, 2001; Seeger, 2001; Zhu, Ghahramani, & Lafferty, 2003; Zhou, Bousquet, Lal, Weston, & Schölkopf, 2004; Chapelle, Schölkopf, & Zien, 2006; Azran, 2007; Camps-Valls, Marsheva, & Zhou, 2007; Zhu, 2008; Mallapragada, Jin, Jain, & Liu, 2009; Zhu & Goldberg, 2009). Superior performance of SSC has been demonstrated in various numerical studies. However, care has to be taken in excise for specific applications (Singh, Nowak, & Zhu, 2008; Lu, 2009). It has been shown in (Lu, 2009), that it is important to ensure that there exists a truly non-trivial relationship between distribution of the unlabeled data and the class labels. SSC has not been tested for process fault diagnosis applications; however it provides a promising tool

for fault diagnosis applications where acquiring training data under fault conditions is challenging but unlabeled data is readily accessible from the SCADA system. The reason is that correlations often exist in different variables of a process due to their physical and functional couplings. Therefore, data collected under the same fault condition tend to fall in the same high density region or on the same manifold structure.

In summary, pattern recognition envelopes a great number of methods for clustering and classification. Many methods have been used as inference engines to diagnose problems in various engineering fields. In fact, scientific studies on FDD applications have been extensive and are still becoming increasingly more popular. This is particularly the case for supervised pattern classification methods. The performance of a supervised classifier can be affected by scarcity of training data for applications in systems like a NPP. SSC provides an interesting alternative if labeled data is rare, but unlabeled data is easily available.

2.1.4 Data Fusion Methods

Multi-sensor data fusion is another technology that has been used for FDD. The terms information fusion and sensor fusion are treated the same as data fusion herein. The idea is to combine information (or data) from several sources (or sensors) to achieve improved estimation results (e.g., accuracy, coverage, and reliability) than that from a single source (Steinberg, Bowman, & White, 1999; Khaleghi, Khamis, Karray, & Razavi, 2013). Data fusion has been studied at data level, feature level, and decision level for applications such as target tracking, remote sensing, medical image fusion and diagnosis, bioinformatics, machine condition monitoring, condition-based maintenance, and process fault diagnosis. The mathematical tools used for data fusion have diverse origins, such as signal-based methods, probabilities, state estimation models, evidence combination models, fuzzy reasoning models, pattern recognition models, and the hybrid of different models. Some renowned algorithms include ordered weighted averaging and voting, Bayes estimator, D-S evidence theory, Kalman filter and extended Kalman filter (EKF), ANN, fuzzy set theory, ensemble of multiple classifiers, particle filter, rough set theory, and Gaussian mixture model (Khaleghi et al., 2013). The D-S evidence theory (Dempster, 1968; Shafer, 1976; Gordon & Shortliffe, 1984; Yager & Liu, 2008; Sentz &

Ferson, 2002) is probably the most famous algorithm for evidence combination in data fusion.

A survey of fault diagnosis applications of data fusion is summarized in Table 2-2. The acronyms used in Table 2-2 are summarized in the nomenclature. It can be observed that such an application usually includes a feature extraction step, so that the features characterize the faults better than the raw input data. Signal-based methods such as spectral analysis, WT, and statistics are often used for this purpose. Multiple features are used by data fusion algorithms, such as D-S theory, to arrive at a unified decision. Multiple pattern recognition models are often used for one problem. The purpose is that classifiers with different models and/or input-output combinations can characterize different aspects of a problem; thus, a more complete understanding of the system conditions is obtained. Results returned by the multiple classifiers are then combined by algorithms such as D-S theory and majority voting to make the final decision.

Table 2-2 shows that signal processing and pattern classification play very important roles in fault diagnosis applications based on data fusion. D-S theory is a popular data fusion technique for FDD, but its applications are mostly limited to simple systems with only a few sensors because the complexity of a D-S evidence model grows exponentially with respect to the number of fault hypotheses and inputs.

Table 2-2: Fault diagnosis applications of data fusion methods

Reference	Application	Data fusion methods	Test system or inputs
(Cai et al., 2014)	Heat pump fault diagnosis	Combine results of two Bayesian networks utilizing sensor data and human observations	A ground source heat pump with eight faults
(Wang, Tamilselvan, & Hu, 2014)	Engine health diagnostics	Combine several classifiers (SVM, BNN, DBN, SOM, and MD) using weighted majority voting	Aircraft engine and rolling bearing diagnostics
(Batista, Badri, Sabourin, & Thomas, 2013)	Bearing fault diagnosis	Combine several SVM classifier using iterative Boolean combination	Simulated vibration signals
(Luo, Yang, Hu, & Hu, 2012)	Fault diagnosis decision making	D-S theory with modified combination rule	One embedded control system with five faults
(Wallace, West, McArthur, & Towle, 2012)	Nuclear reactor monitoring	Multi-agent system based on rules	Data from an advanced gas cooled reactor
(Ghosh, Ng, & Srinivasan, 2011)	Process fault diagnosis	Combine multiple FDI models (EKF, PCA, SOM, ANN) using voting, Bayes rule, and D-S theory	Simulated Tennessee-Eastman process

Table 2-2: Fault diagnosis applications of data fusion methods (continued)

(Jiang, Fu, & Zhang, 2011)	Structural damage identification	Probabilistic neural network	Simulated steel frame
(Loutas, Roulias, Pauly, & Kostopoulos, 2011)	Rotating machinery monitoring	Integrate feature analysis results of different non-destructive test tools using heuristic rules	Gearbox and motor test rig
(Baraldi, Razavi-Far, & Zio, 2010)	NPP transient identification	Combine multiple FCM classifiers by bagged ensemble	Simulated feedwater system of a NPP
(Liu et al., 2009)	Machinery fault diagnosis	Combine FCM classifiers using fuzzy integral	Rolling element bearing and motor
(Niu et al., 2008)	Induction motor fault diagnosis	Combine four classifiers (SVM, LDA, k-NN, ANN) using Bayesian belief and multi-agent algorithms	Current sensors of seven induction motors
(Salahshoor, Mosallaei, & Bayat, 2008)	Detection and diagnosis of sensor and process faults	Extended Kalman filter	Simulated continuous stirred tank reactor (CSTR)
(Basir & Yuan, 2007)	Engine fault diagnosis	D-S theory with modified mass function	Engine with two faults and three sensors
(Zhang, 2006)	Process fault diagnosis	Combine multiple ANN with averaging, voting, etc.	Simulated CSTR
(Yang & Kim, 2006)	Induction motor fault diagnosis	Combine ANN classifiers using D-S theory	Vibration and current signals of a test rig
(Hu, Cai, Li, & Xu, 2005)	Fault diagnosis	Multi-class SVM classifier	Diesel engine with three faults
(Dong, Yan, Yang, & Judd, 2005)	Transformer fault diagnosis	Combine results of different diagnostic tools using D-S theory and fuzzy reasoning	Two operating transformers
(Goebel, 2001)	Aircraft gas turbine engine fault diagnosis	An eight-layer hierarchical weight manipulation process including modules such as vibration analysis, ANN, and fuzzy expert system	Nine faults in the gas path of an engine
(Parikh, Pont, & Jones, 2001)	Fault diagnosis	Combine multiple classifiers with modified D-S theory	Cooling system of a diesel engine
(Wu, Chen, Wang, & Zhou, 2001)	Mechanical fault diagnosis	Combine multiple indices by Bayesian estimation	Different piston-liner wear conditions of a diesel engine
(Chen, Du, & Qu, 1995)	Large machinery fault diagnosis	Combine several features using rules	50 industrial machines

2.1.5 Model-Based Methods

Model-based methods have been extensively studied for FDD in dynamic systems.

Analytical redundancy (Willsky, 1976; Chow & Willsky, 1984) is the core concept that most model-based methods are based on. In model-based FDD, the normal behaviour of a system is represented by a mathematical model. Sensory measurements are estimated analytically from other correlated measurements using the model. Faults result in

violations of the normal relationships represented in the model, leading to statistically abnormal changes in the model residuals, i.e., differences between the analytical estimations and the actual measurements. Therefore, faults can be detected by testing these residuals statistically (Gertler, 1988; Isermann, 2006; Gertler & Singer, 1990; Li & Shah, 2002; Li & Jiang, 2004; Beard, 1971; Clark, 1978; Frank, 1990; Isermann, 1992; Jia & Jiang, 1995; Isermann, 1993). Among the most studied model-based FDD methods are parity equations (Chow & Willsky, 1984; Lou, Willsky, & Verghese, 1986; Gertler & Singer, 1990; Gertler, 1997), diagnostic observers (Beard, 1971; Clark, 1978; Frank, 1990; Frank & Ding, 1997), Kalman filters (Willsky, 1986; Basseville, 1988), and parameter estimation (Isermann, 1984; Isermann, 1993; Li & Jiang, 2004). Subspace methods are also utilized for model-based FDD applications (Verhaegen & Dewilde, 1992; Van Overschee & De Moor, 1994; Van Overschee & De Moor, 1995; Qin & Li, 2001; Dong, Kulcsar, & Verhaegen, 2009). A major limitation of model-based methods is that accurate system models are required, which can be difficult to obtain for complex systems. As a result, practical applications of model-based methods in real systems are still very limited.

2.2 Sensor Placement Methods

The issue of optimal placement of sensors and actuators have been studied for several system design objectives (Jiang & Doraiswami, 1990; Padula & Kincaid, 1999; Xu & Jiang, 2000; Li, 2011). For a FDD system, it is very important to select the suitable set of sensors so that the data collected from the plant are sensitive to changes caused by the faults and that the sensory data can uniquely distinguish different fault conditions. A sensor placement model usually involves three major steps or components: 1) system model; 2) sensor selection criteria; and 3) optimization. A review of optimal sensor placement methods for FDD systems can be found in (Li, 2011).

The system model describes cause-effect relationships between faults and sensors. It is the basis to derive figure of merits as the sensor placement criteria. Methods that have been used for system modeling include fault trees (Lambert, 1977), directed graph (DG) or digraph (Raghuraj, Bhushan, & Rengaswamy, 1999; Li & Upadhyaya, 2011), signed digraph (SDG) (Bhushan & Rengaswamy, 2000a; Bagajewicz, Fuxman, & Uribe, 2004;

Zhang, 2005; Li, 2011), and bond graph (Narasimhan, Mosterman, & Biswas, 1998). DG is the most popular choice for this purpose. It provides a useful tool to model whether a sensor will respond to a particular fault scenario. In a DG, faults and sensors are the nodes and the edges/arcs register the sensitivities between the faults and sensors (Raghuraj et al., 1999; Li, 2011). A bipartite graph can be built from the DG. The bipartite graph contains a set of nodes with all the faults and a set of nodes with all the sensors. To achieve fault observability, based on the bipartite graph, a minimal subset of the sensor nodes is chosen so that all fault nodes are covered by the selected sensor nodes. It is a minimal set covering problem that can be solved using optimization procedures such as greedy search. The problem of achieving diagnosability of all faults can be converted to a fault observability problem with a more complicated bipartite graph, which is derived from the original bipartite graph by adding additional nodes (Raghuraj et al., 1999; Li, 2011). Each additional node corresponds to a pair of faults, which contains the set of sensors that are sensitive to one fault but not to the second fault. It has shown that performing minimum set covering search on the more complicated bipartite graph is a solution to achieve diagnosability for all faults (Raghuraj et al., 1999; Li, 2011).

As to the sensor selection criteria, three mostly chosen objectives are: 1) fault observability or detectability; 2) fault resolution or diagnosability; and 3) sensor network reliability (Ali & Narasimhan, 1993; Ali & Narasimhan, 1995; Bhushan & Rengaswamy, 2000a; Li, 2011). Fault observability deals with the ability to distinguish fault conditions from normal conditions using data collected from a set of sensors. Fault resolution deals with the ability to distinguish different fault conditions from one another. Sensor network reliability is to make sure that fault diagnosis is still guaranteed considering sensor faults and unavailability of certain sensors. The general objectives of sensor placement models are that all fault conditions can be detected from the sensory data, that all fault conditions can be uniquely discriminated, or that certain minimum level of sensor network reliability is achieved. Additional factors are often also considered in the FOM, such as the number of sensors, sensor cost, and sensor reliability. Various FOMs have been defined in the literature such as minimal networks (Bagajewicz & Sanchez, 1999), maximum diagnosability (Namburu, Azam, Luo, Choi, & Pattipati, 2007), maximum

resolution (Bhushan & Rengaswamy, 2000b), minimum cost (Bagajewicz, 1997; Bagajewicz & Sanchez, 2000), maximum reliability (Ali & Narasimhan, 1993; Ali & Narasimhan, 1995), and model prediction accuracy (Musulin, Benqlilou, Bagajewicz, & Puigjaner, 2005). Those FOMs are often formulated as constrained optimization problems (Bhushan & Rengaswamy, 2000a; Bhushan & Rengaswamy, 2000b; Bhushan & Rengaswamy, 2002; Chmielewski, Palmer, & Manousiouthakis, 2002; Bagajewicz et al., 2004).

The final selection of sensors is usually determined by optimization of the FOMs, using methods such as simulated annealing, Tabu search method, genetic algorithm (Namburu et al., 2007; Casillas, Puig, Garza-Castanon, & Rosich, 2013), greedy search (Raghuraj et al., 1999), particle swarm optimization, and mixed integer programming (Bagajewicz, 1997; Bagajewicz & Sanchez, 2000; Bagajewicz & Cabrera, 2002; Bagajewicz et al., 2004).

However, in a practical situation, a fault diagnosis system is usually to be implemented based on availabilities of existing sensors already installed in a system for process control and monitoring. This situation is different from a standard sensor placement problem. In this case, several issues should be addressed. The first is the need to determine whether all the faults are diagnosable with the existing sensors. If the system is already diagnosable, there is no need to search for additional measurements. It is a less important problem to determine a smaller number of sensors that can achieve diagnosability. When analyses show that the existing sensors are not sufficient to achieve fault diagnosability, additional sensors need to be put in place to enhance fault diagnosability. It is desirable to select a minimum set of additional sensors, where it is advantageous to choose additional sensors with high sensitivities to particular non-diagnosable faults and it is indispensable to be able to quantify the influences of installing a specific sensor to the fault diagnosability. However, to the best knowledge of the author, there is no sensor placement model specifically developed to address those practical issues.

The existing methods have several limitations to use for this purpose. First, binary entries are used to represent sensitivities between two nodes in a DG model; thus, different degrees of sensor sensitivities to a fault are not modeled. A consequence is that, if one sensor can respond to a fault but with relatively low sensitivity, it can separate two faults in theory, but the low sensitivity could be insufficient to reliably distinguish the faults in reality. In addition, to list all the sensors that could possibly consider for a sensor placement problem will result in a graphical model with excessive complexity. What's more, building a graph for a complex system with a potentially large number of faults and sensors requires a lot of engineering judgement and system specific experiences, which could be a challenge for practical applications. Furthermore, it is not intuitive to use a DG to guide selection of the additional sensors. One reason is that a fault propagates in a system due to physical couplings among different variables or system states. The selection of additional sensors would be more straightforward if sensitivities between the faults and system states were known, because the additional sensors can be strategically selected to measure the system states with high sensitivities. However, the sensitivities between faults and the system states are not modeled explicitly in current methods. Another reason is that it is not flexible to add new sensors to or remove sensors from the graphical models to test the influence of a particular sensor for diagnosability of certain faults.

2.3 Instrumentation Systems

In this section, industrial I&C technologies are briefly reviewed. Modern I&C systems are playing increasingly important roles in fault diagnosis. For a fault diagnosis system where installation of additional sensors is required, it is especially desirable to be able to build the required infrastructure cost-effectively.

Traditional I&C systems use analog sensors which are wired to centralized controllers. The analog technologies are still widely used in NPPs. Through additional data management systems such as the plant information system developed by OSIsoft, LLC., data from the analog sensors can be acquired, processed, and stored for fault diagnostic analysis.

Digital I&C systems are becoming increasingly popular in industrial systems. Some advantages of digital I&C systems include lower cost, enhanced communications, more powerful diagnostics, and obsolete resistance. Distributed control systems (DCS) are popular for process control. With a DCS, direct process controls are handled by several local controllers distributed in the system. The local controllers acquire measurement data from the field sensors and send out control signals to the field actuators. In addition, the plant-wide data are communicated through data highways, which can be accessed by upper-level supervisory computers for tasks such as condition monitoring, fault diagnosis, and performance optimization.

Wireless I&C technologies (Gutierrez et al., 2001; Agha et al., 2009; Gungor & Hancke, 2009; Akyildiz, Wang, & Wang, 2005; Akyildiz & Wang, 2005) are becoming more and more popular for industrial condition monitoring applications. A WSN has several advantages over a wired system such as no need to install and maintain cables, easier to deploy, flexible to relocate, and lower in cost. WSN provides an effective way to provide new measurements for health monitoring of important assets in an industrial system. WSNs have in fact been deployed in various industries for condition monitoring of machines, processes, pipes, and structural health (Callaway, 2003; Willig, Matheus, & Wolisz, 2005 ; Kadri et al., 2009; Hashemian, 2011; Hashemian & Bean, 2011; Hashemian, Kiger, Morton, & Shumaker, 2011; Jiang, Chen, Bari, & Hashemian, 2014; Oppermann, Boano, & Römer, 2014). However, many challenges still remain for effective deployment of WSN in NPPs (Gungor & Hancke, 2009; Kadri et al., 2009; Bari & Jiang, 2014; Chen, Jiang, Bari, Hashemian, & Wang, 2014; Li et al., 2014; Wang et al., 2014; Yang, 2014), such as cyber security issues, potential eletromagnetic inteferences with other safety-related I&C systems, and resistance to the raditions.

A WSN usually consists of wireless sensor nodes, router nodes, a base station (sink or gateway), and a server. A sensor node contains a transducer, a processor and memory unit, and a radio transceiver. The transducer measures the physical parameter at the senor location. The measurement data is processed by the processor and transmitted wirelessly through the radio transceiver. The radio transceiver can also be designed to receive data from other devices in the sensor network. Data from all the sensor nodes are collected at

the base station, where the data can be shared with other plant networks through means such as Ethernet. Router nodes are used to relay data from sensor nodes to the base station. A separate server is often used for management of the network such as configuration, programming, and data logging.

Data processing with a WSN can be arranged in a centralized or distributed fashion. With a centralized architecture, all sensor measurements are collected to a central location where analysis of the sensory data and decision makings take place. A centralized system is an effective choice for low data-rate applications. The drawbacks include excessive communications, longer latencies, and waste of in-network computation resources (Tham, 2007). With a distributed architecture, analytic computations such as event detection, filtering, feature extraction, and data compression are distributed to devices in the network. Therefore, some limitations associated with a centralized system can be overcome. It is an attractive option for high data-rate applications such as vibration and acoustics monitoring (Tham, 2007; Allen, 2010). However, configuration of a distributed network is less straightforward than a centralized system.

Digital I&C systems have much more enhanced capabilities than analog sensors. However, the full potentials of digital systems for fault diagnosis have not been fully utilized. For example, self-diagnostics in smart sensors usually are limited to problems within the sensor itself, but faults happening outside the sensor cannot be diagnosed. The communication bandwidth could be a bottleneck for an I&C network. The inherent signal processing capabilities of the devices in the network could be used to address this problem. By communicating the on-board processing results other than the raw data, the bandwidth requirement can be reduced dramatically.

2.4 Applications of FDD in NPP

In this section, some applications of FDD methods in NPPs are reviewed. The surveyed applications are summarized into the following six areas: 1) instrument calibration monitoring; 2) instrument dynamic performance monitoring; 3) equipment condition monitoring; 4) reactor core monitoring; 5) loose part monitoring; and 6) transient

identification. FDD methods typically used for those applications are summarized in Table 2-3.

Table 2-3: Applications of fault diagnosis methods in NPPs

	Data-driven	Signal-based	Pattern recognition	Data fusion
Calibration monitoring	✓			
Dynamic performance monitoring		✓		
Equipment monitoring	✓	✓	✓	✓
Reactor core monitoring		✓		
Loose part monitoring		✓	✓	
Transient identification	✓	✓	✓	✓

Instrument calibration monitoring

The steady state performance of an instrument in a NPP can degrade over time, leading to problems such as drift and bias. To deal with these problems, currently, instruments in NPPs have to be calibrated periodically. This often requires a system shutdown or taking the instruments out of service. However, operational experience shows that less than 5% of the manual calibrations are necessary (Hines & Seibert, 2006). The unnecessary calibrations increase plant outage time, staff workload, and radiation exposure. In addition, the reliability of an instrument may be adversely affected by manual interventions. Furthermore, a fault occurring between two consecutive time-based calibrations may not be detected. It is therefore desirable to monitor steady state performance of instruments during plant operation. This is referred to as calibration monitoring. Calibration monitoring can lead to optimal maintenance, enhanced instrument reliability, reduced operation costs, and less radiation exposure for personnel (James, 1996).

A key component in calibration monitoring is accurate estimation of a sensor's output. Steady state performance of the sensor can be validated by comparing its actual output with the estimation. To this end, two FDD approaches can be implemented: hardware redundancy and analytical redundancy.

In hardware redundancy, redundant physical sensors are used to measure one variable. Outputs from the redundant sensors can serve as references for cross-checking each

other. This is the basic idea of the cross calibration technique (Hashemian, 2006), where the average of a set of redundant sensors is considered to be the true value of a variable being measured. A fault in a sensor can be detected if the sensor shows any abnormal deviation from the average. Limitations of hardware redundancy include the need for extra sensors, and it is difficult to detect faulty sensors that drift in the same direction.

Analytical redundancy estimates the output of a sensor analytically from other correlated measurements in the system. Model-based methods can be used in theory, but this is difficult for NPP systems. Data-driven FDD methods are more practical options. MSET and ANN are the most used methods for calibration monitoring in NPPs. Some additional data-driven methods for this purpose include PCA (Kaistha & Upadhyaya, 2001; Ma & Jiang, 2009), ICA (Ding et al., 2004), nonlinear PLS (Rasmussen, Hines, & Uhrig, 2000; Fantoni, Hoffmann, Rasmussen, & Hines, 2002), and AAKR (Garvey & Hines, 2006) etc. The methods have been demonstrated with success using real NPP data (Herzog et al., 1998; Fantoni, 2005). In (Herzog et al., 1998), using a MSET model, the feedwater flow of a PWR plant can be estimated from 29 correlated measurements with a RMS error of only 0.13% of the flow rate at full power. Uncertainty analysis and verification and validation of data-driven calibration monitoring methods are investigated in several papers (Hines & Rasmussen, 2005; Hines & Davis, 2005; Uhrig & Hines, 2005). Performance optimization of those methods has also been studied (Gribok, Hines, Urmanov, & Uhrig, 2002; Hines & Usynin, 2005). Overall, calibration monitoring in NPPs has been extensively studied with potential benefits recognized. Plant monitoring systems developed based on these calibration monitoring methods have been implemented in a number of plants (Hines & Davis, 2005; Fantoni, 2005; GE, 2014).

Instrument dynamic performance monitoring

Dynamic performance is an important aspect of instruments in NPPs. Sensor response time is very important particularly for safety systems. Response time can be defined as the time it takes for the output of a sensor to reach 67.3% of its final steady-state value following a step-change in the input. The time constant of an instrumentation channel should not exceed the maximum value assumed in the safety analyses. However, the

response time of an instrumentation channel can degrade for various reasons, such as air gap in the thermal-well of a temperature sensor, and blockage in the sensing line of pressure sensors (Hashemian, 2004). Testing the response time of an instrumentation channel often requires taking the measurement system out of service. Unfortunately, off-line tests cannot replicate the exact on-line operating conditions. Furthermore, it is very difficult and expensive to carry out these tests frequently. For a self-powered neutron detector (SPND) used in CANDU reactor shutdown systems, its dynamic performance is influenced by the fraction of prompt signal. The signal of a SPND consists of a prompt component and a series of delayed components (Ma, 2006). Only the prompt signal is able to respond to neutron flux change instantaneously. Therefore, it is a requirement for the prompt fraction to be above a minimum limit so that the detector can respond fast enough to overpower accidents (Glöckler, 2003; Demazière & Glöckler, 2004). The prompt fraction of a SPND changes overtime due to material burn-up and defects. The prompt fraction is conventionally tested by comparing SPND outputs with signals from an ex-core ion chamber during a planned shutdown. This requires extensive preparation, and the test frequency is very limited (Demazière & Glöckler, 2004).

Noise analysis, a signal-based method, provides a mean for dynamic performance monitoring of instrumentation channels during plant operation. On top of the steady-state value, noise-like fluctuations often exist at the outputs of an instrumentation channel. With the assumption that the fluctuations are driven by white noise from the process, a model of the instrumentation channel can be generated from the measurement noises, from which the response time can be estimated (Hashemian, 2006; Hashemian & Jiang, 2010). Degradation of dynamic response can be diagnosed by comparing the recently computed response time with what is considered to be normal. Signal analysis methods in both time and frequency domains can be used to extract response time from the measurement noises. In the time domain, an AR model for the measurement noises can be obtained. The step response of the instrumentation channel can be calculated from the AR model coefficients (Hashemian et al., 1988; Kitamura, 1989). In the frequency domain, PSD of the measurement noises is first obtained from which the time constant can be estimated as the inverse of the break frequency (Hashemian, 2006). Noise analysis has also been studied for on-line determination of prompt fractions of SPNDs in CANDU

reactors. It is based on the understanding that only the prompt signal of a SPND is able to follow the neutron flux fluctuation around 0.25 Hz in the reactor caused by reactor regulating systems (Demazière & Glöckler, 2004).

Noise analysis for instrument response time testing has been studied since the 1980s. Plentiful results have been accumulated from laboratory validations and tests using real NPP measurements. Those tests have confirmed that assumptions made in noise analysis-based response time test schemes can satisfy most of the requirements in NPPs. Noise analysis has already become an important diagnostic tool for pressure and temperature measurements in NPPs. In fact, it is the only effective way to test the response time of pressure measurements during NPP operation (Hashemian & Jiang, 2010). Conventional tests can be carried out when a need is indicated by noise analysis; thus, reliability of an instrumentation channel can be enhanced.

Equipment condition monitoring

Normal operation of a NPP depends on satisfactory operation of many components, such as motors, pumps, valves, and compressors. Operational interruptions of these machines can result in million-dollar losses a day. Taking electric motors as an example, there are over 350 motors used to drive pumps, fans, and compressors in a typical PWR plant. Various faults can occur in a motor such as winding faults, insulation degradation, a broken rotor bar, bearing faults, and inadequate lubrication. These faults can result in motor breakdowns. Out of 147 motor failure-related events returned from a search of the licensee event report system maintained by the U.S. NRC, there were over 25 cases which resulted in a reactor trip or scram; thus, it is highly desirable to detect equipment faults as early as possible before they become inoperable. Fault detection provides a way to ensure equipment reliability in addition to periodic inspections. The principle of using data-driven FDD methods for equipment monitoring is similar to instrument calibration monitoring. Several applications of signal-based methods for equipment monitoring will be discussed next. They are vibration monitoring, motor current signature analysis (MCSA), and acoustic emissions monitoring.

Many machine faults are accompanied with abnormal vibrations (amplitudes and/or frequencies). For example, bearing faults in a reactor coolant pump can lead to high vibration (and bearing temperature) that can cause a reactor trip. Misalignment can also cause increased vibration levels for a motor. Vibration monitoring provides a way to monitor the equipment in a NPP. Spectral analysis of vibration signals is a common technique for vibration monitoring. The spectrum of a vibration signal can be trended and compared with fault-free baseline measurements to detect any developing faults. Features in time domain, such as standard deviation and kurtosis of vibration signals are also frequently used for vibration monitoring (Reimche, Südmeren, Pietsch, Scheer, & Bach, 2003). Vibration monitoring has been used routinely in NPPs. New technologies are being developed for better performance. One approach is to use advanced signal processing methods such as TFA and WT (Tandon & Choudhury, 1999; Peng & Chu, 2004; Park, Lee, Kim, Ryu, & Jung, 2006; Sejdić et al., 2009).

For induction motors, an interesting non-invasive monitoring technique is known as motor current signature analysis. It has been shown that the load of an induction motor is related to the stator current. Various mechanical and electrical faults can cause anomalies in the spectrum of stator current. By analyzing the spectrum of the motor current, MCSA has become an important diagnostic tool for detecting induction motor faults such as broken rotator bar, bearing damage, misalignment, and air gap eccentricity (Benbouzid, 2000; Ye, Wu, & Sadeghian, 2003; Mehala & Dahiya, 2007).

Monitoring of acoustic emissions is also considered for applications in NPPs. It mainly relies on signal-based analysis of changes in spectrum and intensity of acoustic signals emitted from equipment and pressure boundaries of NPPs. Acoustic emissions monitoring has been studied for diagnostic applications such as leakages in pressure boundaries (Hessel, Schmitt, Van der Vorst, & Weiss, 1999; Kunze, 1999), bearing damages (Li & Li, 1995), valve wear (Lee et al., 2006), and faults in rotating machineries (Neill, Reuben, Sandford, Brown1, & Steel, 1997).

Reactor core monitoring

In this section, the application of neutron noise analysis for reactor internal vibration monitoring is briefly discussed. Other reactor core monitoring applications, such as reactor core parameter estimation, are left out. A reactor core consists of internal structures, such as fuel bundles, core support barrel assembly, control rods, and in-core instrumentation guide tubes. It is difficult to measure vibrations of reactor internals directly, but it is still desirable to obtain such information indirectly because excessive vibrations pose risks to their structural integrity. A signal-based technique, known as neutron noise analysis, proved to be successful for this application. Nuclear reactors are equipped with ex-core neutron flux detectors for reactor control and protection. Many reactors such as CANDU also have in-core neutron flux detectors for monitoring the in-core neutron flux distribution (Rouben, 1999). Vibrations of reactor internals induce reactivity perturbations which are registered in the noise signals of the neutron detectors. Therefore, analysis of neutron noise provides an effective way to diagnose abnormal vibrations of reactor internals. Identifications of PWR core support barrel vibration using ex-core neutron detector noises are presented in (Robinson et al., 1977; Yun, Koh, Park, & No, 1988; Park et al., 2003). Features extracted from neutron noise for such identification purposes include PSD, cross PSD, coherrence function, and phase differences between ex-core detectors. Neutron noise analysis has also been studied for vibration monitoring of PWR pressure vessel, flux detector guide tubes (Arzhanov & Pázsit, 2002), fuel bundles (Glöckler, 2003), and control rods (Czibok, Kiss, Kiss, Krinisz, & Végh, 2003). Neutron noise analysis has been extensively studied since the 1960s (Thie, 1981; Kolbasseff & Sunder, 2003). WT and TFA have been considered for advanced neutron noise analysis; for example, (Arzhanov & Pázsit, 2002) presented applications of wavelet based analysis of neutron noises to detect and quantify impacting of instrumentation tubes with nearby nuclear fuel assemblies in boiling water reactor due to excessive tube vibrations.

Loose part monitoring

Loose parts may exist in the reactor coolant system (RCS) of a NPP. A loose part can come from internal structures of the RCS due to corrosion, fatigue, and friction. It can also be introduced externally during refuelling and maintenance tests. A loose part can cause damage to SG tubes, reactor internals, and coolant pumps. Such damage may cost millions of dollars to repair (Michela & Puyala, 1988; Szappanos, Kiss, Por, & Kiss, 1999). Loose parts can also get stuck in the path of control rods, and pose safety hazards. In one case, a 7.7 kg austenite plate used to close the inlet hole of a SG during maintenance fell into the RCS of a VVER plant. In addition to causing damage to the SG, 41 fuel assemblies had to be removed from the core. The repair process also led to an additional collective radiation exposure of 370 person*mSv (Gor, 2005).

Loose part monitoring systems (LPMS) have been developed to detect the onset of a loose part, locate the loose part, and estimate the mass of the loose part. Depending on the nature of the loose part, decisions can be made on what actions should be taken. Detecting and diagnosing a loose part mainly relies on acoustic signals generated by the impact of the loose part with the RCS pressure boundary. The signals are picked up by accelerometers mounted at selected locations on the outer RCS boundary. Configurations of the LPMS for a VVER plant and a PWR plant are presented in (Szappanos et al., 1999) and (Kim, Hwang, Lee, Ham, & Kim, 2000), respectively. Filtering techniques are typically used for pre-processing to remove background noises. Loose part detection relies on comparing the pre-processed acoustic signal with a pre-set threshold. Time delays between sensor pairs that detect the same event provide information to locate the loose part. Identifying the precise location of a loose part is still a challenge for existing LPMSs. Mass estimation of the loose part mostly relies on Hertz impact theory which supports the observation that low frequency signal components increase as the mass of the loose part increases. Therefore, the mass of a loose part can be estimated by referring the frequency characteristics (e.g., frequency ratio and center frequency) of the acoustic signal to the baseline measurements (Olma, 1985; Yoon, Park, Choi, Sohn, & Park, 2006).

Significant amount of experience has been gained in the nuclear industry for loose part monitoring (Persson, 1999; Szappanos et al., 1999; Bechtold & Kunze, 1999). Diagnosis is done by experienced operators in first generation LPMSs. Systems with more autonomous diagnostic capabilities emerged later. Pattern recognition methods are increasingly studied to enhance automatic diagnosis. Currently, every NPP in Germany and the Republic of Korea has a LPMS (Uhrig & Hines, 2005). It is an ongoing research topic to apply advanced signal processing methods such as WT (Pokol & Por, 2006), TFA (Kim, Kim, Chung, Park, & Part, 2003; Park & Lee, 2006; Yoon et al., 2006), and ANN (Figedy & Oksa, 2005) to achieve enhanced LPMS performance, e.g. reduced false alarms, more accurate time of detection, and more accurate mass estimation.

Transient identification

Abnormal transients in a NPP can be initiated by equipment failures or external disturbances. A transient must be correctly identified, as soon as possible, so that proper counteractions can be taken to minimize or mitigate the negative consequences. An automatic transient identification system can be a valuable addition to operator knowledge to safeguard the plant and to minimize the negative impacts.

During a transient period, instrument outputs from a NPP may go through patterns that are different from those under normal conditions. The patterns can be different for different transients, severities, and initial conditions. Therefore, transient identification is essentially a pattern recognition problem, but the complexity of a NPP system makes it a very challenging task. Up to now, ANN is the mostly investigated method for NPP transient identifications (Barlett & Uhrig, 1992), with the ANN trained using simulator data. Different schemes based on ANN are summarized in (Uhrig & Tsoukalas, 1999; Uhrig & Hines, 2005). Performances of several ANN algorithms are compared in (Santosh, Vinod, Saraf, Ghosh, & Kushwaha, 2007). It is important to identify transients not considered in the training stage as unlabeled transients, i.e., ‘don't know’ transients. Research has been done to avoid incorrect identification of unlabeled transients using techniques such as probabilistic neural networks (Bartal, Lin, & Uhrig, 1995; Embrechts & Benedek, 2004). Other pattern recognition methods such as fuzzy logic, expert system,

fuzzy clustering and hidden Markov models (Cheon & Chang, 1993; Uhrig & Tsoukalas, 1999; Zio & Baraldi, 2005a; Kwon, 2002) have also been studied for this purpose. Pre-processing using wavelet signal decomposition has also been studied transient identification (Rovero, 2002). Despite those developments, additional research is required before automated transient identification systems can be successfully used in NPP applications.

2.5 Summary

Fault detection and diagnosis methods are reviewed in this chapter. The methods are categorized as data-driven methods, signal-based methods, pattern recognition methods, data fusion methods, and model-based methods. Principles of different categories of methods are discussed and some algorithms are introduced. Their applications in NPPs have also been reviewed. The survey shows that different types of FDD methods have properties desirable for different types of problems. Since an industrial system usually contains components of great diversities, a FDD system needs to deal with potentially diverse types of fault scenarios. Therefore, proper fault diagnosis tools should be selected from the variety of choices. In addition, it should be noted that different types of FDD methods are often used in a collaborative way to solve a FDD problem, e.g., signal-based methods for feature extraction and pattern recognition methods for diagnostic analysis using the features. Some limitations of existing FDD methods have also been identified through the survey, such as performance validation of nonlinear data-driven methods; difficulties of TFA techniques for analysis of multi-component signals; and performance issue of supervised pattern classification methods with limited labeled training data. Further developments to the FDD methods are desirable to overcome those issues.

The methods for selecting the optimal set of sensors for fault diagnosis are also surveyed. The methods ensure that data collected from the sensors can detect and distinguish all fault conditions. Sensor placement models have been developed to solve the issue of fault observability, fault resolution, and sensor network reliability; however, the system models often lack quantitative fault-sensor incidence matrix. The model structures are

not flexible for reconfigurations to guide the placement of additional sensors if they are required for a fault diagnosis system.

Due to advantages such as low cost and flexibilities to deploy, WSN technologies provide effective ways to enhance the SCADA systems of an existing system for condition monitoring and fault diagnosis. Improvement to a standard WSN is desirable to overcome limitations associated with communication bandwidth, diagnosis latency, and various issues for applications in NPPs.

The survey indicates that the selection of sensors, the selection of data analysis methods, and the I&C infrastructures are all important factors to the effectiveness of a FDD system. Therefore, all those factors should be considered for a FDD system. The issue of optimal placement of sensors is first discussed in the next chapter.

Chapter 3

3 Sensor Placement for Fault Diagnosis

Due to physical and functional couplings in a NPP, the effects of a fault can propagate to different places beyond its originating location. As a result, some similar patterns of system responses can be caused by different faults. Consequently, fault diagnosis often involves sophisticated pattern recognition using information collected from multiple locations (Widodo & Yang, 2007; Ma & Jiang, 2014). It is critical to select a suitable set of sensors so that different fault conditions can be uniquely distinguished using data collected from the sensors. This is essentially an optimal sensor placement problem. Sensor placement models are investigated in this chapter. It fills the purpose of step two in the fault diagnosis framework illustrated in Figure 1-1.

A number of sensor placement models have been developed for fault diagnosis systems as reviewed in Chapter 2. However, an important problem has not yet been considered in previous studies. It is the issue of optimal placement of additional new sensors if certain faults cannot be reliably diagnosed with existing sensors in a system. To solve this problem, a model is required to quantify the influences of installing a specific sensor to fault diagnosability, i.e., “the ability to identify the exact fault that has occurred” (Bhushan and Rengaswamy, 2000). Also desirable, are procedures to keep the number of additional sensors at a minimum. Unfortunately, conventional sensor placement models have difficulties for this purpose due to several limitations as reviewed in Chapter 2.

In this Chapter, a sensor placement scheme is developed to solve issues associated with placement of additional sensors. The model provides a method to model fault-sensor sensitivities for a complex system. It can determine whether a set of faults are diagnosable for a given set of sensors. The model can also quantify the effect of adding any specific sensor to improvement in fault diagnosability. Procedures are also derived to guide optimal placement of additional sensors to achieve enhanced fault diagnosability.

The proposed scheme has several unique features. First, the proposed system model is flexible to reconfigure. The model consists of three layers of faults, system states and

sensors. Sensitivities between faults and system states, and system states and sensors are modeled independently. The effects of adding new sensors or removing sensors can be studied by simply adding or removing one row from the sensor sensitivity matrix without affecting the rest of the model. Second, a complex system is decomposed into several less complicated subsystems. Each subsystem is modeled independently. Couplings between subsystems are conveniently modeled by only considering direct correlations between two adjacent subsystems. Therefore, modeling of a complex system becomes easier. In addition, the fault-sensor incidence matrix is quantitative which is more reliable than a binary incidence matrix. Furthermore, a criterion to quantify fault diagnosability is proposed, which is based on the singularities of a quantitative incidence matrix. The proposed diagnosability criterion is improved over conventional methods because it can handle the situation where some sensor response patterns are dissimilar, but the differences are not sufficient to allow a practical fault diagnosis model to reliably discriminate the faults. Finally, additional sensors can be selected straightforwardly to discriminate non-diagnosable faults with the maximum sensitivities. To enhance diagnosability of two faults, a new sensor is placed to measure a system state that has the maximum difference in sensitivities to the two faults.

The proposed sensor placement scheme is validated using some selected loops of the NPCTF which is a simplified physical NPP simulator. The NPCTF system design is shown in (Jiang, Ma, Bari, and Rankin, 2015) and summarized as Appendix A. The selected loops contain seven process control sensors. As summarized in Appendix B, a FMEA indicates that nine fault scenarios are important to the system. Using the proposed sensor placement scheme, it is determined that three pairs of faults are not diagnosable. Three additional sensors are successfully selected that allow diagnosability of all faults. Experimental data collected from the NPCTF demonstrated that fault diagnosability is indeed enhanced by the additional sensors.

3.1 Problem Statement

Consider a system instrumented by a set of sensors $y = \{y(1), y(2), \dots, y(n_y)\}$, where n_y is the total number of sensors. Suppose a set of faults $f = \{f(1), f(2), \dots, f(n_f)\}$ is

considered for a fault diagnosis system, where nf is the total number of faults. Denote $\Xi(y, f) = \{\Xi_1(y, f(1)), \Xi_2(y, f(2)), \dots, \Xi_n(y, f(nf))\}$ as the sensitivities of the sensors in y to the faults in f , where $\Xi_i(y, f(i))$ represents sensor sensitivities to the fault $f(i)$. Diagnosability of two faults (e.g., $f(i)$ and $f(j)$) means that the sensor sensitivities to the two faults are not identical (i.e., $\Xi_i(y, f(i)) \neq \Xi_j(y, f(j))$). Diagnosability of all faults in f means that

$$\forall (i = 1, 2, \dots, nf, j = 1, 2, \dots, nf, i \neq j), \Xi_i(y, f(i)) \neq \Xi_j(y, f(j)) \quad (3-1)$$

When $\Xi(y, f)$ is represented in the form of a fault-sensor incidence matrix, $\Xi_i(y, f(i))$ is a column of the incidence matrix. Then Eq. (3-1) means that no two columns in the incidence matrix are identical.

Note that, in this thesis, the term sensitivity, as in $\Xi(y, f)$, is used as a measure of the causal relationships between two variables, which is different from the conventional definition as a partial derivative of one variable with respect to another variable.

In conventional sensor placement models, $\Xi(y, f)$ is usually binary, i.e., an entry is 0 if a sensor is not affected by a fault and the entry is 1 if a sensor is affected by a fault. Most sensor placement models for fault diagnosis purposes can be considered as a process to find a minimum subset of the sensors $\tilde{y} \subseteq y$, so that diagnosability is satisfied. It is usually solved as a minimum set covering problem (Raghuraj, et al., 1999; Bhushan and Rengaswamy, 2000; Li, 2011). However, there are three problems to use the traditional solutions to guide placement of sensors in an existing NPP.

The first problem is that, with a binary incidence matrix, if a sensor is affected by a first fault but not by a second fault, the two faults are diagnosable. However, if the actual sensor sensitivity to the first fault is low, it may be problematic for a fault diagnosis model in practice. A desirable improvement is to have quantitative sensitivities, i.e., elements in $\Xi(y, f)$ can take any real value within a range, e.g., $\Xi(y, f) \subseteq [-1 \ 1]$. An element of zero means that a sensor is not sensitive to a particular fault at all. An element

of one (or minus one) means that a sensor is affected by a fault. An element between zero and one (or zero and minus one) means that a sensor can be influenced by a fault but with a low sensitivity represented by the absolute value.

The second problem is that Eq. (3-1) does not quantify the differences between $\Xi_i(y, f(i))$ and $\Xi_j(y, f(j))$. As a result, two faults could be diagnosable in principle according to Eq. (3-1), but the actual differences between the sensitivities may not be sufficient for a practical fault diagnosis model. A quantitative measure of the differences between $\Xi_i(y, f(i))$ and $\Xi_j(y, f(j))$, e.g., $\Lambda(\Xi_i(y, f(i)), \Xi_j(y, f(j)))$, is desirable as a more practical criterion to judge diagnosability of two faults. Such a criterion can be represented as

$$\forall (i = 1, 2, \dots, nf, j = 1, 2, \dots, nf, i \neq j), \Lambda(\Xi_i(\tilde{y}, f(i)), \Xi_j(\tilde{y}, f(j))) > \eta \quad (3-2)$$

where η is a threshold. The value of η is dependent on a specific application.

In case that fault diagnosability is not achieved by existing sensors in a system, additional sensors $\bar{y} = \{y(ny + 1), \dots, y(ny + m)\}$ need to be set up, where m is the number of new sensors. Denote the augmented set of sensors as $\tilde{y} = \{y, \bar{y}\}$ and the corresponding sensor-fault sensitivities as $\Xi(\tilde{y}, f)$. A sensor placement model should find a minimum number of additional sensors that ensures diagnosability of all faults in f , i.e.,

$$\text{minimize } [m] \quad (3-3)$$

subjected to Eq. (3-2)

Eq. (3-3) leads to the third problem of conventional sensor placement models: they are difficult to use for optimal placement of additional sensors in an existing system. This is especially true for a system where the effect of a fault could propagate to components far away from the originating location. The reasons have been discussed in Chapter 2. Basically, a new system model needs to be built with all possible additional sensors included. The model could have excessive complexity and thus become difficult to build. In addition, the selection of additional sensors would be more straightforward if

sensitivities between the faults and system states are known; however, they are not available using current methods. A more desirable system model should be able to model such sensitivities explicitly.

The problems to be solved can be summarized as follows: Given a set of sensors $y = \{y(1), y(2), \dots, y(ny)\}$ and a set of faults $f = \{f(1), f(2), \dots, f(nf)\}$, develop a system model $H(y, f) \mapsto \Xi(y, f) \subseteq [-1 \ 1]$ and a measure $\Lambda(\Xi_i(y, f(i)), \Xi_j(y, f(j)))$ so that diagnosability of a fault diagnosis system can be checked for a given threshold η based on the criterion $\forall (i = 1, 2, \dots, nf, j = 1, 2, \dots, nf, i \neq j), \Lambda(\Xi_i(y, f(i)), \Xi_j(y, f(j))) > \eta$. If the diagnosability criterion is not met, reconfigure the model with a set of additional sensors as $H(\tilde{y}, f) \mapsto \Xi(\tilde{y}, f)$, where $\tilde{y} = \{y(ny+1), \dots, y(ny+m)\}$ are the additional sensors and $\tilde{y} = \{y, \bar{y}\}$, and find a minimum subset of \bar{y} (i.e., minimize $[m]$) so that $\forall (i = 1, 2, \dots, nf, j = 1, 2, \dots, nf, i \neq j), \Lambda(\Xi_i(\tilde{y}, f(i)), \Xi_j(\tilde{y}, f(j))) > \eta$ is true.

A sensor placement method is proposed in this research to solve the above problem. Firstly, a system modeling method is developed which can obtain a quantitative incidence matrix. An important feature of the model is that modeling of a complex system can be decomposed to several less complicated models of subsystems. Another important feature is that the model is based on three layers of 1) faults, 2) system states, and 3) sensors. With such a model, additional sensors, if required, can be strategically placed to measure system states that have the maximum differences in sensitivities to undiagnosable faults. With such as model, placement of additional sensors in an existing system becomes straightforward. In fact, procedures to do so have been laid out in this research. Furthermore, a criterion of diagnosability is defined based on the degree of singularities of an incidence matrix. It is useful for practical fault diagnosis systems because the criterion ensures that all columns in the incidence matrix are sufficiently different for a practical fault diagnosis model to separate the faults.

3.2 System Modeling

This section presents details of the modeling method for a complex system. The model structure is shown in Figure 3-1. Besides the faults and sensors, it has an extra layer of

system states which is denoted as $s = \{s(1), s(2), \dots, s(ns)\}$, where ns is the total number of system states. Sensitivities of the system states to the faults are represented by the fault effect matrix B and sensitivities of the sensors to the system states are represented by the sensor sensitivity matrix C .

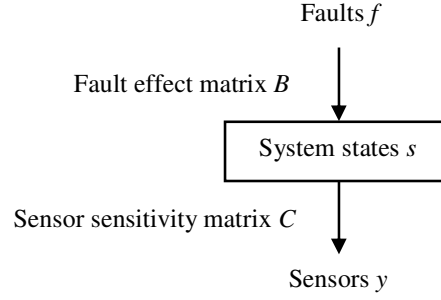


Figure 3-1: Illustration of a system

The sensitivities in the matrices B and C have a range of $[-1 \ 1]$. In the matrix B , an element of zero means that the system state is not sensitive to the particular fault. An element of one (or minus one) means that the system state is affected by a fault. An element between zero and one (or zero and minus one) means that a system state can be influenced by the fault but with a lower sensitivity represented by the absolute value of the entry. Entries in the C matrix can be interpreted similarly.

Even though multiple faults are considered for a system, this research only considers the scenarios that one fault is present at a time. With this assumption, a fault matrix f is defined as $f = I_{nf}$, where I_{nf} is an identity matrix with the dimension of nf . Define a matrix $S_{ns \times nf} \in [-1 \ 1]$ and a matrix $y_{ny \times nf} \subseteq [-1 \ 1]$. The sensitivities can be expressed as

$$S = Bf \quad (3-4)$$

$$y = CS = CBf \quad (3-5)$$

A column in f , e.g., column k , denotes the scenario that fault k has happened. Column k in S represents sensitivities of all system states to fault k . Similarly, each column in y captures sensor sensitivities to fault k . Since f is an identify matrix, it can be obtained that $S = B$, and $y = CB$ is actually the incidence matrix required for diagnosability analysis.

Table 3-1: Illustration of a S matrix

	$f(1)$	$f(2)$	$f(3)$
$s(1)$	1.0	0.1	0.0
$s(2)$	0.0	1.0	1.0
$s(3)$	1.0	1.0	0.8
$s(4)$	0.2	-0.7	-1.0
$s(5)$	0.0	0.0	1.0

Table 3-2: Illustration of a C matrix

		$s(1)$	$s(2)$	$s(3)$	$s(4)$	$s(5)$
y	$y(1)$	1	0	0	0	0
	$y(2)$	0	1	0	0	0
	$y(3)$	0	0	1	0	0
\bar{y}	$y(4)$	0	0	0	0	1

Table 3-3: Illustration of a y matrix

		$f(1)$	$f(2)$	$f(3)$
y	$y(1)$	1.0	0.1	0.0
	$y(2)$	0.0	1.0	1.0
	$y(3)$	1.0	1.0	0.8
\bar{y}	$y(4)$	0.0	0.0	1.0

The structures of the matrices S (i.e., B), C , and y are illustrated in Table 3-1, Table 3-2, and Table 3-3, respectively, using some example sensitivities. An interesting point to note in this example is that, as shown in Table 3-1, the state $s(1)$ is sensitive to $f(2)$ but

only with a low sensitivity of 0.1. As a result, the sensor $y(1)$ is sensitive to $f(2)$ but also with a low sensitivity of 0.1 as shown in Table 3-3. Therefore, the sensor $y(1)$ is able to provide information to distinguish the two faults $f(2)$ and $f(3)$ in theory, but the low sensitivity will make it a challenge for a practical fault diagnosis model. The additional sensor $y(4)$ is sensitive to the states $s(5)$ as shown in Table 3-2. It provides the additional dimension of information to distinguish $f(2)$ and $f(3)$ as shown in Table 3-3. A sensor sensitive to the state $s(4)$ is not a desirable choice because it will be affected by both $f(2)$ and $f(3)$ in similar ways, as can be seen from Table 3-1.

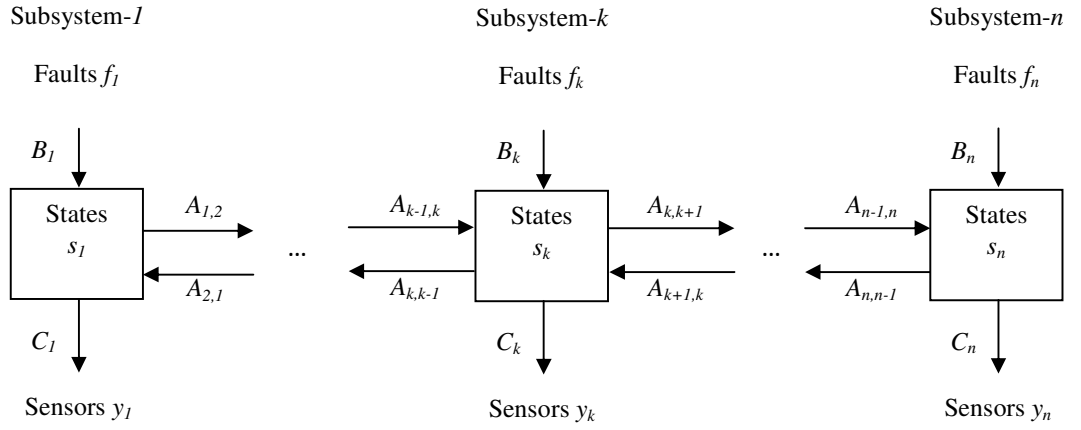


Figure 3-2: System model of a complex system

The sensor sensitivity matrix C is relatively less difficult to obtain because the sensitivity of a sensor to a given system state is usually straightforward. However, for a complex system with potentially a large number of faults and system states, sensitivities between system states and the faults are not obvious at all, especially when the states and faults are located in different parts of the systems, but they are coupled through fault propagations. Therefore, it could be very challenging to obtain the complete fault matrix B for a complex system. To solve this issue, a complex system is decomposed to several coupled subsystems (e.g., n) in the proposed model. Sensitivities between the states and

faults within a subsystem will be easier to model because the number of states and faults to consider is much smaller and relationships between the states and faults are more explicit. Each subsystem can be modeled as Figure 3-1, but couplings between neighboring subsystems are modeled. The complete model can be represented as Figure 3-2, where couplings between two subsystems are represented by the state propagation matrices A . $A_{i,j}$ represents the effects of state changes in S_i of subsystem i on the states S_j of subsystem j . Since a state change can potentially affect both the upstream and the downstream systems, both forward and backward state propagation matrices are defined. Take two subsystems k and $k+1$ for example, $A_{k,k+1}$ represents the effects of forward state propagation from subsystem k to subsystem $k+1$, and $A_{k+1,k}$ represents backward state propagation from subsystem $k+1$ to subsystem k . Suppose the number of states in S_k and S_{k+1} are ns_k and ns_{k+1} , respectively, then the matrix $A_{k,k+1}$ will have a dimension of $ns_{k+1} \times ns_k$. Entries in A are real and fall in the range of $[-1 \ 1]$, representing sensitivity between two states. With a system model structure represented as Figure 3-2, the effects of fault propagation in a complex system can be divided into several easier tasks of modeling couplings between two subsystems. In Figure 3-2, f_k refers to faults happening in the subsystem k and s_k refers to sensors in the subsystem k . Note that only a system with serial subsystems is considered in this model.

Table 3-4: Complete S matrix for a system with subsystems

	f_1	\dots	f_k	\dots	f_n
s_1	S_1^1	\dots	S_1^k	\dots	S_1^n
\dots	\dots	\dots	\dots	\dots	\dots
s_k	S_k^1	\dots	S_k^k	\dots	S_k^n
\dots	\dots	\dots	\dots	\dots	\dots
s_n	S_n^1	\dots	S_n^k	\dots	S_n^n

With a system represented as coupled subsystems as shown in Figure 3-2, the complete S matrix will consists of blocks corresponding to the subsystems as shown in Table 3-4, where S_k^l contains sensitivities of all system states of subsystem k to all faults originated

in the subsystem l . Interpretation of entries in S_k^l is similar to those illustrated in Table 3-1.

Within a subsystem, relationships between faults f_k and the states S_k is shown as

$$S_k^k = B_k f_k \quad (3-6)$$

For convenience, the dimension of f_k is denoted as nf_k ; thus, B_k and S_k^k both have a dimension of $ns_k \times nf_k$. In S_k^k , each column models sensitivities of the states of subsystem k to a fault contained in f_k .

The effects of faults in a subsystem can also propagate to other subsystems, leading to sensitivities states and faults in different subsystems. To take S_k^l for example, f_l (faults in subsystem l) affects the states s_k directly as $S_k^l = B_l f_l$. Denote the overall coupling between subsystem l and subsystem k as $A_{l,k}$. Then S_k^l can be represented as

$$S_k^l = A_{l,k} B_l f_l \quad (3-7)$$

Considering Eq. (3-7), Table 3-4 can now be shown as Table 3-5.

Table 3-5: Complete S matrix for a system with subsystems

	f_1	\dots	f_k	\dots	f_n
s_1	$B_1 f_1$	\dots	$A_{k,1} B_k f_k$	\dots	$A_{n,1} B_n f_n$
\dots	\dots	\dots	\dots	\dots	\dots
s_k	$A_{1,k} B_1 f_1$	\dots	$B_k f_k$	\dots	$A_{n,k} B_n f_n$
\dots	\dots	\dots	\dots	\dots	\dots
s_n	$A_{1,n} B_1 f_1$	\dots	$A_{k,n} B_k f_k$	\dots	$B_n f_n$

Define a row in Table 3-5 as S_k , i.e., $S_k = [A_{1,k} B_1 f_1 \quad \dots \quad B_k f_k \quad \dots \quad A_{n,k} B_n f_n]$.

Sensitivities of sensors in subsystem k to all faults in the system can be computed as

$$y_k = C_k S_k = C_k [A_{1,k} B_1 f_1 \quad \dots \quad B_k f_k \quad \dots \quad A_{n,k} B_n f_n] \quad (3-8)$$

where C_k has a dimension of $ny_k \times ns_k$, with ny_k being the number of sensors in subsystem k . y_k in Eq. (3-8) will have a dimension of $ny_k \times nf$. A column in y_k captures sensitivities of sensors in subsystem k to a particular fault in the system. Eq. (3-8) can be written in another form as

$$\begin{aligned} y_k &= C_k \times [A_{1,k} \quad A_{2,k} \quad \dots \quad A_{k-1,k} \quad I_{ns_k} \quad A_{k+1,k} \quad \dots \quad A_{n,k}] \times \\ &\begin{bmatrix} B_1 & & & & & & & \\ & B_2 & & & & & & \\ & & \dots & & & & & \\ & & & B_{k-1} & & & & \\ & & & & B_k & & & \\ & & & & & B_{k+1} & & \\ & & & & & & B_n & \\ O & & & & & & & \end{bmatrix} \times \begin{bmatrix} f_1 & & & & & & & \\ & f_2 & & & & & & \\ & & \dots & & & & & \\ & & & f_{k-1} & & & & \\ & & & & f_k & & & \\ & & & & & f_{k+1} & & \\ & & & & & & f_{k+1} & \\ & & & & & & & f_n \end{bmatrix} \quad (3-9) \\ &= C_k \times [A_{1,k} \quad A_{2,k} \quad \dots \quad A_{k-1,k} \quad I_{ns_k} \quad A_{k+1,k} \quad \dots \quad A_{n,k}] \times B \times f \end{aligned}$$

where I_{ns_k} is an identity matrix with the dimension ns_k . The matrix f , contains system-wide faults, is defined as

$$f = \begin{bmatrix} f_1 & & & & & & & \\ & f_2 & & & & & & \\ & & \dots & & & & & \\ & & & f_{k-1} & & & & \\ & & & & f_k & & & \\ & & & & & f_{k+1} & & \\ O & & & & & & \dots & \\ & & & & & & & f_n \end{bmatrix} \quad (3-10)$$

Note that the matrix f is in fact an identity matrix I_{nf} with a dimension of nf . The matrix B in Eq. (3-9) is defined as

$$B = \begin{bmatrix} B_1 & & & & & \\ & B_2 & & & & \\ & & B_3 & & O & \\ & & & \dots & & \\ & & & & B_k & \\ & O & & & & \dots \\ & & & & & B_{n-1} \\ & & & & & & B_n \end{bmatrix}_{ns \times nf} \quad (3-11)$$

where ns is the total number of states system wide.

Eq. (3-9) can be created for all subsystems. Putting the results together leads to

$$\begin{bmatrix} y_1 \\ y_2 \\ y_3 \\ \dots \\ y_k \\ \dots \\ y_{n-1} \\ y_n \end{bmatrix} = C \times \begin{bmatrix} I_{ns_1} & A_{2,1} & A_{3,1} & \dots & \dots & \dots & A_{n-1,1} & A_{n,1} \\ A_{1,2} & I_{ns_2} & A_{3,2} & \dots & \dots & \dots & A_{n-1,2} & A_{n,2} \\ A_{1,3} & A_{2,3} & I_{ns_3} & \dots & \dots & \dots & A_{n-1,3} & A_{n,3} \\ \dots & \dots & \dots & \dots & \dots & \dots & \dots & \dots \\ A_{1,k} & A_{2,k} & A_{3,k} & \dots & I_{ns_k} & \dots & A_{n-1,k} & A_{n,k} \\ \dots & \dots & \dots & \dots & \dots & \dots & \dots & \dots \\ A_{1,n-1} & A_{2,n-1} & A_{3,n-1} & \dots & \dots & \dots & I_{ns_{n-1}} & A_{n,n-1} \\ A_{1,n} & A_{2,n} & A_{3,n} & \dots & \dots & \dots & A_{n-1,n} & I_{ns_n} \end{bmatrix} \times B \times f \quad (3-12)$$

where the matrix C is defined as

$$C = \begin{bmatrix} C_1 & & & & & \\ & C_2 & & & & \\ & & C_3 & & O & \\ & & & \dots & & \\ & & & & C_k & \\ & O & & & & \dots \\ & & & & & C_{n-1} \\ & & & & & & C_n \end{bmatrix}_{ny \times ns} \quad (3-13)$$

with ny being the total number of system wide sensors.

Eq. (3-12) models sensitivities between system wide sensors and faults. For simplicity, Eq. (3-12) can be written in a compact form as

$$y = C \times \Phi \times B \times f \quad (3-14)$$

where $y_{nyxf} = [y_1 \ y_2 \ \dots \ y_n]^T$ collects sensitivities of all sensors to all faults. And the matrix Φ is defined as

$$\Phi = \begin{bmatrix} I_{ns_1} & A_{2,1} & A_{2,1} & \dots & \dots & \dots & A_{n-1,1} & A_{n,1} \\ A_{1,2} & I_{ns_2} & A_{3,2} & \dots & \dots & \dots & A_{n-1,2} & A_{n,2} \\ A_{1,3} & A_{2,3} & I_{ns_3} & \dots & \dots & \dots & A_{n-1,3} & A_{n,3} \\ \dots & \dots & \dots & \dots & \dots & \dots & \dots & \dots \\ A_{1,k} & A_{2,k} & A_{3,k} & \dots & I_{ns_k} & \dots & A_{n-1,k} & A_{n,k} \\ \dots & \dots & \dots & \dots & \dots & \dots & \dots & \dots \\ A_{1,n-1} & A_{2,n-1} & A_{3,n-1} & \dots & \dots & \dots & I_{ns_{n-1}} & A_{n,n-1} \\ A_{1,n} & A_{2,n} & A_{3,n} & \dots & \dots & \dots & A_{n-1,n} & I_{ns_n} \end{bmatrix}_{ns \times ns} \quad (3-15)$$

Φ will be denoted as the total state propagation matrix (TSPM) herein. It has a dimension of $ns \times ns$.

Define $\Xi = C \times \Phi \times B = [\Xi_1 \ \Xi_2 \ \dots \ \Xi_{nf}]$ as the fault-sensor incidence matrix. The rows of Ξ correspond to the system wide sensors and the columns correspond to the system wide faults. Ξ_i is the column i of Ξ , which captures sensitivities of all sensors y to the fault corresponding to the column i in the matrix f (i.e., $f(i)$). The procedures to analyze fault diagnosability based on the incidence matrix will be discussed in the next Section.

To compute the incidence matrix, one need to acquire the matrices B , C , and Φ . By decomposing a complex system into subsystems, it becomes easier to model each subsystem, thus the blocks in the B and C matrices. As discussed previously, couplings between any two subsystems (i.e., $A_{k,l}$ and Φ) is far from obvious, but direct coupling between two neighboring subsystems (e.g., $A_{k-1,k}$ and $A_{k+1,k}$) is easier to model.

Fortunately, the propagation process can be modeled using a cascade chain of direct

couplings. For example, state propagations from an upstream subsystem to a downstream subsystem can be represented as

$$A_{i,j(j \leq i-2)} = A_{j+1,j} \times \dots \times A_{i-1,i-2} \times A_{i,i-1} \quad (3-16)$$

Taking advantages of Eq. (3-16), it can be seen that

$$\begin{bmatrix} 0 & 0 & A_{3,1} & & & \\ & 0 & 0 & A_{4,2} & & O \\ & & 0 & 0 & \dots & \\ & & & \dots & \dots & \dots \\ & & & & 0 & 0 & \dots \\ & O & & & \dots & \dots & A_{n,n-2} \\ & & & & & 0 & 0 \\ & & & & & & 0 \end{bmatrix} = \begin{bmatrix} 0 & A_{2,1} & & & & \\ & 0 & A_{3,2} & & & O \\ & & 0 & A_{4,3} & & \\ & & & \dots & \dots & \\ & & & & 0 & A_{k+1,k} \\ & O & & & \dots & \dots & 0 & A_{n,n-1} \\ & & & & & & 0 \end{bmatrix}^2 \quad (3-17)$$

The process can be further extended to higher powers and eventually

$$\begin{bmatrix} 0 & 0 & & & & A_{n,1} \\ & 0 & 0 & & & O \\ & & 0 & 0 & & \\ & & & \dots & \dots & \\ & & & & 0 & 0 \\ & O & & & \dots & \dots & 0 & 0 \\ & & & & & & 0 \end{bmatrix} = \begin{bmatrix} 0 & A_{2,1} & & & & \\ & 0 & A_{3,2} & & & O \\ & & 0 & A_{4,3} & & \\ & & & \dots & \dots & \\ & & & & 0 & A_{k+1,k} \\ & O & & & \dots & \dots & 0 & A_{n,n-1} \\ & & & & & & 0 \end{bmatrix}^{n-1} \quad (3-18)$$

Define a backward state propagation matrix (BSPM) as

$$\Phi_b = \begin{bmatrix} 0 & A_{2,1} & & & & & & \\ & 0 & A_{3,2} & & & & O & \\ & & 0 & \dots & & & & \\ \dots & & & \dots & A_{k+1,k} & & & \\ & & & & 0 & \dots & & \\ \dots & & & & & \dots & A_{n-1,n-2} & \\ & O & & & & & 0 & A_{n,n-1} \\ & & & & & & & 0 \end{bmatrix} \quad (3-19)$$

It can be obtained that

$$\begin{bmatrix} 0 & A_{2,1} & A_{3,1} & \dots & \dots & A_{n-2,1} & A_{n-1,1} & A_{n,1} \\ & 0 & A_{3,2} & A_{4,2} & \dots & \dots & A_{n-1,2} & A_{n,2} \\ & & 0 & A_{4,3} & \dots & \dots & \dots & A_{n,3} \\ & & & \dots & \dots & \dots & \dots & \dots \\ & & & & 0 & \dots & \dots & \dots \\ & & & & & \dots & \dots & A_{n,n-2} \\ O & & & & & & 0 & A_{n,n-1} \\ & & & & & & & 0 \end{bmatrix} = \sum_{j,j=2,\dots,n-1} \Phi_b^j \quad (3-20)$$

Similarly, define a forward state propagation matrix (FSPM) Φ_f as

$$\Phi_f = \begin{bmatrix} 0 & & & & & & & \\ A_{1,2} & 0 & & & & & & O \\ & A_{2,3} & 0 & & & & & \\ & & \dots & \dots & & & & \\ & & & A_{k-1,k} & 0 & & & \\ & & & & \dots & \dots & & \\ & O & & & & A_{n-2,n-1} & 0 & \\ & & & & & & A_{n-1,n} & 0 \end{bmatrix} \quad (3-21)$$

It can be obtained similarly that

$$\begin{bmatrix} 0 & & & & & & & \\ A_{1,2} & 0 & & & & & & O \\ A_{1,3} & A_{2,3} & 0 & & & & & \\ A_{1,4} & A_{2,4} & A_{3,4} & \dots & & & & \\ \dots & \dots & \dots & \dots & \dots & & & \\ \dots & \dots & \dots & \dots & \dots & \dots & & \\ A_{1,n-1} & \dots & \dots & \dots & \dots & A_{n-2,n-1} & 0 & \\ A_{1,n} & A_{2,n} & \dots & \dots & \dots & A_{n-2,n} & A_{n-1,n} & 0 \end{bmatrix} = \sum_{j=2,\dots,n-1} \Phi_f^j \quad (3-22)$$

The total state propagation matrix can then be written as

$$\Phi = \sum_{j=2,\dots,n-1} \Phi_b^j + I_{ns} + \sum_{j=2,\dots,n-1} \Phi_f^j = \Phi_b (I_{ns} - \Phi_b)^{-1} + I_{ns} + \Phi_f (I_{ns} - \Phi_f)^{-1} \quad (3-23)$$

It can be seen from Eq. (3-19) and Eq. (3-21) that the BSPM and FSPM only involve couplings between two adjacent subsystems, which are relatively easy to model. It can also be seen from Eq. (3-23) that the TSPM can be directly obtained from the BSPM and FSPM. Therefore, the potential difficulties of modeling a complex system at once can be eased.

Sensitivities used in the matrices of Eq. (3-11, 3-13, 3-19, and 3-21) can be determined from mathematical modeling of the involved system dynamics. Using experiences in the system dynamics is another way to obtain the sensitivities. It may be less accurate than a rigorous model, but still retains the quantitative nature and is improved over a simple binary choice. Note that the proposed model has not considered influences of system controls.

3.3 Fault Diagnosability Criterion

For all faults to be diagnosable, it is required that no pairs of columns in the incidence matrix Ξ should be the same or very similar so that sensor response patterns to different faults are distinct. To quantify similarities between two columns in Ξ , it is proposed to use the ratio between the two singular values of a matrix consisting of the two columns. The more similar the two columns are to each other, the smaller the second singular value will be, as compared to the first singular value; thus a larger ratio. A higher ratio

means reduced diagnosability for the two faults corresponding to the two columns. In situations where two columns in the incidence matrix are linearly dependent, which occurs when the sensors produce the same respond patterns for the two different faults, then the faults are not diagnosable. In this case, one of the singular values will be zero and the ratio between the two singular values will be infinite.

Checking the singular value ratios of pair-wise column combinations of Ξ provides a way to quantify fault diagnosability. For example for two columns Ξ_i and Ξ_j corresponding to faults $f(i)$ and $f(j)$, a sub-incidence matrix (SIM) can be built as

$$SIM = [\Xi_i \quad \Xi_j] \quad (3-24)$$

Suppose the two singular values of Eq. (3-24) are λ_1 and λ_2 with $\lambda_1 > \lambda_2$, which can be obtained by applying singular value decomposition to the SIM. A fault diagnosability criterion is defined as

$$r_{i,j} = \frac{\lambda_1}{\lambda_2} \leq \eta \quad (3-25)$$

where η is a threshold. If Eq. (3-25) is satisfied, then fault $f(i)$ and $f(j)$ are considered diagnosable. For all the faults to be diagnosable, it is required that the ratios $r_{i,j}$ for all two-column combinations satisfy Eq. (3-25), i.e.,

$$\forall (i = 1, \dots, nf - 1, j = i + 1, \dots, nf), \frac{\lambda_1}{\lambda_2} \Big| [\xi_i, \xi_j] \leq \eta \quad (3-26)$$

Define a $nf \times nf$ fault diagnosability matrix R as

$$R(i, j) = \begin{cases} r_{i,j}, & i = 1, \dots, nf - 1, j = i + 1, \dots, nf \\ 0, & otherwise \end{cases} \quad (3-27)$$

Then the fault diagnosability criterion is that all elements in the matrix R are not larger than a threshold η . In this research, a value of $\eta = 5$ is selected based on experimental data acquired from a physical process.

3.4 Sensor Placement for Diagnosability

This section presents procedures to select a set of additional sensors to ensure diagnosability of all faults if existing process control sensors are not sufficient. In this thesis, the objective is to find the minimum number of additional sensors. The proposed method selects the minimal number of sensors in such a way that they provide the required information. Other related factors, such as cost, or difficulty in installation, etc are not considered. However, the proposed method can potentially be extended to include them.

Define a total fault effect matrix Γ as

$$\Gamma = \Phi \times B \quad (3-28)$$

where Φ and B have been defined in Eq. (3-23) and Eq. (3-11), respectively. Γ models the overall effects of faults on all system states. The rows in Γ are the system states and the columns are the faults.

In order to distinguish two non-diagnosable faults, an additional sensor should be strategically placed to measure a system state with the maximum difference in sensitivities to the two faults. This way, data collected from the additional sensor has the maximum differences in response patterns to the two faults. According to this principle, procedures to place additional sensors to enhance fault diagnosability are proposed as follows:

- 1) Identify a pair of faults not distinguishable according to the fault diagnosability matrix R .
- 2) Find the two columns in Γ corresponding to the faults identified in step 1.
- 3) Subtract the first column from the second column and save the differences as a new column vector.

- 4) Find the maximum absolute value in the vector obtained in step 3 and save the system state corresponding to the row number.
- 5) Select a sensor sensitive to the system state identified in step 4.
- 6) Augment the sensor sensitivity matrix C by an additional row for the new sensor as $C_a = \begin{bmatrix} C \\ c_a \end{bmatrix}$, where c_a is the new row and C_a is the augmented C matrix.
- 7) Update the incidence matrix as $\Xi = C_a \times \Gamma$.
- 8) Update the fault diagnosability matrix R with the new incidence matrix Ξ .
- 9) Repeat steps 1-8 until all faults are diagnosable.
- 10) Eliminate the first additional sensor and update C_a .
- 11) Update the incidence matrix Ξ with the updated C_a in step 10.
- 12) Update the fault diagnosability matrix R .
- 13) Determine fault diagnosability based on the updated R in step 12.
- 14) If all faults are still diagnosable in step 13, confirm deletion of the sensor in step 10.
- 15) If fault diagnosability cannot be satisfied in step 13, restore the deleted sensor in step 10.
- 16) Move to the next additional sensor, and repeat step 11 to 16.

Step 1-9 ensures that all faults are diagnosable with additional sensors. To keep the number of additional sensors at minimal, steps 10-16 can be carried out to eliminate sensors that are added at different stages, but are redundant.

3.5 Experimental Validations

In this section, the modeling concept is first illustrated using an example fluid heating process as shown in Figure 3-3. In the process, working fluid is pumped through a heater, where the fluid temperature is increased. Pressure of the process is maintained by a pressurizer tank that is partially filled with gas. It is assumed that two faults can happen in the system, i.e., heater overpower, denoted as $f(1)$, and spurious opening of the valve CV-1, denoted as $f(2)$. Five system states are considered for the process, including 1)

heater power $s(1)$, 2) fluid flow rate $s(2)$, 3) heater outlet temperature $s(3)$, 4) process pressure $s(4)$, and 5) pressurizer tank level $s(5)$. Furthermore, it is assumed that the process is instrumented with three sensors, i.e., flow sensor F1, denoted as $y(1)$, 2) temperature sensor T1, denoted as $y(2)$, and 3) pressure sensor P1, denoted as $y(3)$. Locations of the three sensors are shown in Figure 3-3.

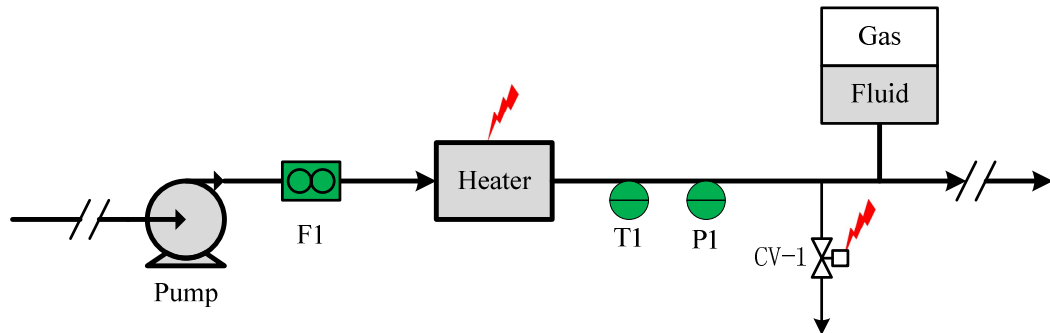


Figure 3-3: An example process to illustrate system modeling

A system model of the process in Figure 3-3 is approximated as

$$f = \begin{bmatrix} 1 & 0 \\ 0 & 1 \end{bmatrix} \quad (3-29)$$

$$B = \begin{bmatrix} 1.0 & 0.0 \\ 0.0 & 0.3 \\ 1.0 & 0.7 \\ 0.1 & -1.0 \\ 0.1 & -1.0 \end{bmatrix} \quad (3-30)$$

$$C = \begin{bmatrix} 0 & 1 & 0 & 0 & 0 \\ 0 & 0 & 1 & 0 & 0 \\ 0 & 0 & 0 & 1 & 0 \end{bmatrix} \quad (3-31)$$

The meaning of the matrix B and C is illustrated using Table 3-6 and Table 3-7, respectively. $B_{1,1}=1$ means that state $S(1; \text{heater power})$ is sensitive to the occurrence of fault $f(1; \text{heater overpower})$, which is straightforward. $B_{1,4} = 0.1$ means that state $S(4; \text{pressure})$ is also affected by $f(1)$, but the influence is less significant. Physically, fault $f(1)$ leads to swell of the working fluid. Therefore, the process pressure will increase. However, the increase is limited because gas in the pressurizer tank is compressible. For a larger air chamber, the sensitivity $B_{1,4}$ will be smaller. $B_{2,4} = -1$ means that fault $f(2; \text{CV-1 open})$ affects state $S(4)$ with high sensitivity, but in the negative direction. Other entries in B can be interpreted similarly. The values in Table 3-6 are illustrative in nature. The best values for a real system depend on actual system parameters. As to the C matrix in Table 3-7, an entry of one means that the sensor is sensitive to the corresponding system state, and a zero means that the sensor is not affected by changes in the state.

Table 3-6: B matrix for the example process

	$f(1; \text{heater overpower})$	$f(2; \text{CV-1 open})$
$s(1; \text{power})$	1.0	0.0
$s(2; \text{flow})$	0.0	0.3
$s(3; \text{temperature})$	1.0	0.7
$s(4; \text{pressure})$	0.1	-1.0
$s(5; \text{level})$	0.1	-1.0

Table 3-7: C matrix for the example process

	$S(1) \text{ (power)}$	$S(2) \text{ (flow)}$	$S(3) \text{ (temperature)}$	$S(4) \text{ (pressure)}$	$S(5; \text{level})$
$y(1; \text{F1})$	0	1	0	0	0
$y(2) \text{ (T1)}$	0	0	1	0	0
$y(3) \text{ (P1)}$	0	0	0	1	0

It can be obtained from Eq. (3-29) to Eq. (3-31) that

$$S = Bf = \begin{bmatrix} 1.0 & 0.0 \\ 0.0 & 0.3 \\ 1.0 & 0.7 \\ 0.1 & -1.0 \\ 0.1 & -1.0 \end{bmatrix} \begin{bmatrix} 1 & 0 \\ 0 & 1 \end{bmatrix} = \begin{bmatrix} 1.0 & 0.0 \\ 0.0 & 0.3 \\ 1.0 & 0.7 \\ 0.1 & -1.0 \\ 0.1 & -1.0 \end{bmatrix} \quad (3-32)$$

$$y = CS \begin{bmatrix} 0 & 1 & 0 & 0 & 0 \\ 0 & 0 & 1 & 0 & 0 \\ 0 & 0 & 0 & 1 & 0 \end{bmatrix} \begin{bmatrix} 1.0 & 0.0 \\ 0.0 & 0.3 \\ 1.0 & 0.7 \\ 0.1 & -1.0 \\ 0.1 & -1.0 \end{bmatrix} = \begin{bmatrix} 0.0 & 0.3 \\ 1 & 0.7 \\ 0.1 & -1.0 \end{bmatrix} \quad (3-33)$$

The first column of y in Eq. (3-33) indicates that only the temperature sensor $y(2)$ has high sensitivity to heater overpower fault $f(1)$. The pressure sensor $y(3)$ is also affected by $f(1)$, but the sensitivity (0.1) is insignificant. Loss of working fluid caused by $f(2)$ influences readings of all three sensors as indicated by the second column of y , i.e., the fault causes slight increase (0.3) in fluid flow rate, considerable increase (0.7) in heater outlet temperature, and dramatic decrease (-1) in system pressure.

The proposed sensor placement model is further validated using selected loops of the NPCTF. A diagram illustrating the selected loops is shown in Figure 3-4. Functions of the selected loops are similar to the primary heat transport system (PHTS) of a NPP. Pump-1 drives water flow in a closed loop. The heater raises the water temperature like a reactor. The water is cooled down in the heat exchanger (HX) by chilled water. The system pressure is maintained by the pressurizer by feeding in compressed air or bleeding air out. Seven sensors for process control are shown in the diagram with solid filling with green color. They are flow sensors F1 and F3, pressure sensors P1 and P4, temperature sensors T1 and T2, and level sensor L3. Some other measurements that can be deployed in the system are also shown but with partial filling. They are Po-12 (CV-12 position), Cu1 (pump-1 current), Po-1 (CV-1 position), Cu2 (heater current), and V2 (chiller pump vibration). The system is decomposed into four subsystems. They are the water cooling subsystem, pressurizer subsystem, water flow subsystem, and water heating subsystem, which will be denoted as subsystem one, two, three and four, respectively. Through a FMEA as summarized in Appendix B, a total of nine faults are identified as critical to the selected NPCTF loops. Components, faults, system states, and sensors of the four subsystems are summarized in Table 3-8. Numberings of the faults, system states, and sensors are also shown in Table 3-8. The system model structure is summarized in Figure 3-5.

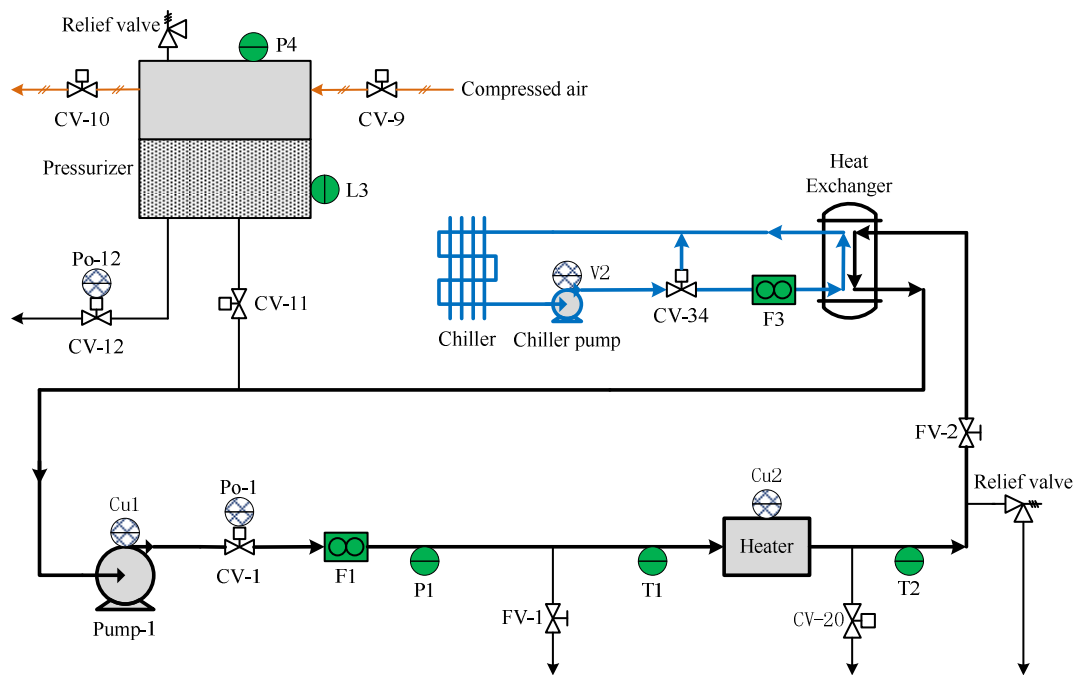


Figure 3-4: Diagram of selected NPCTF loops

Table 3-8: Summary of NPCTF subsystems

Subsystems	Components	Faults	System states	Sensors
Water cooling	Chiller Chiller pump CV-34 HX	$f(1)$: CV-34 spurious close $f(2)$: Chiller pump trip	$S(1)$: primary water temperature at HX exit $S(2)$: primary water flow $S(3)$: chilled water flow $S(4)$: chiller pump speed	$y(1)$: F3 V2
Pressurizer	Pressurizer CV-9 CV-10 CV-11 CV-12	$f(3)$: CV-12 spurious open	$S(5)$: water temperature $S(6)$: air pressure $S(7)$: inventory $S(8)$: boundary open size	$y(2)$: P4 $y(3)$: L3 Po-12
Water flow	Pump-1 CV-1 FV-1	$f(4)$: CV-1 spurious close $f(5)$: Pump-1 trip $f(6)$: FV-1 open	$S(9)$: water temperature $S(10)$: CV-1 outlet pressure $S(11)$: CV-1 inlet flow $S(12)$: outlet flow $S(13)$: inventory $S(14)$: pump-1 speed	$y(4)$: F1 $y(5)$: P1 Cu1
Water heating	Heater CV-20	$f(7)$: HTR overpower $f(8)$: CV-20 spurious open $f(9)$: FV-2 close	$S(15)$: inlet temperature $S(16)$: outlet temperature $S(17)$: inlet pressure $S(18)$: inlet flow $S(19)$: inventory $S(20)$: electric power	$y(6)$: T1 $y(7)$: T2 Cu2

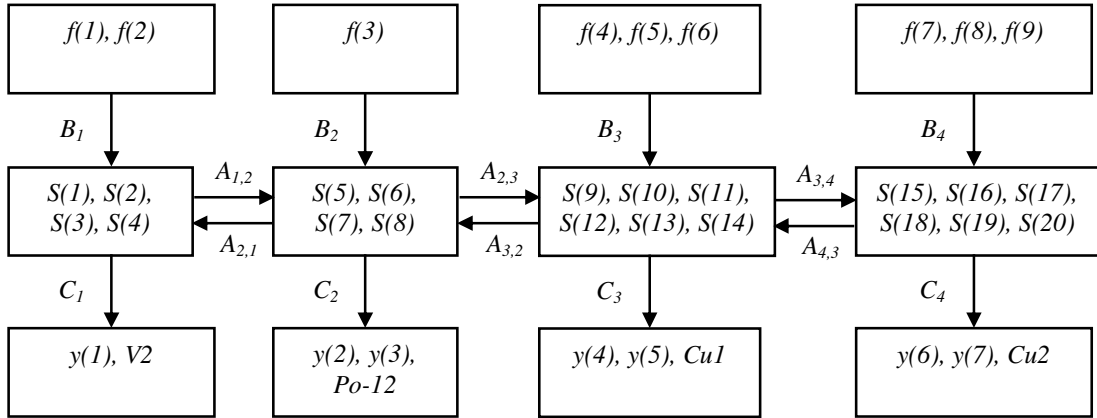


Figure 3-5: Model structure of NPCTF processes

To use the water cooling subsystem as an example, the fault effect matrix for this subsystem, denoted as B_1 , is a 4x2 matrix that relates the two faults, $f(1)$ and $f(2)$, and the four system states $S(1)$, $S(2)$, $S(3)$ and $S(4)$. Based on analysis of the water cooling

subsystem, it is determined that B_1 has a value of $B_1 = \begin{bmatrix} 1.0 & 1.0 \\ 0.0 & 0.0 \\ -0.8 & -1.0 \\ 0.0 & -1.0 \end{bmatrix}$. The meaning of

B_1 is illustrated in Table 3-9. The sensor sensitivity matrix for the water cooling subsystem, denoted as C_1 , is a 1x4 matrix that models sensitivity of the process control sensor $y(1)$ to the four system states. It can be obtained that $C_1 = [0 \ 0 \ 1 \ 0]$. To potentially include an additional sensor $V2$ in the matrix C_1 for enhanced diagnosability, the augmented sensor sensitivity matrix for this subsystem can be shown as

$$C_{1a} = \begin{bmatrix} 0 & 0 & 1 & 0 \\ 0 & 0 & 0 & 1 \end{bmatrix}.$$

Table 3-9: Fault effect matrix for water cooling subsystem

States	Faults	
	$f(1)$: CV-34 spurious close	$f(2)$: chiller pump trip
$S(1)$: primary water temperature at HX exit	1	1
$S(2)$: primary water flow	0	0
$S(3)$: chilled water flow	-0.8	-1
$S(4)$: chiller pump speed	0	-1

The system model results for other subsystems are summarized in Table 3-10.

Interpretations of the matrices are the same as the water cooling subsystem.

Table 3-10: System model results for NPCTF subsystems

Subsystems	Fault effect matrix	Sensor sensitivity matrix
Pressurizer	$B_2 = \begin{bmatrix} 0.0 \\ -1.0 \\ -1.0 \\ -1.0 \end{bmatrix}$	$C_2 = \begin{bmatrix} 0 & 1 & 0 & 0 \\ 0 & 0 & 1 & 0 \end{bmatrix}$
Water flow	$B_3 = \begin{bmatrix} 0.0 & 0.0 & 0.0 \\ -0.7 & -1.0 & -1.0 \\ -1.0 & -1.0 & -0.7 \\ 0.0 & 0.0 & -1.0 \\ 0.0 & -1.0 & 0.0 \end{bmatrix}$	$C_3 = \begin{bmatrix} 0 & 0 & 1 & 0 & 0 & 0 \\ 0 & 1 & 0 & 0 & 0 & 0 \end{bmatrix}$
Water heating	$B_4 = \begin{bmatrix} 0.0 & 0.0 & 0.0 \\ 1.0 & -0.3 & 1.0 \\ 0.0 & -1.0 & 0.8 \\ 0.0 & 0.3 & -1.0 \\ 0.0 & -1.0 & 0.0 \\ 1.0 & 0.0 & 0.0 \end{bmatrix}$	$C_4 = \begin{bmatrix} 1 & 0 & 0 & 0 & 0 & 0 \\ 0 & 1 & 0 & 0 & 0 & 0 \end{bmatrix}$

Couplings between the four subsystems are also modeled to consider the effects of fault propagation. The forward and backward state propagation matrices between the four subsystems are summarized in Table 3-11. For example, the 4x4 matrix of $A_{1,2}$ models how a change in the states of the water cooling subsystem will affect the states of the pressurizer subsystem. Other matrices can be interpreted in similar manners.

Table 3-11: State propagation matrices for NPCTF subsystems

Forward state propagation matrices	Backward state propagation matrices
$A_{1,2} = \begin{bmatrix} 1 & 0 & 0 & 0 \\ 0 & 0 & 0 & 0 \\ 0 & 0 & 0 & 0 \\ 0 & 0 & 0 & 0 \end{bmatrix}$	$A_{2,1} = \begin{bmatrix} 0 & 0 & 0 & 0 \\ 0 & 0 & 0 & 0 \\ 0 & 0 & 0 & 0 \\ 0 & 0 & 0 & 0 \end{bmatrix}$
$A_{2,3} = \begin{bmatrix} 1 & 0 & 0 & 0 \\ 0 & 1 & 0 & 0 \\ 0 & 0 & 0 & 0 \\ 0 & 0 & 0 & 0 \\ 0 & 0 & 1 & 0 \\ 0 & 0 & 0 & 0 \end{bmatrix}$	$A_{3,2} = \begin{bmatrix} 0 & 0 & 0 & 0 & 0 & 0 \\ 0 & 0 & 0 & 0 & 1 & 0 \\ 0 & 0 & 0 & 0 & 1 & 0 \\ 0 & 0 & 0 & 0 & 0 & 0 \end{bmatrix}$
$A_{3,4} = \begin{bmatrix} 1 & 0 & 0 & 0 & 0 & 0 \\ 1 & 0 & 0 & -1 & 0 & 0 \\ 0 & 1 & 0 & 0 & 0 & 0 \\ 0 & 0 & 0 & 1 & 0 & 0 \\ 0 & 0 & 0 & 0 & 1 & 0 \\ 0 & 0 & 0 & 0 & 0 & 0 \end{bmatrix}$	$A_{4,3} = \begin{bmatrix} 0 & 0 & 0 & 0 & 0 & 0 \\ 0 & 0 & 1 & 0 & 0 & 0 \\ 0 & 0 & 0 & 1 & 0 & 0 \\ 0 & 0 & 0 & 1 & 0 & 0 \\ 0 & 0 & 0 & 0 & 1 & 0 \\ 0 & 0 & 0 & 0 & 0 & 0 \end{bmatrix}$

The total fault-effect matrix, incidence matrix, and fault diagnosability matrix of the NPCTF can be obtained by substituting the model parameters in Table 3-9 through Table 3-11 into the proposed model as discussed in previous sections. The results are summarized in Table 3-12 through Table 3-14, respectively.

Table 3-12: Total fault-effect matrix of the NPCTF

	$f(1)$	$f(2)$	$f(3)$	$f(4)$	$f(5)$	$f(6)$	$f(7)$	$f(8)$	$f(9)$
$S(1)$	1.0	1.0	0.0	0.0	0.0	0.0	0.0	0.0	0.0
$S(2)$	0.0	0.0	0.0	0.0	0.0	0.0	0.0	0.0	0.0
$S(3)$	-0.8	-1.0	0.0	0.0	0.0	0.0	0.0	0.0	0.0
$S(4)$	0.0	-1.0	0.0	0.0	0.0	0.0	0.0	0.0	0.0
$S(5)$	1.0	1.0	0.0	0.0	0.0	0.0	0.0	0.0	0.0
$S(6)$	0.0	0.0	-1.0	0.0	0.0	-1.0	0.0	-1.0	0.0
$S(7)$	0.0	0.0	-1.0	0.0	0.0	-1.0	0.0	-1.0	0.0
$S(8)$	0.0	0.0	1.0	0.0	0.0	0.0	0.0	0.0	0.0
$S(9)$	1.0	1.0	0.0	0.0	0.0	0.0	0.0	0.0	0.0
$S(10)$	0.0	0.0	-1.0	-0.7	-1.0	-1.0	0.0	-1.0	0.8
$S(11)$	0.0	0.0	0.0	-1.0	-1.0	0.3	0.0	0.3	-1.0
$S(12)$	0.0	0.0	0.0	-1.0	-1.0	-0.7	0.0	0.3	-1.0
$S(13)$	0.0	0.0	-1.0	0.0	0.0	-1.0	0.0	-1.0	0.0
$S(14)$	0.0	0.0	0.0	0.0	-1.0	0.0	0.0	0.0	0.0
$S(15)$	1.0	1.0	0.0	0.0	0.0	0.0	0.0	0.0	0.0
$S(16)$	1.0	1.0	0.0	1.0	1.0	0.7	1.0	-0.3	1.0
$S(17)$	0.0	0.0	-1.0	-0.7	-1.0	-1.0	0.0	-1.0	0.8
$S(18)$	0.0	0.0	0.0	-1.0	-0.7	0.0	0.3	0.0	-1.0
$S(19)$	0.0	0.0	-1.0	0.0	0.0	-1.0	0.0	-1.0	0.0
$S(20)$	0.0	0.0	0.0	0.0	0.0	0.0	1.0	0.0	0.0

Table 3-13: Incidence matrix for process control sensors of the NPCTF

	$f(1)$	$f(2)$	$f(3)$	$f(4)$	$f(5)$	$f(6)$	$f(7)$	$f(8)$	$f(9)$
$y(1)$	-0.8	-1.0	0.0	0.0	0.0	0.0	0.0	0.0	0.0
$y(2)$	0.0	0.0	-1.0	0.0	0.0	-1.0	0.0	-1.0	0.0
$y(3)$	0.0	0.0	-1.0	0.0	0.0	-1.0	0.0	-1.0	0.0
$y(4)$	0.0	0.0	0.0	-1.0	-1.0	0.3	0.0	0.3	-1.0
$y(5)$	0.0	0.0	-1.0	-0.7	-1.0	-1.0	0.0	-1.0	0.8
$y(6)$	1.0	1.0	0.0	0.0	0.0	0.0	0.0	0.0	0.0
$y(7)$	1.0	1.0	0.0	1.0	1.0	0.7	1.0	-0.3	1.0

Table 3-14: Fault diagnosability matrix of the NPCTF with process control sensors

	$f(1)$	$f(2)$	$f(3)$	$f(4)$	$f(5)$	$f(6)$	$f(7)$	$f(8)$	$f(9)$
$f(1)$	0.00	19.89	1.07	1.51	1.46	1.32	2.43	1.15	1.49
$f(2)$	0.00	0.00	0.00	1.32	1.41	1.26	2.41	1.11	1.46
$f(3)$	0.00	0.00	0.00	1.32	1.41	4.78	1.73	8.29	1.35
$f(4)$	0.00	0.00	0.00	0.00	12.86	1.54	2.45	1.14	1.89
$f(5)$	0.00	0.00	0.00	0.00	0.00	1.59	2.41	1.14	1.58
$f(6)$	0.00	0.00	0.00	0.00	0.00	0.00	2.14	3.57	1.22
$f(7)$	0.00	0.00	0.00	0.00	0.00	0.00	0.00	1.83	2.43
$f(8)$	0.00	0.00	0.00	0.00	0.00	0.00	0.00	0.00	1.71
$f(9)$	0.00	0.00	0.00	0.00	0.00	0.00	0.00	0.00	0.00

Table 3-14 shows that three pairs of faults ($f(1), f(2)$), ($f(4), f(5)$), and ($f(3), f(8)$) cannot be diagnosed from the seven process control sensors. The procedures presented in Section 4.4 are applied to place additional sensors to enhance diagnosability of the six faults. Take the pair ($f(1), f(2)$) for example. The first and second column in the total fault-effect matrix in Table 3-12 reveals that the maximum difference of the two faults are in the state $S(4)$; chiller pump speed). $S(4)$ is not affected by the first fault $f(1)$, but it is sensitive to the second fault $f(2)$; therefore, it is desirable to place an additional sensor to measure $S(4)$. The choice is the vibration sensor V2 that measures the pump vibration which is correlated to the chiller pump speed. When V2 is included into the augmented sensor sensitivity matrix, the singular value ratio corresponding to the two faults is reduced from 19.89 to 3.76, which means that ($f(1), f(2)$) can be diagnosed. In a similar way, two more sensors Cu1 and Po-12 are selected to enhance diagnosability of ($f(4), f(5)$) and ($f(3), f(8)$), respectively. The final fault diagnosability matrix with the three additional sensors considered is presented in Table 3-15. It can be seen that all faults can be diagnosed. It is also determined that none of the three additional sensors can be eliminated to possibly reduce the number of new sensors.

Table 3-15: Fault diagnosability matrix of NPCTF with three additional sensors

	$f(1)$	$f(2)$	$f(3)$	$f(4)$	$f(5)$	$f(6)$	$f(7)$	$f(8)$	$f(9)$
$f(1)$	0.00	3.76	1.23	1.51	1.46	1.32	2.43	1.15	1.49
$f(2)$	0.00	0.00	1.00	1.50	1.29	1.22	2.48	1.15	1.46
$f(3)$	0.00	0.00	0.00	1.39	1.29	2.95	2.00	3.43	1.39
$f(4)$	0.00	0.00	0.00	0.00	3.70	1.54	2.45	1.14	1.89
$f(5)$	0.00	0.00	0.00	0.00	0.00	1.48	2.49	1.17	1.56
$f(6)$	0.00	0.00	0.00	0.00	0.00	0.00	2.14	3.57	1.22
$f(7)$	0.00	0.00	0.00	0.00	0.00	0.00	0.00	1.83	2.43
$f(8)$	0.00	0.00	0.00	0.00	0.00	0.00	0.00	0.00	1.71
$f(9)$	0.00	0.00	0.00	0.00	0.00	0.00	0.00	0.00	0.00

To further demonstrate improvement in fault diagnosability enabled by the additional sensors, all faults except pump-1 trip are physically simulated on the NPCTF. The fault pump-1 trip is skipped because it is interlocked to other safety functions of the NPCTF. Nine sets of data are acquired from the NPCTF with a sampling interval of one second. The first data set is acquired when the system is operating under steady state normal operations. Each of the other eight sets of data is acquired with a different fault simulated. The faults are simulated independently starting with the steady state normal condition. The experimental settings are summarized in Table 3-16.

Table 3-16: Summary of NPCTF experiments

Fault location	NPCTF operation	Fault hypothesis	Experiment data set
N/A	Normal steady state	$f(0)$	1
CV-34	Close CV-34 in manual mode	$f(1)$	2
Chiller	Stop chiller pump in manual mode	$f(2)$	3
CV-12	Open CV-12 to a high opening in manual mode	$f(3)$	4
CV-1	Set CV-1 at a low opening in manual mode	$f(4)$	5
FV-1	Manually open FV-1 to a high position	$f(6)$	6
Heater	Set heater power high in manual mode	$f(7)$	7
CV-20	Force open CV-20 in manual mode	$f(8)$	8
FV-2	Manually close FV-2 to a low opening	$f(9)$	9

The experimental data are first illustrated in Figure 3-6 using three process control sensors $y(4; F1)$, $y(3; L3)$ and $y(6)(T1)$. The data are further illustrated in Figure 3-7 using three sensors $y(4; F1)$, $y(5; P1)$, and $y(7)(T2)$. As highlighted in Figure 3-6, it can be seen that different faults can have similar sensor response patterns. For example, both $f(1)$ and $f(2)$ lead to increased temperature T1 due to loss of cooling water. The

experimental data for both faults fall in the same region. The two faults cannot be distinguished by a diagnosis model that is trained based on the three sensors. It is also the case for the measurement data for the fault clusters of $(f(3), f(6)$ and $f(8))$, $(f(4)$ and $f(9))$, as well as $(f(7)$ and $f(0))$.

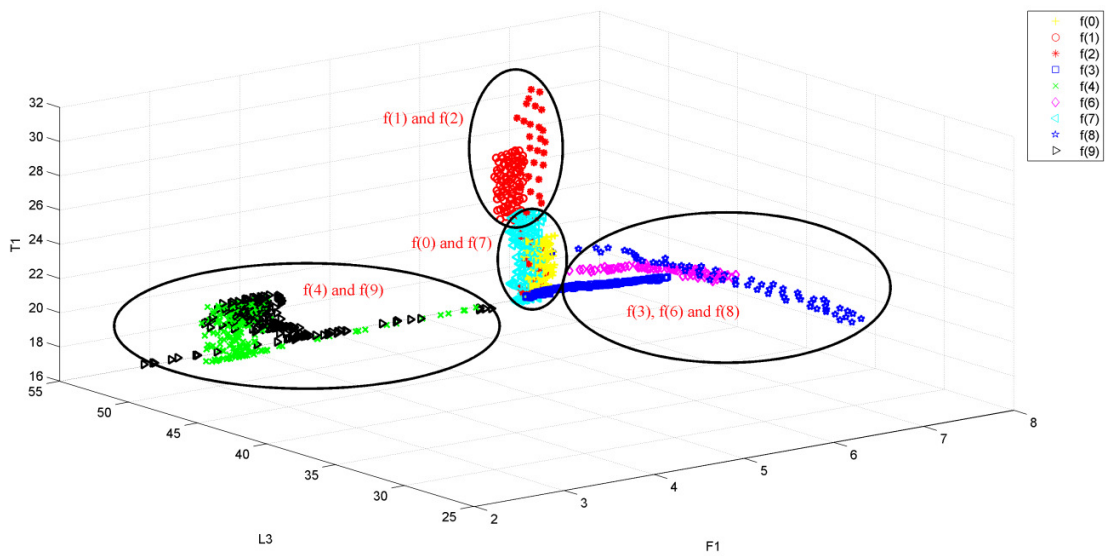


Figure 3-6: Illustration of NPCTF experimental data

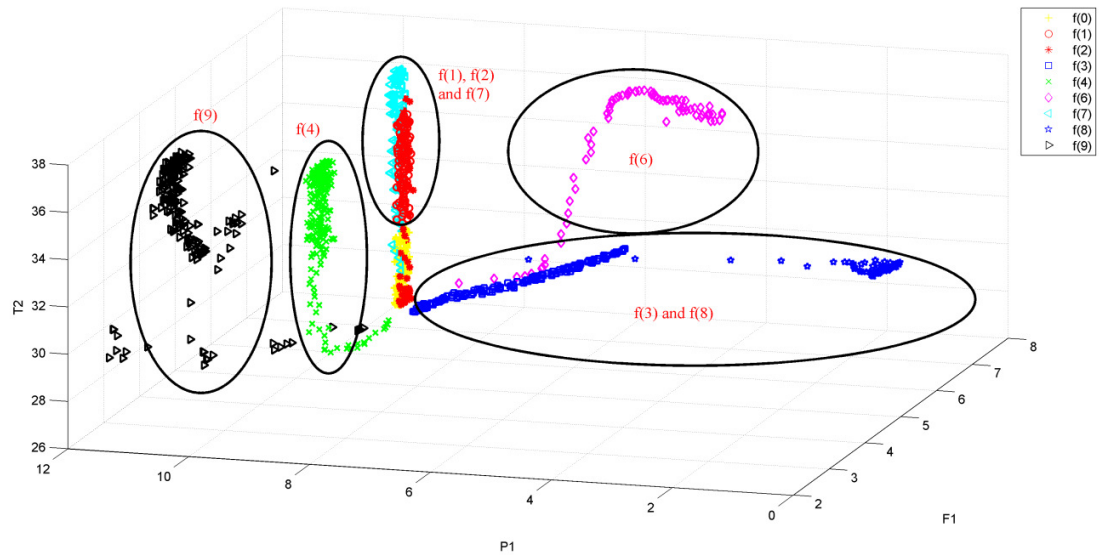


Figure 3-7: Further illustration of NPCTF experimental data

When Figure 3-7 is examined, it can be seen that the faults $f(4)$ and $f(9)$ can be distinguished by the sensor P1 because $f(9)$ leads to increased pressure, but the pressure is not affected by $f(4)$. It is also observed that the fault $f(6)$ is separated from $f(3)$ and $f(8)$ because increased temperature T2 is only caused by $f(6)$. However, the pairs of $(f(1), f(2))$ and $(f(3), f(8))$ still cannot be distinguished. The experiment results in Figure 3-6 and Figure 3-7 are consistent with the fault diagnosability results produced by the proposed model.

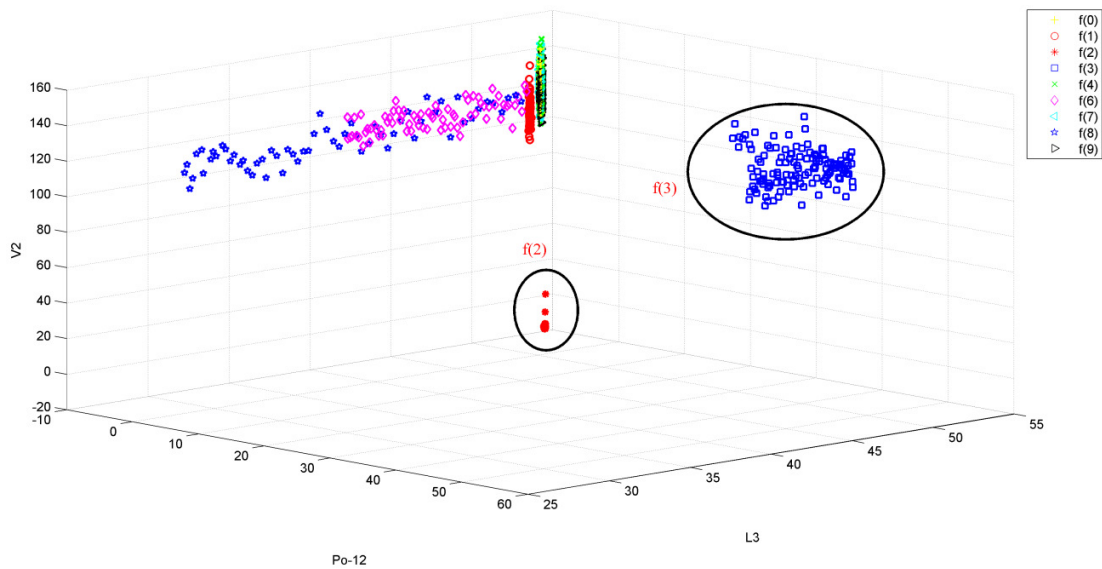


Figure 3-8: Illustration NPCTF experimental data with additional sensors

The experiments also show that diagnosability of $(f(1), f(2))$ and $(f(3), f(8))$ can be dramatically enhanced with the additional sensors. Measurement data from the two additional sensors V2 and Po-12 are plotted in Figure 3-8 together with the data of $y(3; L3)$. For the case of $f(1)$ and $f(2)$, it can be seen that the vibration measurement of V2 remains normal for $f(1)$, but it dropped to around zero when $f(2)$ was simulated. The sensor V2 provides a clear indication of which type of fault has happened. The results for the case of $f(3)$ and $f(8)$ are similar. The data provided by Po-12 separated $f(3)$ and $f(8)$ noticeably. Figure 3-8 proves that the proposed procedures to place additional sensor to enhance diagnosability are effective for the NPCTF system.

3.6 Conclusion

A sensor placement methodology is proposed in this chapter. In this scheme, a quantitative fault-sensor incidence matrix can be conveniently obtained from the system model. The degrees of singularity of the incidence matrix provide a practical measure of fault diagnosability. When additional sensors are required for enhanced diagnosability, proposed procedures can guide the placement of the most appropriate sensors.

Validations using a physical nuclear power plant simulator prove that the proposed scheme is indeed a flexible and effective tool for placement of additional sensors to enhance fault diagnosability of a technical system.

The proposed sensor placement model identifies the set of additional sensors required for a fault diagnosis. However, actual installation of the sensors in an existing NPP could be a very challenging task. In the next chapter, a cost-effective way to set up additional sensors using WSN is discussed.

Chapter 4

4 Wireless Sensor Networks for Fault Diagnosis

It is demonstrated in the previous chapter that additional sensors can be required for a fault diagnosis system. However, instrumentation wiring in harsh environment of a NPP could cost as much as two thousand dollars per foot (Shankar, 2004; Kadri, Rao, & Jiang, 2009). The excessive cost can diminish the values of the fault diagnosis system.

As reviewed in Chapter 2, WSN is especially attractive for installing additional sensors in existing plants and remote locations. Building a WSN is usually much less expensive than a wired system due to savings in cabling and deployment time. Therefore, WSN provides a flexible and cost-effective way to install sensors necessary for fault diagnosis. The review in Chapter 2 shows that a centralized system can cause issues for a fault diagnosis system such as excessive communications and longer diagnosis latencies (Tham, 2007). The limitations can be overcome by distributing fault diagnosis related computations (such as event detection, feature extraction, and diagnostic analysis) to devices in the network.

In this chapter, a WSN to support implementation of fault diagnosis systems is designed. The design leverages the inherent computing capabilities of the devices in a WSN to achieve distributed in-network data processing and fault diagnosis. The WSN itself consists of three levels: wireless sensor nodes at the field level, local diagnosis nodes at the local process level, and a central decision station at the system level. A wireless sensor node measures a process variable in the field. The sensor nodes are grouped into clusters according to the nature of the physical process (e.g., pressurizer, feed water system, and heat transport system). Within each cluster, multiple process variables are continuously measured by several sensor nodes. One node within each cluster is dedicated with the tasks to collect and integrate measurements from other sensors in the cluster, and to perform fault diagnosis at a local level. This node is referred to as 'local diagnosis node'. Data analysis in a local diagnosis node consists of a first level of data aggregation. Local diagnosis results from each cluster are then wirelessly forwarded to a

central station for final decision making, annunciation or alarm generation. This consists of a second level of data aggregation.

As a proof of concept, a prototype WSN has been deployed for the NPCTF processes presented in Chapter 3. The WSN system uses seven sensors of the NPCTF to diagnose six faults in the process. More specifically, seven MEMSIC IRIS wireless motes (MEMSIC, 2014) are connected to the NPCTF sensors, acting as field level sensor nodes. These sensors are organized in three clusters for three processes of the NPCTF. Three additional IRIS motes are programmed as local diagnosis nodes for the three clusters. On board the local diagnosis nodes, a Naive Bayes based decision-making scheme has been implemented to carry out real-time diagnosis. Results of the local diagnosis nodes are communicated to a central station where decisions are made based on fusion of the local diagnosis results. Experimental tests show that the system can diagnose all the faults correctly and promptly. Note that the main objective of this system is to prove the concept of using WSN for fault diagnosis. Simple data processing methods are used. They can be modified when a specific application is considered. In addition, more issues such as cyber security, electromagnetic interferences, regulations, and engineering feasibilities need to be considered when deployed in real NPPs, but they are beyond the scope of this thesis.

4.1 Wireless Sensor Network Design

The architecture of the designed WSN is illustrated in Figure 4-1. It consists of three levels of sensor nodes, local diagnosis nodes, and central station.

The sensor nodes are installed in the fields to measure physical parameters such as pressure and temperature. The sensory data are converted to digital signals and communicated through radio transceivers. Besides the measurement function, a sensor node is also able to receive signals from other sensors in the communication range and relay the data. In addition, a sensor node can also be programmed to process signals measured from the process as well as signals received from other sensors wirelessly.

This capacity enables on-board feature extraction and diagnostic analysis. The sensor nodes are grouped into clusters according to their positions in the system.

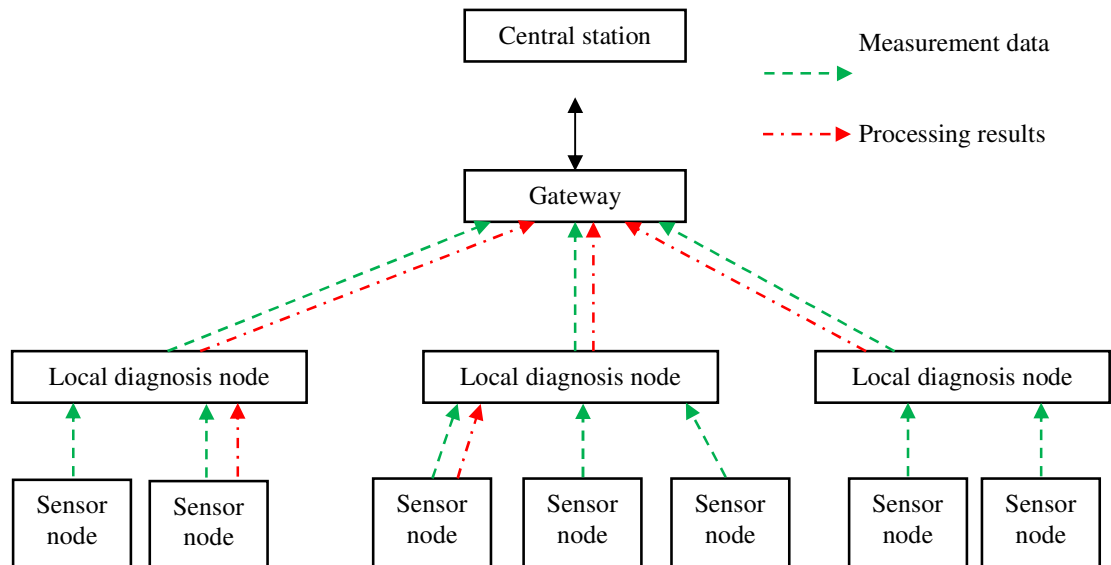


Figure 4-1: Architecture of prototype WSN for NPCTF fault diagnosis

Signals from the sensor nodes are communicated to the corresponding local diagnosis node for the cluster. Signal processing and diagnostic analysis are performed in the local diagnosis nodes. The main objective of the local diagnostic analysis is to analyze the current condition of a subsystem using information from the most relevant sensors. The purpose of local diagnosis is threefold. First, the local diagnosis models can deal with problems within a subsystem promptly. If a fault within a subsystem can be reliably diagnosed with the local sensor nodes (i.e., no information outside the cluster is required), the local diagnosis models can be designed to make decisions based on the diagnosis. By dealing with faults close to the origins, the amount of latency is kept at minimal. The second usage of local diagnosis nodes is to optimize the information to be communicated through the wireless network by using in-network signal processing such as filtering, compression and diagnostics. By communicating the processing results instead of the raw data, the required data-rate and bandwidth can be reduced. Finally, local diagnosis nodes can be designed as integral parts to support diagnosis of more

complex problems. For a complex system, building a single diagnosis engine to handle a large number of faults and sensors all together is difficult. The problem may be decomposed into several less complicated components by carefully designing the component models and the strategy to fuse the results of the components. A local diagnosis node can be designed to handle tasks of such a component.

Selected sensory data and the diagnostic processing results are sent to the central station through a gateway. For the sensory data acquired from the process, the central station presents the data to the plant engineers and stores the data for further references. For faults already diagnosed at the local diagnosis level, the central station is a location for presentation of the results, annunciation, alarm generation, or further processing. A complete picture of the system's operation condition is also constructed in the central station using the plant-wide information. For this purpose, a variety of information fusion methods that have been reviewed in Chapter 2 can be utilized, such as ordered weighted averaging, majority voting, ensemble of several classifiers, and expert systems.

4.2 Diagnostic Models Used in a Prototype WSN

A prototype WSN is implemented on the NPCTF as a proof of concept. The system considers six faults in the NPCTF. Wireless sensor modules are connected to seven sensors of the NPCTF which provide the information used to diagnose the six faults. The faults and sensors are listed in Table 4-1. In addition, the sensors are grouped to three clusters as indicated in Table 4-1. No signal processing is implemented for the sensor nodes because it is a low data-rate application.

Table 4-1: Faults and sensors used for prototype WSN system

	Group one	Group three	Group two
Process faults	CV-1 close FV-1 open Heater overpower FV-2 close	CV-12 open	CV-34 close
Wireless sensors	F1, P1, T1 and T2	P4 and L3	F3

As a proof of concept, Naive Bayes classification models are implemented on the local diagnosis nodes as local diagnosis engines. Naive Bayes classifier will be briefly discussed in the context of assigning discrete class labels $y \in \{0,1,2,\dots,k\}$ based on a set of process measurements $x = (x_1, x_2, \dots, x_n)$, where n is the total number of sensors or input features. The annotation is slightly different from that in Chapter 3. The pattern classification task is to find the most probable class labels give the set of inputs as

$$y = \arg \max_i p(y = i|x) \quad (4-1)$$

Based on the Bayes rule, the *posterior* probability $p(y = i|x)$ can be represented as

$$p(y = i|x) \propto p(y = i)p(x|y = i) \quad (4-2)$$

The *a priori* distribution $p(x|y = i)$ is a joint distribution of the class label y on the multiple inputs, which can be explicitly represented according to the chain rule as

$$p(x|y = i) = p(x_1|y = i)p(x_2|y = i, x_1)\dots p(x_n|y = i, x_1, x_2, \dots, x_{n-1}) \quad (4-3)$$

The joint distributions in Eq. (4-3) could be very difficult to estimate in practice. Naive Bayes classifier is based on the assumption that all input features are independent, i.e.,

$$\forall(i, j) : p(x_i|y, x_j) = p(x_i|y) \quad (4-4)$$

As a result, Eq. (4-2) can be written as

$$p(y = i|x) \propto p(y = i) \prod_{j=1}^n p(x_j|y = i) \quad (4-5)$$

where $p(x_j|y = i)$ is the *a priori* probability distribution of x_j when the fault $y = i$ happens. With the assumption that the likelihood of occurrence is equal for all hypotheses, the classification rule is reduced to

$$y = \arg \max_{i, i=1, \dots, 7} \prod_{j=1}^n p(x_j | y = i) \quad (4-6)$$

In the WSN implemented for the NPCTF system, three Naive Bayes classification models are designed, each for one local diagnosis node. To keep the model structure simple, all classifiers are designed to compute probabilities of all seven hypotheses (normal and six faults), using sensors within the corresponding clusters. The *a priori* distributions are fit using test data. The distribution functions are summarized in Table 4-2. Note that those classifiers are not designed to achieve the best possible classification performance. The main purpose is to demonstrate a fault diagnosis system using WSN technologies.

Table 4-2: *A priori* distributions for local diagnosis models

Fault location	Cluster 1				Cluster 2		Cluster 3
	F1	P1	T1	T2	P4	L3	F3
Normal	$N(6.6, 0.5)$	$N(9.1, 0.3)$	$N(20.0, 1.5)$	$N(29.2, 1.5)$	$N(6.0, 0.3)$	$R(50.0, 4.5)$	$N(28.0, 8.0)$
CV-1	$R(0.5, 1.5)^*$	$N(8.3, 0.3)$	$N(20.0, 1.5)$	$R(43.0, 3.0)$	$N(6.0, 0.3)$	$R(50.0, 4.5)$	$N(28.0, 8.0)$
FV-1	$N(10.0, 1.5)^{**}$	$R(0.5, 3.0)$	$N(20.0, 1.5)$	$R(43.0, 3.0)$	$R(0.5, 1.3)$	$R(20.0, 6.0)$	$N(28.0, 8.0)$
Heater	$N(6.6, 0.5)$	$N(9.1, 0.3)$	$N(20.0, 1.5)$	$R(43.0, 3.0)$	$N(6.0, 0.3)$	$R(50.0, 4.5)$	$N(28.0, 8.0)$
FV2	$R(0.5, 1.5)$	$R(17.0, 2.5)$	$N(2.0, 1.5)$	$R(43.0, 3.0)$	$N(6.0, 0.3)$	$R(50.0, 4.5)$	$N(28.0, 8.0)$
CV-34	$N(6.6, 0.5)$	$N(9.1, 0.3)$	$R(32.0, 2.5)$	$R(43.0, 3.0)$	$N(6.0, 0.3)$	$R(50.0, 4.5)$	$R(2.5, 3.3)$
CV-12	$N(6.6, 0.5)$	$R(0.5, 3.0)$	$N(20.0, 1.5)$	$N(29.2, 1.5)$	$R(0.5, 1.3)$	$R(20.0, 6.0)$	$N(28.0, 8.0)$

* $R(a, b) = \frac{x}{b^2} \exp(-\frac{(x-a)^2}{2b^2})$, where x is the input signal

** $N(a, b) = \frac{2}{\sqrt{2\pi}b^2} \exp(-\frac{(x-a)^2}{2b^2})$, where x is the input signal

Within each local diagnosis node, probabilities of all of the seven hypotheses are computed using sensors in the corresponding cluster. The results are further scaled to a sum of 100%. To use cluster two as an example, normalized probabilities of the fault hypotheses are estimated as

$$p_n(y = i | P4, L3) = \frac{p(y = i | P4, L3)}{\sum_{i=1}^7 p(y = i | P4, L3)} 100\% \quad (4-7)$$

The three local diagnosis nodes provide independent estimations of the probabilities of the seven hypotheses. In the central station, the normalized probabilities provided by the three local diagnosis nodes are averaged as the final results. The system status is decided as the hypothesis with the highest probability at the central station. Mathematically, the final probabilities are

$$p(y|F1, P1, T1, T2, P4, L3, F3) = \frac{p_n(y|F1, P1, T1, T2) + p_n(y|P4, L3) + p_n(y|F3)}{3} \quad (4-8)$$

and the system status is determined as

$$y = \arg \max_{i, i=1, \dots, 7} p(y = i | F1, P1, T1, T2, P4, L3, F3) \quad (4-9)$$

Even though simple diagnosis models are selected for the prototype system, experiments prove that all the fault conditions can be correctly and promptly diagnosed when the faults are physically simulated on the NPCTF.

4.3 Prototype Implementations

The WSN prototype is implemented on the NPCTF using MEMSIC (then Crossbow) wireless products (MEMSIC, 2014). The sensor nodes and local diagnosis nodes are based on the IRIS wireless motes. IRIS motes programmed as sensor nodes are connected to 4-20mA measurements from the NPCTF through the prototyping areas of MDA100 sensor boards. Motes programmed as local diagnosis nodes are not connected to physical inputs. Instead, they collect measurement data from the designated sensor nodes. The measurement data and local diagnosis results are collected to a laptop central station through a MIB520 USB gateway. Programmes on the sensor nodes and local diagnosis nodes are downloaded also through the MIB520 gateway. The WSN system is developed using the TinyOS operating system (TinyOs, 2014). The Naive Bayes models are developed in the C language and downloaded to the local diagnosis nodes. Data fusion and other high level functions such as data visualization and logging are executed on the laptop.

4.4 Experimental Results

In this section, the experimental results with the prototype WSN system on the NPCTF are presented. The objective of these tests is to investigate the performance of the WSN for diagnosis of practical faults. For the tests, all six faults are manually introduced, one at a time, while the NPCTF is in a normal steady state operating condition. The normal steady state conditions are summarized in Table 4-3. As listed in Table 4-4, the six fault hypotheses are designated with distinct class numbers 1-6 and the normal operating condition is identified as class number 0.

Table 4-3: NPCTF settings for normal steady state operation

Component	Setting	Control mode	Comments
Pump-1	Full power	Automatic	
CV-1	70%	Manual	
Heater	70%	Manual	
Chiller thermostat	17 °C, 1 °C differential	Automatic	Standalone control
CV-34	50%	Manual	
Pressurizer level	40%	Manual	
Pressurizer pressure	6.0 psi	Manual	

Table 4-4: Fault hypotheses for WSN test

Fault	Class number for hypothesis
Normal	0
FV-2 close	1
CV-1 close	2
FV-1 open	3
CV-12 open	4
CV-34 close	5
Heater overpower	6

The tests with each of the six faults are conducted as follows. The NPCTF is initially set to normal operating condition, so that the process status is determined as ‘normal’ by the central station (class level 0). A fault is then manually introduced. The fault causes some process parameters to deviate from the normal condition, and their current values are measured by the sensors. The sensor measurements are forwarded to the corresponding local diagnosis node, which performs a local classification and sends results to the central

station. The central station determines the current system status using local diagnosis results from all local diagnosis nodes, and classifies the fault as identified by the class level.

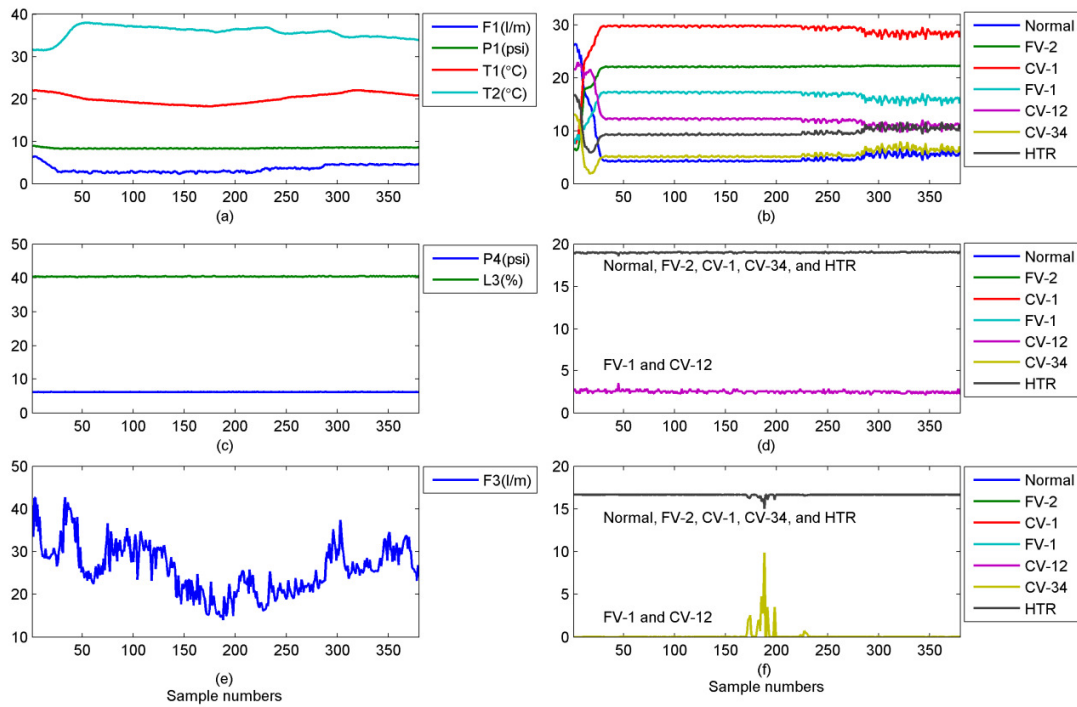


Figure 4-2: Illustration of CV-1 fault experiment, (a), (c) and (e) sensor readings, and (b), (d) and (f), fault hypotheses probabilities computed by local diagnosis nodes in Cluster-1, 2 and 3, respectively.

The fault diagnosis process in the WSN system is illustrated in the following using the case “fault at CV-1” (class label 2, i.e., CV-1 partially close) which belongs to Cluster-1 (Table 4-1). The measurements from the sensors (right after the fault is introduced in the process) from clusters 1, 2 and 3 are shown in Figure 4-2 (a), (c) and (e), respectively. The vertical axes in the three figures are the values of wireless sensor readings. As shown in Figure 4-2 (a), the flow rate F1 has gradually decreased due to the fault as it forces a partial closure of CV-1. As a result, the heater outlet temperature T2 has

increased (due to a lower water flow rate). The pressure P1 is also decreased slightly due to higher pressure drop through CV-1.

Corresponding local diagnosis results by the local diagnosis node in Cluster-1 are shown in Figure 4-2 (b). As shown, in the beginning, the system has been classified as ‘normal’ (the normal hypothesis having the highest probability), as the fault is still developing and changes in the sensor readings are not yet significant. However, the probability for the hypothesis of CV-1 fault increases quickly to become the highest as the water flow rate drops. This demonstrates that using the proposed approach, the fault can be correctly diagnosed by the local diagnosis node as soon as the fault symptoms are clear, especially if the fault belongs to the same cluster.

The sensor measurements and local diagnosis results for Cluster-2 are shown in Figure 4-2 (c) and (d), respectively. As shown, CV-1 fault does not affect the readings of the two sensors in this cluster. The hypotheses of normal, FV-2 fault, CV-1 fault, CV-34, and heater fault have the same *posterior* probabilities in Cluster-2, as the same *a priori* distribution is used for those hypotheses. Similar reasoning applies for hypotheses FV-1 fault and CV-12 fault. The signals and corresponding local diagnosis results for Cluster-3 are shown in Figure 4-2 (e) and (f), respectively.

The final diagnosis and decision making process at the central station are shown in Figure 4-3. The fault hypotheses probabilities, sent by all three local diagnosis nodes, are first averaged in the central station, shown in Figure 4-3. As shown, the patterns are very similar to those of the Cluster-1. The probabilities of CV-1 fault have increased quickly, and the fault is correctly diagnosed by the central station; however, the correct diagnosis is done only after a brief moment which is needed to allow for fault progression.

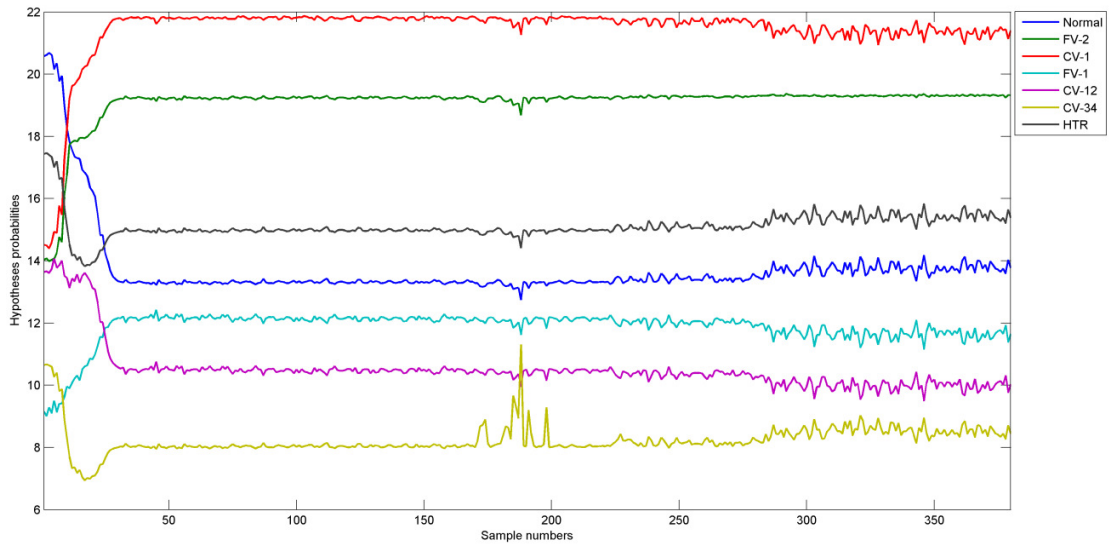


Figure 4-3: Illustration of final diagnosis results by the central station for test with CV-1 fault.

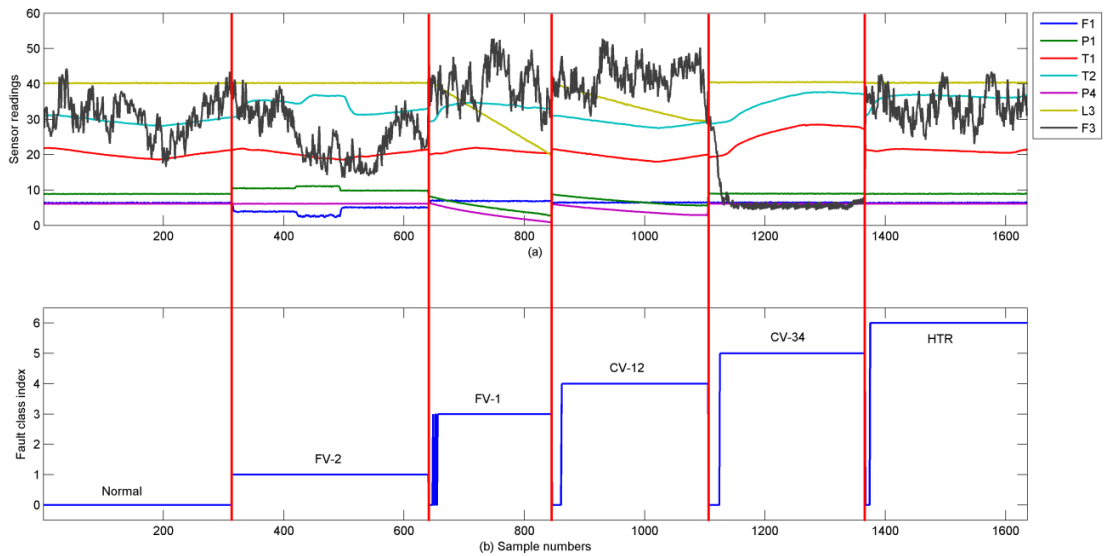


Figure 4-4: System status diagnosis under normal condition and faults FV-2, FV-1, CV-12, CV-34 and heater, (a) measurement signals, (b) fault class level as classified by the central station.

The experiment results for normal condition and other five fault scenarios are collectively presented in Figure 4-4. The real signals from the seven sensors are shown in the Figure

4-4 (a), and final classification results by the central station (corresponding to the measurement signal above) are shown in the Figure 4-4 (b). It is noted that the central station decides the status based on the information provided by the local diagnosis node, not the actual signal; however, the signals are shown here to better understand the effectiveness of the proposed system. To illustrate, consider the fault cases of FV-1 open and CV-12 open. When either of the two faults occurs, the pressurizer level L3 drops steadily due to the loss of inventory. The pressurizer pressure P4 also drops in both cases due to the expansion of the air. Coolant pressure P1 also drops due to lower P4. Based on these phenomena, two fault scenarios cannot be distinguished. However, this can be diagnosed using additional information, in this case, using T2. With FV-1 open, coolant flow to the heater is significantly by-passed, causing higher than normal heater outlet temperature, T2. Conversely, with CV-12 open, the coolant flow is not affected; thus, T2 remains normal. The proposed WSN system has used this information to distinguish the fault scenarios, and has correctly identified both faults. This has clearly demonstrated the feasibility of the proposed scheme, as it can successfully diagnose the faults correctly, despite the fact that different faults can sometime exhibit similar response patterns among multiple process variables.

As further shown in Figure 4-4, the proposed system has been able to diagnose all system states correctly. It is noted that there can be some misclassifications at the very inception of the fault; however, this is because the fault symptoms are not developed sufficiently right away, and the WSN system can correctly classify a fault as soon as the symptoms become relatively significant.

4.5 Conclusion

A wireless sensor network with distributed in-network signal processing and two levels of data aggregation is designed for fault diagnosis. A prototype system is implemented on a physical nuclear power plant simulator. Experimental tests have demonstrated the usefulness of the proposed approach, as the system can correctly diagnose all faults created in the simulator, despite the challenge that the faults often cause similar patterns of changes in the process measurements. The proposed WSN can conveniently acquire

additional information from a process and/or equipment beyond what are normally available through existing SCADA systems which can be utilized to improve the quality of fault diagnosis. The experiments indicate that although each device in a WSN has limited capability, a distributed WSN system can be used for fault diagnosis applications to improve the safety and operational efficiency of a NPP.

For the WSN, the fault diagnosis model is trained using experimental data collected under actual fault conditions. However, it will be very difficult, if possible, to operate a NPP under actual fault conditions to acquire the necessary data to train a fault diagnosis model. Therefore, a fault diagnosis model that can be used with scarce training data will be a valuable tool for applications in NPPs. This issue is addressed in the next chapter.

Chapter 5

5 Semi-Supervised Classification for Fault Diagnosis

Sensor placement models as discussed in Chapter 3 ensure that all faults are diagnosable. If additional sensors are required, a WSN (as discussed in Chapter 4) can be used to acquire the necessary data for fault diagnostic analysis. Nevertheless, a proper fault diagnostic model is still indispensable for a fault diagnosis system to be effective. This chapter deals with fault diagnostic reasoning as step seven of the process fault diagnosis framework illustrated in Figure 1-1.

The processes in a technical process are governed by physical laws such as balances of mass, energy, and momentum. When different types of process faults happen in the system, the normal physical balances are altered in different ways. As a result, different patterns of system response can be observed. By carefully selecting the sensors so that the faults can be uniquely characterised by the sensor responses, diagnosis of process faults can then be formulated as a pattern classification problem.

Pattern classification is the process of assigning discrete output class labels based on features extracted from the input data. Majorities of the fault diagnosis applications use so-called supervised pattern classification models, where training data with fault class labels are used first to train a classifier. The classifier subsequently processes new measurements for fault classification. However, for applications in systems such as a NPP, it could be difficult to obtain reliable labeled data to train a classifier. One reason is that one cannot simply create real faults in a NPP to collect training data. Although some databases under fault conditions are available, they may not coincide with the faults classes considered in the diagnostic classifier. The use of a NPP simulator is another way to generate training data, but there are modeling errors between simulator responses and real plant responses. Lack of reliable labeled data can skew the boundaries of a classifier. As a result, false classification can be induced when applied to real measurement data.

A fault diagnosis scheme based on semi-supervised classification is proposed in this chapter to address this issue. In SSC, both labeled data and unlabeled data are utilized to

train a classifier which can then be used to classify the unlabeled data. A SSC model can achieve superior performance when the labeled data set is small but unlabeled data are abundant. In addition, higher degree of uncertainties in the labeled data should be tolerated.

In the proposed fault diagnosis scheme, faults to be considered by the diagnostic system are first defined. Sensors that can be used to diagnose the faults are also selected. Labeled data for these faults are then generated through various means, such as simulation, experiments on scaled physical mock-ups, or experiences in the system. If the presence of fault is detected, sensory measurements are acquired from the plant and treated as unlabeled data. They are integrated with the labeled data samples to train a SSC model. The model subsequently estimates class labels of the unlabeled inputs; thus, the fault hypotheses of the new measurement data.

The proposed scheme is validated using a desktop simulator of a CANDU NPP and selected loops of the NPCTF. Three types of fault are considered in the CANDU simulator. As to the NPCTF, the faults identified in Chapter 3 for sensor placement case studies are considered. The NPCTF faults will be classified using the sensors selected in Chapter 3. Classification results have shown that all faults can be successfully diagnosed, even though the labeled data has considerable amount of uncertainties and the size of the labeled data is significantly smaller than typically required in a supervised model.

5.1 Fault Diagnosis as a Semi-Supervised Classification Problem

Suppose k faults can happen in a system and m sensors are used to diagnose the faults. The sensor outputs sampled at the time t are collected into a vector $x_t \in R^{1 \times m}$. Denote the fault i as hypothesis Hi and the fault class label $y = i$. Normal operation is denoted as $H0$ and the class label is $y = 0$. A set of training data is available as $D^l = \{X^l, Y^l\} = \{(x_i^l, y_i)\}_{i=1, \dots, nl}$, where nl is the total number of training data samples, X^l contains all the inputs and Y^l contains the class labels corresponding to X^l . When a fault is detected during system operation, a set of new measurements $X^u = \{x_i^u\}_{i=1, \dots, nu}$ are

acquired by the plant SCADA system, where nu is the number of unlabeled new measurements. The objective of a fault diagnosis system is to determine what type of fault has happened by testing the best match between the new measurements and the training data. This is essentially a pattern classification problem of assigning discrete labels of fault hypotheses $y \in \{0,1,2,\dots,k\}$ to a set of new data X'' , given a set of training data D' . In this chapter, X' and X'' will be referred to as the labeled data and unlabeled data, respectively.

To implement the pattern classification system, generally a classification function $g_i(y=i|x)$ is defined for each class which characterizes the match of the inputs x to the class $y=i$. The classification results can be obtained as

$$y = \arg \max_{i, i=1,\dots,k} g_i(y=i|x) \quad (5-1)$$

The classification function can be modeled from a generative approach to learn the joint probability distribution of the inputs x and the class label y . The classification function can also be modeled from a discriminative approach to find a direct map from the inputs to the class label. Bayes classifier is one of the most popular generative classifiers, which uses the posterior probability as the classification function as

$$g_i(y=i|x) = p(y=i|x) \quad (5-2)$$

Through the Bayes rule, Eq. (5-2) is equivalent to

$$g_i(y=i|x) \propto p(x|y=i)p(y=i) \quad (5-3)$$

where $p(x|y=i)$ is the *prior* distribution of the measurements for the class $y=i$ and $p(y=i)$ is the probability distribution of the class $y=i$.

To use a generative classification model, the distribution $p(x|y=i)$ must be estimated from the training data, which can be solved using various techniques such as maximum

likelihood estimation (MLE). In MLE, it is assumed that $p(x|y=i, \theta)$ belongs to certain distribution and θ represents the parameters of the selected distribution. With the conventional supervised pattern classification model, MLE estimates the value of θ by maximizing the log likelihood of $p(D^l|\theta)$ (Duda et al., 2000; Alpaydin, 2010; Webb & Copsey, 2011) as

$$\log p(D^l|\theta) = \log \prod_{j=1}^{nl} (p(x_j, y_j|\theta)) = \sum_{j=1}^{nl} \log p(y_j|\theta) p(x_j|y_j, \theta) \quad (5-4)$$

$$\hat{\theta} = \arg \max_{\theta} (\log p(D^l|\theta)) \quad (5-5)$$

With a discriminative model, the classification functions are designed to find decision regions or boundaries that separate the classes. The linear discriminant function is a popular choice for discriminative classification (Alpaydin, 2010; Duda et al., 2000; Webb & Copsey, 2011). The SVM algorithm learns the discriminant function as a hyperplane that separates two classes with the maximum margin (Webb & Copsey, 2011; Vapnik, 1998). With a supervised classification model, the parameters in the discriminant functions must be learned from the training data $\{X^l, Y^l\}$.

If size of the training data set D^l is small, the training data may not cover all the scenarios considered for the classification tasks. As a result, considerable errors may exist in the estimated parameters or decision boundaries of a classification model. Consequently, performance of a supervised classifier can be affected considerably.

In the case when the training data set is small, but abundant unlabeled data is available, i.e. $nu \gg nl$, the semi-supervised pattern classification models can provide enhanced performance. In semi-supervised classification, both labeled and unlabeled data are used to train the classifier. To take the Bayes model for example, the model parameters θ are now required to maximize the joint log likelihood defined on both the labeled training data D^l as well as the unlabeled instances X^u , i.e. (Zhu & Goldberg, 2009),

$$\begin{aligned}
\log p((D^l, X^u)|\theta) &= \log \prod_{j=1}^{nl} p((x_j^l, y_j)|\theta) \prod_{i=1}^{nu} p(x_i^u|\theta) \\
&= \sum_{j=1}^{nl} \log p(y_j|\theta) p(x_j|y_j, \theta) + \sum_{i=1}^{nu} \log p(x_i|\theta)
\end{aligned} \tag{5-6}$$

When Eq. (5-6) is compared to Eq. (5-4), it can be seen that information contained in the unlabeled data also contributes to the MLE estimation of the distribution parameters. The results will be different from those obtained from the labeled data only. Since the unlabeled data may cover additional regions not available from the limited training data, the differences can lead to enhanced performance. Note that Eq. (5-4) and Eq. (5-6) are used to illustrate the connections and differences between supervised and semi-supervised pattern classification modeling. In fact, the unlabeled data can be integrated into a pattern classification model through various means as shown in the related studies (Blum & Mitchell, 1998; Blum & Chawla, 2001; Seeger, 2001; Chapelle et al., 2002; Zhu et al., 2003; Chapelle & Zien, 2004; Zhou et al., 2004; Belkin et al., 2006; Chapelle et al., 2006; Azran, 2007; Zhu, 2008; Zhu & Goldberg, 2009).

Semi-supervised classification is generally based on the clustering assumption that nearby data points likely belong to the same class, and the manifold assumption that data points lie in the same manifold structure are likely to be in the same class (Chapelle et al., 2006; Niyogi, 2013). A SSC model can achieve superior performance because the classifier can be designed to avoid cutting through the high density regions or the manifolds with the availability of unlabeled data. On the other hand, correlations often exist in the process measurements due to physical and functional couplings. Therefore, data generated with the same fault tends to fall in the same high density region or on the same manifold structure. For those reasons, SSC provides a promising modeling approach for fault diagnosis in industrial systems like a NPP.

Supervised and semi-supervised classification is compared in Figure 5-1 using a simple two-class problem, where the input is a vector of two variables $x = (h_1, h_2)$ and the classes are designed as $y = 1 | h_2 = 0.25$ and $y = 2 | h_2 = 0.75$. The desirable classifier boundary is at $h_2 = 0.5$, as shown in Figure 5-1(a) using the red dashed line. Suppose two training

data samples are available as $D^l = \{d_1, d_2\} = \{ \{(-0.5, 0.25), 1\}, \{(0.5, 0.75), 2\} \}$, which are shown in Figure 5-1 as the large size blue circle and green triangle, respectively. If a supervised 1-nearest neighbor (1-NN) classifier (Bishop, 2006) is trained based on d_1 and d_2 , the classification boundary is essentially a line vertical to the line connecting d_1 and d_2 . This boundary is shown as the red solid line in Figure 5-1(a), which is considerably different from the truth. Some new unlabeled data in the range of $h_1 \in [-1, 1]$ are generated and classified by the 1-NN classifier. The results are shown in Figure 5-1(a), where data classified to the two classes is represented using the smaller size circles and triangles, respectively. It is observed that a large portion of the unlabeled data is misclassified by the supervised classifier.

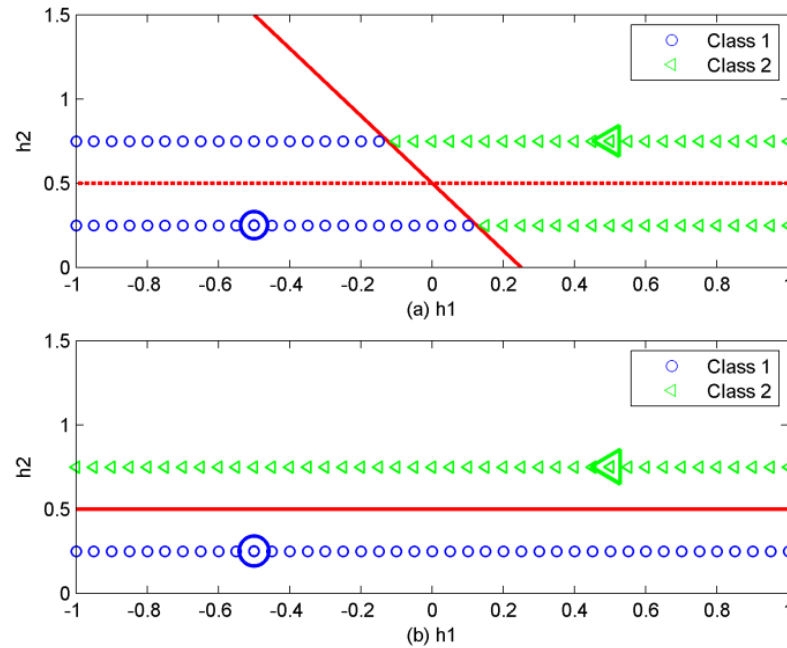


Figure 5-1: Supervised classification based on (a) 1-nearest neighbor; (b) semi-supervised classification

The unlabeled data and training data is also processed by a SSC model and the results are presented in Figure 5-1(b). It is observed that all unlabeled data is correctly classified, and the classifier avoids cutting through the two high density regions of the unlabelled

data. It is a substantial improvement as compared to the results shown in Figure 5-1(a).

It should be noted that even though SSC has demonstrated superior performance in numerous studies, it should not be taken for granted that indiscriminate inclusion of unlabeled data in a pattern classification model will lead to improved performance (Singh et al., 2008; Lu, 2009). For instance, it has been shown in (Lu, 2009) that it is important to make sure that there is indeed a non-trivial relationship between distribution of the unlabeled data and the class labels.

5.2 Semi-Supervised Classification Algorithms for Fault Diagnosis

Several SSC algorithms have been developed in recent years (Zhu, 2008; Zhu & Goldberg, 2009; Seeger, 2001; Chapelle et al., 2006). A graph-based SSC algorithm in (Zhou et al., 2004) is utilized in this research due to its classification performance and the ability to perform multi-class classification with one classifier. This algorithm can be considered as a combination of spectral clustering (Shi & Malik, 2000; Ng et al., 2001) and label propagation on a data graph (Zhu, 2005). First, a graph $G(V, E)$ is built for a data matrix $X = \{x_i\}_{i=1, \dots, n}$, where the vertices V are the data points in X and E are edges connecting the vertices. A weight w_{ij} is assigned to the edge connecting vertices i and j , which can be computed as

$$w_{ij} = \exp\left(-\frac{(x_i - x_j)^2}{2\sigma^2}\right), i \neq j \quad (5-7)$$

where σ is a constant. $w_{ij} = 0$ if $i=j$. An affinity matrix W is built with weights for all the data points.

A diagonal degree matrix D can then be defined as

$$D = \text{diag}\{D_{ii}\} = \text{diag}\{\sum_j w_{ij}\} \quad (5-8)$$

Elements in W quantify similarities between two data samples and elements in D quantify the total weights for every data sample. An example data graph is shown in Figure 5-2 to

illustrate the concept. The circles in Figure 5-2 are the vertices, representing the input data points. The two filled circles represent labeled data for two classes, as shown by the legend. The lines connecting the vertices are the edges. The numbers beside the edges are the weights. In a complete data graph, all pairs of data points are connected, but only some of the connections are shown in Figure 5-2, so that the graph is not excessively crowded. A higher weight means that the two data points are more similar or closer to each other. When a label propagation process is performed on the graph, a higher weight means that the likelihood of receiving label information from the other data point is higher. It is intuitively reasonable to partition the data points in Figure 5-2 in such a way that data below the dashed line belong to class one and data above the dashed line belong to class two.

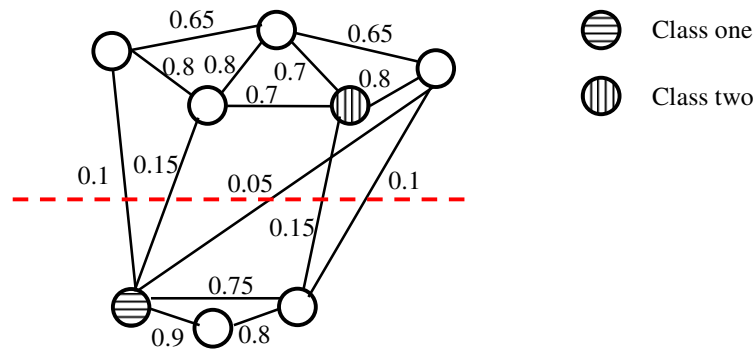


Figure 5-2: An example data graph

Spectral clustering is formulated as a graph cut problem so that edges between different clusters have low weights and edges within the same cluster have high weights.

Minimizing the graph cut functions becomes an eigenvalue problem (Ng et al., 2001) as

$$Lu = \lambda Du \quad (5-9)$$

where u is an eigenvector and L takes the form

$$L = D^{-1/2}WD^{-1/2} \quad (5-10)$$

SSC is achieved by integrating spectral clustering with some labeled data. Create the input data matrix $X = \begin{bmatrix} X^l \\ X^u \end{bmatrix} \in R^{n \times m}$, where $n = nl + nu$ is the total number of labeled and unlabeled data. Define a $n \times (k + 1)$ classification matrix F . Each row in F represents the similarities of one data sample to all the classes to be assigned. The label of a data point x_i is obtained by $y_i = \arg \max_{j, j=1, \dots, k+1} F_{ij}$.

In the algorithm in (Zhou et al., 2004), every data point spreads its label information to the neighboring points with the matrix L controlling the likelihoods. The label spread process iterates until the system is stable. It is more likely for a labeled data to propagate its label information to data in the same high density region or on the same manifold structure. Referring to the example in Figure 5-2, the data points above the dashed line are more likely to propagate their label information to each other than to the rest of the graph. When a convergent stable state is achieved, the unlabeled data points are more likely to possess label information from the labeled node for class two. It is the same situation for the data points below the dashed line.

Mathematically, the classification matrix F is obtained iteratively as (Zhou et al., 2004)

$$F(t+1) = \alpha L F(t) + (1 - \alpha) Y \quad (5-11)$$

where α is a parameter between 0 and 1 that controls the relative importance of the two terms on the right side. It is seen in Eq. (5-11), that the classification is based on information received from its neighbors (the first term) and initial information (the second term). The convergent value of F can be obtained as (Zhou et al., 2004; Camps-Valls et al., 2007)

$$F^* = (1 - \alpha)(I - \alpha L)^{-1} Y \quad (5-12)$$

and the class label of an unlabeled data is obtained as

$$y_i = \arg \max_{j, j=1, \dots, k+1} F_{ij}^* \quad (5-13)$$

The complete SSC algorithm can be summarized as follows: 1) Collect labeled data and unlabeled data into a data matrix X and initiate the label matrix Y ; 2) Form the weight matrix W as $w_{ij} = \exp(-(x_i - x_j)^2 / 2\sigma^2), i \neq j$ and $w_{ii} = 0$; 3) Compute the diagonal degree matrix D as $D = \text{diag}\{D_{ii}\} = \text{diag}\{\sum_j w_{ij}\}$; 4) Compute $L = D^{-1/2}WD^{-1/2}$; 5) Compute the classification matrix F as $F = (1 - \alpha)(I - \alpha L)^{-1}Y$; and 6) Label a data point as

$$y_i = \arg \max_{j, j=1, \dots, k+1} F_{ij}^*.$$

A fault diagnosis scheme based on SSC is developed and illustrated in Figure 5-3.

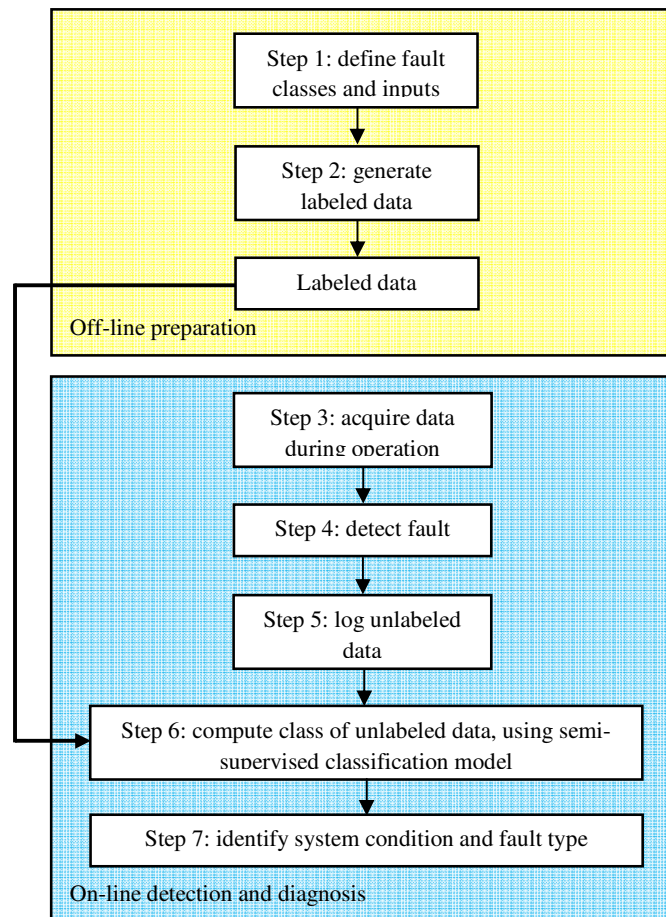


Figure 5-3: Proposed fault diagnosis scheme based on SSC

At Step 1, the fault types considered are determined first. One can use techniques such as failure mode and effect analysis for this purpose. Class labels are assigned to the fault hypothesis. Inputs to the SSC model are also selected, so that all the faults can be distinguished. The sensor placement method proposed in Chapter 4, or other sensor placement methods reviewed in Chapter 2, can be used to select the sensors for this purpose. Labeled training data are then generated in Step 2. For this purpose, measured data with real faults, historical operation data, operating experience, and numerical simulations can all be considered to generate the labeled data. Step 1 and Step 2 are performed off-line. At Step 3, new measurements are acquired during system operation. Step 4 is a process which detects potential faults based on the new measurements. If a fault is detected, the new measurements in sequel will be logged as the unlabeled data, which is known as Step 5. In Step 6, both the labeled and the unlabeled data are processed by a SSC model to determine the most appropriate class labels for the unlabeled new measurements. Based on the fault class designation, at Step 7, the class labels are assigned to identify whether the system is normal or what type of faults has most likely occurred. Step 3 to step 7 are intended for on-line fault detection and diagnosis.

5.3 Experimental Validations

In this part, the developed scheme is validated by two case studies using a desktop CANDU NPP simulator and the NPCTF. In the case studies, the data matrix X for the graph-based SSC algorithm is constructed as

$$X = \begin{bmatrix} X_{n0 \times m} \\ X_{n1 \times m} \\ \dots \\ X_{nk \times m} \\ X_{nu \times m} \end{bmatrix} \quad (5-14)$$

where nk represents the size of labeled data for class $y = k$ and nu is the number of unlabeled data. The classification matrix F is initiated as shown in Eq. (5-15). A zero matrix of the size $nu \times (k + 1)$ is set for the unlabeled data. For a labeled data point, the

entry i of the corresponding row vector is set to unity with the rest set to zero. For $H0$, the last entry is set to unity.

$$Y = \begin{bmatrix} [0,0,0,\dots,1]_{n0 \times (k+1)} \\ [1,0,0,\dots,0]_{n1 \times (k+1)} \\ [0,1,0,\dots,0]_{n2 \times (k+1)} \\ \dots \\ [0,0,\dots,1,0]_{nk \times (k+1)} \\ [0,0,\dots,0,0]_{nu \times (k+1)} \end{bmatrix} \quad (5-15)$$

5.3.1 Case study using CANDU NPP simulator

The desktop simulator is developed and maintained by Ontario power generation (OPG) for training of plant operators. It is capable of simulating one entire CANDU unit in real-time with high fidelity. Different types of faults can also be simulated. This case study involves faults introduced in the pressurizer, feedwater, and main steam systems. These faults can affect various subsystems in the plant with some common symptoms.

The first simulated fault is spurious open of one pressurizer steam bleed valve (SBV). The SBV is used to reduce pressure in the heat transport system by bleeding steam out. The second fault is a spurious close of one boiler level control valve (BLCV) that is used to control the steam generator level by regulating the feedwater flow rate. In addition, a low position fault is simulated to the backup BLCV. The third fault is spurious open of one main steam safety valve (MSSV) which is used to protect the steam line.

The following seven process variables are used as the model inputs: (1) gross reactor power (%), (2) reactor outlet header (ROH) pressure (kPa), (3) SG level, (4) SG pressure (kPa), (5) feedwater flow (kg/s), (6) steam flow from SG to the balance header (kg/s), and (7) balance header pressure (kPa).

As summarized in Table 5-1, four sets of data are acquired from the simulator. The simulations are all initiated with full power steady state (FPSS) condition. No fault is

inserted for the first simulation. Each of the other three simulations has one different fault simulated.

Table 5-1: Validation data sets using CANDU NPP simulator

Data set	Simulation condition	Fault hypothesis	Class label
1	Normal operation	$H0$	0
2	One BLCV fail close first; the backup BLCV has a 30% position fault	$H1$	1
3	One SBV stuck open at 80%	$H2$	2
4	MSSV fail open	$H3$	3

One out of every twenty data points of the first data set is used as the labeled training data for $H0$. Four data points are selected from each of the other data sets as the labeled data points for $H1$, $H2$, and $H3$. The rest of the data in all data sets are treated as unlabeled data.

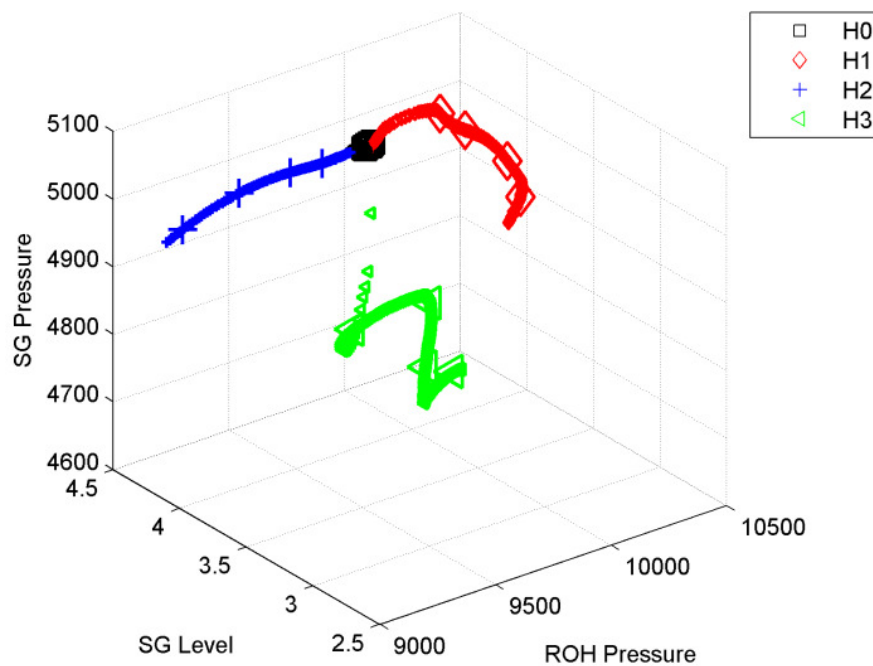


Figure 5-4: Illustration of CANDU NPP classification results

Classification results are first illustrated in Figure 5-4 using three variables, i.e., SG pressure, SG level, and ROH pressure. The labeled data is shown in Figure 5-4 as the

larger size symbols, and the unlabeled data is represented using the smaller size symbols. Different shapes and colors are used to distinguish the classes. It can be observed that the unlabeled data are all classified to the correct classes as the measurements change outside the region of fault free data.

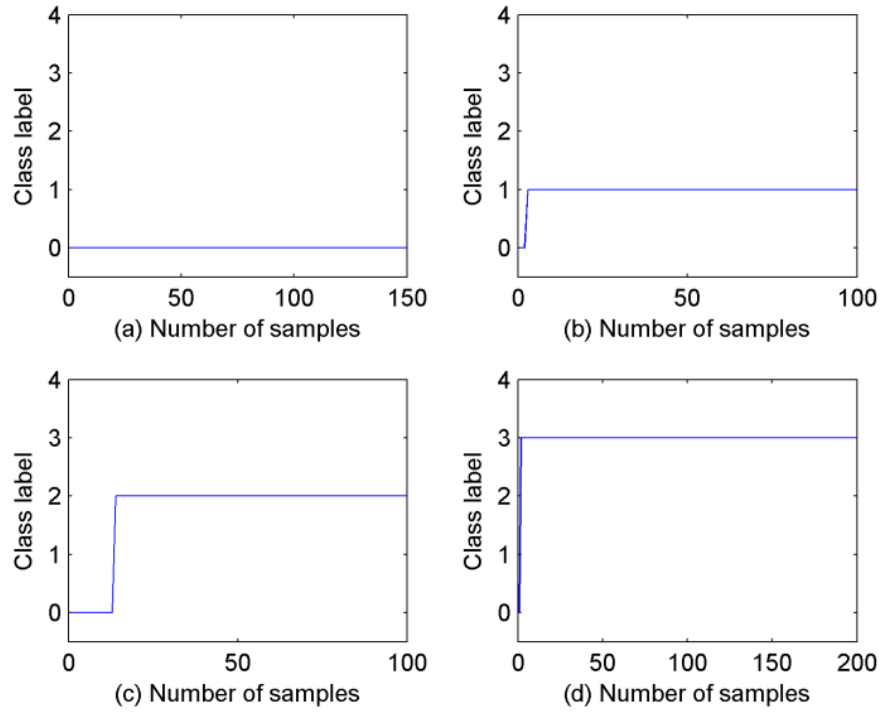


Figure 5-5: Computed class labels for the CANDU NPP data sets with: (a) normal operation $H0$; (b) BLCV fault $H1$; (c) SBV fault $H2$; and (d) MSSV fault $H3$

The class labels estimated for the four data sets are plotted in Figure 5-5. All data points with normal operation are correctly classified as hypothesis $H0$ and are shown in Figure 5-5(a). For the data sets with faults as shown in Figure 5-5(c-d), the data are initially classified as normal because the data contain FPSS condition in the beginning. The faults are all correctly classified shortly. It is demonstrated in Figure 5-4 and Figure 5-5 that the SSC model is able to distinguish all three faults with a small number of labeled data.

5.3.2 Case study using NPCTF

The developed scheme is also validated using the NPCTF loops used in Chapter 3. A diagram of the NPCTF loops is illustrated again in Figure 5-6 for convenient reference. The system mainly consists of a pump, a heater, a heat exchanger, a chiller system and a pressurizer system. Pump-1 drives the primary water flow and CV-1 controls the flow rate. The water temperature is raised in the heater, simulating the function of a reactor. The heated water is cooled in the HX using chilled water supplied by the chiller system, simulating the heat sink function of a SG. The pressurizer tank controls the system pressure by feeding in compressed air through CV-3, or bleeding air out through CV-4. Two manual valves FV-1 and FV-2 are used to simulate pipe breaks or flow blockage. CV-20 is a valve that belongs to the passive cooling system of the NPCTF. The rest of the passive cooling system is not shown because it is not relevant to this case study. Valve openings of the NPCTF can be set manually in manual control mode, or regulated by the controller in automatic control mode.

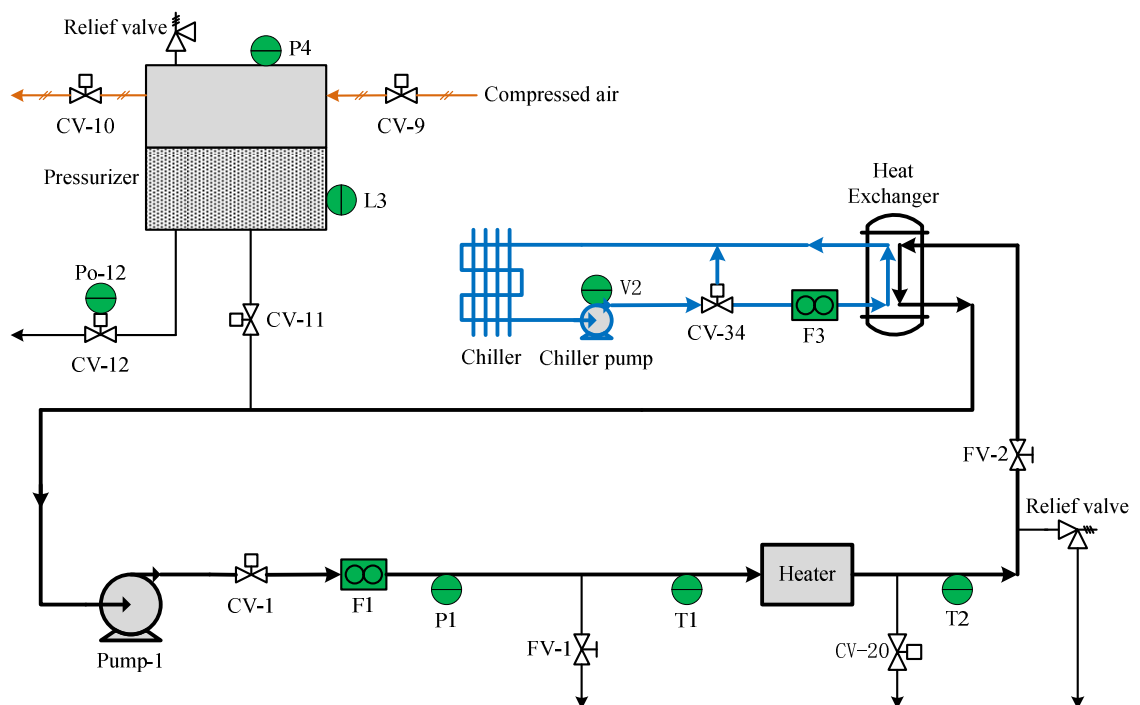


Figure 5-6: Diagram of selected NPCTF loops

In this case study, the same faults and sensors identified in Chapter 4 are considered. However, the fault ‘pump-1 trip’ is skipped because it is interlocked to other safety functions of the NPCTF. In addition, as the current sensor Cu1 is selected only to diagnose pump-1 related fault, this current sensor is also dropped from the case study. As discussed in Chapter 4, the two faults CV-12 open and CV-20 open have similar response patterns and the sensor Po-12 is added to distinguish the faults. To reduce the complexity of the SSC model, those two faults are combined to one hypothesis of *loss of coolant inventory* (LOCI). If a LOCI hypothesis is diagnosed by a SSC model, the data will be further classified by considering the value of the valve position measurement Po-12. Similarly, the two faults CV-34 close and chiller pump stop are combined as the hypothesis *loss of cooling capacity* (LOCC) and the two faults are distinguished by the vibration sensor V2. Po-12 and V2 are not included in the SSC model as input to reduce the complexity. In addition, it is determined that all the faults are diagnosable without the sensor F3; thus, the sensor is dropped out of the SSC model to keep the computation process efficient. Furthermore, the temperature difference T2-T1 between the heater outlet and inlet is used as an input data instead of using T2 directly. The reason is that the temperature difference is more directly correlated to other process parameters, such as flow rate F1 and heater power. The considered faults are listed in Table 5-2. The selected sensors are F1, L3, P1, P4, T1, T2, Po-12, and V2, as shown in Figure 5-6. The SSC model inputs are F1, L3, P1, P4, T1, and T2-T1. Po-12 and V2 are used to analyze LOCI and LOCC further.

Table 5-2: NPCTF faults considered for SSC-based fault diagnosis model

Fault location	NPCTF operation	Fault hypothesis	Class label	Experiment data set
N/A	Normal steady state	<i>H0</i>	0	1
FV-1	Manually open FV-1 to a high position	<i>H1</i>	1	2
CV-12	Open CV-12 to a high opening in manual mode	<i>H2-A</i>	2	3
CV-20	Force open CV-20 in manual mode	<i>H2-B</i>	2	4
Heater	Set heater power high in manual mode	<i>H3</i>	3	5
CV-34	Close CV-34 in manual mode	<i>H4-A</i>	4	6
Chiller	Stop chiller pump in manual mode	<i>H4-B</i>	4	7
CV-1	Set CV-1 at a low opening in manual mode	<i>H5</i>	5	8
FV-2	Manually close FV-2 to a low opening	<i>H6</i>	6	9

Nine sets of data are acquired from the NPCTF with a sampling interval of one second. One data set is acquired when the system is operating under steady state normal operations. Each of the other eight sets of data is acquired with a different fault. The faults are simulated independently starting with the steady state normal condition. The NPCTF settings for the normal steady state operations are summarized in Table 5-3. When the normal steady state operation is set, the target is to set the level L3 at 50% and the pressure P4 at 6psi. However, variations may exist when the condition is set with different runs. The other values are not directly set. Instead, they are the results of other process settings.

Table 5-3: NPCTF settings for normal steady state operation

Component	Setting	Control mode	Comments
Pump-1	Full power	Automatic	
CV-1	70%	Manual	
Heater	70%	Manual	
Chiller thermostat	17 °C, 1 °C differential	Automatic	Standalone control
CV-34	50%	Manual	
Pressurizer level	50%	Manual	
Pressurizer pressure	6.0 psi	Manual	

Statistics of the model input signals under normal operation are presented in Table 5-4.

Table 5-4: Statistics of normal NPCTF operation data

Variable and unit	Minimum	Maximum	Average	Standard deviation
F1 (l/m)	6.36	6.73	6.54	0.09
L3 (%)	49.77	49.86	49.81	0.18
P1 (psi)	9.08	9.25	9.16	0.03
P4 (psi)	6.00	6.03	6.02	0.01
T1 (°C)	17.98	21.37	19.49	1.00
T2-T1 (°C)	9.08	9.85	9.55	0.23
Po-12 (%)	0.67	1.01	0.09	0.06
V2 (10 ⁻³ ips)	107.93	162.04	132.85	7.63

Based on the data in Table 5-4 and the steady state settings, a fault is considered being detected if any sensor output exceeds the thresholds listed in Table 5-5.

Table 5-5: NPCTF fault detection thresholds

Variable and unit	Lower bound	Higher bound
F1 (l/m)	6.0	7.0
L3 (%)	48.0	N/A
P1 (psi)	8.9	9.4
P4 (psi)	5.8	N/A
T1 (°C)	17.0	22.5
T2-T1 (°C)	8.5	11.0
Po-12 (%)	N/A	30
V2 (10 ⁻³ ips)	100	N/A

Two different ways are used to generate the labeled data in this case study. The first one is to generate labeled data based on dynamic relations among different variables in the NPCTF. The responses of related process variables to a fault can be anticipated from the dynamic relations; thus, some expected sensor outputs can be estimated. It provides a way to incorporate previous experiences and knowledge to assist the pattern classification task. This method is used to generate the training data for the faults related to FV-1, CV-20, chiller, and FV-2 as summarized in Table 5-6. To use the case of FV-2 as an example, with FV-2 partially closed, water flow in the primary loop is partially blocked; thus, the flow rate F1 will drop and the pressure P1 will increase. In addition, the temperature difference across the heater T2-T1 will increase due to the reduced flow. No substantial changes in other measurements are expected. Based on this knowledge and the normal values presented in Table 5-4, six labeled data points are generated as follows: F1 has a range of 5.5 to 3.0; P1 has a range of 10.0 to 12.0; T2-T1 has a range of 10 to 14; and values of other variables are selected as random numbers in the normal ranges. Six labeled data are also generated for the other three faults in a similar fashion. The fault sensitivity matrix obtained in Chapter 4 can be referred to understand the effects of the faults on the sensors. The labeled data are summarized in Table 5-7. As expected, the training data generated based on rough understanding of the system dynamics will probably contain considerable uncertainties. If more accurate models are available to simulate the dynamic relations, they can also be used to generate the labeled data. Unfortunately, a dependable simulation model for the NPCTF is not yet available.

Table 5-6: Labeled data generation for NPCTF fault diagnosis

Fault hypothesis		Labeled data generation method	Number of labeled data	Class label in SSC model
Normal		Samples from a test run	10	0
FV-1		Expected system dynamics	6	1
LOCI	CV-12	Selected samples from the test data set	2	2
	CV-20	Expected system dynamics	6	
Heater		Selected samples from the test data set	2	3
LOCC	CV-34	Selected samples from the test data set	2	4
	Chiller	Expected system dynamics	6	
CV-1		Selected samples from the test data set	2	5
FV-2		Expected system dynamics	6	6

Table 5-7: Labeled data for SSC model

Fault location	F1	L3	P1	P4	T1	T2-T1
FV-1	7.0	49.0	7.0	5.5	19.5	10.0
	7.2	47.0	6.5	5.0	20.5	12.0
	7.1	46.0	6.0	4.0	19.0	15.0
	6.9	44.0	5.5	3.0	21.0	13.0
	7.3	43.0	5.0	2.5	20.0	12.0
	7.0	42.0	4.5	2.0	18.5	16.0
CV-12	6.3	48.7	8.6	5.3	18.7	9.4
	6.4	45.9	7.3	4.2	19.5	9.2
CV-20	7.0	49	5.5	5.5	20.0	9.1
	7.1	47.5	3.0	5.0	19.5	9.0
	7.2	46.0	2.5	4.0	19.0	8.9
	6.9	44.0	2.0	3.0	21.0	8.7
	7.1	43.0	1.5	2.5	20.5	8.6
	7.3	42.0	1.0	2.0	18.5	8.5
Heater	6.4	49.9	9.1	6.0	17.9	13.6
	6.5	49.8	9.1	6.2	19.8	14.5
CV-34	6.2	50.5	8.9	6.0	23.6	9.0
	6.2	50.3	9.1	5.9	25.8	9.2
Chiller	6.3	50.0	9.0	5.8	23.0	9.0
	6.5	50.2	9.2	6.0	25.0	8.5
	6.7	50.4	9.4	6.2	27.0	8.0
	6.2	49.8	9.1	5.9	29.0	8.3
	6.4	49.6	9.3	6.1	26.0	7.8
	6.6	50.0	9.5	6.0	28.0	7.3
CV-1	3.53	49.9	8.5	6.0	17.7	10.9
	3.3	49.9	8.6	6.0	17.5	16.0
FV-2	5.5	50.2	10.0	6.0	18.0	10.0
	5.0	50.0	10.5	6.1	19.0	10.5
	4.5	49.5	11.0	5.9	20.0	11.0
	4.0	50.1	11.0	6.0	18.5	12.0
	3.5	49.8	11.5	6.2	19.5	13.0
	3.0	50.1	12.0	6.1	20.5	14.0

The second way to get labeled data for the SSC model is to pick some samples from the test data set as labeled data. A noise term can be added as if the labeled data is obtained with another off-line test. For the normal hypothesis H_0 , every forty data points of the first data set are used as the labeled data. It is a valid method to produce the labeled data because the system can repeat the normal steady state operations to generate data. For the faults related to CV-12, heater, CV-34, and CV-1, only two data samples are picked from the corresponding test data sets as labeled training data. Values of the labeled data are summarized in Table 5-7 also. The reason that labeled data can be produced in such a way is that, for some fault scenarios, the actual effects can be physically tested or emulated. The frequency and severity of a test can be very limited to control the stress within the safety boundaries, but it provides a viable way to understand the real system dynamics.

The class labels estimated by the SSC model for the eight test runs with faults are shown in Figure 5-7. The fault locations are shown at the bottom of each plot. The horizontal axes of the plots are the number of samples which is equivalent to time in seconds.

For the fault due to FV-1 open, all the data are correctly classified to fault hypothesis H_1 except the first two data points. The first two data are classified as normal. Fault detection is triggered by low pressure which responds fast to opening of FV-1; however, changes in other parameters such as temperature could be slower. Therefore, at the beginning of the data set, unique symptoms due to the fault have not been fully developed, and the misclassification at the beginning is acceptable. The case for the fault of spurious open of CV-12 is similar to FV-1. The data at the beginning are misclassified as normal, but correct classification is achieved subsequently. The number of misclassified data is larger because the physical movement of CV-12 is slow. Therefore, it takes longer to simulate the fault on the NPCTF. The test data, the faults at CV-20, the heater, and CV-34 are correctly classified. For the chiller fault, fault detection is triggered by the vibration signal V2 as soon as the chiller is stopped. However, it takes much longer for the loss of cooling capacities to manifest in other process parameters, particularly temperature. Therefore, the first about 20 seconds of data are misclassified to normal which is reasonable. Fault detection will be delayed if the vibration sensor is not available, and the

correct diagnosis will appear sooner in the plot. The results for the two faults in CV-1 and FV-2 can be interpreted similarly.

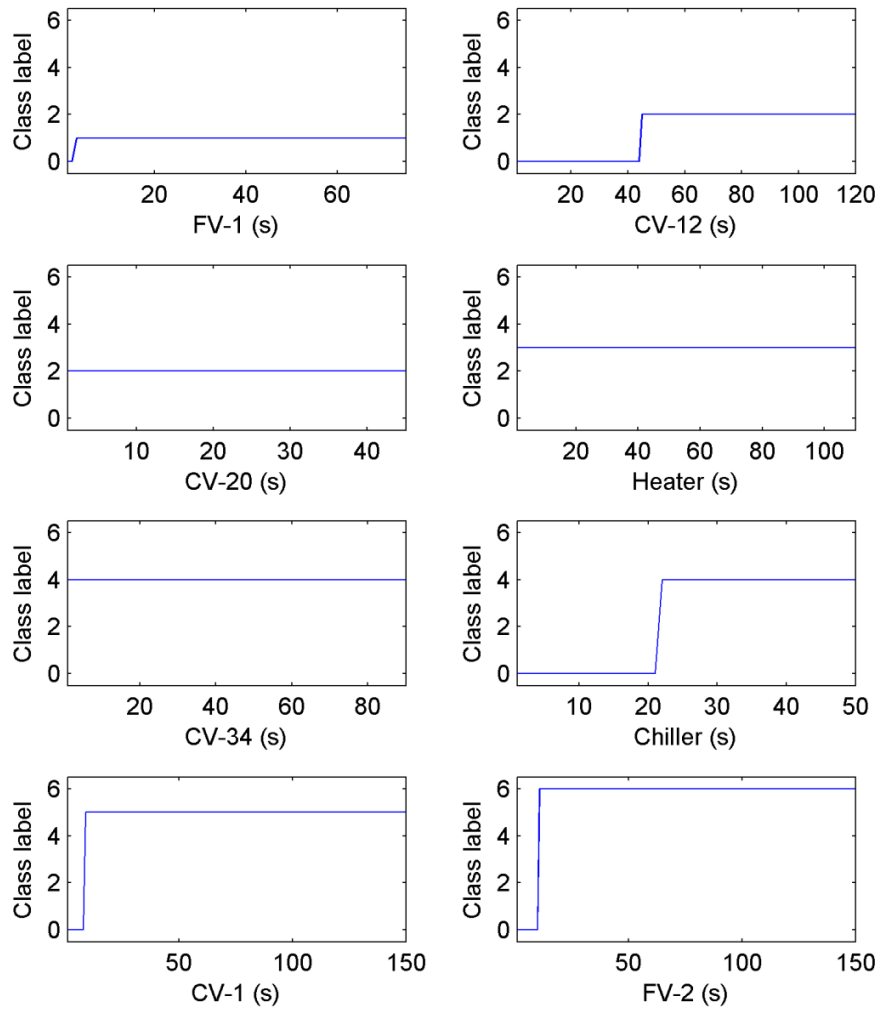


Figure 5-7: Estimated class labels of NPCTF test data

Furthermore, it is shown in Figure 5-7 that the test data for faults in CV-12 and CV-20 are all classified as class two in the SSC model which is loss of coolant inventory as summarized in Table 5-6. When a LOCI condition is diagnosed, the two possible faults can be easily separated by referring to the CV-12 opening signal of Po-12. It is demonstrated by the plot in Figure 5-8. Similarly, faults in CV-34 and chiller are all

diagnosed as the LOCC condition in the SSC model. Those two faults can be distinguished by the vibration signal V2.

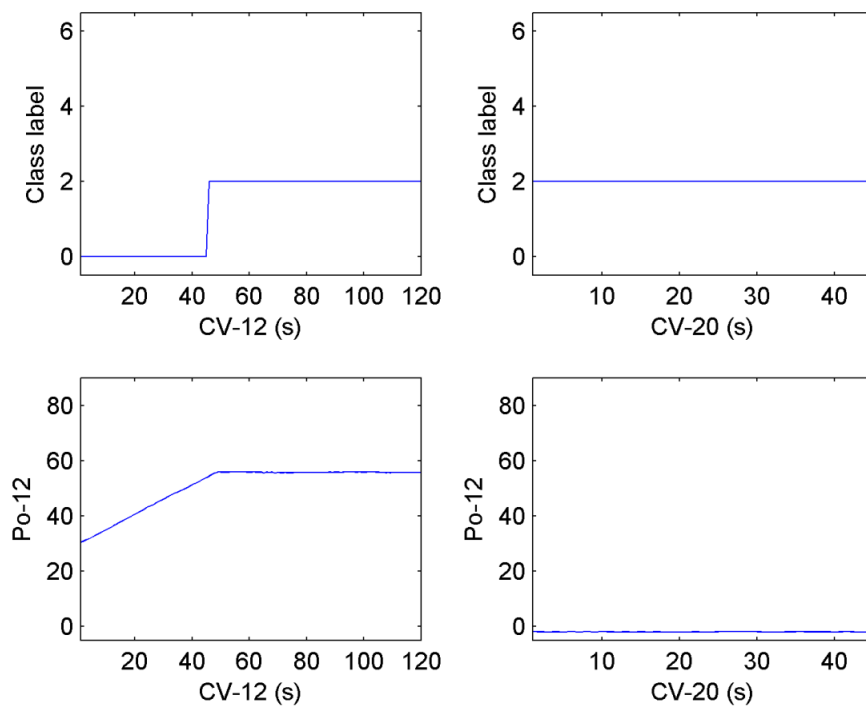


Figure 5-8: Diagnosis results of test data with loss of coolant inventory faults

The classification results of the test data sets are illustrated in Figure 5-9 using three variables F1, L3 and T2-T1. The labeled data points are shown in the figure as the larger size symbols, and the unlabeled data are shown as the smaller size symbols. In addition, different classes are represented using different symbol shapes and colors. For the data set with FV-1 fault shown as pink circles, it can be seen that the labeled data, shown as the larger size circles, has considerable uncertainties as compared to the measured data, shown as the smaller size circles. The reason is that the six labeled data points are generated based on coarse analysis of the relations among the variables without mathematical models or experimental tests. However, the experimental data with fault are correctly classified. The situation is similar for the data with fault at FV-2, shown as the black triangles. When the test data for the FV-1 fault and LOCI fault (including CV-12

open and CV-20 open) is compared, it can be seen that they all lead to decreased level L3 because of loss of inventory. FV-1 is obviously separated from the two faults considered as LOCI because of the different patterns in temperature response. FV-1 simulates a pipe break before the heater inlet. The actual coolant flow to cool the heater is reduced when FV-1 is open. Consequently, the temperature difference across the heater will increase considerably. The inventory loss through CV-12 and CV-20 does not reduce the flow through the heater. Therefore, the temperature difference is not affected significantly. The opening of CV-20 will actually increase the upstream coolant flow, which is similar to the case of FV-1 opening. However, the amount of increase is relatively small; thus, to distinguish the faults at CV-20 and CV-12 based on the information of flow increase is less reliable than the temperature difference. This is another reason to treat the two faults as one hypothesis in the SSC, besides the consideration of the model complexity. When the faults at CV-1 and FV-2 are concerned, their effects on the three variables used for the plot is similar. As a result, it can be seen that the two sets of data lie in the same region in the Figure 5-9. The two faults are separated by the different effects on coolant pressure, which will be illustrated later. The data with heater overpower are correctly classified.

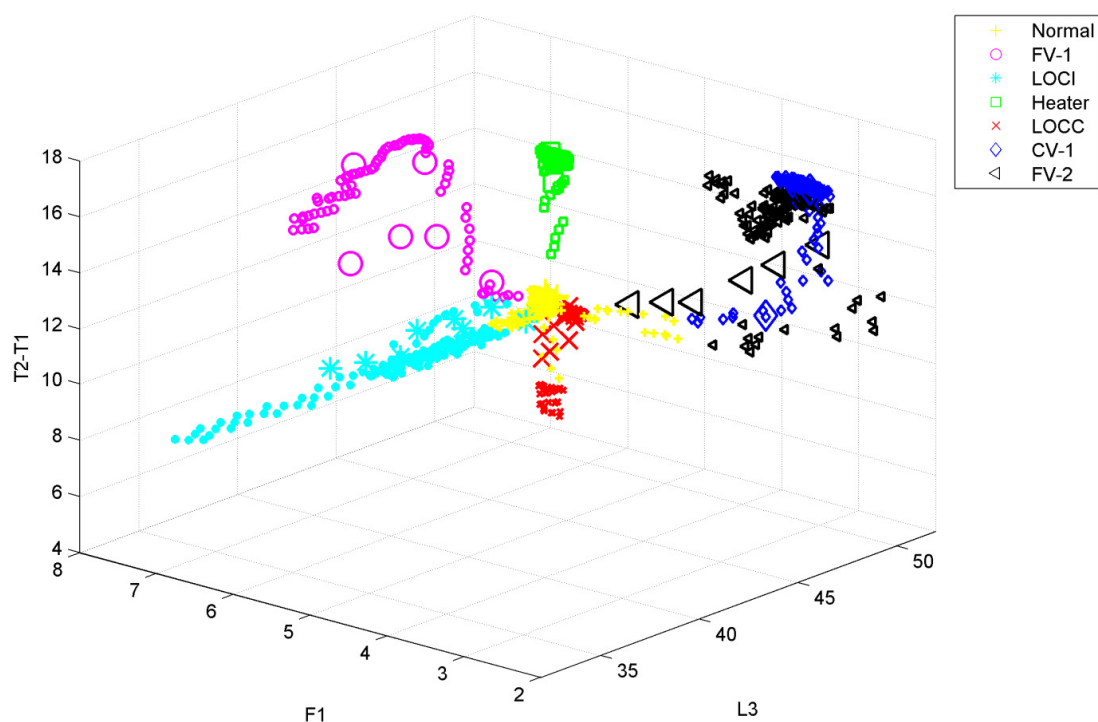


Figure 5-9: Illustration of the classification results of NPCTF test data

Classification results of the test data are further illustrated in Figure 5-10 using three variables P1, F1 and T1. The shapes and colors of the symbols are consistent with those in Figure 5-9. The differences between the data with CV-1 fault and FV-2 fault now become clear, as the FV-2 fault will lead to increased coolant pressure P1, but the CV-1 fault is accompanied by slight decrease in P1. The unique characteristics of the two faults (CV-34 close and chiller trip) considered as LOCC are also clearer in this plot. LOCC is the only hypothesis that will lead to abnormal increase in T1.

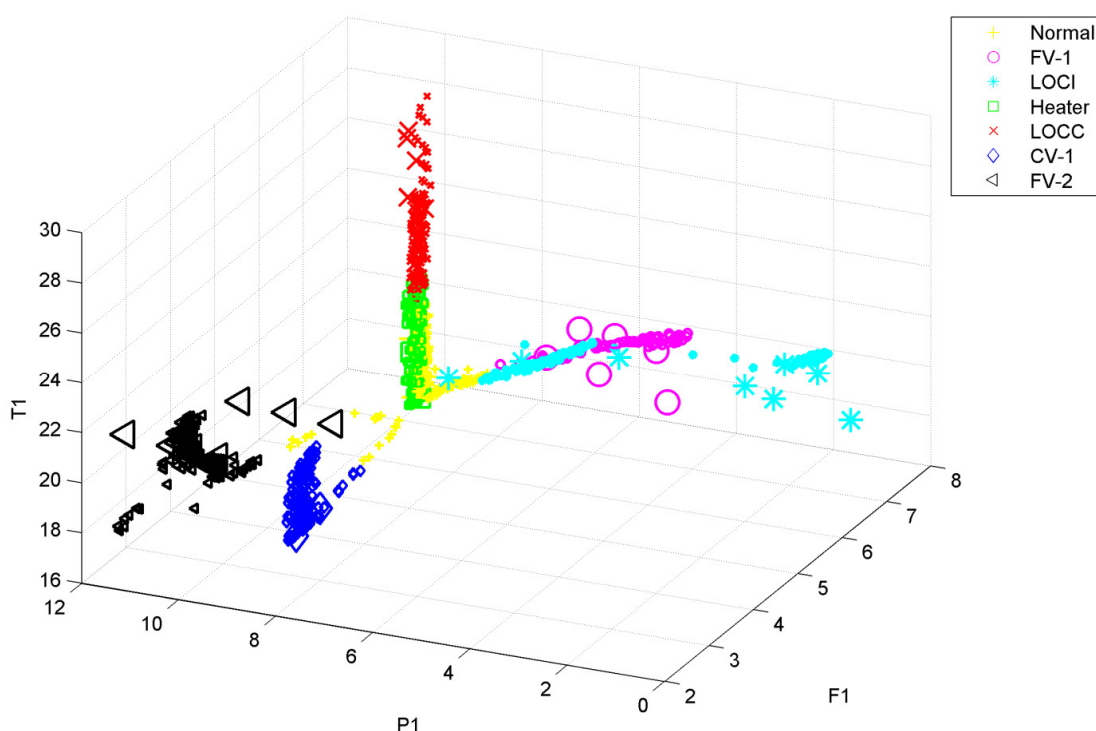


Figure 5-10: Further illustration of the classification results of NPCTF test data

Overall, satisfactory classification results of the eight fault scenarios are obtained using the SSC model. Considering the fact that the training data contains sizable uncertainties and the size of the labeled data is significantly smaller than that is typically required in a supervised model, the experimental tests demonstrated that the proposed SSC-based fault diagnosis scheme is a promising tool for diagnosis of process faults.

5.4 Conclusion

A fault diagnosis method based on semi-supervised classification is proposed for applications in NPP. Applications to a CANDU NPP using data from a training simulator and a physical NPP simulator show that, even though only a few labeled data with uncertainties are used to train a classification model, all faults considered can be correctly diagnosed. The experimental validations demonstrate that the proposed scheme is a promising tool for fault diagnosis in NPP, where it is usually difficult to obtain reliable training data for a supervised classification model.

In the experimental case studies, raw measurement data from the sensors are used directly as the inputs to the pattern classification model. However, in other fault diagnosis applications such as a system involving machine vibrations, features extracted from the raw data are often more suitable inputs to the pattern classification model. In fact, the quality of the feature extraction step has a direct impact on the performance of the subsequent analysis. Therefore, advancement to related signal processing algorithms is always an integral part to improvement in fault diagnosis performance. In the next chapter, a signal processing algorithm based on time-frequency analysis is proposed for applications involving time-varying and multi-component signals.

Chapter 6

6 Equipment Condition Monitoring using Modified S-Transform

This chapter deals with advanced signal processing methods for feature extractions as an integrated part of the process fault diagnosis framework illustrated in Figure 1-1. In this chapter, equipment condition monitoring based on processing of monitoring signals such as vibration is studied. As reviewed in Chapter 2, time-frequency analysis methods are increasingly used for this purpose. The S-transform is particularly suitable to study the time-frequency characteristics of a non-stationary signal. However, the standard ST has limitations for analysis of a signal with multiple components.

In this research, two methods for design of modified S-transform window functions are developed to improve the time-frequency localization performance. In the first method, the window width is represented by a sigmoid function, and its shape can be easily tuned in frequency domain; thus, greater control over the window width becomes feasible over a wide range of frequencies. As an illustrative example, a MST algorithm is developed based on a Gauss error function.

Following the idea of modifying the standard window function directly in the frequency domain, a second MST design method is proposed. In the frequency domain, a modified window is obtained as the product of the standard window function and an additional shaping function. Using the shaping function as a tuning tool, a series of MST with different characteristics can be obtained. In fact, other MST algorithms can be viewed as special cases of this general method. As an illustrative example, one MST algorithm is designed where the shaping function is the Fourier transform of another Gaussian window function. The width of the shaping function can be selected to achieve specified frequency localization.

The proposed MST algorithms have been successfully validated using signals from a physical vibration test system. Vibration signals containing different non-stationary characteristics, such as bursts and time-varying components across a wide range of frequencies, have been effectively captured. The results have convincingly shown that

the MST algorithms can indeed improve the time-frequency localization, as compared to both standard ST and classical methods such as STFT. The proposed MST algorithms have also been used for vibration monitoring of the NPCTF water pipes. The results indicate that the proposed algorithm can enhance the diagnostic capability of losing structure support for the pipe, as compared to the standard ST.

6.1 S-Transform for Time-Frequency Analysis

The S-Transform (ST) of a signal $x(t)$ is defined as (Stockwell et al., 1996)

$$ST(t, f) = \int_{-\infty}^{\infty} x(\tau) w(t - \tau) \exp(-j2\pi f \tau) d\tau \quad (6-1)$$

where $w(t)$ is a Gaussian window function expressed as follows

$$w(t) = \frac{1}{\sigma\sqrt{2\pi}} \exp\left(\frac{-t^2}{2\sigma^2}\right) \quad (6-2)$$

The parameter σ represents the window width in time domain. However, it is also a frequency-dependent quantity as

$$\sigma(f) = \frac{1}{|f|} \quad (6-3)$$

where f is the analysis frequency. Thus, the window function of a standard ST has the form

$$w(t) = \frac{|f|}{\sqrt{2\pi}} \exp\left(\frac{-f^2 t^2}{2}\right) \quad (6-4)$$

and the ST of $x(t)$ can be written as

$$ST(t, f) = \frac{|f|}{\sqrt{2\pi}} \int_{-\infty}^{\infty} x(\tau) \exp\left(\frac{-f^2 (t - \tau)^2}{2}\right) \exp(-j2\pi f \tau) d\tau \quad (6-5)$$

Using convolution principle, Eq. (6-5) can also be written as (Stockwell et al., 1996)

$$ST(t, f) = \int_{-\infty}^{\infty} X(\alpha + f)W(\alpha, f) \exp(j2\pi\alpha t) d\alpha = F^{-1}(X(\alpha + f)W(\alpha, f)) \quad (6-6)$$

where F^{-1} represents the inverse Fourier transform, $X(\alpha)$ is the Fourier transform of the signal $x(t)$, and $W(\alpha, f)$ is the Fourier transform of the window function $w(t)$ evaluated at the analysis frequency f as (Jeffrey, 2000)

$$W(\alpha, f) = \exp\left(\frac{-2\pi^2\alpha^2}{f^2}\right) \quad (6-7)$$

Eq. (6-6) indicates that, to compute $ST(t, f)$ at analysis frequency f , one needs to shift $X(\alpha)$ by $-f$, compute $W(\alpha, f)$, evaluate the product $X(\alpha + f)W(\alpha, f)$, and subsequently perform an inverse Fourier transform of $X(\alpha + f)W(\alpha, f)$. The frequency representation, $X(\alpha)$, needs to be evaluated only once and then shifted for different analysis frequencies. $X(\alpha + f)W(\alpha, f)$ can be viewed as a filtering operation on the shifted input signal $X(\alpha + f)$ by a band-pass filter $W(\alpha, f)$. The standard deviation of a Gaussian shaped window in frequency domain as in Eq. (6-7) is defined as the *window width* herein.

One issue associated with the standard ST, as shown in Eq. (6-7), is that the window width is the analysis frequency f . The frequency resolution deteriorates as the analysis frequency increases. This can be problematic when the signal being analyzed contains high frequency components. Furthermore, if the signal being analyzed is corrupted by additive noise, higher degree of artifacts would also appear in the higher frequency regions, which can skew the TFD (Pinnegar & Mansinha, 2003).

Different attempts have been made to modify the standard ST to achieve tradeoff in time and frequency resolution, particularly for high frequency regions. Two of the most acclaimed MST modification formulas in the literature are presented herein. The time domain window width is scaled by a parameter k in (Mansinha et al., 1997) as

$$\sigma(f) = \frac{k}{|f|} \quad (6-8)$$

Consequently, the window function becomes

$$W(\alpha, f) = \exp\left(\frac{-2\pi^2\alpha^2}{\left(\frac{f}{k}\right)^2}\right) \quad (6-9)$$

As shown, the window width becomes $\frac{f}{k}$ in the frequency domain. If the value of k is greater than unity, the resulting width will be narrower than that of the window in a standard ST. Therefore, the frequency resolution can be improved at the expense of time resolution due to the uncertainty principle (Papoulis, 1977). In (Assous & Boashash, 2012), the parameter k can be replaced by a linear function of the analysis frequency f for greater control over the window width. For convenience, a MST using a window in Eq. (6-9) will be referred to as the algorithm MST-1(k) herein in this chapter.

The window width can also be modified by a parameter p as in (Djurovic et al., 2008):

$$\sigma(f) = \frac{1}{|f|^p} \quad (6-10)$$

As a result, the frequency domain window function becomes

$$W(\alpha, f) = \exp\left(\frac{-2\pi^2\alpha^2}{f^{2p}}\right) \quad (6-11)$$

The frequency domain window width becomes f^p . For $p \in (0,1)$ the width is reduced to achieve improved frequency resolution with tradeoff in time resolution. Optimization procedures can be used to determine the most suitable p for the optimal energy concentration. A MST based on Eq. (6-11) will be referred to as algorithm MST-2(p) herein for convenience.

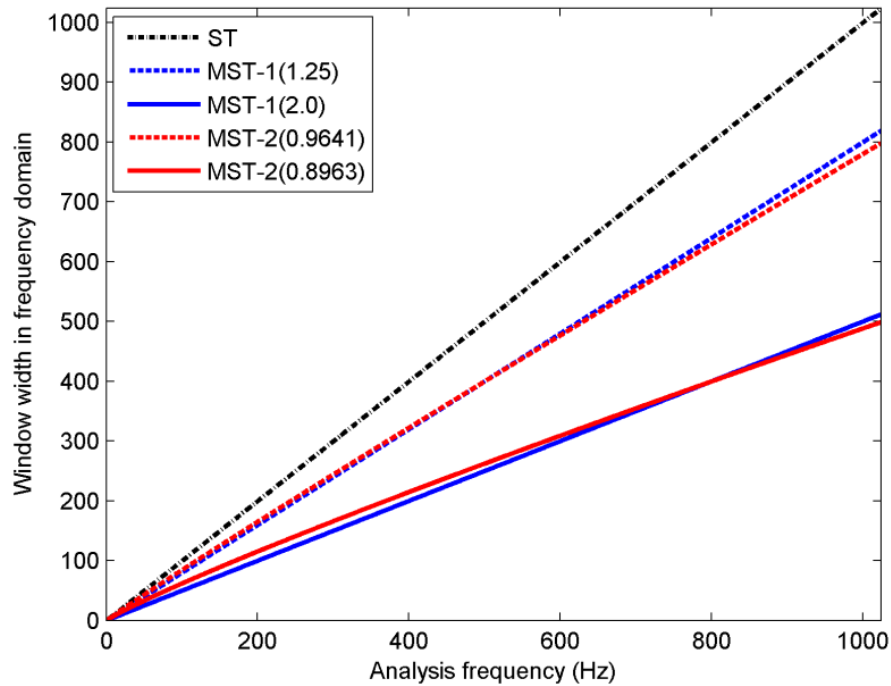


Figure 6-1: Frequency domain window width of two MST algorithms

The window widths of standard ST and MST-1 and MST-2 with two different tuning parameters are shown as a function of the analysis frequency in Figure 6-1. They are known as the window width profile herein. MST-1 has a linear window width profile for a given value of the tuning parameter as indicated in Eq. (6-9). MST-2 also has an approximate linear window width profile for a chosen tuning parameter. Since the time-frequency resolution tradeoff is directly controlled by the window width, the time-frequency localization capabilities of MST-1 and MST-2 could vary considerably at different frequency regions. As a result, a parameter optimal for one signal component may produce unacceptable results for another signal component in a different frequency region.

A simple example could be used to highlight such deficiencies. Suppose a signal has three frequency components at 800 Hz, 500 Hz, and 100 Hz. Furthermore, assume that a frequency domain window width of 400 will be considered to be desirable for time-

frequency resolution for both the 800 Hz and 500 Hz components, but a standard window width of 100 is acceptable for 100 Hz component.

As shown in Table 6-1, if the tuning parameters are selected optimal for 500 Hz component, MST-1 and MST-2 will have window width of 640 and 629, respectively, for the 800 Hz component, which are considerably wider than desirable. This can lead to deteriorated frequency localization. Similarly, if the tuning parameters are optimized for 800 Hz component, MST-1 and MST-2 will end up with window width of 250 and 262, respectively, for the 500 Hz component, which are too narrow in this case. Consequently, it leads to unacceptable time resolution. For 100 Hz component, both MST-1 and MST-2 have narrower than desired window widths.

Table 6-1: Frequency domain window widths of two MST for example frequencies

Algorithm	$f=800$ Hz	$f=500$ Hz	$f=100$ Hz
Desired window width	400	400	100
MST-1(1.25)	640	400	80
MST-2(0.9641)	629	400	85
MST-1(2.0)	400	250	50
MST-2(0.8963)	400	262	62

The desirable window is identical to ST in the low frequency region, i.e. a linear width profile. In the medium and high frequency regions, the desirable profile is essentially a flat line with a width of 400, so that the 500 Hz and 800 Hz components have the same time-frequency resolutions. The joint profile cannot be conveniently achieved with the existing MST algorithms. Therefore, a MST with greater tuning flexibilities of the window width profile will be beneficial improvement for effective analysis of such signals with multiple components.

6.2 Modified S-transform

In this paper, a sigmoid function of the analysis frequency $S(f, \beta)$ is chosen to be the general window function as

$$\sigma(f) = \frac{1}{S(f, \beta)} \quad (6-12)$$

where β represents a collection of tuning parameters to control the shape of a sigmoid function $S(f)$. The window will have a frequency domain width of $S(f, \beta)$. As f increases from zero to the maximum analysis frequency f_m , $S(f, \beta)$ also increases from zero to a maximum value with a shape similar to the right side half of a sigmoid curve. To use the Gauss error function as an example, $S(f, \beta)$ can be defined as

$$S(f) = a * f_m * \text{erf}\left(\frac{b * f}{f_m}\right) \quad (6-13)$$

where a and b are two tuning parameters and $\text{erf}(x)$ is the Gauss error function defined as

$$\text{erf}(x) = \frac{2}{\sqrt{\pi}} \int_0^x \exp(-t^2) dt \quad (6-14)$$

A MST using Eq. (6-13) as the window width function will be referred to as algorithm MST-3 (a, b) herein in this chapter.

The main advantage of a sigmoid function is that it can realize different window width profiles simply by varying tuning parameters. As for MST-3(a, b), parameter a controls the amplitude and parameter b controls shape of the profile. A greater value of a will result in a wider width window in frequency domain. The effect of the parameter b is illustrated in Figure 6-2. As b increases, the window width grows faster at low frequencies and then reaches a flatter tail across the higher frequencies. In addition, the differences in the window width between medium frequency regions and high frequency regions become smaller. Therefore, for a signal with components at both medium and high frequencies, a greater b can potentially result in a satisfactory time-frequency resolution for a range of signal components.

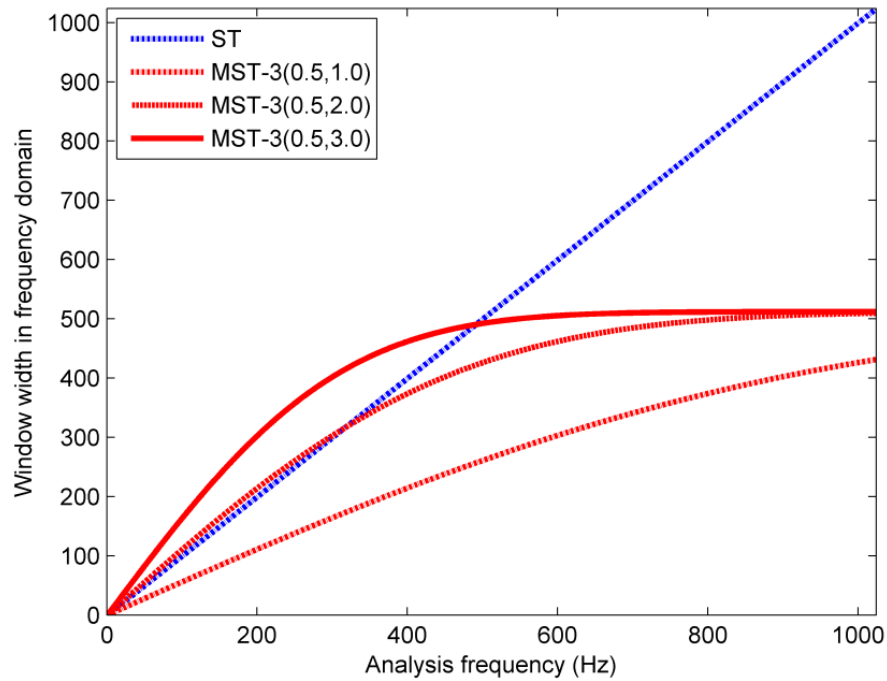


Figure 6-2: Effect of parameter b for MST-3(a, b)

Tuning flexibilities of MST-3 is further demonstrated in Table 6-2 using the earlier example. It can be observed that, as far as the window width is concerned, MST-3 with tuning parameters (0.9315, 0.5) is very similar to MST-1(2.0) and MST-2(0.8963) in Table 6-1. Likewise, MST-3(1.4462, 0.5) is similar to MST-1(1.25) and MST-2(0.9641). However, if the tuning parameters are chosen to be (0.4, 2.2), the window widths of MST-3 become significantly closer to the desired values.

Table 6-2: Frequency domain window width of MST-3 for example frequencies

Model	$f=800$ Hz	$f=500$ Hz	$f=100$ Hz
Desired window width	400	400	100
MST-3(0.9315, 0.5)	400	258	53
MST-3(1.4462, 0.5)	621	400	82
MST-3(0.4, 2.2)	403	357	98

To obtain an even more flexible window width profile, a user-defined function can be fitted. First, the shape of a desirable window profile can be sketched by specifying

window widths for some critical analysis frequencies. A smooth curve (e.g., polynomial) connecting the user-specified points can then be fitted. This approach gives flexibility to obtain any shapes desirable for a specific application.

A window shaping method for MST to meet specific frequency localization is also developed. A modified frequency domain window function $\hat{W}(\alpha, f)$ is obtained as the product of the standard window $W(\alpha, f)$ and a shaping function $\tilde{W}(\alpha, f)$:

$$\hat{W}(\alpha, f) = W(\alpha, f) \tilde{W}(\alpha, f) \quad (6-15)$$

For simplicity, $W(\alpha, f)$, $\tilde{W}(\alpha, f)$, $\hat{W}(\alpha, f)$ will be referred to as the original window, shaping function, and modified window, respectively.

By choosing a desired shaping function, one can ensure that $\hat{W}(\alpha, f)$ meets the needs of specific applications. This concept will be illustrated through design of a MST with a specific width of \hat{f} for a signal component at f Hz. For this purpose, a Gaussian shaping function is selected. One advantage of a Gaussian shaping function is that the product of multiple Gaussian functions is still Gaussian. Suppose the width of the shaping function is f_0 , Eq. (6-15) can be rewritten as

$$\hat{W}(\alpha, f) = \exp\left(\frac{-2\pi^2\alpha^2}{f^2}\right) \exp\left(\frac{-2\pi^2\alpha^2}{f_0^2}\right) = \exp\left(-2\pi^2\alpha^2\left(\frac{1}{f_0^2} + \frac{1}{f^2}\right)\right) \quad (6-16)$$

As shown, width of the modified window \hat{f} is related to f_0 as

$$\frac{1}{\hat{f}^2} = \frac{1}{f_0^2} + \frac{1}{f^2} \quad (6-17)$$

Substitute the application specific numbers of f and \hat{f} into Eq. (6-17) will give the solution of f_0 and, thus, the shaping function. For example, if the window width of 400 is needed for a signal at 800 Hz, using Eq. (6-17), one can obtain $f_0 = 462$.

Subsequently, the shaping function can be chosen as $\tilde{W}(\alpha, f) = \exp(\frac{-2\pi^2\alpha^2}{462^2})$. A MST with a window function described in Eq. (6-16) will be called algorithm MST-4(f_0) herein.

For the example in Table 6-1, a shaping function is designed to achieve the desirable window width profile. For this purpose, a shaping function is selected as

$$\tilde{W}(\alpha, f) = \begin{cases} 1, & f \leq f_0 \\ \exp(\frac{-\pi^2\alpha^2}{2}(\frac{1}{f_0^2} - \frac{1}{f^2})), & f > f_0 \end{cases} \quad (6-18)$$

which leads to the modified window of

$$\hat{W}(\alpha, f) = \begin{cases} \exp(\frac{-\pi^2\alpha^2}{2f^2}), & f \leq f_0 \\ \exp(\frac{-\pi^2\alpha^2}{2f_0^2}), & f > f_0 \end{cases} \quad (6-19)$$

Choosing $f_0 = 400$ Hz leads to the window width of 400, 400, and 100 for the 800 Hz, 500 Hz and 100 Hz signal, respectively, which satisfies the desired frequency localization exactly.

If interpreted in the frequency domain, many other MST algorithms can be considered as special cases of Eq. (6-15). For MST-1, it can be shown that

$$\hat{W}(\alpha, f) = \exp(\frac{-2\pi^2\alpha^2 k^2}{f^2}) = W(\alpha, f) \exp(-2\pi^2\alpha^2(\frac{k^2}{f^2} - \frac{1}{f^2})) \quad (6-20)$$

Similarly for MST-2,

$$\hat{W}(\alpha, f) = \exp(\frac{-2\pi^2\alpha^2}{f^{2p}}) = W(\alpha, f) \exp(-2\pi^2\alpha^2(\frac{1}{f^{2p}} - \frac{1}{f^2})) \quad (6-21)$$

And for MST-3,

$$\hat{W}(\alpha, f) = \exp\left(\frac{-2\pi^2\alpha^2}{S(f)^2}\right) = W(\alpha, f) \exp\left(-2\pi^2\alpha^2\left(\frac{1}{S(f)^2} - \frac{1}{f^2}\right)\right) \quad (6-22)$$

Even though the design concept for a modified window using a shaping function is straightforward, determination of the best shaping function for a specific application can still be challenging.

6.3 Experimental Validations

In this section, performance of the proposed MST-3 and MST-4 algorithms is validated using a physical vibration test system. The setup for the vibration test platform is shown in Figure 6-3. Vibration signals are generated by a U56001 vibration generator. Input signals to the vibration generator are produced by an arbitrary waveform generator. Sinusoidal input signals with the continuous, burst, and sweep type waveforms are used. The vibration is measured by a PCB353B33 accelerometer, and the signals are acquired through a NI 9234 USB data acquisition module at a sampling rate of 2 kHz. Case studies involved in the validations are briefly summarized in Table 6-3.

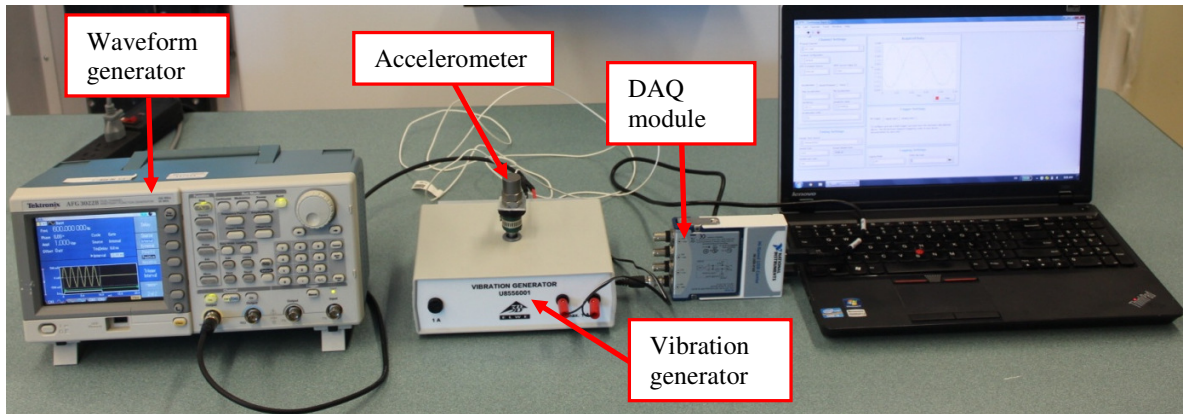


Figure 6-3: Setup of vibration test system

Table 6-3: Summary of experimental case studies using vibration test system

Case study	Purpose	Signal components	Related figures and tables
I	Demonstrate advantages and necessities of MST	Two bursts	Figure 6-4 and Figure 6-5
II	Validate MST-4	One burst	Figure 6-6 and Table 6-4
III	Illustrate tuning flexibility of MST-3	Constant with several frequencies	Figure 6-7, Table 6-5 and Table 6-6
IV	Validate performance of MST-3 as compared to existing MST algorithms and classical TFA techniques	Two bursts and one constant	Figure 6-8 and Figure 6-9
V	Demonstrate performance of MST-3 and MST-4 for a different type of signal	One sweep and one constant	Figure 6-10
VI	Test performance of MST-3 for signals with lower signal to noise ratio (SNR)	Constant at 700Hz	Figure 26 and Table 34

Case study I

Advantage of MST over standard ST is illustrated using a vibration signal with two trains of burst components. The first component $x_1(t)$ has a central frequency of 750 Hz and a period of 15ms. The second component $x_2(t)$ has a central frequency of 500 Hz and a period of 15ms. The combined signal $x(t)$ can be expressed in Eq. (6-23)

$$\begin{aligned}
 x_1(t) &= \begin{cases} \sin(2\pi 750t), t \in [2n, 2n+1) \times 7.5ms \\ 0, t \in [2n+1, 2(n+1)) \times 7.5ms \end{cases} \\
 x_2(t) &= \begin{cases} \sin(2\pi 500t), t \in [2n, 2n+1) \times 7.5ms \\ 0, t \in [2n+1, 2(n+1)) \times 7.5ms \end{cases} \\
 x(t) &= x_1(t) + x_2(t)
 \end{aligned} \tag{6-23}$$

where t is time, $n = \{0, 1, 2, 3, \dots\}$ is a non-negative integer sequence, and ms stands for a million seconds. The signal components are generated independently by the waveform generator and normalized to unity standard deviations.

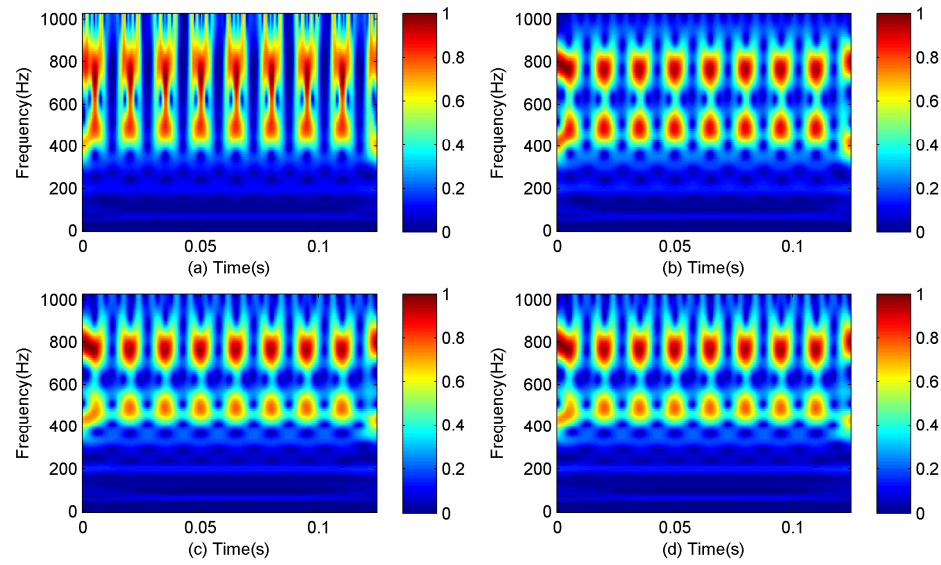


Figure 6-4: Results of case study I as TFDs produced by (a) ST; (b) MST-3(0.4, 2.2); (c) MST-2(0.9083); and (d) MST-1(1.8345)

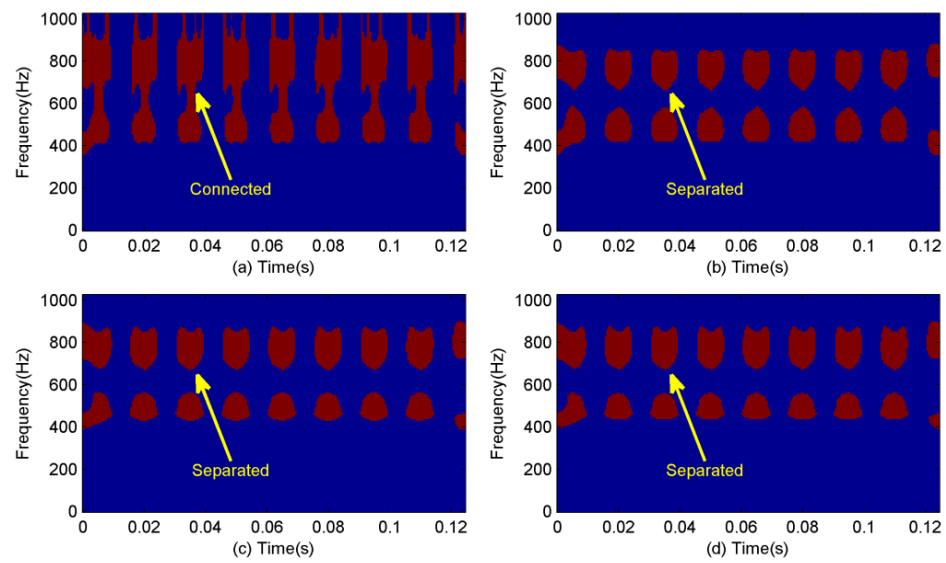


Figure 6-5: Threshold of the results in Figure 6-4 at 0.5

TFDs of the signal $x(t)$ are computed by ST, MST-3(0.4, 2.2), MST-2(0.9083), and MST-1(1.8345). The tuning parameters are selected so that the three MST models have the same width for the 750 Hz component for consistency. No optimization is used here. A section of the TFD results (125ms) are normalized and presented in Figure 6-4. As far as the two burst components are concerned, the TFDs of ST are connected in frequency and the bursts become non-distinguishable. This can further be seen in Figure 6-5 where results in Figure 6-4 are processed by a threshold at 0.5. As shown in the rest of Figure 6-4 and Figure 6-5, other MST algorithms are capable of separating the two components due to the improved frequency resolution for high frequencies.

Case study II

To validate performance of MST-4, a burst similar to a single component in Eq. (6-23) is generated with the central frequency at 800 Hz. A section of the TFDs produced by ST, MST-4(462), MST-2(0.8963), and MST-1(2.0) are presented in Figure 6-6. The widths of the MST windows are chosen to be 400 for the 800 Hz signal component for cross-validation purposes.

As can be seen from Figure 6-6, MST-4, MST-2 and MST-1 all produce improved frequency localization over ST, due to the fact that they all have reduced window width in this region. To quantify the frequency localization performance, the average frequency range is measured where the amplitude of the TFDs in Figure 6-6 is over 0.5. The results for all four windows are summarized in Table 6-4. It can be seen that MST-4 improved the index to 163.7 from 296.4 of ST, which is an improvement of almost 45%.

Differences between the result of MST-4 and those of MST-2 and MST-1 are less than 1%. This is due to the fact that all three MST models have the same width at 800 Hz and similar profiles in the nearby region. Table 6-4 demonstrated that the shaping function designed for MST-4 met the design objective satisfactorily.

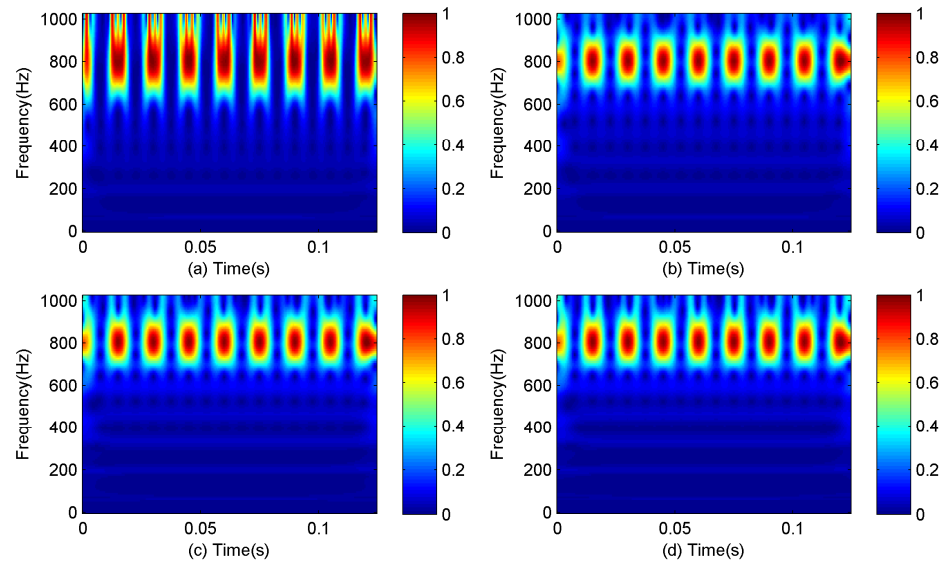


Figure 6-6: Results of case study II as TFDs produced by (a) ST; (b) MST-4(462); (c) MST-2(0.8963); and (d) MST-1 (2.0)

Table 6-4: Frequency localization index for the data shown in Figure 6-6

Signal	ST	MST-4(462)	MST-2(0.8963)	MST-1(2.0)
800 Hz	296.4 Hz	163.7 Hz	164.4 Hz	165.2 Hz

Case study III

Tuning flexibilities of MST-3 have already been illustrated in Table 6-2 and Figure 6-2. It is further demonstrated using Table 6-5 with more analysis frequencies. The cases presented in Table 6-5 are further implemented by physical experiments using the vibration test system and the results are presented in Figure 6-7. The previously defined frequency localization index is used to quantify the results in Figure 6-7, and the findings are summarized in Table 6-6.

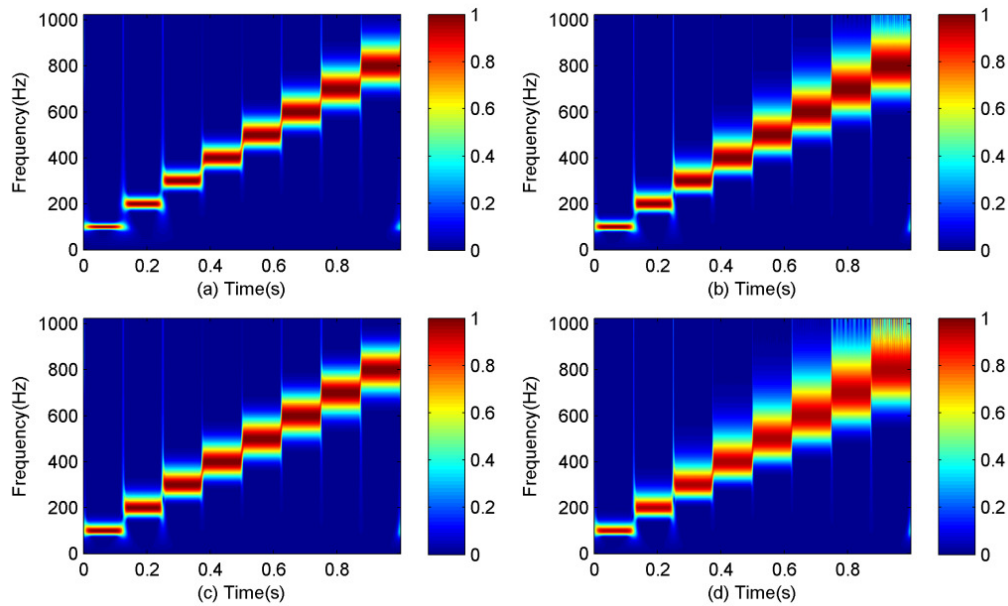


Figure 6-7: Results of case study III as TFDs produced by (a) MST-3(0.9315, 0.5); (b) MST-3(1.4462, 0.5); (c) MST-3(0.4, 2.2); and (d) standard ST

Table 6-5: Frequency domain window widths for three MST-3 parameter settings

Analysis frequency	MST-3 (0.9315,0.5)	MST-3 (1.4462,0.5)	MST-3 (0.4,2.2)	ST
100 Hz	53	82	98	100
200 Hz	105	163	187	200
300 Hz	157	243	261	300
400 Hz	208	322	318	400
500 Hz	258	400	357	500
600 Hz	307	476	382	600
700 Hz	354	550	395	700
800 Hz	400	621	403	800

Table 6-6: Frequency localization index for the data shown in Figure 6-7

Analysis frequency	MST-3 (0.9315,0.5)	MST-3 (1.4462,0.5)	MST-3 (0.4,2.2)	ST
100 Hz	20	32	38	37
200 Hz	39	62	72	74
300 Hz	59	93	99	111
400 Hz	78	123	119	148
500 Hz	98	153	133	186
600 Hz	116	182	142	223
700 Hz	133	209	148	260
800 Hz	151	236	151	299

As discussed before, MST-3 (0.9315, 0.5) and MST-3 (1.4462, 0.5) both have approximate linear window width profiles. It means the frequency localization index will become increasingly bigger as the analysis frequency becomes higher. The difference between the two is the rate of increase. Those features are confirmed by the second and third columns in Table 6-5 and Table 6-6. They can also be observed from the TFDs shown in Figure 6-7(a-b). With the tuning parameters (0.4, 2.2), the window width profile of MST-3 is nonlinear with a fast increase at low frequencies, and it becomes flatter for higher frequencies. The nonlinearity can be observed in the fourth column of Table 6-5 and Table 6-6. For example, with a 100 Hz increase in analysis frequency, the performance index in Table 6-6 has an increase of about 19, 29, and 37 for MST-3(0.9315, 0.5), MST-3(1.4462, 0.5), and ST, respectively, for the whole frequency range. However, MST-3(0.4, 2.2) has an increase of 34 in the low frequency end, which is similar to ST, but the increase is only 3 in the high frequency end. Those observations support the fact that MST-3 enables greater tuning flexibility for a wider range of analysis frequencies.

Case study IV

The advantage of the greater tuning flexibility of MST-3 is demonstrated through this case study. In this case, the signal contains two burst components with a period of 10ms and one continuous component with a constant frequency at 100 Hz. The signal can be expressed as Eq. (6-24)

$$\begin{aligned}
 x_1(t) &= \begin{cases} \sin(2\pi 750t), t \in [2n, 2n+1) \times 5.0ms \\ 0, t \in [2n+1, 2(n+1)) \times 5.0ms \end{cases} \\
 x_2(t) &= \begin{cases} \sin(2\pi 400t), t \in [2n, 2n+1) \times 5.0ms \\ 0, t \in [2n+1, 2(n+1)) \times 5.0ms \end{cases} \\
 x_3(t) &= \sin(2\pi 100t) \\
 x(t) &= x_1(t) + x_2(t) + x_3(t)
 \end{aligned} \tag{6-24}$$

TFDs of the signal are plotted in Figure 6-8. As shown in Figure 6-8 (b), the MST-3 algorithm generally has improved energy concentration for the signal components as compared to the standard ST in Figure 6-8. The two burst components in both time and

frequency can be distinguished. The reason for this is that the window width profile has been tuned to have a flat shape across the high and medium frequency regions. There is freedom to choose the width amplitude for optimal resolution tradeoff in those regions. In contrast, when MST-2 and MST-1 are designed to have similar frequency resolution for the 750 Hz signal component (as shown in Figure 6-8(c) and Figure 6-8(d)) time resolution for the 400 Hz component deteriorated to the extent that the burst becomes indistinguishable in the time domain. Likewise, when MST-2 and MST-1 are tuned to have similar time resolution for the 400 Hz component, as shown in Figure 6-8(e) and Figure 6-8(f), frequency resolution for the 750 Hz component has been compromised considerably. Overall, MST-3 has the best tradeoff in time-frequency resolution.

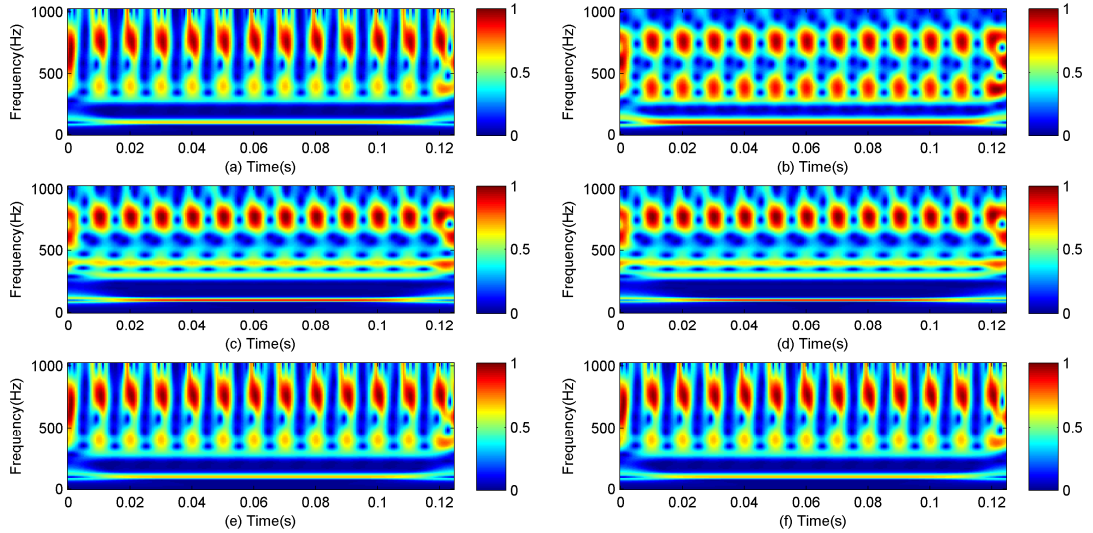


Figure 6-8: Results of case study IV as TFDs produced by a) ST; (b) MST-3 (0.42, 3.0); (c) MST-2 (0.9157); (d) MST-1 (1.7472); (e) MST-2 (0.995); and (f) MST-1 (1.03)

To compare MST-3 with classical TFA algorithms, TFDs of the signal used in Figure 6-8 are also computed using STFT and smoothed pseudo Wigner-Ville distribution (SPWVD). The results of STFT are shown in Figure 6-9. It is seen that a STFT with a narrow time domain window ($\sigma = 0.0017$) will have a poor frequency resolution for

the 100 Hz signal component while a larger window width (sigma = 0.0078) will lead to loss of time resolution for the burst signals. The SPWVD has difficulty detecting the burst signals and the results are not shown here for the interest of space. This study shows that MST-3 has clear advantages for time-frequency localization compared to the mentioned classical algorithms.

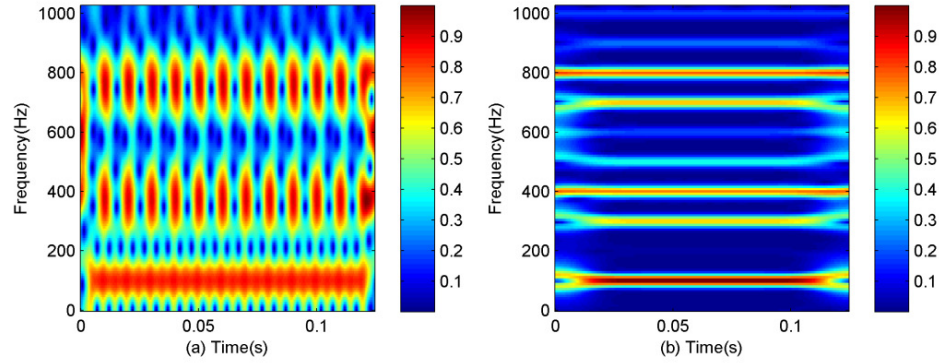


Figure 6-9: TFDs produced by short-time Fourier transform for the signal in Fig. 8 using (a) narrow time domain window and (b) wide time domain window

Case study V

Up to now, burst type signals were mainly used to validate the MST algorithms. To examine their performance with respect to other types of non-stationary signals, two vibration signals are generated with sweep type waveforms (Chirp signals). The first sweep signal, as shown in Eq. (6-25), has a start frequency of 200 Hz and a stop frequency of 750 Hz, with a rise time of 50ms and a return time of 50ms. The second sweep signal, as shown in Eq. (6-26), also has a start frequency of 200 Hz and a stop frequency of 750 Hz. However, it has a rise time of 50ms, a hold time of 25ms and a return time of 50ms. A continuous signal component with a constant frequency of 100 Hz is also added to illustrate performance at low frequency regions.

$$\begin{aligned}
 x_1(t) &= \begin{cases} \sin(2\pi(200 + 11t)t), & t \in [2n, 2n+1) \times 50ms \\ \sin(2\pi(750 - 11t)t), & t \in [2n+1, 2(n+1)) \times 50ms \end{cases} \\
 x_2(t) &= \sin(2\pi 100t) \\
 x(t) &= x_1(t) + x_2(t)
 \end{aligned} \tag{6-25}$$

$$\begin{aligned}
 x_1(t) &= \begin{cases} \sin(2\pi(200 + 11t)t), t \in [5n, 5n + 2) \times 25ms \\ \sin(2\pi 750t), t \in [5n + 2, 5n + 3) \times 25ms \\ \sin(2\pi(750 - 11t)t), t \in [5n + 3, 5(n + 1)) \times 25ms \end{cases} \\
 x_2(t) &= \sin(2\pi 100t) \\
 x(t) &= x_1(t) + x_2(t)
 \end{aligned} \tag{6-26}$$

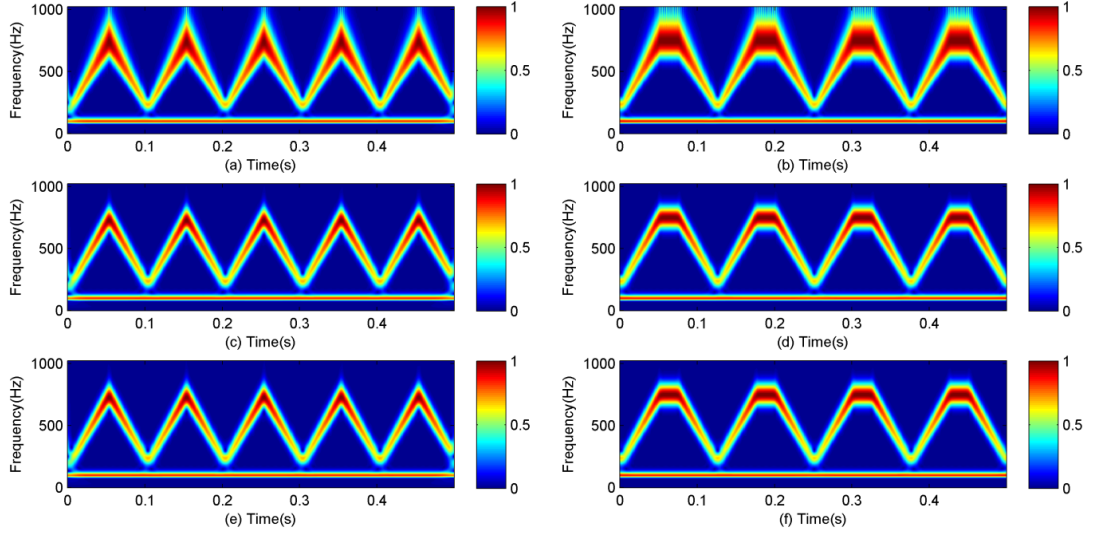


Figure 6-10: TFDs of sweep signals produced by (a) ST for sweep signal one; (b) ST for sweep signal two; (c) MST-3(0.4, 2.2) for sweep signal one; (d) MST-3(0.4, 2.2) for sweep signal two; (e) MST-4(462) for sweep signal one; and (f) MST-4(462) for sweep signal two

TFDs of the two signals are presented in Figure 6-10 and compared with the standard ST. For both signals, the frequency localizations of ST become increasingly dispersive as the frequency increases. In contrast, MST-3 [Figure 6-10(c) & (d)] and MST-4 [Figure 6-10(e) & (f)] can track the time-varying signals well across the entire frequency range with noticeably improved frequency resolution at high-frequency regions. At the same time, both MST-3 and MST-4 can distinguish the continuous component satisfactorily.

Case study VI

In this case study, the MST-3 algorithm is tested for signals with different signal to noise ratios (SNRs). For this purpose, a constant vibration signal at 700Hz is acquired from the vibration test system. Two Gaussian noise terms are added to the vibration signal independently to generate test signals with different SNRs. In the first case, the standard deviation of the noise is half of that of the vibration signal, i.e., the test signal has a SNR of approximately 6 dB. In the second case, the standard deviation of the noise is set equal to the vibration signal; thus, the test signal has a SNR of 0 dB.

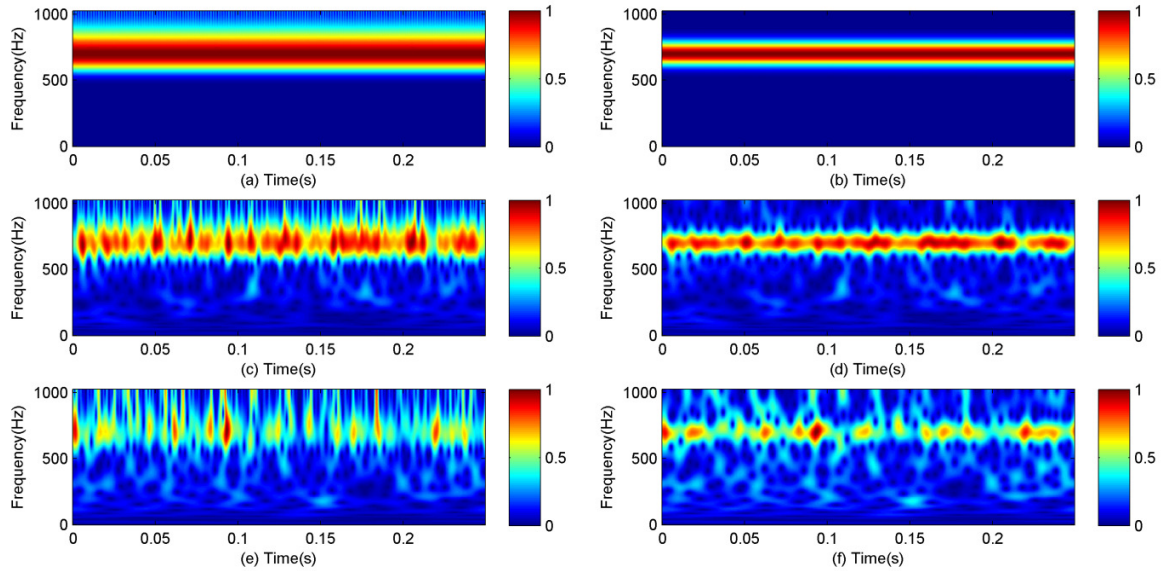


Figure 6-11: Comparison of TFDs with different SNRs for (a) ST without noise; (b) sigmoid MST (0.4, 2.2) without noise; (c) ST with 6 dB SNR; (d) sigmoid MST (0.4, 2.2) with 6 dB SNR; (e) ST with 0 dB SNR; and (f) sigmoid MST (0.4, 2.2) with 0 dB SNR.

TFDs of the test signals are computed using ST and MST-3(0.4, 2.2), and the results are plotted in Figure 6-11. Without additional noise, ST [Figure 6-11(a)] and MST-3 [Figure 6-11(b)] both produce clean TFDs, with MST-3 possessing finer frequency localization. As the SNR decreases with the increased level of noise, the TFDs of ST [Figure 6-11(c) & (e)] become increasingly noisier especially in the high frequency regions. MST-3 [Figure 6-11(d) & (f)] is also affected by the decreased qualities of the test signals.

However, when it is compared with the standard ST, it can be observed that the energy concentration of MST-3 is improved over ST. The improvement in performance is consistent for test signals with different SNRs.

The frequency localization performance of the tests shown in Figure 6-11 is quantified by the index defined in *case study II*. The experiments are repeated ten times, and the average frequency location indices are summarized in Table 6-7. It can be seen that the MST-3 algorithm has considerably improved frequency localization for all three scenarios.

Table 6-7: Frequency localization index for vibration signals with different SNRs

Analysis method	No additional noise	6 dB SNR	0 dB SNR
ST	272	204	183
Sigmoid MST (0.4, 2.2)	148	122	105

Besides the vibration test system, the MST-3 algorithm is used for vibration monitoring of a water pipe on the NPCTF, as illustrated in Figure 6-12. The system mainly consists of a water storage tank, a Jabsco 31820 diaphragm pump, and pipes and valves to supply water to three loops. The vibration DAQ system shown in Figure 6-3 is used to measure pipe vibrations near the pump outlet. A structural pipe support is installed near the vibration sensor. The support can be deliberately removed to simulate a fault. A picture of the actual system is shown in Figure 6-13. The pump has four piston-diaphragm units, and its speed is dependent on outlet pressure. Experiments show that the pump vibration mainly consists of a burst type signal around 400 Hz during strokes.

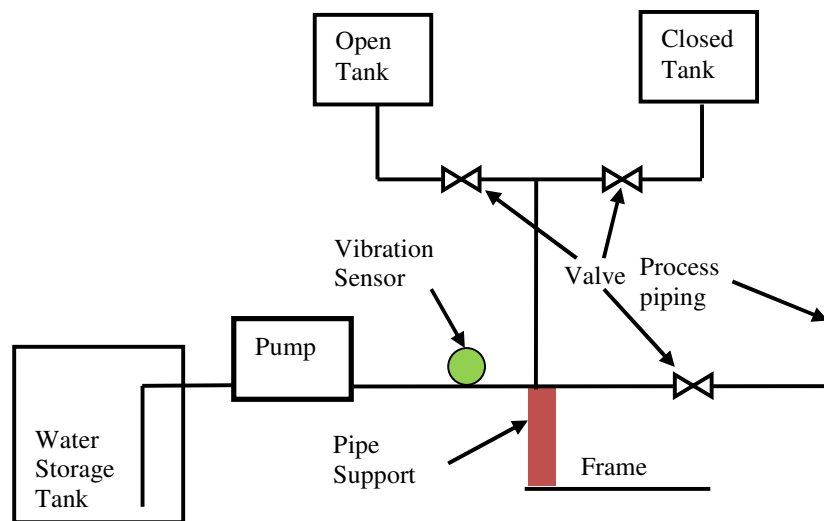


Figure 6-12: Illustration of the pipe vibration monitoring system

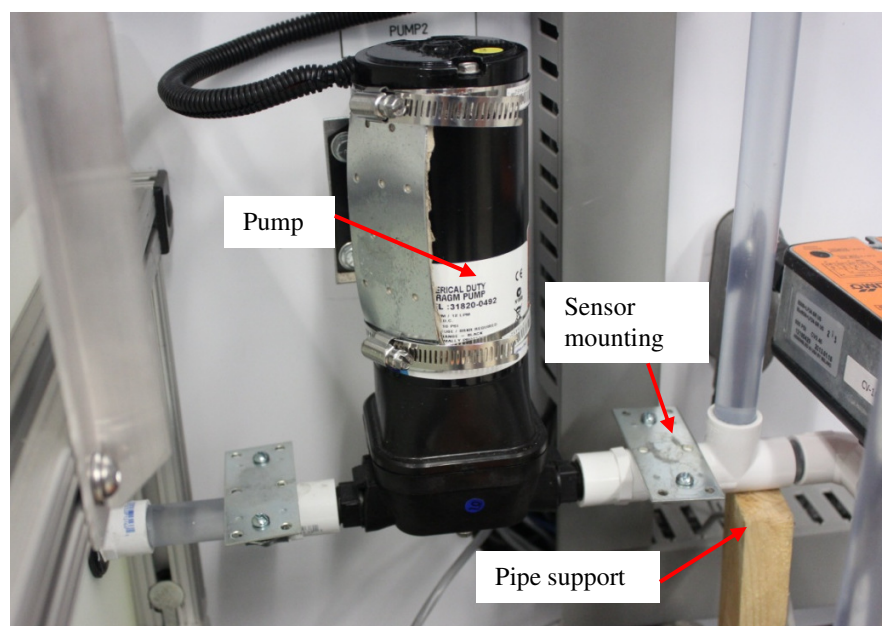


Figure 6-13: Picture of the pipe vibration monitoring system

The objective of the tests is to validate the effectiveness of the proposed MST-3 algorithm for characterization of real world signals for condition monitoring and fault detection. For this purpose, several tests with different pump speeds and structural support scenarios have been carried out. The pump speed can be changed by setting different valve openings in the downstream of the pump. Collapsed structural support is simulated by removing the pipe support. Results for four tests are summarized in Table 6-8. The results from the first two tests are discussed in more detail.

Table 6-8: Summary of pipe vibration tests

Test number	Pump speed	Pipe support
I	Low	Yes
II	Low	No
III	High	Yes
IV	High	No

TFDs of pipe vibration Test-I are shown in Figure 6-14(a-b). Results after imposing a threshold to the TFDs at 0.368 are represented in Fig. 6-14(c-d). It can be observed that the vibration signal consists of two burst type components. The component at the lower frequency is consistent with the pump vibration. The second component has a frequency of about 800 Hz. Comparing Figure 6-14 (c) and Figure 6-14(d), it becomes clear that MST-3 (0.3, 2.0) apparently has improved frequency localization for the higher frequency signal component, which is further confirmed in Table 6-9.

The frequency localization capabilities of ST and MST-3 are listed in Table 6-9 as the average frequency range where signal is considered in Figure 6-14(c) and Figure 6-14(d). Time localization is defined in a similar fashion and listed in Table 6-9. MST-3 enables enhanced analysis of the vibration in terms of frequency localization; for example, MST-3 produces a localization index of 50.4, while ST is 113.9 for 800 Hz component. Furthermore, the trade-off in time resolution is acceptable considering that MST-3 gives sufficient time details to distinguish and localize the bursts. For example, it can be obtained that the time interval between two consecutive bursts is about 3.9ms, which is consistent for both MST-3 and standard ST.

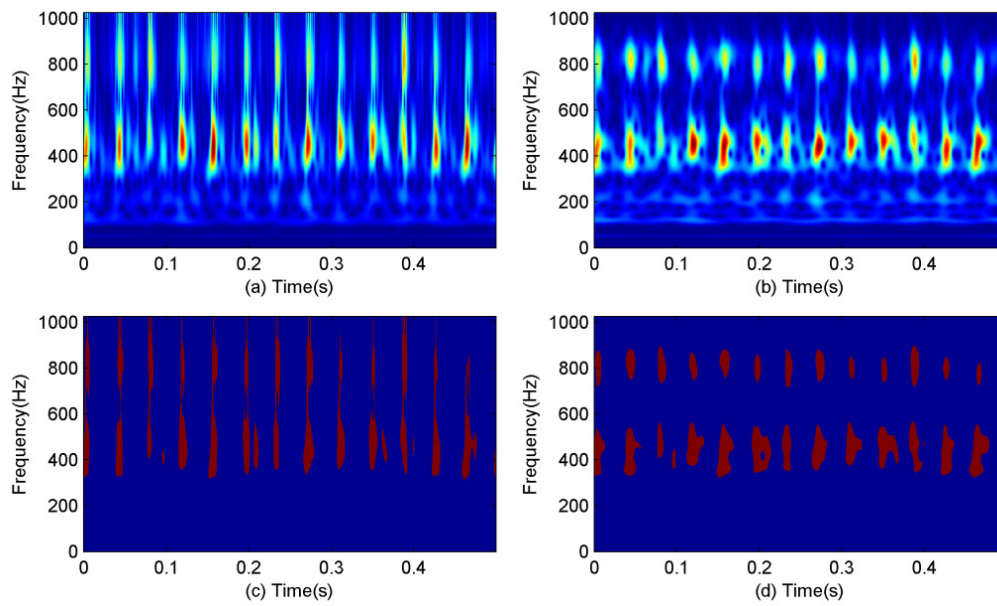


Figure 6-14: Results of pipe vibration Test-I as TFDs produced by (a) ST and (b) MST-3(0.3, 2.0). The TFDs are threshold at 0.368 and shown in (c) for ST and (d) for MST-3(0.3, 2.0)

Table 6-9: Time and frequency localization index for pipe vibration Test-I

Localization index	Signal component	MST-3(0.3, 2.0)	S-transform
Frequency (Hz)	400 Hz	60.3	84.5
Frequency (Hz)	800 Hz	50.4	113.9
Time (ms)	400 Hz	10.0	7.0
Time (ms)	800 Hz	5.1	3.3

The results of pipe vibration Test-II are presented in Figure 6-15. TFDs for the 400 Hz component remain similar. It can be seen that the 800 Hz component disappeared and a new burst type component at 230 Hz is detected. Figure 6-15(d) shows that the 230 Hz component can be distinguished from the 400 Hz one by MST-3. However, they are indistinguishable in ST as shown in Figure 6-15(c).

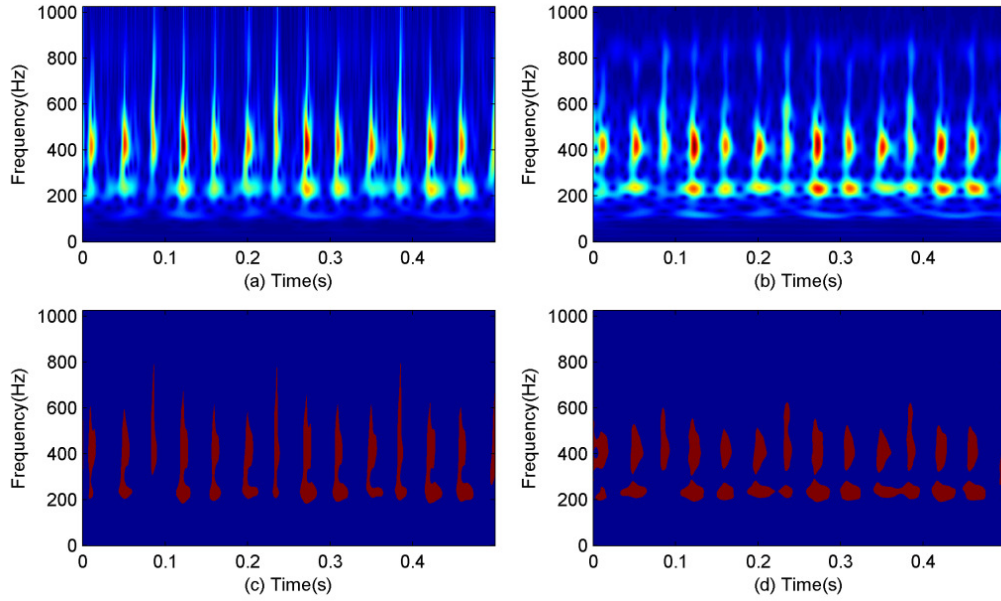


Figure 6-15: Results of pipe vibration Test-II as TFDs produced by (a) ST and (b) MST-3(0.3, 2.0). The TFDs are threshold at 0.368 and shown in (c) for ST and (d) for MST-3(0.3, 2.0)

Results of pipe vibration Test-III and Test-IV are collectively represented in Figure 6-16. It is seen that the vibration signal contains components similar to the cases of low speed, but the time interval between the two bursts is much shorter at about 1.6ms. In Figure 6-16, it can be seen that the TFD of ST is too dispersive in the high frequency regions to provide reliable indication of the signal frequency. In comparison, MST-3, as shown in Figure 6-16(b), concentrates the signal energy to a narrower range near 800 Hz. At the same time, MST-3 is able to distinguish the other burst at lower frequency with time-frequency resolution comparable to ST. Similarly for Test-IV as shown in Figure 6-16(c-

d), MST-3 also has enhanced time-frequency concentration to locate the signal components.

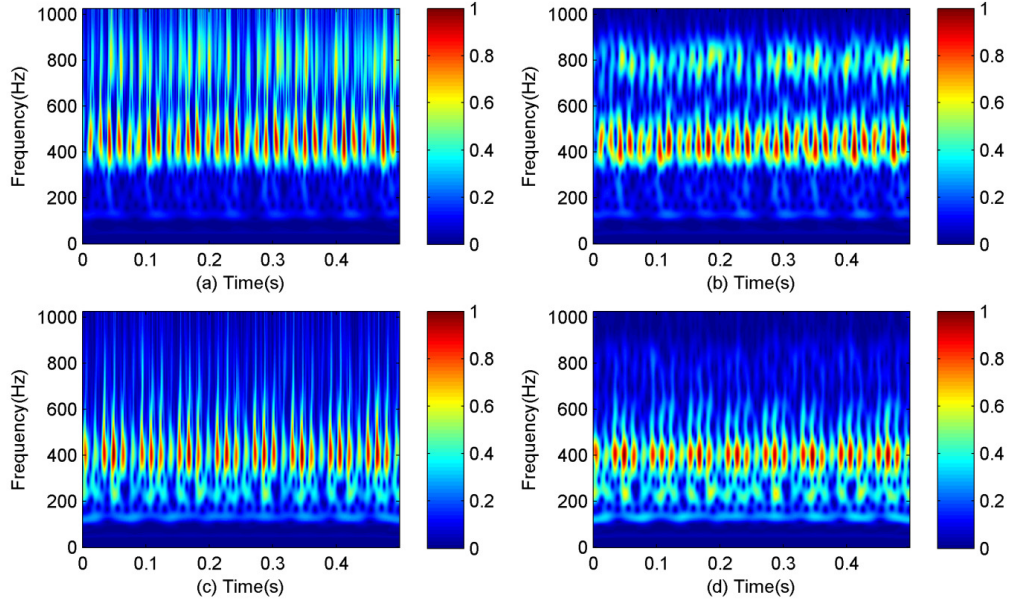


Figure 6-16: Results of pipe vibration test -III and test-IV as TFDs produced by (a) ST for test-III; (b) MST-3(0.3, 2.0) for test-III; (c) ST for test-IV; and (d) MST-3(0.3, 2.0) for test-IV

The test results successfully demonstrate that the MST-3 algorithm is capable of characterizing the pipe vibration under normal conditions. The results have also indicated that MST-3 can indeed enhance the fault diagnostic capability of standard ST.

Note that a threshold is used to compute the frequency localization index. With a higher threshold, the frequency localization index will be smaller. Thus, the index will be greatly influenced by the selected threshold. However, setting a universally acceptable threshold is difficult, because the presence or absence of a signal can be application dependent. Domain specific knowledge may be required to make a sensible choice. In the current example, the results of the standard S-transform and the modified S-transform are affected in the same way as the threshold varies.

6.4 Conclusion

The proposed MST algorithms make it possible for users to design desirable windows to meet specific frequency localization requirements for a given application. Furthermore, using a sigmoid function, the modified window design problem has effectively been reduced to selection of some tuning parameters. With a prior knowledge of the signal being analyzed for a given application, optimization techniques can be used to facilitate the window design process. The experimental validation results using vibration signals show that the new window design methods can provide superior time-frequency resolution for time-varying signals with multiple components, where the classical time-frequency analysis methods and standard S-transform method may fail. The results have also shown that, by observing changes in characteristics of the TFD of vibration signals, one can effectively detect faults occurred in components of an industrial system.

A pattern classification model has been successfully validated in Chapter 5 and a signal processing algorithm is tested satisfactorily in this chapter. Nevertheless, the performance of the experiments used in those two studies is dependent on the fact that the sensory data used therein are fault-free. If the measurement data is affected by sensor faults, erroneous fault diagnosis results can be induced. Therefore, it is very important to ensure that the sensors used for a fault diagnosis system are in good conditions. In the next chapter, a sensor validation method based on the KPCA algorithm is studied.

Chapter 7

7 Sensor Validations using KPCA

This chapter deals with sensor validations as step ten of the process fault diagnosis framework illustrated in Figure 1-1. Several methods have been developed for FDI in sensors. A popular practice is to install redundant sensors, where a sensor can be cross checked with the redundant measurements to detect fault. With triple redundancies, a faulty sensor can be isolated from the remaining good ones. However, increased cost and complexity are associated with the increased number of sensors. Another approach is to use analytical redundancy to estimate the output of a sensor from correlated sensors. Data-driven models have been successfully used for this purpose and PCA is one of the most used techniques. As reviewed in Chapter 2, the kernel PCA model has been developed as a generalization of PCA. However, KPCA still has limitations for sensor FDI, particularly for isolation of multiple sensor faults.

In this chapter, a need for sensor validation is first illustrated using the fault diagnosis experiments discussed in Chapter 5. A sensor FDI scheme based on KPCA is then studied.

7.1 Sensor Faults on Diagnosis Performance

In this section, case studies are carried out using the NPCTF system to show influences of the sensor validation module on the fault classification performance. In the case studies, sensor faults are added to NPCTF sensors. The SSC model discussed in Chapter 5 is repeated with faulty sensor readings and the results are compared against the normal results. It is shown that considerable false classifications are induced by the sensor faults. Therefore, integration of the sensor validation module is important to ensure satisfactory performance of the fault diagnosis system.

In the case studies, sensor bias is added to NPCTF sensor measurements. The erroneous data are substituted into the SSC model presented in Chapter 5. Influences of the sensor faults are checked by comparing the classification results with the normal results shown

in Figure 5-7 of Chapter 5. The results of four case studies, as summarized in Table 7-1, are presented.

Table 7-1: Summary of case studies with sensor faults

Case study	Faulty sensor	Magnitude of bias
I	T2	3.0 °C
II	T2	-3.0 °C
III	P1	2.5 psi
IV	P1	-2.5 psi

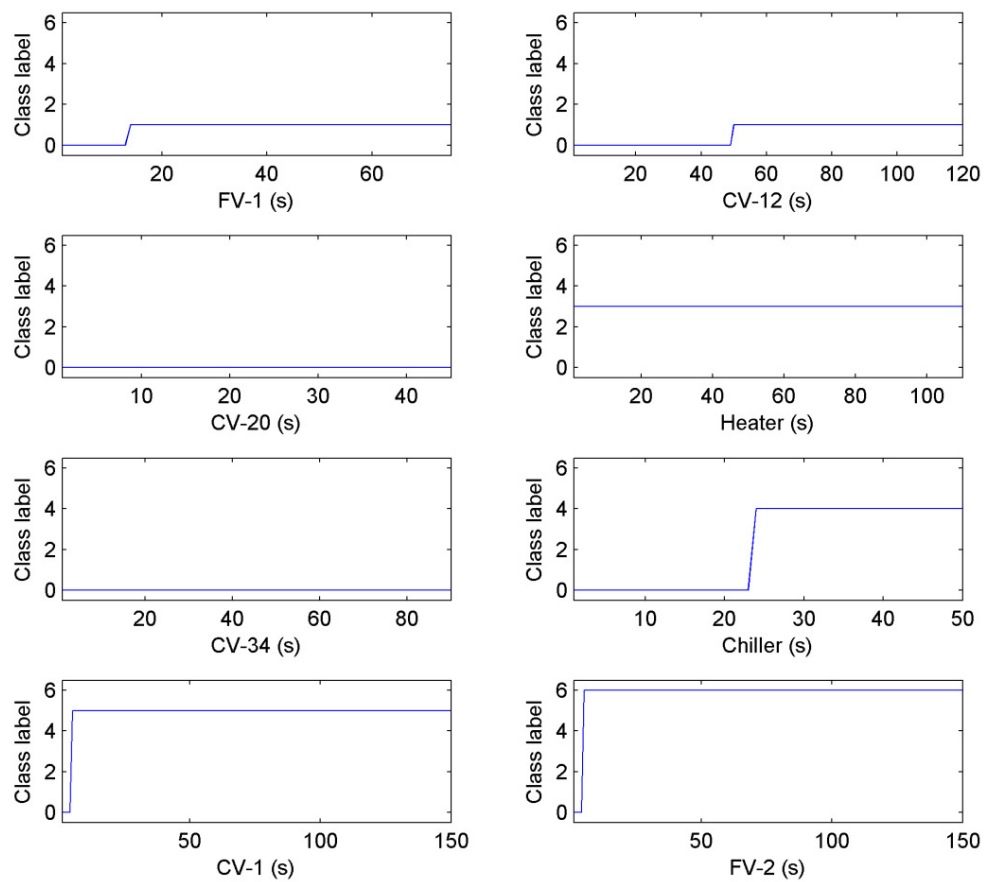


Figure 7-1: Classification results of NPCTF test data with positive bias in T2

In *case study I*, the same sets of test data used in Chapter 5 to validate the SSC model are used. However, a bias of 3.0 °C is added to the sensor T2. Test data containing erroneous

T2 measurements are then substituted into the same SSC model. The classification results are presented in Figure 7-1. By comparing the results in Figure 7-1 with those in Figure 5-7, it can be observed that the FV-1 fault is correctly classified, but with longer delays. The two faults associated with CV-12 and CV-20 are classified wrongly. So is the case for the fault with CV-34. Results for the other faults are not altered significantly. This case study shows that a sensor fault can have profound impact on the performance of a fault diagnosis model.

Case study II is carried out in a similar fashion, but the magnitude of the bias in T2 is set to -3.0°C . The classification results of the test data are shown in Figure 7-2. By comparison with the previous case study and the normal results, it can be observed that four of the faults (CV-12, CV-20, heater, and chiller) are completely misdiagnosed.

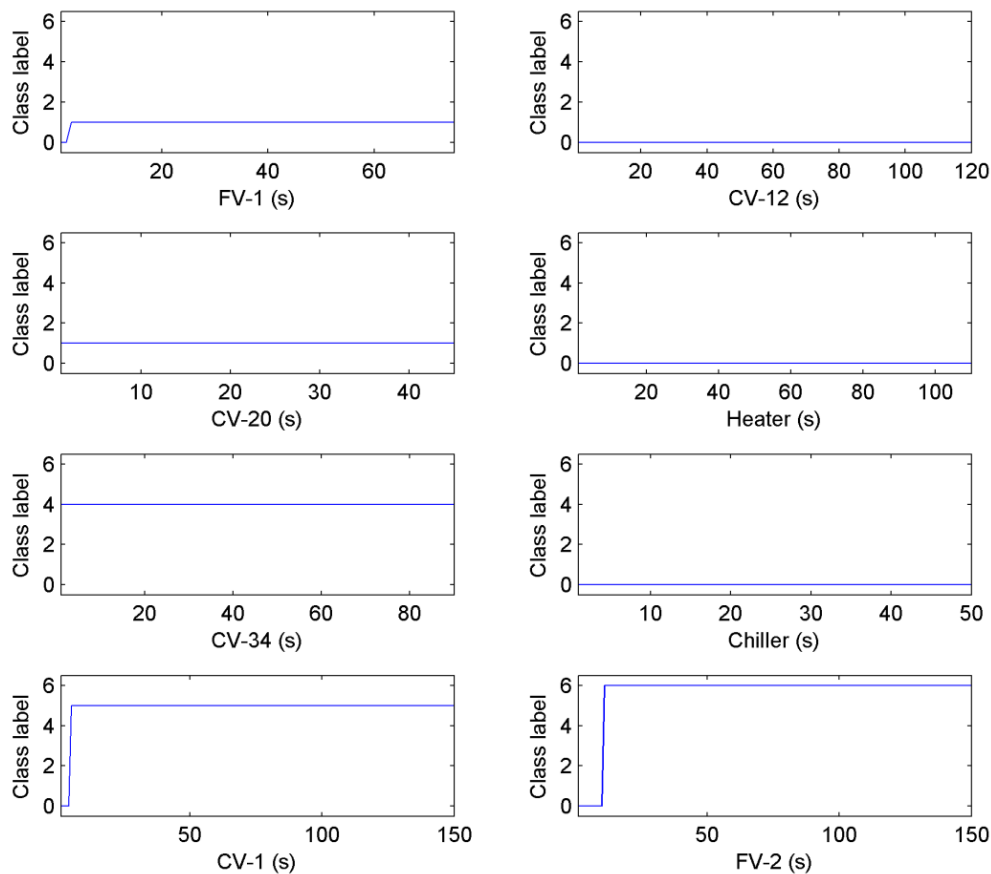


Figure 7-2: Classification results of NPCTF test data with negative bias in T2

The results for *case study III* and *case study IV* are shown in Figure 7-3 and Figure 7-4, respectively. Effects of the sensor faults on the classification performance vary, but the same conclusions drawn from the previous two case studies are supported that a faulty sensor can lead to considerable incorrect fault diagnosis results. Therefore, it is important to include a sensor validation module in a fault diagnosis system.

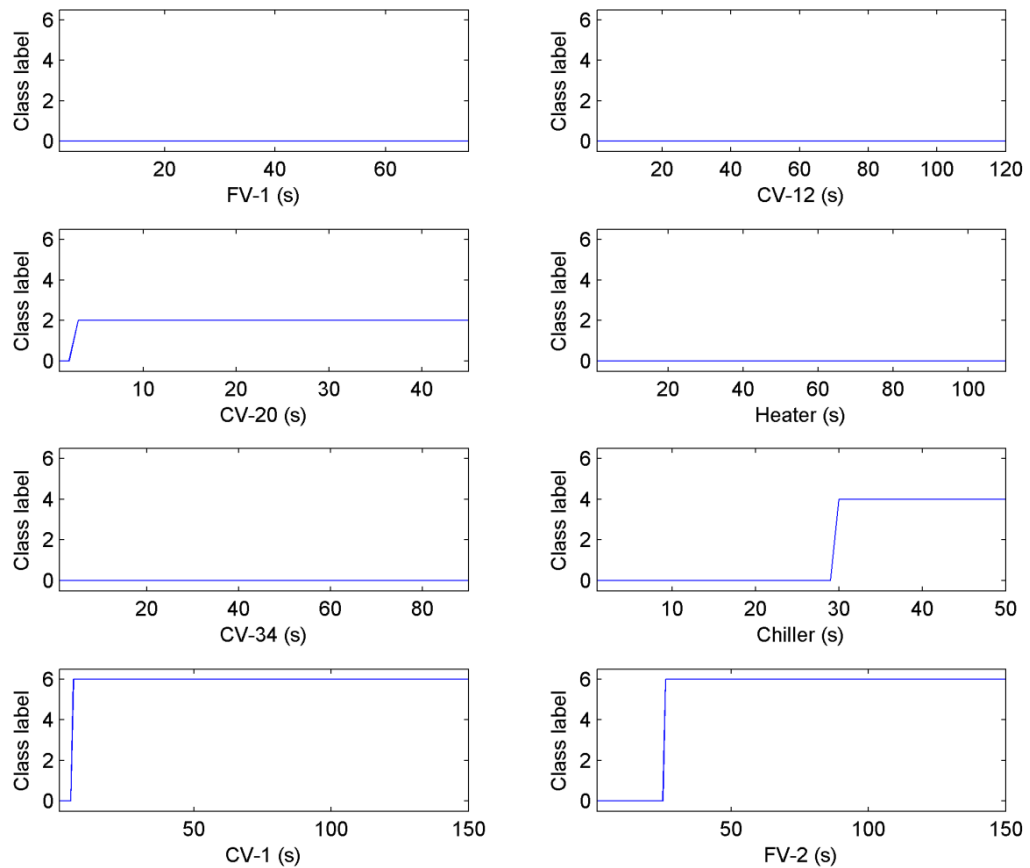


Figure 7-3: Classification results of NPCTF test data with positive bias in P1

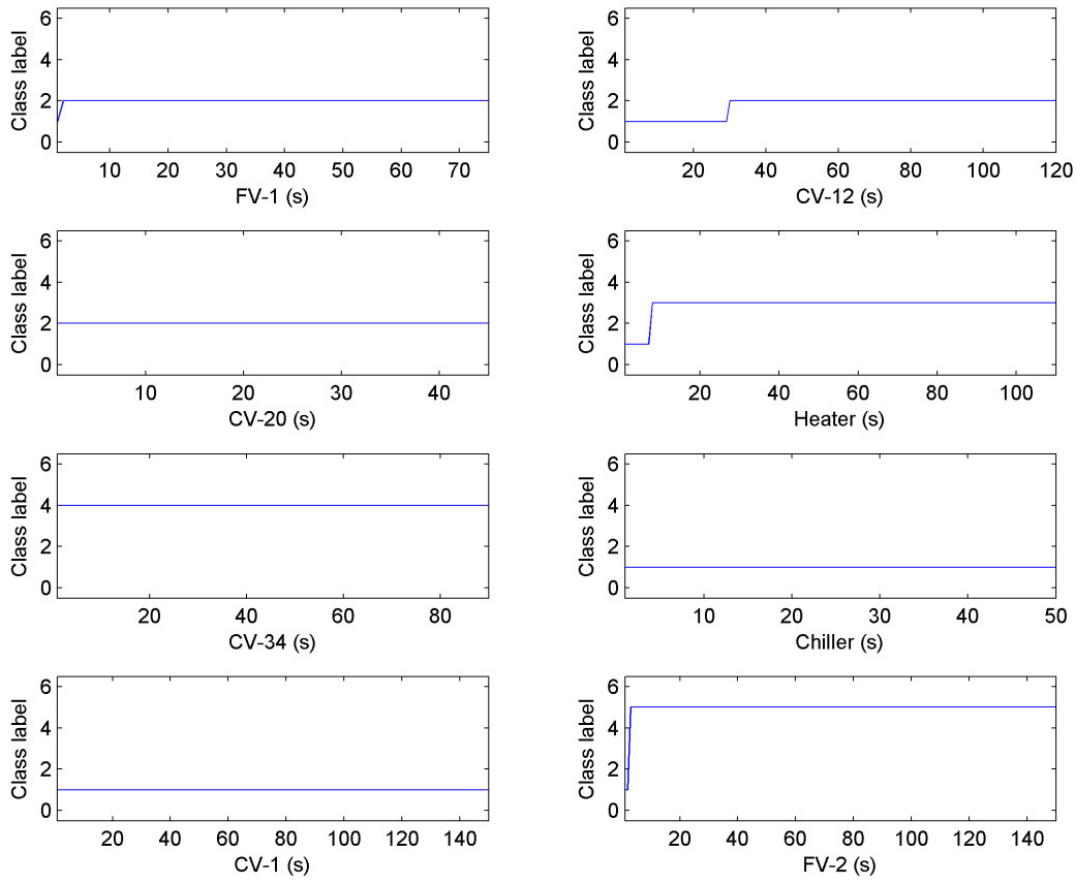


Figure 7-4: Classification results of NPCTF test data with negative bias in P1

7.2 Sensor Fault Detection and Isolation using KPCA

In this section, a sensor FDI method based on KPCA is developed. The method is validated using real measurements from a NPP.

7.2.1 KPCA for sensor FDI

In this research, KPCA is applied to sensor FDI. The technique uses the average sensor reconstruction errors for fault identification. The average reconstruction errors provide useful information about the directions and magnitudes of detected faults, which are not available from existing fault isolation techniques. Furthermore, average reconstruction errors can isolate and identify multiple faults that exist simultaneously when existing

fault isolation techniques are problematic. Therefore, the approach based on average reconstruction errors can outperform the fault index approach and linear PCA for fault isolation and identification.

Before the discussion of KPCA, some background on PCA is first given. In PCA, measurement data are projected onto a lower dimensional principal subspace, where most important variances in the data are captured. Projections to the residual (non-principal) subspaces are considered noises. Faults in the data will break down the normal relationships and lead to statistically unusual increase in the residuals. Mathematically, with a training data matrix $X \in R^{m \times n}$, where n is the number of variables/sensors and m is the number of samples, a PCA model is trained as

$$\lambda p = Cp \quad (7-1)$$

where $C \in R^{n \times n}$ is the covariance matrix of X , λ are the eigenvalues and p are the eigenvectors. When a set of new measurements $x \in R^{1 \times n}$ becomes available, estimations of x are obtained as

$$x = \hat{x} + e = \sum_{i=1}^l x p_i p_i^T + \sum_{j=l+1}^n x p_j p_j^T \quad (7-2)$$

where $\hat{x} = \sum_{i=1}^l x p_i p_i^T$ is an estimation of x , $e \in R^{1 \times n}$ is a vector of the prediction errors or residuals, and $l < n$ is the number of retained principal components. l is usually selected so that the ratio between the sum of l leading eigenvalues and the sum of all eigenvalues

is higher than a selected threshold, i.e., $\frac{\sum_{i=1}^l \lambda_i}{\sum_{j=1}^n \lambda_j} \geq 0.9$, where 0.9 is an example threshold.

Faults in x will lead to unusual increase in the residuals of a PCA model. Statistics, such as squared prediction error $SPE = \|e\|^2$, can be calculated to detect the fault by comparing with a threshold δ^2 (Wise & Gallagher, 1996). One renowned fault isolation technique

for PCA is to reconstruct the output of a sensor, e.g. sensor j , using the remaining sensors (Dunia et al., 1996). A SVI can be computed as the ratio between the SPE after reconstruction of sensor j , SPE_j , and the SPE without any reconstruction, i.e.

$$\eta_j = \frac{SPE_j}{SPE}$$

Because the residuals can only be considerably reduced after the output of a faulty sensor is replaced by the reconstructed value, a considerable reduction in η_j indicates that sensor j is faulty (Dunia et al., 1996).

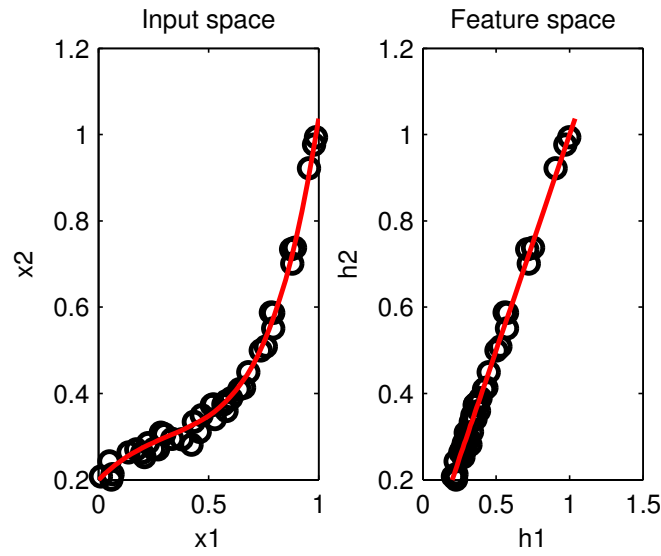


Figure 7-5: Illustration of advantages of nonlinear PCA

KPCA is a nonlinear generalization of PCA procedures (Schölkopf et al., 1998). The general principle of KPCA is illustrated in Figure 7-5. If the relationship between two variables is nonlinear as shown in the left graph of Figure 7-5, fitting a linear PCA model to the original input space may lead to large errors. If the data are firstly mapped into a feature space H through a nonlinear mapping function, linear relationship in the feature space can be obtained, as shown in the second graph of Figure 7-5. Linear PCA procedures can then be directly carried out in the feature space as a simple eigenvalue problem. This is the general principle of KPCA. To this end, two problems may be raised: how to select an appropriate nonlinear mapping function and how to deal with the

usually intimidating dimensions in the feature space. Fortunately, those two problems can be avoided with the use of kernel functions. By replacing dot products in the feature space with kernel functions defined in the input space, the nonlinear mapping can be computed implicitly, and the PCA problem in the feature space reduces to a simple eigenvalue problem (Schölkopf et al., 1998). The theory behind the kernel method is explored in detail in a number of works (Aizerman et al., 1964; Schölkopf & Smola, 2002; Shaw-Taylor & Cristianini, 2004).

Mathematical formulations of KPCA can be written as follows (Schölkopf et al., 1998).

For X , its covariance matrix in the feature space, \bar{C} , is represented as

$$\bar{C} = \frac{1}{m} \sum_{j=1}^m \Phi(x_j) \Phi(x_j)^T, \text{ where } m \text{ is the number of samples and } \Phi(x) \text{ represents } x \text{ in the}$$

feature space. The eigenvalues and eigenvectors of \bar{C} can be found by solving

$$\lambda p = \bar{C} p \quad (7-3)$$

Explicit calculation of \bar{C} and solution of Eq. (5-3) are usually difficult, if even possible.

Noting that all solutions p with $\lambda \neq 0$ lie in the span of $\Phi(x_1), \dots, \Phi(x_m)$, Eq. (7-3) can be written as

$$\lambda (\Phi(x_j) \cdot p) = (\Phi(x_j) \cdot \bar{C} p), j = 1, \dots, m \quad (7-4)$$

and there exist coefficients α_i such that

$$p = \sum_{i=1}^m \alpha_i \Phi(x_i) \quad (7-5)$$

A kernel matrix $K \in R^{m \times m}$ can be computed as

$$K_{i,j} = (\Phi(x_i) \cdot \Phi(x_j)) = k(x_i, x_j) \quad (7-6)$$

where $(\Phi(x_i) \cdot \Phi(x_j))$ is the dot product of $\Phi(x_i)$ and $\Phi(x_j)$. An effective kernel function is a Gaussian kernel defined as

$$k(a,b) = \exp\left(-\frac{\|a-b\|^2}{2\sigma^2}\right) \quad (7-7)$$

where σ is a constant variance to be specified. Combining Eq. (7-4)–(7-6) transforms the eigenvalue problem of Eq. (7-3) to a much simpler problem as follows

$$m\lambda\alpha = K\alpha \quad (7-8)$$

where α is a vector consisting of the unknown coefficients α_i .

For a new test point x , its projection to the j th principal component in the feature space, called score, can be calculated as

$$w_j = (p_j \cdot \Phi(x)) = \sum_{i=1}^m \alpha_i^j k(x_i, x) \quad j = 1, \dots, l \quad (7-9)$$

where l is the number of retained principal components. Eq. (7-6)–(7-9) form the major procedures of a KPCA model.

The procedures to detect and identify faults using a KPCA model are similar to those of linear PCA. In fact, they have been discussed in recent publications in analogy to linear PCA. For a new data point, with the scores as defined in Eq. (7-9) available, a SPE index can be computed and compared with a predetermined threshold δ^2 for fault detection, i.e., presence of a fault can be declared if the SPE exceed δ^2 (Shi, Liu, & Zhang, 2009)

$$\text{SPE} = \sum_{j=1}^m w_j^2 - \sum_{j=1}^l w_j^2 > \delta^2 \quad (7-10)$$

The threshold developed in linear PCA can also be directly used for KPCA as (Choi et al., 2005)

$$\delta^2 = \theta_1 \left[\frac{c_\alpha \sqrt{2\theta_2 h_0^2}}{\theta_1} + 1 + \frac{\theta_2 h_0 (h_0 - 1)}{\theta_1^2} \right]^{\frac{1}{h_0}} \quad (7-11)$$

where $\theta_i = \sum_{j=l+1}^m \lambda_j^i$ for $j = 1, 2, 3$, $h_0 = 1 - (2\theta_1\theta_3 / 3\theta_2^2)$, and c_α is the standard normal deviation corresponding to the upper $(1 - \alpha)$ percentile.

It is more complicated to isolate and identify faults in KPCA than in linear PCA. For fault isolation, the popular contribution plot technique cannot be directly applied in nonlinear cases. Reconstruction-based method is an alternative way to isolate faults in linear PCA. However, it is difficult to find a straightforward inverse mapping from the feature space to the original input space. A technique developed for de-noising applications using KPCA (Mika, Schölkopf, et al., 1999; Takahashi & Kurita, 2002) can be adopted for reconstruction. The technique presented in (Rathi, Dambreville, & Tannenbaum, 2006) can also be used for the reconstruction. The motivation behind the technique in (Mika, Schölkopf, et al., 1999) and (Takahashi & Kurita, 2002) is to find a vector z as an approximation of a test point x in the input space. Reconstruction of $\Phi(x)$ in the feature space can be defined by the projection operator P_l as

$$P_l \Phi(x) = \sum_{i=1}^l w_i p_i \quad (7-12)$$

By minimizing $\rho(z) = \|\Phi(z) - P_l \Phi(x)\|^2$, an iterative scheme to obtain z can be found as

$$z(d+1) = \frac{\sum_{i=1}^m \beta_i k(x_i, z(d)) x_i}{\sum_{i=1}^m \beta_i k(x_i, z(d))} \quad (7-13)$$

where $\beta_i = \sum_{j=1}^l w_j \alpha_i^j$ and d is the number of iterations.

After a converged value of z , say \bar{z} , is obtained, $\text{SPE}_{i,i=1,\dots,n}$ can be calculated with the original measurement of sensor i , x_i , being replaced by the reconstruction \bar{z}_i . A fault index can be calculated for each sensor as $\eta_i = \text{SPE}_i / \text{SPE}$ for $i = 1, \dots, n$. In case that the

sensor j is faulty, SPE_j will be considerably reduced in comparison with $SPE_{i,i \neq j}$.

Therefore, a considerable reduction in fault index η_j indicates that sensor j is faulty.

This principle has been discussed in (Choi et al., 2005). However, this technique may not always give satisfactory results, especially when, at one time, more than one sensor is problematic. It is difficult to isolate multiple faults because with multiple faults in the measurement data, the reduction in SPE may not be significant after reconstruction of any single sensor. For a situation where one of the faulty sensors is the main source of the abnormal increase in SPE, this faulty sensor can possibly be isolated by the fault index, but the other faulty sensors with less significant contributions to the increased SPE may not be isolated. Fault index does not provide information about the direction and magnitude of an isolated fault.

The average reconstruction errors, denoted as $\mu \in R^{b \times n}$, can be preferred indices for fault isolation and identification, especially in the presence of multiple faults. μ could be conveniently obtained as

$$\mu = \sum_{i=1}^q (x(i) - \bar{z}(i)) / q \quad (7-14)$$

where q is the length of a set of new test data, $x(i) \in R^{b \times n}$ is a point in the test data set, and $\bar{z}(i)$ contains reconstructions of $x(i)$. The average deviations of the actual sensor outputs from the reconstructed values provide useful information about the directions and magnitudes of sensor performance degradation. This diagnostic information is not normally available in existing fault isolation techniques. Another advantage of this technique is that it can identify more than one faulty sensor at a time, regardless of their respective contributions to the increase in SPE. Those advantages are supported by the numerical validation results to be presented later. It is suggested in this research to examine the results of Eq. (7-14) for fault isolation and identification prior to calculating the fault index for KPCA-based FDD applications.

7.2.2 Numerical validations

To validate performance of the KPCA-based FDI method, measurements from 29 transmitters in a pressurized water reactor plant have been used. The transmitters measure eight variables of the nuclear steam supply system as summarized in Table 7-2. Six sets of data are obtained at six different periods within one fuel cycle as summarized in Table 7-3. Each set of data contains twelve-hour measurements, sampled every 10 seconds, from the 29 transmitters. Therefore, each data set contains about 4,320 samples for each sensor.

Table 7-2: NPP sensors used for KPCA validations

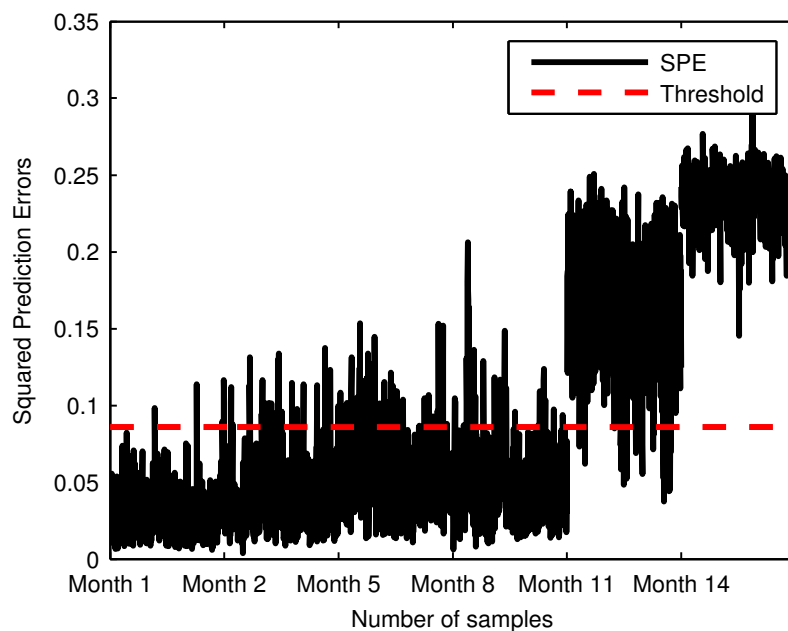
Transmitter	Measured variable
1-4	Steam pressure
5-6	SG level wide range
7-10	SG level narrow range
11-14	SG feedwater flow
15-18	Pressurizer pressure
19-22	Pressurizer level
23-26	Reactor coolant system pressure
27-29	Steam flow

Data set one is obtained from the first month in a new fuel cycle when the instrumentations in the plant have just undergone maintenance; thus, this data set is used as the benchmark data in this study. A KPCA model is trained using the first 500 samples of data set one. When the model is applied to another 500 samples of data set one for validation, the average reconstruction errors are all less than 0.2% of the full spans of the respective sensors. The KPCA model is then applied to the other five data sets to detect and identify sensor faults in them. Considering the space constraint, results for 500 samples of each data set are presented and discussed herein. Note that the KPCA model actually detects and identifies sensor performance degradations over time as reflected in the measurement data. The performance changes are considered as sensor faults in this research. However, other possibilities such as sensor recalibration cannot be excluded.

Table 7-3: NPP data set for KPCA validation

Data set	Description
1	Data from month 1 of the fuel cycle
2	Data from month 2 of the fuel cycle
3	Data from month 5 of the fuel cycle
4	Data from month 8 of the fuel cycle
5	Data from month 11 of the fuel cycle
6	Data from month 14 of the fuel cycle

For fault detection, squared prediction errors of the KPCA model are computed. The results for 500 samples of each of the six data sets are shown in Figure 7-6. It can be seen that the SPEs obviously exceed the threshold for the measurements of data set 5 (month 11 of the fuel cycle) and data set 6 (month 14 of the fuel cycle). Faults in the measurements of data sets 5 and 6 are detected. In comparison with results of the training data (month 1 of the fuel cycle), the SPEs exceed the threshold more often for data set 3 (month 5 of the fuel cycle) and data set 4 (month 8 of the fuel cycle), signifying potential presence of developing faults in the sensors.

**Figure 7-6: Results of fault detection in NPP data using KPCA**

To isolate and identify the detected fault, reconstructions of the test data are computed. The average reconstruction errors for the twenty-nine sensors for data set 3 to 6 are presented in Figure 7-7. In Figure 7-8, the average reconstruction errors are presented as percentages of the full spans of the respective sensors.

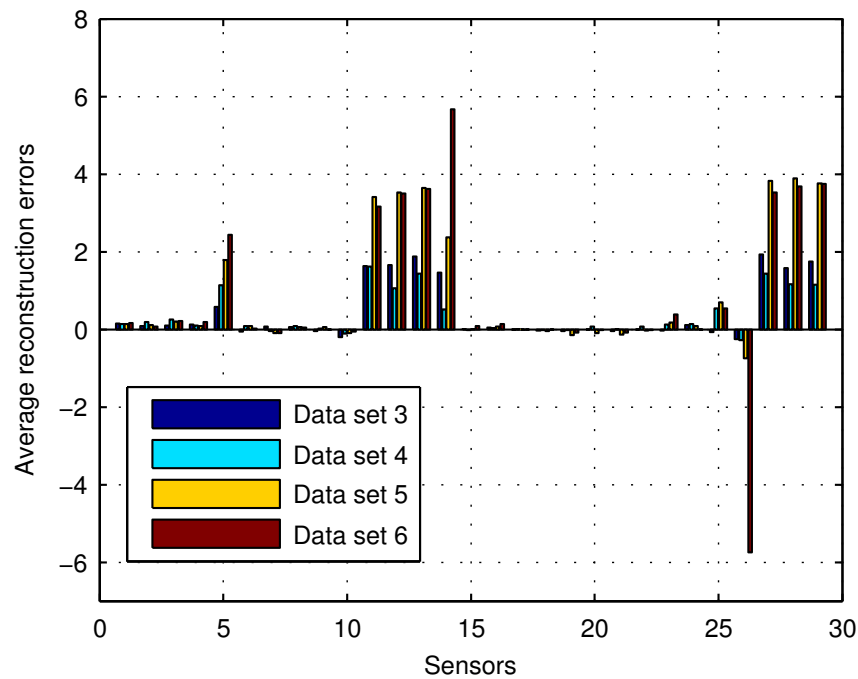


Figure 7-7: Average reconstruction errors (absolute value) of KPCA for NPP data

For data set 6, notable performance changes are observed from Figure 7-7 for sensor 5, sensor 11-14, and sensor 26-29. When measured in terms of percentages in Figure 7-8, with over 2% differences between the actual measurements and their reconstructed values, faults in sensor 5 and sensor 26 are most noticeable. The performance changes for sensor 11-14 and 27-29 are less significant in this perspective, but still considerable, especially for sensor 14. In a summary, sensors 5 and 26 are isolated as faulty sensors for data set 6. Sensor 5 is faulty for data set 5, but sensor 26 appears normal. Directions and magnitudes of the faults can be observed from the graphs. Potential problems in sensors 11-14 and 27-29, especially sensor 14, can be suspected. Due to higher levels of noises in

those sensors, faults in those sensors are not affirmative. Taking into consideration the results for data set 3 and 4, it can be observed that the average reconstruction errors of sensor 5 grow increasingly larger over time, showing a pattern of sensor drift in the upward direction, i.e., the indicated SG level by sensor 5 becomes increasingly larger than the actual level over time. The reconstruction errors of sensor 26 are small, except for data set 6 when dramatic increase in the negative direction is observed. This could be the result of a fault that occurred after the eleventh month of the fuel cycle when data set 5 is acquired. In addition, special attention should be paid to sensors 11-14 and 27-29 during the next calibration.

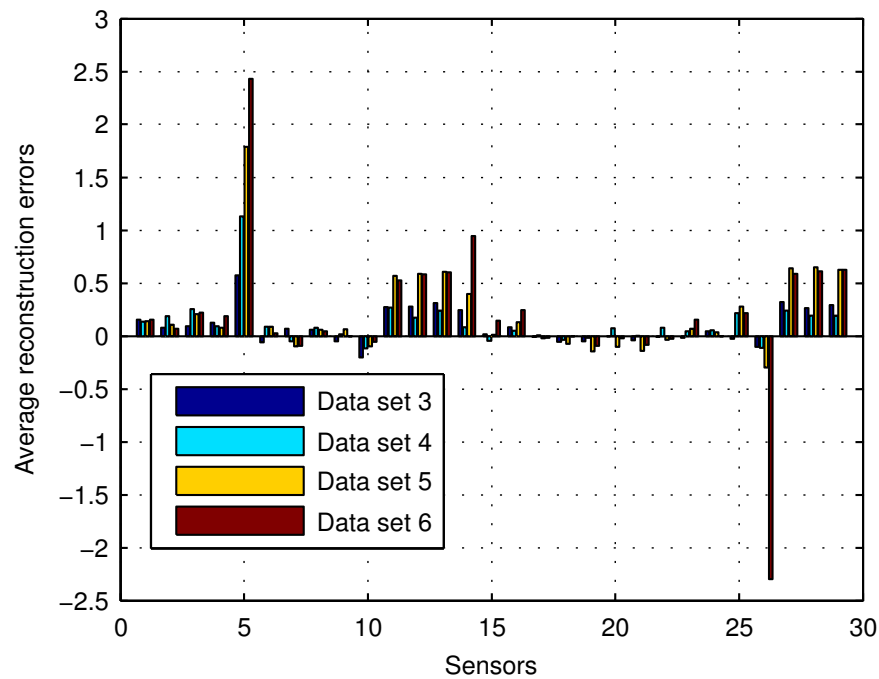


Figure 7-8: Average reconstruction errors (percentage) of KPCA for NPP data

To compare performance of the average reconstruction error-based fault identification technique with the fault index approach, fault indices are computed for all twenty-nine sensors. The results of four sensors for data set 6 are presented in Figure 7-9. The fault isolation performance is not satisfactory with this approach. Though sensor 26 may be isolated through this technique, reductions in the fault index for sensor 5 are small.

Therefore, sensor 5 cannot be isolated as faulty. The results for sensor 14 and 28 are also not conclusive. Furthermore, the fault indices do not provide information about the directions and magnitudes of the faults.

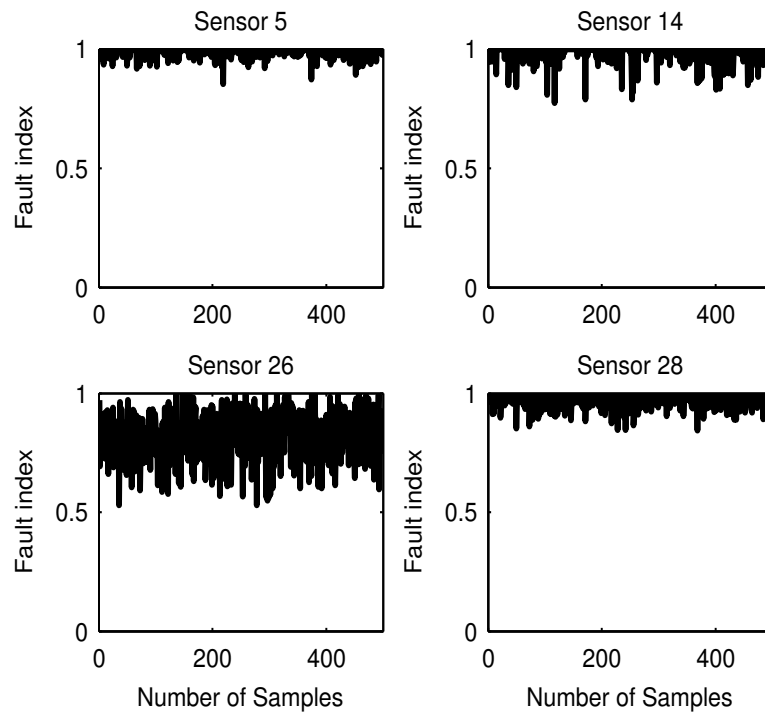


Figure 7-9: Fault indices for selected sensors of NPP data

The data used for this study are all obtained during steady state plant operation near the same operating point. There is no significant nonlinearity in the data, thus, linear PCA has comparable performance to KPCA for fault detection in this case. For problems where nonlinearity in the data cannot be neglected, KPCA is expected to outperform PCA. For fault isolation in linear PCA, the output of one sensor is reconstructed using the remaining sensors. Therefore, in the presence of more than one faulty sensor, it is difficult to perform reliable fault isolation based on sensor reconstruction. In this case, the average reconstruction errors of KPCA provide more reliable conclusions because in KPCA all of the sensors can be reconstructed simultaneously from the faulty-free training data. This is another advantage of KPCA over PCA.

7.3 Conclusion

The fault diagnosis methods validated in Chapter 5 is tested herein using data containing sensor faults. It can be concluded from the studies that sensor faults can cause considerable erroneous fault diagnosis results. Therefore, a sensor validation should be included in a practical fault diagnosis system.

KPCA is applied for sensor validations. Performance changes in multiple sensors can be detected and identified. The average reconstruction errors could be more effective in isolation and identification of multiple faults than both the fault index technique and linear PCA-based approaches. Results of the numerical validations also support this conclusion. Overall, it is demonstrated that the KPCA-based method is a promising tool for condition assessment of instruments in a complex industrial system such as a NPP.

The scheme studied in this chapter is most suitable for a system operating near a steady state to monitor the static performance of sensors, as well as the conditions of other equipment. The outcomes of the monitoring system can be used for condition-based maintenance to prevent a minor fault from developing into major failures. They can also provide evidences of failure precursors that can be considered in the diagnosis analysis to identify the root causes of detected faults. Thus, such a scheme is an important part of an integrated fault diagnosis system.

Chapter 8

8 Summary, Conclusion, and Future Work

8.1 Summary

In this research, several methods and systems have been investigated to deal with different aspects of an integral framework for fault diagnosis in NPPs. To determine whether a given set of sensors is sufficient to ensure diagnosability of the faults considered in a fault diagnosis system, the optimal sensor placement model developed in this research can be used. If additional sensors are indeed required for the fault diagnosis system, the sensor placement model can also be used to find a minimum number of additional sensors so that fault diagnosability can be achieved. To physically install the additional sensors that are identified by the sensor placement model, the wireless sensor networks system proposed in this research can be used so that measurement data can be acquired from the plant in cost-effective ways. When fault is detected from the collected measurement data, the fault diagnosis scheme based on semi-supervised pattern classification can then be applied to analyze the data to identify what type of fault has happened. To use a pattern classification model for diagnosis of equipment condition, a feature extraction step is often required to process the raw measurement data. In this research, the modified S-transform algorithm is developed for processing of vibration signals that are popular for equipment conditions monitoring applications. To ensure that the pattern classification methods (for diagnosis of fault type) and feature extraction methods (for monitoring of equipment condition) do not suffer from erroneous measurement data, the proposed sensor validation scheme based on kernel principal component analysis can be used to monitor the conditions of the sensors in a NPP. The results of condition monitoring can not only help to prevent failures in a NPP, but can also provide evidences for root cause analysis of the detected faults. Finally, the simplified physical NPP simulator can be used to validate performance of methods and systems developed for fault diagnosis applications in NPPs.

By integrating the studied methods and systems into a suite of diagnostic tools, the values and performance of the diagnosis system can potentially be enhanced. For example, the

sensors required to diagnose the faults simulated on the NPCTF are determined by the sensor placement model, and data collected from the sensors are used by the SSC model to effectively identify what faults have happened. Without the suitable suite of sensors, diagnosis of the faults cannot be achieved regardless of how advanced the diagnosis model is. In addition, the WSN prototype can effectively collect data from the sensors and feed the data into a similar diagnosis system. Even though a complete integration and thorough demonstration of all the proposed methods have not been implemented under a unified framework on the simplified NPP simulator, the methods and systems developed in this research have created the foundation for future development of integral fault diagnosis system.

In such an integrated fault diagnosis system, the data from the existing SCADA systems and additional ones collected by a WSN system can be used together to achieve improved diagnostic performance. An online monitoring system assesses the conditions of the sensors and equipment in the plant and provides key information for condition-based maintenance. When a fault is detected, additional data are subsequently acquired, processed to extract necessary features, and to identify the natures and root causes of the fault. Such information can then be used to create an effective maintenance strategy.

8.2 Conclusion

An optimal sensor placement model is proposed in this research to guide placement of additional sensors. Validations of the proposed sensor placement model show that the following objectives have been achieved.

- A quantitative sensor-fault incidence matrix can be obtained from the proposed system modeling technique.
- The proposed modeling technique can model a system as several less complicated modules.
- The proposed diagnosability criterion can accommodate different performances of different fault diagnosis systems. It can handle the situation where sensor response patterns are dissimilar, but the differences are not sufficient to allow a practical diagnosis model to reliably discriminate the faults.

- The influence of a specific sensor on fault diagnosability can be tested by addition of new sensors or removal of unnecessary sensors from the model.
- The proposed method can be used to select additional sensors with the maximum sensitivity to distinguish un-diagnosable faults.

The prototype wireless sensor network is only tested preliminarily with simple signal processing models. The following properties of the system are demonstrated by the experimental studies.

- The WSN is flexible to deploy. It acquires process measurements effectively.
- The WSN can be programmed to implement distributed in-network signal processing and fault diagnosis.
- The WSN can be effectively used for condition monitoring and process fault diagnosis in industrial systems.

A process fault diagnosis scheme based on semi-supervised classification is proposed. Experimental validations show that the proposed scheme has several desirable features.

- A semi-supervised classification model is able to achieve satisfactory fault diagnosis results using significantly less training data than what is typically required in a supervised model.
- A semi-supervised classification model is able to tolerate considerable uncertainties in the training data.
- The proposed scheme is a promising tool for fault diagnosis in industrial systems when it is difficult to obtain labeled data to train a supervised classification model.

A time-frequency analysis algorithm based on modified S-transform is proposed which utilizes the sigmoid function and other shaping functions to modify the frequency domain window width of standard S-transform. The numerical studies show that:

- The proposed approach makes it possible for users to design desirable windows to meet specific frequency localization requirements for a given application.

- Using a sigmoid function, the modified window design problem has effectively been reduced to selection of some tuning parameters.
- The new window design methods can provide superior time-frequency resolution for time-varying signals with multiple components, where the classical time-frequency analysis methods and standard S-transform method may fail.
- By observing changes in time-frequency characteristics of vibration signals, one can use the proposed algorithms to effectively detect faults occurred in a system.

A sensor fault detection and isolation scheme based on kernel principal component analysis is studied in this research. The numerical studies support the conclusions that:

- The average reconstruction errors of KPCA are more effective in fault diagnosis than existing techniques.
- Performance changes in multiple sensors can be detected and identified.
- The KPCA-based method is a promising tool for on-line condition assessment of instruments in an industrial system such as a NPP.

The nuclear power plant process control test facility has successfully supported the research in several methods and systems for fault diagnosis. It is observed that:

- Multiple process faults can be effectively simulated.
- The instrumentation system allows independent access to process measurements through wired data acquisition systems and wireless devices.

The methods investigated in this research are integrated into a proposed fault diagnosis framework. Values of the methods to the overall performance of a fault diagnosis system have been demonstrated through the numerous experimental studies. It can be observed that:

- A proper set of sensors should be selected for a fault diagnosis system, so that fault diagnosability is ensured. Installation of additional sensors can be required for practical implementations.

- Sensor faults can affect the fault diagnosis results considerably. Sensor validation is important to guarantee performance of the fault diagnosis system.
- The fault diagnosis model should accommodate constraints of a practical problem. When a conventional supervised classification model is unreliable due to limited availability of training data, semi-supervised classification models may provide improved performance.
- By using improved feature extraction techniques, enhanced diagnosis of equipment conditions can be achieved.

8.3 Future Work

This research encompassed multiple areas related to process fault diagnosis. Even though the principles and effectiveness of the several proposed algorithms and systems have been demonstrated within the scope, there are interesting issues that can be further investigated. Some possible topics include:

- More comprehensive evaluation of the WSN prototype in terms of signal processing capabilities, communication constraints, energy consumption, and scalability are needed to integrate the WSN with existing SCADA systems for a fault diagnosis system.
- Integrate the studied methods to create a complete FDD system and to demonstrate their effectiveness of the integrated system on the NPCTF.
- Extend the sensor placement model for processes with feedback controls, closed loops, and parallel loops.
- Develop adaptive and dynamic semi-supervised classification models for fault diagnosis.

Bibliography

- Agha, K. A., Bertin, M.-H., Dang, T., Guitton, A., Minet, P., Val, T., & Viollet, J.-B. (2009). Which wireless technology for industrial wireless sensor networks? The development of OCARI technology. *IEEE Transactions on Industrial Electronics*, 56, 4266-4278.
- Aizerman, M., Braverman, E., & Rozonoer, L. (1964). Theoretical foundations of the potential function method in pattern recognition learning. *Automation and Remote Control*, 25, 821–837.
- Akyildiz, I. F., & Wang, X. (2005). A survey on wireless mesh networks. *IEEE Communications Magazine*, 43, S20-S30.
- Akyildiz, I. F., Wang, X., & Wang, W. (2005). Wireless mesh networks: a survey. *Computer Networks*, 47, 445–487.
- Aldrich, C., & Auret, L. (2013). *Unsupervised process monitoring and fault diagnosis with machine learning methods*, London: Springer.
- Ali, Y., & Narasimhan, S. (1993). Sensor network design for maximizing reliability of linear processes. *American Institute of Chemical Engineering Journal*, 39, 820-828.
- Ali, Y., & Narasimhan, S. (1995). Redundant sensor network design for linear processes. *American Institute of Chemical Engineering Journal*, 41, 2237-2249.
- Allen, M. (2010). VoxNet: Reducing latency in high data rate applications. In E. Elena Gaura, L. Girod, J. Brusey, M. Allen & G. Challen (Eds.), *Wireless sensor networks: deployments and design frameworks*: Springer.
- Alpaydin, E. (2010). *Introduction to machine learning* (2nd ed.): The MIT Press.
- Aminian, F., & Aminian, M. (2001). Fault diagnosis of analog circuits using bayesian neural networks with wavelet transform as preprocessor. *Journal of Electronic Testing: Theory and Applications*, 17, 29-36.

- Aminian, M., & Aminian, F. (2000). Neural-network based analog-circuit fault diagnosis using wavelet transform as preprocessor. *IEEE Transactions on Circuits and Systems II: Analog and Digital Signal Processing*, 47, 151 - 156.
- Antonino-Daviu, J. A., Riera-Guasp, M., Pineda-Sanchez, M., & Perez, R. B. (2009). A critical comparison between DWT and hilbert–huang-based methods for the diagnosis of rotor bar failures in induction machines. *IEEE Transactions on Industry Applications*, 45, 1794 - 1803.
- Arzhanov, V., & Pázsit, I. (2002). Detecting impacting of BWR instrument tubes by wavelet analysis. In D. Ruan & P. F. Fantoni (Eds.), *Power plant surveillance and diagnostics: applied research and diagnostics* (pp. 157-174): Springer.
- Assous, S., & Boashash, B. (2012). Evaluation of the modified S-transform for time-frequency synchrony analysis and source localization. *EURASIP Journal on Advances in Signal Processing*, 49, 1-18.
- Aydin, I., Karakose, M., & Akin, E. (2008). *Artificial immune inspired fault detection algorithm based on fuzzy clustering and genetic algorithm methods*. CIMSA 2008.
- Azran, A. (2007). *The rendezvous algorithm: multiclass semi-supervised learning with Markov random walks*. Proceedings of the 24th international conference on Machine learning.
- Bach, F. R., & Jordan, M. I. (2003). Kernel independent component analysis. *The Journal of Machine Learning Research*, 3, 1-48.
- Bagajewicz, M. (1997). Design and retrofit of sensor networks in process plants. *American Institute of Chemical Engineering Journal*, 43, 2300-2306.
- Bagajewicz, M., & Cabrera, E. (2002). New MILP formulation for instrumentation network design and upgrade. *American Institute of Chemical Engineering Journal*, 48, 2271-2282.

- Bagajewicz, M., Fuxman, A., & Uribe, A. (2004). Instrumentation network design and upgrade for process monitoring and fault detection. *American Institute of Chemical Engineering Journal*, 50, 1870-1880.
- Bagajewicz, M., & Sanchez, M. (1999). Design and upgrade of nonredundant and redundant linear sensor networks. *American Institute of Chemical Engineering Journal*, 45, 1927-1938.
- Bagajewicz, M., & Sanchez, M. (2000). Cost-optimal design of reliable sensor networks. *Computers and Chemical Engineering*, 23, 1757-1762.
- Bakshi, B. R. (1999). Multiscale PCA with application to multivariate statistical process monitoring. *AIChE Journal*, 44, 1596-1610.
- Baraldi, P., Razavi-Far, R., & Zio, E. (2010). *A method for estimating the confidence in the identification of nuclear transients by a bagged ensemble of FCM classifiers*. NPIC&HMIT 2010, Las Vegas, Nevada.
- Baraldi, P., Razavi-Fara, R., & Zio, E. (2011). Bagged ensemble of Fuzzy C-Means classifiers for nuclear transient identification. *Annals of Nuclear Energy*, 38, 1161-1171.
- Bari, A., & Jiang, J. (2014). Deployment strategies for wireless sensor networks in nuclear power plants. *Nuclear Technology*, 187, 82-95.
- Barlett, E. B., & Uhrig, R. E. (1992). Nuclear power plant status diagnostics using an artificial neural network. *Nuclear Technology*, 97, 272-281.
- Bartal, Y., Lin, J., & Uhrig, R. E. (1995). Nuclear power plant transient diagnostics using artificial neural networks that allow 'don't-know' classifications. *Nuclear Technology*, 110, 436-449.
- Basir, O., & Yuan, X. (2007). Engine fault diagnosis based on multi-sensor information fusion using Dempster-Shafer evidence theory. *Information Fusion*, 8, 379-386.

- Basseville, M. (1988). Detecting changes in signals and systems-a survey. *Automatica*, 24, 309-326.
- Batista, L., Badri, B., Sabourin, R., & Thomas, M. (2013). A classifier fusion system for bearing fault diagnosis. *Expert Systems with Applications*, 40, 6788-6797.
- Baudat, G., & Anouar, F. (2000). Generalized discriminant analysis using a kernel approach. *Neural Computation*, 12, 2385-2404.
- Beard, R. V. (1971). *Failure accommodation in linear systems through self-reconfiguration*. (Ph.D. Thesis), MIT, Cambridge, MA, USA.
- Bechtold, B., & Kunze, U. (1999). KUES'95-The modern diagnostic system for loose parts monitoring. *Progress in Nuclear Energy*, 34, 221-230.
- Belkin, M., Niyogi, P., & Sindhvani, V. (2006). Manifold regularization: a geometric framework for learning from labeled and unlabeled examples. *Journal of Machine Learning Research*, 7, 2399-2434.
- Benbouzid, M. E. H. (2000). A review of induction motors signature analysis as a medium for faults detection. *IEEE Transactions on Industrial Electronics*, 47, 984-993.
- Bhushan, M., & Rengaswamy, R. (2000a). Design of sensor location based on various fault diagnostic observability and reliability criteria. *Computers and Chemical Engineering*, 24, 735-741.
- Bhushan, M., & Rengaswamy, R. (2000b). Design of sensor network based on the signed directed graph of the process for efficient fault diagnosis. *Industrial and Engineering Chemistry Research*, 39, 999-1019.
- Bhushan, M., & Rengaswamy, R. (2002). Comprehensive design of a sensor network for chemical plants based on various diagnosability and reliability criteria-1. framework. *Industrial and Engineering Chemistry Research*, 41, 1826-1839.
- Bishop, C. M. (2006). *Pattern recognition and machine learning*. New York: Springer.

- Blum, A., & Chawla, S. (2001). *Learning from labeled and unlabeled data using graph mincuts*. Proceedings of the Eighteenth International Conference on Machine Learning.
- Blum, A., & Mitchell, T. (1998). *Combining labeled and unlabeled data with co-training*. Proceedings of the eleventh annual conference on Computational learning theory.
- Box, G. E. P., & Jenkins, G. M. (1970). *Time series analysis : forecasting and control* San Francisco Holden-Day.
- Broughton, J. M., Kuan, P., Petti, D. A., & Tolman, E. L. (1989). A scenario of the Three Mile Island unit 2 accident. *nuclear technology*, 87, 34-53.
- Cai, B., Liu, Y., Fan, Q., Zhang, Y., Liu, Z., Yu, S., & Ji, R. (2014). Multi-source information fusion based fault diagnosis of ground-source heat pump using Bayesian network. *Applied Energy*, 114, 1-9.
- Callaway, E. H. (2003). *Wireless sensor networks: architectures and protocols*: Auerbach Publications.
- Camps-Valls, G., Marsheva, T. V., & Zhou, D. (2007). Semi-supervised graph-based hyperspectral image classification. *IEEE Transactions on Geoscience and Remote Sensing*, 45, 3044-3054.
- Casillas, M. V., Puig, V., Luis E. Garza-Castanon, L. E., & Rosich, A. (2013). Optimal sensor placement for leak location in water distribution networks using genetic algorithms. *Sensors*, 13, 14984-15005.
- Chan, A. M. C., & Ahluwalia, A. K. (1992). Feedwater flow measurement in u.s. nuclear power generation stations. *EPRI-TR--101388*: Electric Power Research Institute.
- Chapelle, O., Schölkopf, B., & Zien, A. (2006). *Semi-supervised learning* (O. Chapelle, B. Schölkopf & A. Zien Eds.). Cambridge, Massachusetts: The MIT Press.
- Chapelle, O., Weston, J., & Schölkopf, B. (2002). Cluster kernels for semi-supervised learning. *Advances in Neural Information Processing Systems*, 15, 585-592.

- Chapelle, O., & Zien, A. (2004). Semi-supervised classification by low density separation.
- Chen, D., Jiang, J., Bari, A., Hashemian, H. M., & Wang, Q. (2014). *Challenges and prospects of equipment health monitoring with wireless sensor network in nuclear power plants*. ISOFIC2014, Jeju, Republic of Korea.
- Chen, J., & Liu, K. (2002). On-line batch process monitoring using dynamic PCA and dynamic PLS models. *Chemical Engineering Science*, 57, 63-75.
- Chen, Y. D., Du, R., & Qu, L. S. (1995). Fault features and large rotating machinery and diagnosis using sensor fusion. *Journal of Sound and Vibration*, 188, 227-242.
- Cheon, S. W., & Chang, S. H. (1993). Application of neural networks to a connectionist expert system for transient identification in nuclear power plant. *Nuclear Technology*, 102, 177-191.
- Chiang, L. H., Kotanchek, M. E., & Kordon, A. K. (2004). Fault diagnosis based on Fisher discriminant analysis and support vector machines. *Computers & Chemical Engineering*, 28, 1389-1401.
- Chiang, L. H., Russell, E. L., & Braatz, R. D. (2000). *Fault detection and diagnosis in industrial systems*: Springer.
- Chiang, L. H., Russell, E. L., & Braatz, R. D. (2000). Fault diagnosis in chemical processes using Fisher discriminant analysis, discriminant partial least squares, and principal component analysis. *Chemometrics and Intelligent Laboratory Systems*, 50, 243-252.
- Chmielewski, D., Palmer, T., & Manousiouthakis, V. (2002). On the theory of optimal sensor placement. *American Institute of Chemical Engineering Journal*, 48, 1001-1012.
- Choi, H.-I., & Williams, W. J. (1989). Improved time-frequency representation of multicomponent signals using exponential kernels. *IEEE Transactions on Acoustics, Speech and Signal Processing*, 37, 862-871.

- Choi, S., Lee, C., Lee, J., Park, J., & Lee, I. (2005). Fault detection and identification of nonlinear processes based on kernel PCA. *Chemometrics and Intelligent Laboratory Systems*, 75, 55-67.
- Chow, E. Y., & Willsky, A. S. (1984). Analytical redundancy and the design of robust failure detection systems. *IEEE Transactions on Automatic Control*, 29, 603-614.
- Clark, R. N. (1978). Instrument fault detection. *IEEE Transactions on Aerospace and Electronic Systems*, 14, 456-465.
- Clarke, D. W. (2000). Intelligent Instrumentation. *Transactions of the Institute of Measurement and Control*, 22, 3-27.
- Cohen, L. (1966). Generalized phase-space distribution functions. *Journal of Mathematical Physics*, 781-786.
- Cohen, L. (1989). Time-frequency distributions-a review. *Proceedings of the IEEE*, 77, 941-981.
- Cohen, L. (1995). *Time-frequency analysis*. Englewood Cliffs, N.J Prentice Hall.
- Cohen, L., & Posch, T. E. (1985). Positive time-frequency distribution functions. *IEEE transactions on acoustics, speech, and signal processing*, 33, 31-38.
- Czibok, T., Kiss, G., Kiss, S., Krinizs, K., & Végh, J. (2003). Regular neutron noise diagnostics measurements at the hungarian Paks NPP. *Progress in Nuclear Energy*, 43, 67-74.
- Dasarathy, B. V. (2003). Information fusion as a tool in condition monitoring. *Information Fusion*, 4, 71-73.
- Dash, P. K., Panigrahi, B. K., & Panda, G. (2003). Power quality analysis using S-transform. *IEEE Transactions on Power Delivery*, 18, 406-411.
- Demazière, C., & Glöckler, O. (2004). *On-line determination of the prompt fraction of in-core neutron detectors in CANDU reactors*. PHYSOR 2004, Chicago, IL, USA.

- Dempster, A. P. (1968). A generalization of Bayesian inference. *Journal of the Royal Statistical Society Series B*, 30, 205-247.
- Ding, J., Gribok, V. A., Hines, W. J., & Rasmusse, B. (2004). Redundant sensor calibration monitoring using independent component analysis and principal component analysis. *Real-Time Systems*, 27, 27-47.
- Ding, S. X. (2012). Model-based fault diagnosis techniques: design schemes, algorithms and tools. London: Springer
- Ding, S. X. (2014). *Data-driven design of fault diagnosis and fault-tolerant control systems*: Springer.
- Djurovic, I., Sejdic, E., & Jiang, J. (2008). Frequency-based window width optimization for S-transform. *International Journal of Electronic Commerce*, 62, 245-250.
- Dong, D., & McAvoy, T. J. (1996). Nonlinear principal component analysis-based on principal curves and neural networks. *Computers & Chemical Engineering*, 20, 65-78.
- Dong, J., Kulcsar, B., & Verhaegen, M. (2009). *Subspace based fault detection and identification for LPV systems*. Proceedings of 7th IFAC Symposium on Fault Detection, Supervision and Safety of Technical Processes, Barcelona, Spain.
- Dong, M., Yan, Z., Yang, L., & Judd, M. D. (2005). Fault diagnosis model for power transformers based on information fusion. *Measurement Science and Technology*, 16, 1517-1524.
- Dougherty, G. (2013). *Pattern recognition and classification: an introduction*: Springer.
- Du, Y., Chi, Y., & Wu, X. (2008). *The application of information fusion in fault diagnosis and equipment monitoring*. The 27th Chinese Control Conference, Kunming.
- Duda, R. O., Hart, P. E., & Stork, D. G. (2000). *Pattern classification* (2nd ed.): Wiley-Interscience.

- Dunia, R., Qin, J. S., Edgar, F. T., & McAvoy, J. T. (1996). Identification of faulty sensors using principal component analysis. *AIChE Journal*, 42, 2797-2812.
- Dunia, R., & Qin, S. J. (1998). Joint diagnosis of process and sensor faults using principal component analysis. *Control Engineering Practice*, 6, 457-469.
- Embrechts, M. J., & Benedek, S. (2004). Hybrid identification of nuclear power plant transients with artificial neural networks. *IEEE Transactions on Industrial Electronics*, 51, 686-693.
- Fantoni, P. F. (2005). Experiences and applications of PEANO for online monitoring in power plants. *Progress in Nuclear Energy*, 46, 206-225.
- Fantoni, P. F., Hoffmann, M., Rasmussen, B., & Hines, J. W. (2002). *The use of non-linear partial least squares methods for on-line process monitoring as an alternative to artificial neural networks*. FLINS 2002, Gent, Belgium.
- Feng, Z., Liang, M., & Chu, F. (2013). Recent advances in time-frequency analysis methods for machinery fault diagnosis: a review with application examples. *Mechanical Systems and Signal Processing*, 38, 165-205.
- Figedy, S., & Oksa, G. (2005). Modern methods of signal processing in the loose part monitoring system. *Progress in Nuclear Energy*, 46, 253-267.
- Frank, P. M. (1990). Fault diagnosis in dynamic systems using analytical and knowledge-based redundancy-a survey and some new results. *Automatica*, 26, 459-474.
- Frank, P. M., & Ding, S. X. (1997). Survey of robust residual generation and evaluation methods in observer-based fault detection systems. *Journal of Process Control*, 7, 403-424.
- Gan, G., Ma, C., & Wu, J. (2007). *Data clustering: theory, algorithms, and applications*: Society for Industrial and Applied Mathematics.

- Garvey, R. D., & Hines, J. W. (2006). *An adaptive distance measure for use with nonparametric models*. NPIC&HMIT 2006, Albuquerque, NM, USA.
- GE. (2014). Proficy SmartSignal. Retrieved Aug 28, 2014, from <http://www.ge-ip.com/products/proficy-smartsignal/p3704>
- Geladi, P., & Kowalski, B. R. (1986). Partial least-squares regression: a tutorial. *Analytica Chimica Acta*, 185, 1-17.
- Gertler, J. J. (1988). Survey of model-based failure detection and isolation in complex plants. *IEEE Control Systems Magazine*, 8, 3-11.
- Gertler, J. J. (1997). Fault detection and isolation using parity relations. *Control Engineering Practice*, 5, 653-661.
- Gertler, J. J. (1998). *Fault detection and diagnosis in engineering systems*: CRC Press.
- Gertler, J. J., Li, W., Huang, Y., & McAvoy, T. (1999). Isolation enhanced principal component analysis. *AIChE Journal*, 45, 323-334.
- Gertler, J. J., & Singer, D. (1990). A new structural framework for parity equation-based failure detection and isolation. *Automatica*, 26, 381-388.
- Ghosh, K., Ng, Y. S., & Srinivasan, R. (2011). Evaluation of decision fusion strategies for effective collaboration among heterogeneous fault diagnostic methods. *Computers and Chemical Engineering*, 35, 342-355.
- Glöckler, O. (2003). Reactor noise measurements in the safety and regulating systems of candu stations. *Progress in Nuclear Energy*, 43, 75-82.
- Goebel, K. (2001). Architecture and design of a diagnostic information fusion system. *Artificial Intelligence for Engineering Design, Analysis and Manufacturing*, 15, 335-348.
- Gor, P. (2005). *Early warning acoustic system for nuclear power plant*. TCM-IAEA, Knoxville, Tennessee, U.S.

- Gordon, J., & Shortliffe, E. H. (1984). The Dempster-Shafer theory of evidence. *Rule-Based Expert Systems: The MYCIN Experiments of the Stanford Heuristic Programming Project*, 3, 832-838.
- Gottlieb, C., Arzhanov, V., Gudowski, W., & Garis, N. (2006). Feasibility study on transient identification in nuclear power plants using support vector machines. *nuclear technology*, 155, 67-77.
- Gribok, A. V., Hines, J. W., Urmanov, A., & Uhrig, R. E. (2002). Heuristic, systematic, and informational regularization for process monitoring. *International Journal of Intelligent Systems*, 17, 723-749.
- Gröchenig, K. (2001). *Foundations of time-frequency analysis*. Boston: Birkhäuser.
- Gross, K. C., Wegerich, S. W., Singer, R. M., & Mott, J. E. (1996). USA Patent No. US5764509 A.
- Gungor, V. C., & Hancke, G. P. (2009). Industrial wireless sensor networks: challenges, design principles, and technical approaches. *IEEE Transactions on Industrial Electronics*, 56, 4258-4265.
- Gutierrez, J. A., Naeve, M., Callaway, E., Bourgeois, M., Mitter, V., & Heile, B. (2001). IEEE 802.15.4: a developing standard for low-power low-cost wireless personal area networks. *IEEE Network*, 15, 12-19.
- Hamilton, J. D. (1994). *Time series analysis*. Princeton, N.J., USA: Princeton University Press.
- Hashemian, H. M. (2004). *Sensor performance and reliability*. Research Triangle Park, NC: The Instrumentation, Systems, and Automation Society.
- Hashemian, H. M. (2006). *Maintenance of process instrumentation in nuclear power plant. berlin heidelberg*: Springer.

Hashemian, H. M. (2011). Wireless sensors for predictive maintenance of rotating equipment in research reactors. *Annals of Nuclear Energy*, 38, 665–680.

Hashemian, H. M., & Bean, W. C. (2011). Sensors for next-generation nuclear plants: fiber-optic and wireless. *Nuclear Science and Engineering*, 169, 262–278.

Hashemian, H. M., & Jiang, J. (2010). Using the noise analysis technique to detect response time problems in the sensing lines of nuclear plant pressure transmitters. *Progress in Nuclear Energy*, 52, 367-373.

Hashemian, H. M., Kiger, C. J., Morton, G. W., & Shumaker, B. D. (2011). Wireless sensor applications in nuclear power plants. *Nuclear Technology*, 173, 8-16.

Hashemian, H. M., Thie, J. A., Upadhyaya, B. R., & Holbert, K. E. (1988). Sensor response time monitoring using noise analysis. . *Progress in Nuclear Energy*, 21, 583-592.

He, Q. P., Qin, S. J., & Wang, J. (2005). A new fault diagnosis method using fault directions in Fisher discriminant analysis. *AIChE Journal*, 51, 555-571.

Herzog, J. P., Wegerich, S. W., & Gross, K. C. (1998). *MSET modeling of Crystal River-3 venturi flow meters*. The 6th International Conference on Nuclear Engineering San Diego, CA, USA.

Hessel, G., Schmitt, W., Van der Vorst, K., & Weiss, F. P. (1999). A neural network approach for acoustic leak monitoring in the VVER-400 pressure vessel head. *Progress in Nuclear Energy*, 34, 173-183.

Hines, J. W., & Davis, E. (2005). Lessons learned from the U.S. nuclear power plant on-line monitoring programs. *Progress in Nuclear Energy*, 46, 176-189.

Hines, J. W., & Rasmussen, B. (2005). Online sensor calibration monitoring uncertainty estimation. *Nuclear Technology*, 151, 281-288.

Hines, J. W., & Seibert, R. (2006). Technical review of on-line monitoring techniques for performance assessment volume 1: state-of-the-art (NUREG/CR-6895). Washington DC: United States Nuclear Regulatory Commission.

Hines, J. W., & Usynin, A. (2005). MSET performance optimization through regularization. *Nuclear Engineering and Technology*, 37, 177-184.

Hlawatsch, F., & Boudreaux-Bartels, G. F. (1992). Linear and quadratic time-frequency signal representations. *IEEE Signal Processing Magazine*, 9, 21-67.

House, J. M., Lee, W. Y., & Shin, D. R. (1999). Classification techniques for fault detection and diagnosis of an air-handling unit. *ASHRAE Transactions*, 105, 1987-1997.

Hsu, C., & Lin, C. (2002). A comparison of methods for multiclass support vector machines. *IEEE Transactions on Neural Networks*, 13, 415-425.

Hu, Z., Cai, Y., Li, Y., & Xu, X. (2005). Data fusion for fault diagnosis using multi-class Support Vector Machines. *Journal of Zhejiang University SCIENCE*, 6A, 1030-1039.

Huang, N. E., Shen, Z., & Long, S. R. (1999). A new view of nonlinear water waves: the Hilbert spectrum. *Annual Review of Fluid Mechanics*, 31, 417-457.

Huang, N. E., Shen, Z., Long, S. R., Wu, M. C., Shih, H. H., Zheng, Q., Yen, N. C., Tung, C. C., & Liu, H. H. (1998). The empirical mode decomposition and the Hilbert spectrum for nonlinear and non-stationary time series analysis. *Proceedings of the Royal Society A*, 454, 903-995.

Hunt, J. S. (1986). The exponentially weighted moving average. *Journal of Quality Technology*, 18, 203-209.

Hyvärinen, A., & Oja, E. (2000). Independent component analysis: algorithms and applications. *Neural Networks*, 13, 411-430.

- Ichtertz, F. (2007). An Examination of the FF Standard Diagnostics Profile. Retrieved Nov 06, 2014, from http://www.fieldbus.org/images/stories/international/emea/middle-east/presentations/M07_12_fichtertz_ff_std_diagnostic_profile_5.12.07.pdf
- Isermann, R. (1984). Process fault detection based on modeling and estimation methods-a survey. *Automatica*, 20, 387-404.
- Isermann, R. (1992). Estimation of physical parameters for dynamic processes with application to an industrial robot. *International Journal of Control*, 55, 1287-1298.
- Isermann, R. (1993). Fault diagnosis of machines via parameter estimation and knowledge processing-tutorial paper. *Automatica*, 29, 815-835.
- Isermann, R. (2005). Model-based fault-detection and diagnosis - status and applications. *Annual Reviews in Control*, 29, 71-85.
- Isermann, R. (2006). *Fault-diagnosis systems: an introduction from fault detection to fault tolerance*: Springer.
- Isermann, R., & Balle, P. (1997). Trends in the application of model-based fault detection and diagnosis of technical processes. *Control Engineering Practice*, 5, 709-719.
- Jain, A. K., & Dubes, R. C. (1988). *Algorithms for clustering data*. Upper Saddle River, NJ, USA: Prentice-Hall, Inc. .
- Jain, A. K., Duin, R. P. W., & Mao, J. (2000). Statistical pattern recognition: a review. *IEEE Transactions on Pattern Analysis and Machine Intelligence*, 22, 4-37.
- Jain, A. K., Murty, M. N., & Flynn, P. J. (1999). Data clustering: a review. *ACM Computing Surveys*, 31, 264-323.
- James, R. W. (1996). *Calibration through on-line monitoring of instrument channels*. The 1996 IEEE Nuclear Science Symposium, Anaheim, CA, USA.
- Jaradat, M. A. B., & Langari, R. (2009). A hybrid intelligent system for fault detection and sensor fusion. *Applied Soft Computing*, 9, 415-422.

- Jeffrey, A. (2000). *Handbook of mathematical formulas and integrals* (2nd ed.): Academic Press.
- Jia, F., & Jiang, J. (1995). A robust fault diagnosis scheme based on signal modal estimation. *International Journal of Control*, 62, 461-475.
- Jiang, J., Chen, D., Bari, A., & Hashemian, H. M. (2014). *Technical survey on applications of wireless sensor networks in nuclear power plants*. ISOFIC2014, Jeju, Republic of Korea.
- Jiang, J., & Doraiswami, R. (1990). *Selection of optimal monitoring locations in real-time intelligent reconfigurable control systems*. Proceedings of the 5th IEEE International Symposium on Intelligent Control, pp. 766-770, Philadelphia, USA.
- Jiang, S., Fu, C., & Zhang, C. (2011). A hybrid data-fusion system using modal data and probabilistic neural network for damage detection. *Advances in Engineering Software*, 42, 368-374.
- Jiang, J., Ma, J., Bari, A., & Rankin, D. J. *A physical simulator in supporting of research and development for instrumentation and control systems in nuclear power plants*. Proceedings of the 9th International Conference on Nuclear Plant Instrumentation, Control & Human-Machine Interface Technologies, Charlotte, NC, USA, Feb. 23-26, 2015.
- Joachims, T. (1999). *Transductive inference for text classification using support vector machines*. Proceedings of the Sixteenth International Conference on Machine Learning.
- Jolliffe, I. T. (2002). *Principal component analysis* (2nd ed.): Springer.
- Kadri, A., Rao, R. K., & Jiang, J. (2009). Low-power chirp spread spectrum signals for wireless communication within nuclear power plants. *Nuclear Technology*, 166, 156-169.
- Kaistha, N., & Upadhyaya, R. B. (2001). Incipient fault detection and isolation of field devices in nuclear power systems using principal component analysis. *Nuclear Technology*, 136, 221-230.

- Kesavan, P., & Lee, J. H. (1997). Diagnostic tools for multivariable model-based control systems. *Industrial & Engineering Chemistry Research*, 36, 2725-2738.
- Khaleghi, B., Khamis, A., Karray, F. O., & Razavi, S. N. (2013). Multisensor data fusion: a review of the state-of-the-art. *Information Fusion*, 14, 28-44.
- Kidam, K., Hurme, M., & Hassim, M. H. (2010). Technical analysis of accident in chemical process industry and lessons learnt. *Chemical Engineering Transactions*, 19, 451-456.
- Kim, J. S., Hwang, I. K., Lee, D. Y., Ham, C. S., & Kim, T. H. (2000). Development of a mass estimation algorithm using the impact test data of nuclear power plant. *Journal of Korean Nuclear Society*, 32, 227-234.
- Kim, Y. B., Kim, S. J., Chung, H. D., Park, Y. W., & Part, J. H. (2003). A study of technique to estimate impact location of loose part using Wigner-Ville distribution. *Progress in Nuclear Energy*, 43, 261-266.
- Kitamura, M. (1989). Fault detection in nuclear reactors with the aid of parametric modelling methods. In R. Patton, P. M. Frank & R. Clark (Eds.), *Fault diagnosis in dynamic systems: theory and applications* (pp. 311-360). London, UK: Prentice Hall.
- Kolbasseff, A., & Sunder, R. (2003). Lessons learned with vibration monitoring systems in german nuclear power plants. *Progress in Nuclear Energy*, 43, 159-165.
- Kolen, P. T. (1994). Self-Calibration/Compensation Technique for Microcontroller-Based Sensor Arrays. *IEEE Transactions on Instrumentation and Measurement*, 43, 620-623.
- Korbicz, J., Koscielny, J. M., Kowalczyk, Z., & Cholewa, W. (2004). *Fault diagnosis: models, artificial intelligence, applications*: Springer.
- Kourti, T., & MacGregor, F. J. (1996). Multivariate SPC methods for process and product monitoring. *Journal of Quality Technology*, 28, 409-428.

- Kramer, M. A. (1991). Nonlinear principal component analysis using autoassociative neural networks. *AIChE Journal*, 37, 233–243.
- Kramer, M. A. (1992). Autoassociative neural networks. *Computers & Chemical Engineering*, 16, 313-328.
- Ku, W., Storer, R. H., & Georgakis, C. (1995). Disturbance detection and isolation by dynamic principal component analysis *Chemometrics and Intelligent Laboratory Systems*, 30, 179-196.
- Kunpeng, Z., San, W. Y., & Soon, H. G. (2009). Wavelet analysis of sensor signals for tool condition monitoring: A review and some new results. *International Journal of Machine Tools & Manufacture*, 49, 537-553.
- Kunze, U. (1999). Experience with the acoustic leakage monitoring system ALUES in 17 VVER plants. *Progress in Nuclear Energy*, 34, 213-220.
- Kwon, K. C. (2002). Hidden markov model based transient identification in NPPs. In D. Ruan & P. F. Fantoni (Eds.), *Power Plant Surveillance and Diagnostics: Applied Research and Diagnostics* (pp. 91-106): Springer.
- Lambert, H. E. (1977). Fault trees for locating sensors in process systems. *Chemical Engineering Progress*, 73, 81-85.
- Lee, C., Choi, S. W., & Lee, I. (2004). Sensor fault identification based on time-lagged PCA in dynamic processes. *Chemometrics and Intelligent Laboratory Systems*, 70, 165-178.
- Lee, J., Lee, M., Kim, J., Luk, V., & Jung, Y. (2006). A study of the characteristics of the acoustic emission signals for condition monitoring of check valves in nuclear power plants. *Nuclear Engineering and Design*, 236, 1411-1421.
- Lee, J., Yoo, C., Choi, S., Vanrolleghem, P. A., & Lee, I. (2004). Nonlinear process monitoring using kernel principal component analysis. *Chemical Engineering Science*, 59, 223-234.

- Lee, J. M., Qin, S. J., & Lee, I. B. (2007). Fault detection of non-linear processes using kernel independent component analysis. *The Canadian Journal of Chemical Engineering*, 85, 526-536.
- Li, B., Zhang, P., Liu, D., Mi, S., Ren, G., & Tian, H. (2011). Feature extraction for rolling element bearing fault diagnosis utilizing generalized S transform and two-dimensional non-negative matrix factorization. *Journal of Sound and Vibration*, 330, 2388-2399.
- Li, C. J., & Li, S. Y. (1995). Acoustic emission analysis for bearing condition monitoring. *Wear*, 185, 67-74.
- Li, F. (2011). *Dynamic modeling , sensor placement design, and fault diagnosis of nuclear desalination systems*. (Ph.D.), University of Tennessee, Knoxville.
- Li, F., & Upadhyaya, B. R. (2011). Design of sensor placement for an integral pressurized water reactor using fault diagnostic observability and reliability criteria. *Nuclear Technology*, 173, 17-25.
- Li, L., Wang, Q., Deng, C., Alexander, Q., Sur, B., Chen, D., & Jiang, J. (2014). *Radiation resistance test of wireless sensor node and the radiation shielding calculation*. ISOFIC2014, Jeju, Republic of Korea.
- Li, W., & Jiang, J. (2004). Isolation of parametric faults in continuous-time multivariable systems: a sampled data-based approach. *International Journal of Control*, 77, 173-187.
- Li, W., & Qin, S. J. (2001). Consistent dynamic pca based on error-in-variables subspace identification. *Journal of Process Control*, 11, 661-678.
- Li, W., & Shah, S. L. (2002). Structured residual vector-based approach to sensor fault detection and isolation. *Journal of Process Control*, 12, 429-443.
- Li, W., Yue, H. H., Valle-Cervantes, S., & Qin, S. J. (2000). Recursive PCA for adaptive process monitoring. *Journal of Process Control*, 10, 471-486.

- Liang, B., Iwnicki, S. D., & Zhao, Y. (2013). Application of power spectrum, cepstrum, higher order spectrum and neural network analyses for induction motor fault diagnosis. *Mechanical Systems and Signal Processing*, 39, 342-360.
- Liu, X., Ma, L., & Mathew, J. (2009). Machinery fault diagnosis based on fuzzy measure and fuzzy integral data fusion techniques. *Mechanical Systems and Signal Processing*, 23, 690-700.
- Lou, X. C., Willsky, A. S., & Verghese, G. C. (1986). Optimally robust redundancy relations for failure detection in uncertain systems. *IEEE Transactions on Automatic Control*, 31, 333-344.
- Loutas, T. H., Roulias, D., Pauly, E., & Kostopoulos, V. (2011). The combined use of vibration, acoustic emission and oil debris on-line monitoring towards a more effective condition monitoring of rotating machinery. *Mechanical Systems and Signal Processing*, 25, 1339-1352.
- Lu, T. (2009). *Fundamental limitations of semi-supervised learning*. University of Waterloo.
- Luo, H., Yang, S., Hu, X., & Hu, X. (2012). Agent oriented intelligent fault diagnosis system using evidence theory. *Expert Systems with Applications*, 39, 2524-2531.
- Ma, J. (2006). *Self-powered detectors for power reactors: an overview*. The 30th Annual CNA/CNS Student Conference., Toronto, Canada.
- Ma, J., & Jiang, J. (2009). *A fault detection and isolation technique for in-core flux detectors*. NPIC&HMIT 2009, Knoxville, Tennessee, USA.
- Ma, J., & Jiang, J. (2011). Applications of fault detection and diagnosis methods in nuclear power plants: A review. *Progress in Nuclear Energy*, 53, 255-266.
- Ma, J., & Jiang, J. (2012). Detection and identification of faults in NPP Instruments using Kernel Principal component Analysis. *Journal of Engineering for Gas Turbines and Power*, 134, 032901.

- Mallapragada, P. K., Jin, R., Jain, A. K., & Liu, Y. (2009). SemiBoost: boosting for semi-supervised learning. *IEEE Transactions on Pattern Analysis and Machine Intelligence*, 31, 2000 - 2014.
- Mansinha, L., Stockwell, R. G., Lowe, R. P., Eramian, M., & Schincariol, R. A. (1997). Local S-spectrum analysis of 1-D and 2-D data. *Physics of the Earth and Planetary Interiors*, 103, 329-336.
- McFadden, P. D., Cook, J. G., & Forster, L. M. (1999). Decomposition of gear vibration signals by the generalized S-transform. *Mechanical Systems and Signal Processing*, 13, 691-707.
- Mehala, N., & Dahiya, R. (2007). Motor current signature analysis and its applications in induction motor fault diagnosis. *International Journal of Systems Applications, Engineering and Development*, 2, 29-35.
- Mehrotra, K., Mohan, C. K., & Ranka, S. (1997). *Elements of artificial neural networks*. Cambridge, MA, USA: MIT Press.
- MEMSIC. (2014). Wireless sensor networks. Retrieved Oct 02, 2014, from <http://www.memsic.com/wireless-sensor-networks/>
- Michela, B., & Puyala, C. (1988). Operational and economical experience with vibration and loose parts monitoring systems on primary circuits of PWRs. *Progress in Nuclear Energy*, 21, 469-473.
- Mika, S., Ratsch, G., Weston, J., Scholkopf, B., & Muller, K. (1999, 23-25 Aug). *Fisher discriminant analysis with kernels*. Proceedings of the 1999 IEEE Signal Processing Society Workshop, Madison, WI, USA.
- Mika, S., Schölkopf, B., Smola, A., Müller, K. R., Scholz, M., & Rätsch, G. (1999). Kernel PCA and de-noising in feature spaces. *Advances in Neural Information Processing Systems*, 11, 536-542.

- Montgomery, D. C. (2005). *Introduction to statistical quality control* (5th ed.): John Wiley.
- Moshkbar-Bakhshayesh, K., & Ghofrani, M. B. (2013). Transient identification in nuclear power plants: a review. *Progress in Nuclear Energy*, 67, 23-32.
- Murty, M. N., & Devi, V. S. (2011). *Pattern recognition: an algorithmic approach*: Springer.
- Musulin, E., Benqlilou, C., Bagajewicz, M., & Puigjaner, L. (2005). Instrumentation design based on optimal kalman filtering. *Journal of Process Control*, 15, 629-638.
- Namburu, S. M., Azam, M. S., Luo, J., Choi, K., & Pattipati, K. R. (2007). Data-driven modeling, fault diagnosis and optimal sensor selection for HVAC chillers. *IEEE Transactions on Automation Science and Engineering*, 4, 469-473.
- Narasimhan, S., Mosterman, P., & Biswas, G. (1998). *A systematic analysis of measurement selection algorithms for fault isolation in dynamic systems*. Proceedings of the 9th International Workshop on Principles of Diagnosis, Cape Cod.
- Neill, G. D., Reuben, R. L., Sandford, P. M., Brown1, E. R., & Steel, J. A. (1997). Detection of incipient cavitation in pumps using acoustic emission. *Proceedings of the Institution of Mechanical Engineers, Part E: Journal of Process Mechanical Engineering*, 211, 267-277.
- Ng, A. Y., Jordan, M. I., & Weiss, Y. (2001). On spectral clustering: analysis and an algorithm. *Advances in Neural Information Processing Systems*, 14, 849-856.
- Nieman, W., & Singer, R. (2002). Detection of incipient signal or process faults in co-generation plant using the plant ecm system. In D. Ruan & F. P. Fantoni (Eds.), *Power Plant Surveillance and Diagnostics: Applied Research with Artificial Intelligence* (pp. 121-134): Springer.

- Niu, G., Widodo, A., Son, J. K., Yang, B. S., Hwang, D. H., & Kang, D. S. (2008). Decision-level fusion based on wavelet decomposition for induction motor fault diagnosis using transient current signal. *Expert Systems with Applications*, 35, 918-928.
- Niyogi, P. (2013). Manifold regularization and semi-supervised learning: some theoretical analyses. *Journal of Machine Learning Research*, 14, 1229-1250.
- Nomikos, P., & MacGregor, J. F. (1994). Monitoring batch processes using multiway principal component analysis. *AIChE Journal*, 40, 1361-1375.
- Olma, B. J. (1985). Source location and mass estimation in loose parts monitoring of LWR's. *Progress in Nuclear Energy*, 15, 583-594.
- Onchis, D. M., Yan, R., & Rajmic, P. (2014). Time–frequency methods for condition based maintenance and modal analysis. *Signal Processing*, 96, 4-5.
- Oppermann, F. J., Boano, C. A., & Römer, K. (2014). A decade of wireless sensing applications: survey and taxonomy. In H. M. Ammari (Ed.), *The art of wireless sensor networks: volume 1: fundamentals*: Springer-Verlag Berlin Heidelberg.
- Oukhellou, L., Debiolles, A., Denœux, T., & Aknin, P. (2010). Fault diagnosis in railway track circuits using Dempster–Shafer classifier fusion. *Engineering Applications of Artificial Intelligence*, 23, 117-128.
- Padula, S. L., & Kincaid, R. K. (1999). Optimization strategies for sensor and actuator placement: NASA/TM-1999-209126.
- Palade, V., & Bocaniala, C. D. (2006). *Computational intelligence in fault diagnosis*. London: Springer.
- Pan, Y., Chen, J., & Li, X. (2010). Bearing performance degradation assessment based on lifting wavelet packet decomposition and fuzzy c-means. *Mechanical Systems and Signal Processing*, 24, 559–566.
- Papoulis, A. (1977). *Signal analysis*. New York: McGraw-Hill.

- Parikh, C. R., Pont, M. J., & Jones, N. B. (2001). Application of Dempster–Shafer theory in condition monitoring applications: a case study. *Pattern Recognition Letters*, 22, 777–785.
- Park, G. Y., Lee, C. K., Kim, J. T., Ryu, J. S., & Jung, H. S. (2006). *Identification of nuclear components degradation by time-frequency ridge pattern*. NPIC&HMIT 2006, Albuquerque, NM.
- Park, J., Lee, J. H., Kim, T. R., Park, J. B., Lee, S. K., & Koo, I. S. (2003). Identification of reactor internals' vibration modes of a korean standard PWR using structural modeling and neutron noise analysis. *Progress in Nuclear Energy*, 42, 177-186.
- Park, J. H., & Lee, J. H. (2006). Application of continuous wavelet transform to the impact location estimation of the loose part monitoring system (LPMS). *International Journal of Nuclear Science and Technology*, 2, 233-240.
- Patton, R. J., & Chen, J. (1997). Observer-based fault detection and isolation: robustness and applications. *Control Engineering Practice*, 5, 671-682.
- Paya, B. A., Esat, I. I., & Badi, M. N. M. (1997). Artificial neural network based fault diagnostics of rotating machinery using wavelet transforms as a preprocessor. *Mechanical Systems and Signal Processing*, 11, 751-765.
- Peng, Z. K., & Chu, F. L. (2004). Application of the wavelet transform in machine condition monitoring and fault diagnostics: a review with bibliography. *Mechanical Systems and Signal Processing*, 18, 199-221.
- Peng, Z. K., Tse, P. W., & Chu, F. L. (2005). A comparison study of improved Hilbert–Huang transform and wavelet transform: Application to fault diagnosis for rolling bearing. *Mechanical Systems and Signal Processing*, 19, 974–988.
- Persion, J. V. (1999). Commercial nuclear reactor loose part monitoring setpoints. *Progress in Nuclear Energy*, 34, 203-211.

- Pinnegar, C. P., & Mansinha, J. (2003). Time-local spectral analysis for non-stationary time series: the S-transform for noisy signals. *Fluctuations and Noise Letters*, 3, 357-364.
- Pinnegar, C. R., & Mansinha, L. (2003a). The bi-Gaussian S-transform. *SIAM Journal on Scientific Computing*, 24, 1678-1692.
- Pinnegar, C. R., & Mansinha, L. (2003b). The S-transform with windows of arbitrary and varying shape. *Geophysics*, 68, 381-385.
- Pokol, G., & Por, G. (2006). The advanced loose part monitoring system (ALPS) and wavelet analysis. *International Journal of Nuclear Science and Technology*, 2, 241-252.
- Powner, E. T., & Yalcinkaya, F. (1995). Intelligent Sensors: Structure and System. *Sensor Review*, 15, 31-35.
- Press, D. (2003). *Guidelines for failure mode and effects analysis (FMEA), for automotive, aerospace, and general manufacturing industries*. Boca Raton, Fla.: CRC Press.
- Qian, S. (2002). *Introduction to time-frequency and wavelet transforms*. Upper Saddle River, N.J.: Prentice Hall.
- Qin, S. J. (1998). Recursive PLS algorithms for adaptive data modeling. *Computers and Chemical Engineering*, 22, 503-514.
- Qin, S. J. (2003). Statistical process monitoring: basics and beyond. *Journal of Chemometrics*, 17, 480-502.
- Qin, S. J. (2012). Survey on data-driven industrial process monitoring and diagnosis. *Annual Reviews in Control*, 36, 220-234.
- Qin, S. J., & Li, W. (1999). Detection, identification, and reconstruction of faulty sensors with maximized sensitivity. *AIChE Journal*, 45, 1963-1976.
- Qin, S. J., & Li, W. (2001). Detection and identification of faulty sensors in dynamic processes. *AIChE Journal*, 47, 1581-1593.

- Qin, S. J., & McAvoy, T. J. (1992). Nonlinear PLS modeling using neural networks. *Computers and Chemical Engineering*, 16, 379-391.
- Raghuraj, R., Bhushan, M., & Rengaswamy, R. (1999). Locating sensors in complex chemical plants based on fault diagnostic observability criteria. *American Institute of Chemical Engineering Journal*, 45, 310-322.
- Rasmussen, B., Hines, J. W., & Uhrig, R. E. (2000). *Nonlinear partial least squares modeling for instrument surveillance and calibration verification*. MARCON 2000, Knoxville, TN, USA.
- Rathi, Y., Dambreville, S., & Tannenbaum, A. R. (2006). *Statistical shape analysis using kernel PCA*. Proceedings of SPIE 6064, San Jose, CA, USA.
- Rehorn, A. G., Sejdic, E., & Jiang, J. (2006). Fault diagnosis in machine tools using selective regional correlation. *Mechanical Systems and Signal Processing*, 20, 1221-1238.
- Reimche, W., Südmersen, U., Pietsch, O., Scheer, C., & Bach, F. W. (2003). *Basics of vibration monitoring for fault detection and process control*. The 3rd Pan-American Conference for Non-Destructive Testing, Rio de Janeiro, Brazil.
- Robinson, J. C., Hardy, J. W., Shamblin, G. R., & Wolff, C. L. (1977). Monitoring of core support barrel motion in pwr's using ex-core detectors. *Progress in Nuclear Energy*, 1, 369-378.
- Rogovin, M., & Frampton, J., G. T. (1980). Three Mile Island: a report to the commissioners and to the public, vol. I: U. S. Nuclear Regulatory Commission.
- Rosipal, R., & Kramer, N. (2006). Overview and recent advances in partial least squares. *Lecture Notes in Computer Science*, 3940(34-51).
- Rouben, B. (1999). CANDU fuel management course. Retrieved Sep 03, 2014, from <http://canteach.candu.org/library/20031101.pdf>

- Roverso, D. (2002). Plant diagnostics by transient classification: the ALADDIN approach. *International Journal of Intelligent Systems*, 17, 767-790.
- Russell, E. L., Chiang, L. H., & Braatz, R. D. (2000). Fault detection in industrial processes using canonical variate analysis and dynamic principal component analysis. *Chemometrics and Intelligent Laboratory Systems*, 51, 81-93.
- Saidia, L., Fnaiech, F., Henao, H., Capolino, G.-A., & Cirrincione, G. (2013). Diagnosis of broken-bars fault in induction machines using higher order spectral analysis. *ISA Transactions*, 52, 140-148.
- Salahshoor, K., Mosallaei, M., & Bayat, M. (2008). Centralized and decentralized process and sensor fault monitoring using data fusion based on adaptive extended Kalman filter algorithm. *Measurement*, 41, 1059-1076.
- Santosh, T. V., Vinod, G., Saraf, R. K., Ghosh, A. K., & Kushwaha, H. S. (2007). Application of artificial neural networks to nuclear power plant. *Reliability Engineering and System Safety* 92, 1468-1472.
- Schölkopf, B., & Smola, A. (2002). *Learning with kernels: support vector machines, regularization, optimization, and beyond*: The MIT Press, Cambridge, MA.
- Schölkopf, B., Smola, A., & Müller, K.-R. (1998). Nonlinear component analysis as a kernel eigenvalue problem. *Neural Computation*, 10, 1299-1319.
- Seeger, M. (2001). Learning with labeled and unlabeled data. Edinburgh, UK: University of Edinburgh.
- Sejdic, E., Djurovic, I., & Jiang, J. (2008). A window width optimized S-transform. *EURASIP Journal on Advances in Signal Processing*(672941).
- Sejdić, E., Djurović, I., & Jiang, J. (2009). Time–frequency feature representation using energy concentration: an overview of recent advances. *Digital Signal Processing*, 19, 153-183.

Sentz, K., & Ferson, S. (2002). Combination of evidence in Dempster-Shafer theory: Sandia National Laboratory.

Shafer, G. (1976). *A mathematical theory of evidence*: Princeton University Press.

Shankar, R. (2004). EPRI's wireless technology newsletter - July 2004: Electric Power Research Institute.

Shaw-Taylor, J., & Cristianini, N. (2004). *Kernel methods for pattern analysis*: Cambridge University Press.

Shi, H., Liu, J., & Zhang, Y. (2009). *An optimized kernel principal component analysis algorithm for fault detection*. The 7th IFAC Symposium on Fault Detection, Supervision and Safety of Technical Processes, Barcelona, Spain.

Shi, J., & Malik, J. (2000). Normalized cuts and image segmentation. *IEEE Transactions on Pattern Analysis and Machine Intelligence*, 22, 888-905.

Singh, A., Nowak, R. D., & Zhu, X. (2008). Unlabeled data: now it helps, now it doesn't. *Advances in Neural Information Processing Systems*, 21, 1513-1520.

Stamatis, D. H. (2003). *Failure mode and effect analysis : FMEA from theory to execution*. Milwaukee, Wisc.: ASQ Quality Press.

Steinberg, A. N., Bowman, C. L., & White, F. E. (1999). Revisions to the JDL data fusion model. *Proceedings of SPIE*, 3719.

Stockwell, R. G., Mansinha, L., & Lowe, R. P. (1996). Localization of the complex spectrum: the S Transform. *IEEE Transactions on Signal Processing*, 44, 998-1001.

Sun, H., Xue, Z., Du, Y., & Sun, L. (2010). *Power transformer fault diagnosis based on fuzzy C-means clustering and multi-class SVM*. The 2010 International Conference on Machine Learning and Cybernetics.

- Szappanos, G., Kiss, J. J., Por, G., & Kiss, J. M. (1999). Analysis of measurements made by helps loose part detection system during installation and operation periods. *Progress in Nuclear Energy*, 34, 184-193.
- Takahashi, T., & Kurita, T. (2002). Robust de-noising by kernel PCA *Artificial Neural Networks—ICANN 2002*: Springer Berlin Heidelberg.
- Tandon, N., & Choudhury, A. (1999). A review of vibration and acoustic measurement methods for the detection of defects in rolling element bearings. *Tribology International*, 32, 469-480.
- Tavner, P., Ran, L., Penman, J., & Sedding, H. (2008). *Condition monitoring of rotating electrical machines* (2 ed.): Stylus Publishing.
- Teppola, P., Mujunen, S., & Minkkinen, P. (1999). Adaptive Fuzzy C-Means clustering in process monitoring. *Chemometrics and Intelligent Laboratory Systems*, 45, 23-38.
- Tham, C.-K. (2007). SensorGrid architecture for distributed event classification. In N. P. Mahalik (Ed.), *Sensor Networks and Configuration: Fundamentals, Standards, Platforms, and Applications*: Springer.
- Thie, J. A. (1981). *Power reactor noise*. LaGrange Park, Illinois: American Nuclear Society.
- TinyOs. (2014). Retrieved Oct 06, 2014, from <http://www.tinyos.net/>
- Tombs, M. (2002). Intelligent and Self-Validating Sensors and Actuators. *Computer & Control Engineering Journal*, 13, 218-220.
- Ueda, M., Tomobe, K., Setoguchi, K., & Endou, A. (2002). Application of autoregressive models to in-service estimation of transient response for LMFBR process instrumentation. *Nuclear Technology*, 137, 163-168.
- Uhrig, R. E., & Hines, J. W. (2005). Computational intelligence in nuclear engineering. *Nuclear Engineering and Technology*, 37, 127-138.

- Uhrig, R. E., & Tsoukalas, L. H. (1999). Soft computing techniques in nuclear engineering applications. *Progress in Nuclear Energy*, 34, 13-75.
- Upadhyaya, R. B., Zhao, K., & Lu, B. (2003). Fault monitoring of nuclear power plant sensors and field devices. *Progress in Nuclear Energy*, 43, 337-342.
- Van Overschee, P., & De Moor, B. (1994). N4SID: Subspace algorithms for the identification of combined deterministic-stochastic systems. *Automatica*, 30, 75-93.
- Van Overschee, P., & De Moor, B. (1995). A unifying theorem for three subspace system identification algorithms. *Automatica*, 31, 1853-1864.
- Vapnik, V. (1998). *Statistical learning theory*. : John Wiley & Sons.
- Venkatasubramanian, V., Rengaswamy, R., & Kavuri, S. N. (2003). A review of process fault detection and diagnosis: part II: qualitative models and search strategies. *Computers & Chemical Engineering*, 27, 313-326.
- Venkatasubramanian, V., Rengaswamy, R., Kavuri, S. N., & Yin, K. (2003). A review of process fault detection and diagnosis: part III: process history based methods. *Computers & Chemical Engineering*, 27, 327-346.
- Venkatasubramanian, V., Rengaswamy, R., Yin, K., & Kavuri, S. N. (2003). A review of process fault detection and diagnosis: part I: quantitative model-based methods. *Computers & Chemical Engineering*, 27, 293-311.
- Venkatasubramanian, V., Vaidyanathan, R., & Yamamoto, Y. (1990). Process fault detection and diagnosis using neural networks I: steady state processes. *Computers and Chemical Engineering*, 14, 699-712.
- Verhaegen, M., & Dewilde, P. (1992). Subspace model identification part I. the output-error state-space model identification class of algorithms. *International Journal of Control*, 56, 1187-1210.

- Von Luxburg, U. (2007). A tutorial on spectral clustering. *Statistics and Computing*, 17, 395-416.
- Wallace, C. J., West, G. M., McArthur, S. D. J., & Towle, D. (2012). Distributed data and information fusion for nuclear reactor condition monitoring. *IEEE Transactions on Nuclear Science*, 59, 182-189.
- Wang, D., & Man, Z. (2014). Special issue: Data-driven fault diagnosis of industrial systems. *Information Sciences*, 259, 231-233.
- Wang, P., Tamilselvan, P., & Hu, C. (2014). Health diagnostics using multi-attribute classification fusion. *Engineering Applications of Artificial Intelligence*, 32, 192–202.
- Wang, Q., Li, L., Jiang, J., Bari, A., Deng, C., Sur, B., & Chen, D. (2014). *Experimental evaluation of wireless communication channels under radiation environment*. ISOFIC2014, Jeju, Republic of Korea.
- Watanabe, K., Matsura, I., Abe, M., Kubota, M., & Himmelblau, D. M. (1989). Incipient fault diagnosis of chemical processes via artificial neural networks. *American Institute of Chemical Engineers Journal*, 35, 1803-1812.
- Webb, A. R. (1996). An approach to non-linear principal components analysis using radially symmetric kernel functions. *Statistics and Computing*, 6, 159-168.
- Webb, A. R., & Copsey, K. D. (2011). *Statistical pattern recognition* (3rd ed.): Wiley.
- White, A. M., Gross, K. C., Kubic, W. L., & Wigeland, R. A. (1994). US5586066 A.
- Widodo, A., & Yang, B. S. (2007). Support vector machine in machine condition monitoring and fault diagnosis. *Mechanical Systems and Signal Processing*, 21, 2560-2574.
- Willig, A., Matheus, K., & Wolisz, A. (2005). Wireless technology in industrial networks. *Proceedings of the IEEE*, 93, 1130 - 1151.

- Willsky, A. S. (1976). A survey of design methods for failure detection in dynamic systems. *Automatica*, 12, 601-611.
- Willsky, A. S. (1986). Detection of abrupt changes in dynamic systems. In M. Basseville & A. Benveniste (Eds.), *Detection of abrupt changes in signals and dynamical systems* (pp. 27-49): Springer.
- Wise, B. M., & Gallagher, N. B. (1996). The process chemometrics approach to process monitoring and fault detection. *Journal of Process Control*, 6, 329-348.
- Wold, S. (1994). Exponentially weighted moving principal components analysis and projections to latent structures. *Chemometrics and Intelligent Laboratory Systems*, 23, 149-161.
- Wu, J., & Liu, C. (2009). An expert system for fault diagnosis in internal combustion engines using wavelet packet transform and neural network. *Expert Systems with Applications*, 36, 4278-4286.
- Wu, X., Chen, J., Wang, W., & Zhou, Y. (2001). Multi-index fusion-based fault diagnosis theories and methods. *Mechanical Systems and Signal Processing*, 15, 995-1006.
- Xu, Y., & Jiang, J. (2000). *Optimal sensor location in closed-loop control systems for fault detection and isolation*. Proceedings of the 2000 American Control Conference, Chicago, IL.
- Yager, R. R., & Liu, L. (Eds; 2008). *Classic works of the Dempster-Shafer theory of belief functions*: Springer.
- Yan, R., Gao, R. X., & Chen, X. (2014). Wavelets for fault diagnosis of rotary machines: A review with applications. *Signal Processing*, 96, 1-15.
- Yang, B. S., & Kim, K. J. (2006). Application of Dempster-Shafer theory in fault diagnosis of induction motors using vibration and current signals. *Mechanical Systems and Signal Processing*, 20, 403-420.

- Yang, S. H. (2014). *Wireless sensor networks: principles, design and applications*: Springer.
- Ye, H., Wu, B., & Sadeghian, A. (2003). Current signature analysis of induction motor mechanical faults by wavelet packet decomposition. *IEEE Transactions on Industrial Electronics*, 50, 1217-1228.
- Yoon, D. B., Park, J. H., Choi, Y. C., Sohn, C. H., & Park, O. K. (2006). *An improvement of mass estimation capability in loose parts monitoring by using time-frequency analysis*. NPIC&HMIT 2006, Albuquerque, NM.
- Yoon, S., & MacGregor, J. F. (2004). Principal-component analysis of multiscale data for process monitoring and fault diagnosis. *AIChE Journal*, 50, 2891-2903.
- Yu, D., Yang, Y., & Cheng, J. (2007). Application of time–frequency entropy method based on Hilbert–Huang transform to gear fault diagnosis. *Measurement*, 40, 823–830.
- Yun, W. Y., Koh, B. J., Park, I. Y., & No, H. C. (1988). Neutron noise analysis for PWR core motion monitoring. *Journal of the Korean Nuclear Society*, 20, 253-264.
- Zaytoon, J., & Lafortune, S. (2013). Overview of fault diagnosis methods for discrete event systems. *Annual Reviews in Control*, 37, 308-320.
- Zhang, G. (2005). *Optimum sensor localization/selection in a diagnostic/prognostic architecture*. (Ph.D.), Georgia Institute of Technology
- Zhang, J. (2006). Improved on-line process fault diagnosis through information fusion in multiple neural networks. *Computers and Chemical Engineering*, 30, 558-571.
- Zhang, Y., & Qin, S. J. (2007). Fault detection of nonlinear processes using multiway kernel independent component analysis. *Industrial & Engineering Chemistry Research*, 46, 7780-7787.
- Zhou, D., Bousquet, O., Lal, T. N., Weston, J., & Schölkopf, B. (2004). Learning with local and global consistency. *Advances in Neural Information Processing Systems*, 16.

- Zhu, X. (2005). *Semi-supervised learning with graphs*. (Ph.D.), Carnegie Mellon University.
- Zhu, X. (2008). Semi-supervised learning literature survey *Computer Sciences Technical Report 1530*: University of Wisconsin–Madison.
- Zhu, X., Ghahramani, Z., & Lafferty, J. (2003). *Semi-supervised learning using gaussian fields and harmonic functions*. The 20th International Conference on Machine Learning
- Zhu, X., & Goldberg, A. B. (2009). *Introduction to semi-supervised learning*: Morgan and Claypool Publishers.
- Zhu, Z., & Song, Z. (2011). A novel fault diagnosis system using pattern classification on kernel FDA subspace. *Expert Systems with Applications*, 38, 6895–6905.
- Zio, E., & Baraldi, P. (2005a). Evolutionary fuzzy clustering for the classification of transients in nuclear component. *Progress in Nuclear Energy*, 46, 282-296.
- Zio, E., & Baraldi, P. (2005b). Identification of nuclear transients via optimized fuzzy clustering. *Annals of Nuclear Energy*, 32, 1068–1080.
- Zio, E., & Gola, G. (2006). Neuro-fuzzy pattern classification for fault diagnosis in nuclear components. *Annals of Nuclear Energy*, 33, 415-426.

Appendices

Appendix A: NPP Process Control Test Facility

The NPCTF is a system that physically simulates major processes of a typical nuclear power plant, including the main pump, reactor, steam generator, pressurizer, main steam system, turbine, and generator. The NPCTF also includes systems that simulate the NPP inventory control system, two independent shutdown systems, and a passive emergency core cooling system. The process control loops of the NPCTF are designed to simulate the working principles of major control functions in a NPP, including coolant flow control, reactor power control, pressure and inventory controls for the heat transport system, steam generator level control, steam generator pressure control, steam pressure control, and turbine speed control. The NPCTF also has safety protection control and emergency core cooling control. A front view of the complete NPCTF system is shown in Figure A-1.

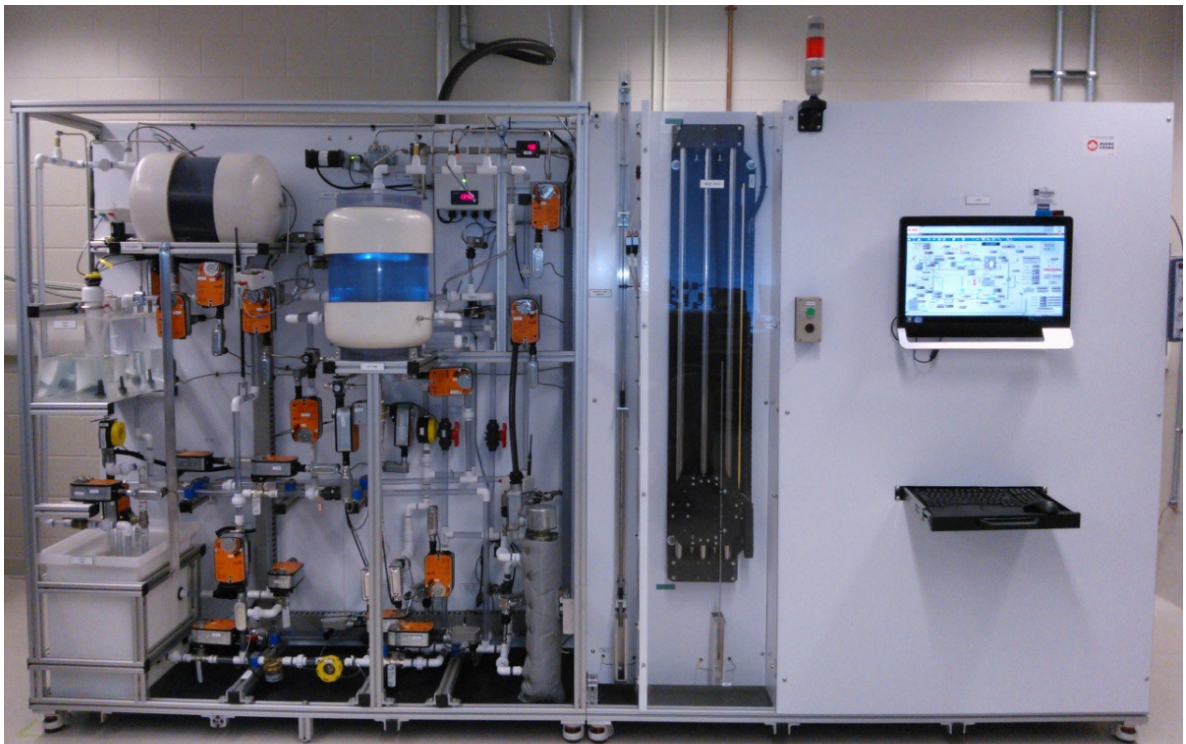


Figure A-1: Front view of the NPCTF

The NPCTF can be operated in three different modes. The first mode is normal mode. The NPCTF operates in a closed water loop with a pressurizer. It is the default operation mode that simulates a normal operating NPP. The second mode is solid mode. It operates in a closed water loop without a pressurizer. It simulates the solid modes of a NPP in special situations such as warm up. The third operation mode is open mode. In this mode, the coolant flows in an open loop. The system is no longer a NPP simulator, but a general purpose process control facility.

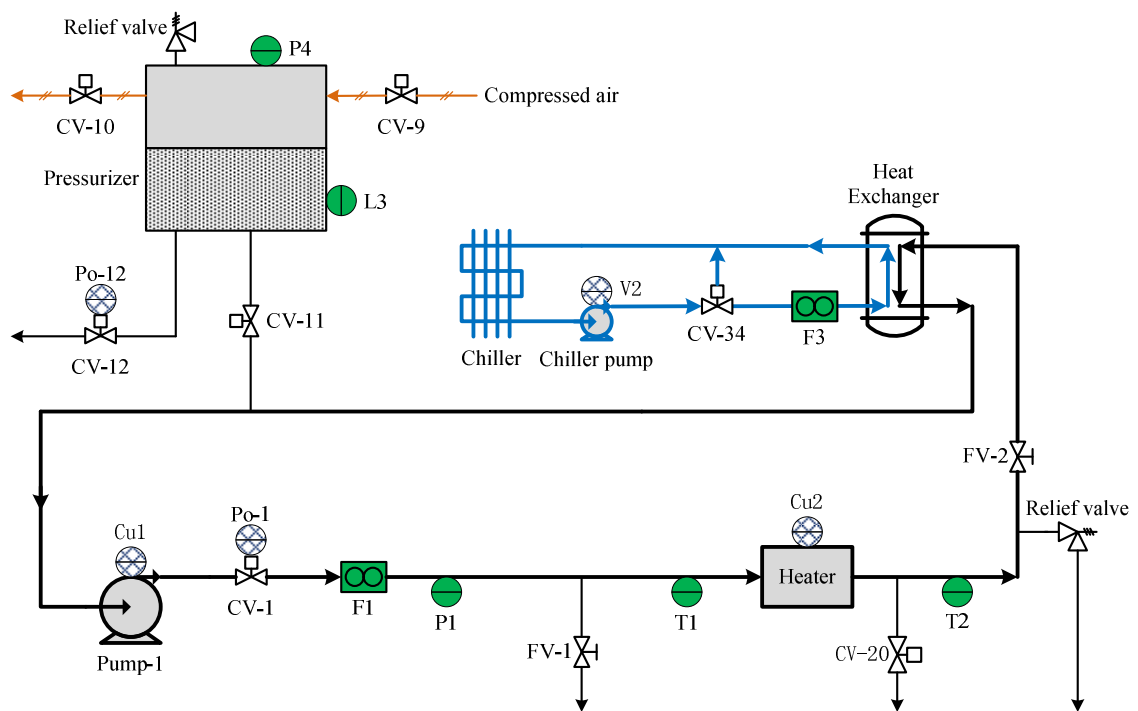


Figure A-2: Diagram of selected NPCTF loops

Because only selected loops with the normal operation mode are used for experimental validations reported in this thesis, only the selected components will be explained in more details in this appendix. A diagram of the selected NPCTF loops has been shown in Figure A-2. It is shown again here, as Figure A-2, for easier reference. Pump-1 simulates the main pump of a NPP. It provides the pressure head to driven coolant flow in the

closed water loop. CV-1 is a proportional valve that can be used to regulate the coolant flow rate F1. The sensor P1 measures the coolant pressure. The heater is a 7.5kW electric heater that simulates the reactor of a NPP. The heater power can be regulated linearly. The temperature sensors T1 and T2 measure the cold leg and hot leg temperature, respectively. The heat exchanger (HX) simulates the steam generator of a NPP. Coolant flows on one side of the HX and chilled water flows on the second side. The exit coolant temperature is cooled by the chilled water flow. The chilled water is supplied by a fan-cooled chiller system. A three valve CV-34 is used to control the chilled water flow rate to the HX, and the flow is measured by the sensor F3. A pressurizer is connected to the coolant system through an on/off type valve CV-11. CV-11 is set open with the normal operation mode. The pressurizer pressure can be regulated by feeding compressed air in through CV-9 or bleeding air out through CV-10. CV-12 is part of the inventory control system. The rest of the inventory control system is not shown because they are not considered in this research. FV-1 and FV-2 are two manual valves that can be used to introduce fault. CV-20 is an on/off type valve that belongs to the emergency core cooling system (ECCS). The rest of the ECCS is not shown because they are not used in this thesis. Two relief valves are installed to protect the system from potentially dangerous high pressure.

Table A-1: Control loops of the considered NPCTF system

Controlled parameter	Feedback signal	Manipulated variable	Comments
Coolant flow	F1	CV-1 opening	N/A
Hot leg temperature	T2	Heater current	N/A
Cold leg temperature	T3	CV-34 opening	T3 (not shown in Figure A-2) is equivalent to T1
Pressurizer pressure	P4	CV-9 & CV-10 openings	CV-9 to increase P4, and CV-10 to decrease P4
Pressurizer level	L3	CV-12 and CV-16 openings	CV-12 to decrease L3. CV-16 (not show in Figure A-2) is connected to a feed pump to increase L3 if required

The system shown in Figure A-2 contains several control loops, as summarized in Table A-1. The control loops can be set in automatic control mode, when the controller will regulate the manipulated variables to track the corresponding set-points. The control can

also be put in manual mode when the operator can set the valve openings and heater power manually. In addition, all the valves in the NPCTF have physical measurements of the valve positions. The position signals will be referred to as “Po-xx”, where xx is the number of the valve.

The current NPCTF has several characteristics in real operations. First, the heater needs a minimum flow rate of 2 l/m to operate. If the flow is lower than 2 l/m, the heater will trip as self-protection. For this reason, the CV-1 and FV-2 need certain minimum openings to keep the heater working, and the pump-1 cannot be tripped. Second, the chiller has standalone chilled water temperature control based on a thermostat. The thermostat has a minimum differential temperature of 1°C. The cooling fan of the chiller will stop when the chilled water temperature is 1°C below the set-point, and the fan will not start until the chilled water temperature is 1°C above the set-point. Due to inertial, the chilled water temperature actually varies over 2°C. In addition, the cooling capacity of the chiller is much more than the heater power. Therefore, the coolant temperature at the HX exit (equivalent to T1) is actually more influenced by the chilled water temperature than the chilled water flow. This problem is further compromised by the fact that the CV-34 has a relatively long response time. As a result, the coolant temperature T1 cannot be accurately controlled by the chilled water flow rate through regulating CV-34. Instead, T1 actually fluctuates around the set-point in response to the chilled water temperature. Furthermore, the chilled water flow measurement F3 has significant noise and uncertainties. A possible reason is trapped air bubbles in the chilled water flow path.

Various faults can be injected into the NPCTF. The first way is to open or close the manual valves FV-1 and FV-2. The second way is to set the valve openings in abnormal values in manual control mode. For example, CV-12 and CV-20 can be forced open to create scenarios of loss of coolant accidents. This method applies to all the valves. Similarly, the heater power can also be put in manual control mode to simulate abnormal power levels. Finally, the chiller system can be tripped manual to stop the chiller, chiller pump, and cooling fan.

The instrumentation and control system of the NPCTF is also specially designed for versatile interfaces with PLC, DCS, fieldbus systems, and wireless systems. Specifically, all the sensors have industrial standard 4-20mA output signals. Each 4-20mA signal is divided into four independent and identical current signals using a current splitter. One of the four channels is used for the standalone DCS-based control system. The DCS is configured to archive all the process measurements with a sampling interval of one second. Two of the redundant signal channels are connected to a junction box for interface with external I&C systems. The measurement signals to the sensor nodes in the prototype WSN system are actually drawn from the junction box, but the sensor nodes are physically installed near the measurement locations. The NPCTF is also designed to be independently operable by different control systems. For this purpose, mechanisms are included to select control signals from different control systems. This is not discussed further because it is not utilized in this research. The current splitters, control signal selection systems, and the junction box containing interfaces to external control systems are shown in Figure A-13.

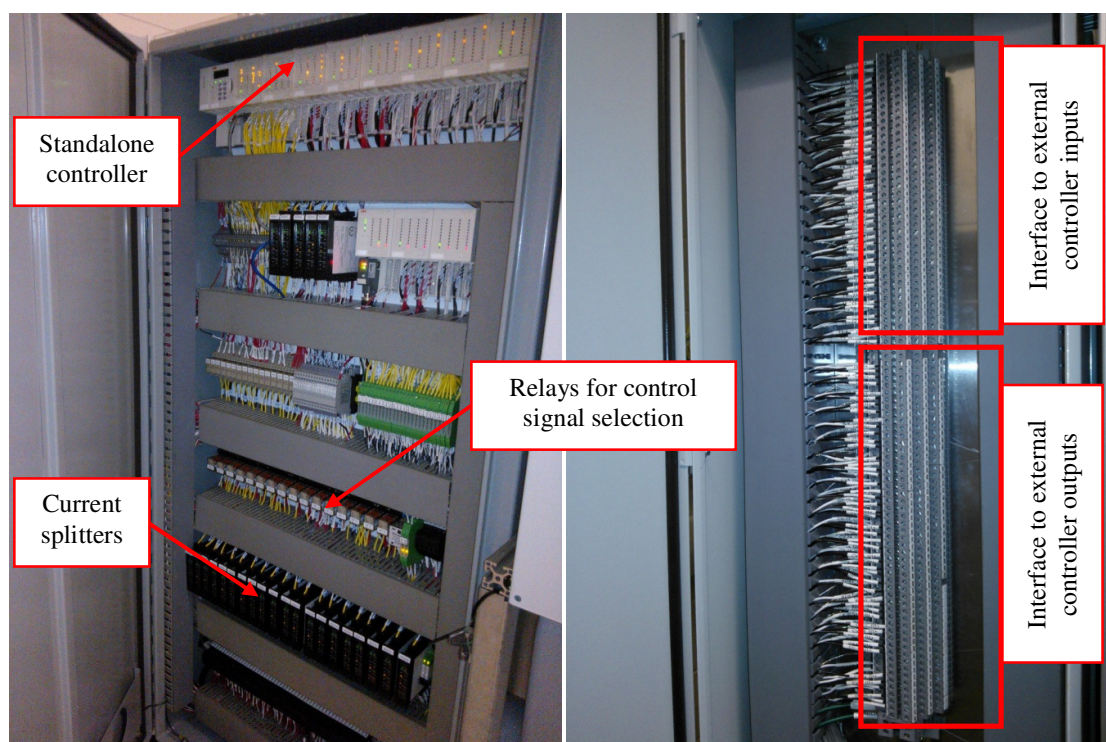


Figure A-3: Pictures of selected components of the NPCTF I&C system

Appendix B: FMEA of Selected NPCTF Loops

FMEA of selected NPCTF loops used for sensor placement studies is shown in Table A-2. The faults with a risk priority number of no less than 200 are considered for the sensor placement studies.

Table A-2: FMEA of selected NPCTF loops

Step in process	Mode of Failure	Cause of Failure	Effects of Failure	Degree of Severity (1-10)	Frequency of Occurrence (1-10)	Likelihood of Detection (1-10)	Risk Priority Number	Control Action
Circulation Pump	Pressure head low	Pump-1 trip	Loss of coolant flow to HTR	7	5	8	280	Cu1
Primary water flow control	Flow high	CV-1 fail open	Coolant flow high	1	5	6	30	Po-1
	Flow low	CV-1 fail close	Coolant flow to HTR restricted	6	5	8	240	Po-1
Pipe between pump and heater	Inventory loss	FV-1 open	Loss of pres., inventory, and coolant flow to HTR	8	6	10	480	N/A
Heater	Power low	Power failure	Loss of heat source	1	5	2	10	Cu2
	Power high	Power too high	Excessive heat	7	4	8	224	Cu2
Pipe between heater and HX	Flow restrained	FV-2 closed	Coolant flow to HTR restricted	6	6	10	360	N/A
	Inventory loss	CV-20 open	Loss of pres. and inventory	6	5	8	240	Po-34
Chilled water system	Chilled water low	Chiller-pump trip	Loss of heat sink	6	5	8	240	V2
		CV-34 fail close	Loss of heat sink	6	5	8	240	Po-34
	Chilled water high	CV-34 fail open	Coolant temp. low	1	4	2	8	Po-34
Pressurizer	Pressure low	CV-10 fail open	Coolant pressure low	5	5	2	50	Po-10
	Pressure high	CV-9 fail open	Coolant pressure high	3	4	2	24	Po-9
	Inventory loss	CV-12 fail open	Loss of pres. and inventory	5	5	8	200	Po-12

Curriculum Vitae

Name: Jianping Ma

Post-Secondary Education and Degrees: Xi'an Jiaotong University
Xi'an, Shaanxi, China
2001-2005, B. E.

The University of Western Ontario
London, Ontario, Canada
2005-2008, M. E. Sc.

The University of Western Ontario
London, Ontario, Canada
2008-2015, Ph.D. Candidate

Related Work Experience: Research Assistant and Teaching Assistant
The University of Western Ontario
London, Ontario, Canada
2005-2015

Publications:

Jianping Ma and Jin Jiang, "Optimal Placement of Additional Sensors in Nuclear Power Plants for Fault Diagnosis," (submitted).

Jin Jiang, Jianping Ma, Ataul Bari, and Drew Rankin. *Physical Simulator for Training and Research in Nuclear Power Plant Instrumentation and Control Systems and Technologies*, Patent Pending, U.S. Patent Application 62120411, Filed on Feb 25, 2015.

Jin Jiang, Jianping Ma, Ataul Bari, and Drew J. Rankin, "A Physical Simulator in Supporting of Research and Development for Instrumentation and Control Systems in Nuclear Power Plants," *the 9th International Conference on Nuclear Plant Instrumentation, Control & Human-Machine Interface Technologies*, Charlotte, NC, USA, Feb. 23-26, 2015.

Ataul Bari, Jianping Ma, and Jin Jiang, "Demonstration of Wireless Sensor Networks based Fault Diagnosis," *the 9th International Conference on Nuclear Plant Instrumentation, Control & Human-Machine Interface Technologies*, Charlotte, NC, USA, Feb. 23-26, 2015.

Jianping Ma and Jin Jiang, "Semi-Supervised Classification for Fault Diagnosis in Nuclear Power Plants," *Nuclear Engineering and Technology* (2015), Vol. 47, pp. 176-

186, 2015.

Jianping Ma and Jin Jiang, "Analysis and Design of Modified Window Shapes for S-Transform to Improve Time-Frequency Localization," *Mechanical Systems and Signal Processing*, Vol. 58-59, pp. 271–284, 2015.

Jianping Ma and Jin Jiang, "Semi-Supervised Classification for Fault Diagnosis in Nuclear Power Plants," *International Symposium on Future I&C for Nuclear Power Plants and International Symposium on Symbiotic Nuclear Power Systems 2014*, Jeju, Republic of Korea, Aug. 24-28, 2014.

Jianping Ma and Jin Jiang, "Detection and Identification of Faults in NPP Instruments using Kernel Principal Component Analysis," *Journal of Engineering for Gas Turbines and Power*, Vol. 134, 032901, 2012.

Jianping Ma and Jin Jiang, "Applications of Fault Detection and Diagnosis Methods in Nuclear Power Plants: A Review," *Progress in Nuclear Energy*, Vol. 53, pp. 255-266, 2011.

Jianping Ma and Jin Jiang, "Fault Detection and Identification in NPP Instruments Using Kernel Principal Component Analysis," *The 18th International Conference on Nuclear Engineering*, Xi'an, Shaanxi, China, May 17-21, 2010.

Jianping Ma and Jin Jiang, "Applications of Fault Diagnosis in Nuclear Power Plants: An Introductory Survey," *the 7th IFAC Symposium on Fault Detection, Supervision and Safety of Technical Processes*, Barcelona, Spain, June 30 - July 3, 2009.

J. Ma and J. Jiang, "A Fault Detection and Isolation Technique for In-Core Flux Detectors," *the 6th International Conference on Nuclear Plant Instrumentation, Control & Human-Machine Interface Technologies*, Knoxville, Tennessee, USA, April 5-9, 2009.